PROCEEDINGS
of the
4th JOINT MEETING
of the
UJNR PANEL
on
EARTHQUAKE - PREDICTION TECHNOLOGY

Washington, D.C., USA

天然資源の開発利用に関する日米会議

地震予知技術専門部会

第4回合同部会会議録

於アメリカ合衆国、ワシントン, D. C.

1984年3月　　March, 1984

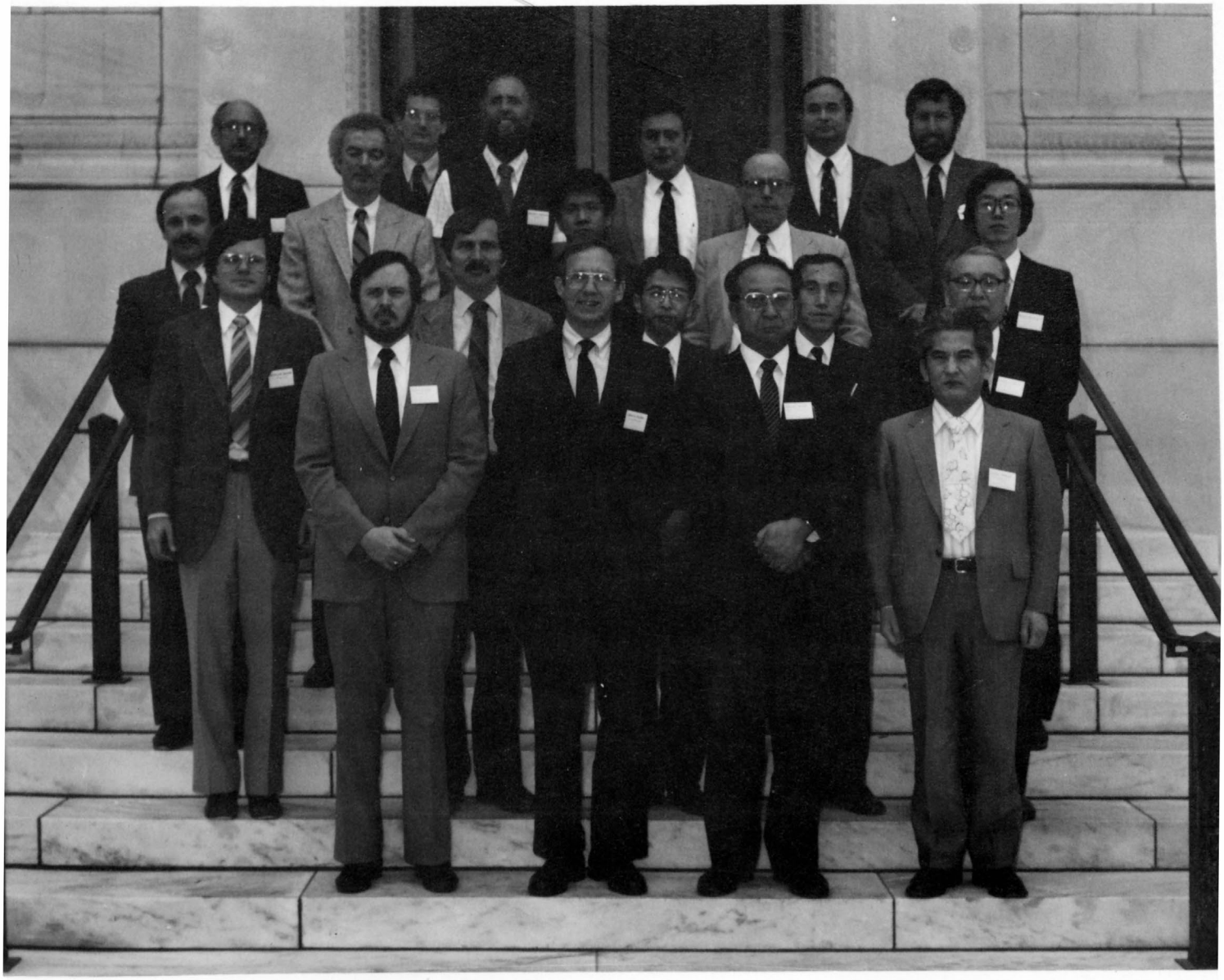

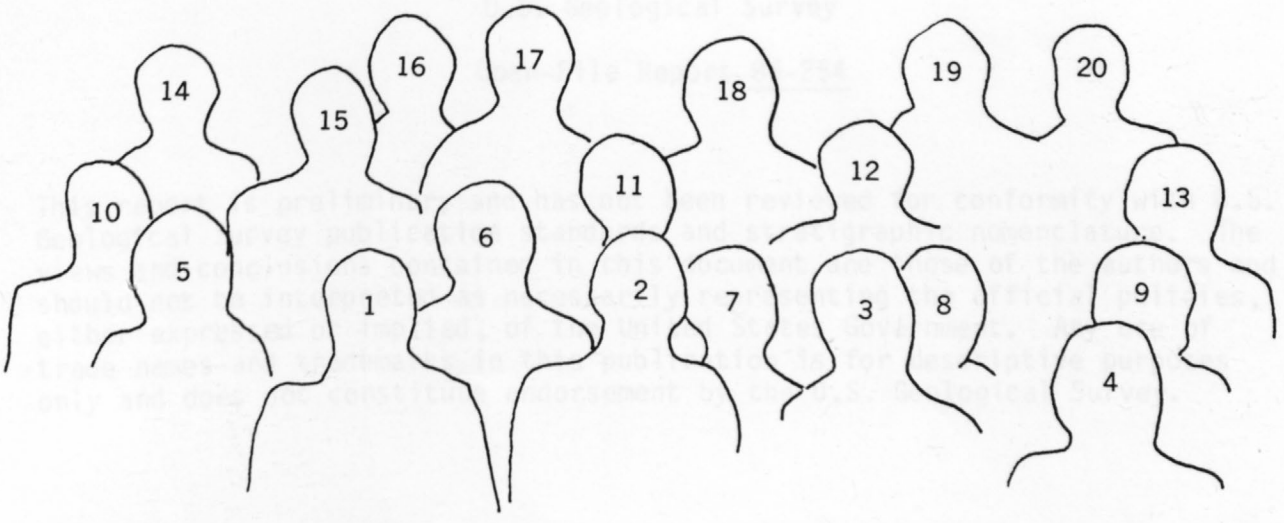

1. David P. Russ, 2. Dr. John Filson, 3. Dr. Minoru Tazima, 4. Dr. Kazuo Hamada, 5. Dr. Gary Mavko, 6. Dr. David Hill, 7. Mr. Hitoshi Haruyama, 8. Dr. Tadanao Ohishi, 9. Dr. Tsuneji Rikitake, 10. Dr. James H. Dieterich, 11. Dr. Yoshiro Nakahori, 12. Dr. Edward Flinn, 13. Dr. Masakatsu Sasada, 14. Dr. Carl Kisslinger, 15. Dr. Leonard Johnson, 16. Dr. Robert Wesson, 17. Dr. Wayne Thatcher, 18. Captain John Bossler, 19. Dr. Charles Bufe, 20. Dr. Mark Zoback

20
19
18
17
16
15
14
13
12
11
10
9
8
7
6
5
4
3
2
1

PROCEEDINGS OF THE

FOURTH JOINT MEETING OF THE U.S. - JAPAN CONFERENCE

ON NATURAL RESOURCES

(UJNR) PANEL ON EARTHQUAKE PREDICTION TECHNOLOGY

MARCH 26-27, 1984

Panel Chairman:

John R. Filson

U.S. Geological Survey

Reston, Virginia 22092

U.S.A.

Minoru Tazima

Geographical Survey Institute

Kitazato-1, Yatabe-Machi

Tsukuba-Gun, Ibaraki-Ken 305

Japan

U.S. Geological Survey

Open-File Report 86-254

TABLE OF CONTENTS

Introduction

The Fourth Joint Meeting of UJNR Panel on Earthquake Prediction Technology was held at the National Academy of Sciences in Washington, D.C., during the week of March 20, 1984. This panel, which was established in 1978, is the newest of 17 panels under the United States/Japan Cooperative Program in National Resources (UJNR). The UJNR program is based on a 1964 Cabinet-level agreement to foster the exchange of scientists, information, equipment, and knowledge between government agencies in Japan and the United States concerned with problems involving natural resources.

Dr. Minoru Tazima, Geographical Survey Institue, headed the Japanese Delegation of four Panel Members and three observers. From the United States, nine Panel members and twelve observers attended the technical sessions on March 26 and 27.

In addition to the technical session, the Japanese delegation visited the U.S. Naval Observatory, NASA - Goddard Space Center, NOAA - Office of Charting and Geodetic Services, Defense Advanced Research Projects Agency, and the U.S. Geological Survey in Menlo Park, California and in Reston, Virginia.

The scientific papers presented during the technical sessions are summarized in these proceedings. The papers represent an important part of the mutual exchange of information fostered by this panel on progress and problems in research on earthquake prediction in Japan and the United States.

JAPANESE MEMBERS OF THE UJNR PANEL

Dr. Minoru Tazima, Chairman*
Director General
Geographical Survey Institute
Kitazato-1, Yatabe-Machi
Tsukuba-Gun, Ibaraki-Ken 305

Dr. Kazuo Hamada*
Senior Researcher
Second Research Division
National Research Center
for Disaster Prevention
3-1, Tennodai, Sakura-Mura
Niihari-Gun, Ibaraki-Ken 305

Mr. Hitoshi Haruyama, Secretary*
Director,
Crustal Dynamics Department
Geographical Survey Institute
Kitazato-1, Yatabe-Machi
Tsukuba-Gun, Ibaraki-Ken 305

Dr Sadaiku Hattori
Director
International Institute of Seismology
and Earthquake Engineering
Building Research Institute
Tatehara-1 Oho-Machi
Tsukuba-Gun Ibaraki-Ken 305

Mr. Shigeru Kato
Research Officer
Ocean Surveys Division
Hydrographic Department
Maritime Safety Agency
5-3-1 Tsukiji Chuo-Ku
Tokyo 104

Dr. Nobuhiro Kawajiri
Deputy Director
Kashima Branch
Radio Research Laboratories
893-1 Hirai Kashima-Machi
Kashima-Gun, Ibaraki-Ken 314

Dr. Tadanao Ohishi*
Chief
Applied Optics Section
First Division
National Research Laboratory
of Metrology
1-1-4 Umezono Sakura-Mura
Niihari-Gun, Ibaraki-Ken 305

Mr. Koji Ono
Director
Environmental Geology Department
Geological Survey of Japan
1-1-3 Higashi Yatabe-Machi
Tsukuba-Gun, Ibaraki-Ken 305

Mr. Kazuo Sato
Director
Earthquake Disaster Prevention
Department
Public Works Research Institute
Asahi-1 Toyosato-Machi
Tsukuba-Gun Ibaraki-Ken 305

Dr. Norio Yamakawa
Head
Seismological Division
Department of Observation
Japan Meteorological Agency
1-3-4 Ote-Machi Chiyoda-Ku
Tokyo 100

*Members in attendance at the meeting

UNITED STATES MEMBERS OF THE UJNR PANEL

Dr. John Filson, Chairman*
Chief, Office of Earthquakes, Volcanoes, and Engineering
U.S. Geological Survey
National Center, MS-905
Reston, VA 22092

Mr. Leon L. Beraton*
Chief, Earth Science Branch
Div. of Health, Siting, and Waste Management
U.S. Nuclear Regulatory Comm.
Washington, D.C. 20555

Rear Admiral John D. Bossler*
Director, Charting and Geodetic Services
National Oceanic and Atmospheric Administration
6001 Executive Blvd.
Rockville, MD 20852

Dr. James H. Dieterich*
Research Geophysicist, Office of Earthquakes, Volcanoes & Engineering
U.S. Geological Survey
345 Middlefield Road, MS-77
Menlo Park, CA 94025

Dr. Edward Flinn*
Chief Scientist, Geodynamics Resource Observation Division
National Aeronautics and Space Administration
Center for Seismic Studies
1300 North 17th Street
Suite 1450
Arlington, VA 22209

Dr. David P. Hill*
Research Geophysicist, Office of Earthquakes, Volcanoes, and Engineering
U.S. Geological Survey
345 Middlefield Road, MS-77
Menlo Park, CA 94025

Dr. Leonard Johnson*
Program Director, Seismology and Deep Earth Structure
Div. of Earth Sciences
National Science Foundation
1800 G. Street, N.W.
Washington, D.C. 20550

Mr. Richard W. Krimm*
Director, Office of Natural and Technological Hazards
Federal Emergency Management Agency
500 C Street, S.W.
Washington, D.C. 20472

Dr. Wayne Thatcher*
Research Geophysicist, Office of Earthquakes, Volcanoes, and Engineering
U.S. Geological Survey
345 Middlefield Road, MS-77
Menlo Park, CA 94025

Dr. Robert L. Wesson*
Research Geophysicist, Office of Earthquakes, Volcanoes, and Engineering
U.S. Geological Survey
National Center, MS-922
Reston, VA 22092

*Members in attendance at the meeting

JAPANESE OBSERVERS

Dr. Yoshiro Nakahori
Geographical Survey Institute
Kitazato-1, Yatabe-Machi
Tsukuba-Gun, Ibaraki-Ken 305

Dr. Tsuneji Rikitake
Nihon University
Department of Earth Sciences
10-302, 4-1 Sakurajosui
Setagaya, Tokyo 156
Japan

Dr. Masakatsu Sasada
Geological Survey of Japan
1-1-3 Higashi, Yatabe, Tsukuba-Gun
Ibaraki-Ken 305
Japan

UNITED STATES OBSERVERS

Dr. Joseph Berg
National Academy of Sciences
Washington, D.C.

Dr. Roger Bilham
Lamont-Doherty Geological
Observatory
Palisades, New York

Captain John Bossler
National Geodetic Survey
Washington, D.C.

Dr. Charles Bufe
U.S. Geological Survey
Reston, Virginia

Dr. Robert Hamilton
U.S. Geological Survey
Reston, Virginia

Dr. Leonard Johnson
National Science Foundation
Washington, D.C.

Dr. Carl Kisslinger
CIRES
Boulder, Colorado

Dr. Ian MacGregor
National Science Foundation
Washington, D.C.

Dr. Gary Mavko
U.S. Geological Survey
Menlo Park, California

Dr. Frank Press
National Academy of Sciences
Washington, D.C.

Dr. Carl Romney
Center for Seismic Studies
Rosslyn, Virginia

Dr. David Russ
U.S. Geological Survey
Reston, Virginia

Dr. Mark Zoback
U.S. Geological Survey
Menlo Park, California

WELCOMING BY DR. JOHN R. FILSON

On behalf of the U.S. panel members and their guests I would like to extend our warm welcome to the members of the Japanese panel and their guests to Washington, D.C. and to the Fourth Joint Meeting of the United States/Japan Committee on Natural Resources Panel on Earthquake Prediction.

The panel, which was established in 1978, is the newest of 17 panels under the United States/Japan Cooperative Program in Natural Resources. The program is based on a 1964 Cabinet-level agreement to foster the exchange of scientists, information, equipment, and knowledge between government agencies concerned with problems involving natural resources.

I am particularly pleased to have the opportunity to welcome and renew my acquaintance with Dr. Minoru Tazima, Director-General of the Geographical Survey, Institute of Japan. I am also pleased to welcome the rest of the Japanese panel members and their guest, Professor Rikitake to the meeting.

OPENING REMARKS BY DR. MINORU TAZIMA

It is my great pleasure to have an opportunity of greeting you at the Fourth Joint Meeting of the United States/Japan Natural Resources Panel on Earthquake Prediction Technology in Washington, D.C. With the resignation of Mr. Keiji Nishimura, the former General Director of the Geographical Survey Institute, I am now the chairman of the Japanese members.

On behalf of the Japanese side, I would like to convey my gratitude to Dr. Filson, the Chairman of the United States side, and the Panel members for inviting me. As you already know, a great number of earthquakes occur all over the world and cause repeated disasters. In Japan, a big earthquake occurred in the northern part of the Japan Sea last May. Approximately 100 people were injured by tsunamis (tidal waves) which resulted from the quake.

Needless to say, earthquake prediction is extremely important since it helps protect life and property of people from disaster.

The Fifth Earthquake Prediction Project of Japan which will start in April of 1985, encompasses earthquake prediction and observation research. In Japan, VLBI (Very-long Baseline Interferometry) and multi-laser instruments are being developed, and refraction studies are underway.

At this joint meeting, the important results of our earthquake studies will be discussed. I believe that the papers presented and discussions held will significantly contribute to earthquake prediction technology world-wide.

I would like to introduce the members of the Japanese Panel and guests. The members attending are Dr. Kazuo Hamada of the National Research Center for Disaster Prevention, Mr. Hitoshi Haruyama of the Geographical Survey Institute, Dr. Tadanao Ohishi of the National Research Laboratory of Metrology and I am from the Geographical Survey Institute.

Japanese Panel members have traditionally been affiliated with government agencies. However, in view of the fact that important research occurs in the academic community, I welcome with great pleasure Dr. Rikitake of Nihon University. Our other guests are Dr. Masakatsu Sasada of the Geological Survey of Japan, and Dr. Yoshiro Nakahori of the Geographical Survey Institute.

As is customary, the Chairman of the hosting panel is the Chairman of the committee, therefore Dr. Filson is going to assume the Chairmanship today.

OPENING REMARKS BY DR. JOHN FILSON

I would like to take this opportunity to discuss the importance of the Panel meetings and introduce the United States Panel members and guests.

The Congress of the United States has a great interest in the domestic

earthquake prediction program and is aware of the committment to earthquake prediction made by the Japanese government and its scientists. Every year when the United States program is reviewed by Congress, we can be assured of being asked one question. That question is "Are you aware of the status of the Japanese earthquake prediction program and their latest results?" Primarily due to this panel and the exchange of information and scientists carried out under the aegis of this panel, we can happily answer this question in the affirmative. We look forward to a productive meeting and again welcome our visitors who have journeyed so far to join us. I would now like to introduce the United States panel members and our guests.

The members of the Panel are Richard Krimm, Associate Director for State and Local Programs, from the Federal Emergency Management Agency, Dr. Edward Flinn of the National Aeronautics and Space Administration, Dr. James Dieterich of the U.S. Geological Survey, Dr. Wayne Thatcher of the U.S. Geological Survey, Dr. Robert Wesson of the U.S. Geological Survey, and Dr. David Hill, past Chairman of the U.S. side of this panel. Dr. Carl Kisslinger is our designate consulting member. Our other guests are Dr. Frank Press who is a distinguished seismologist and the current President of the National Academy of Sciences, Dr. Robert Hamilton, Chief Geologist of the Geological Survey, Dr. Carl Romney from the Center for Seismic Studies, Dr. Ian MacGregor of the National Science Foundation, and Dr. Roger Bilham from Lamont-Doherty Geological Observatory. Also, Dr. Mark Zoback of the U.S. Geological Survey, Dr. Gary Mavko of the Geological Survey, Dr. David Russ of the U.S. Geological Survey, and Dr. Charles Bufe of the Geological Survey. Part of the secretariat helping us in the organization of the meeting is Mrs. Carolyn Hearn.

RESOLUTIONS OF THE FOURTH JOINT MEETING

U.S.-JAPAN PANEL ON EARTHQUAKE PREDICTION TECHNOLOGY

U.J.N.R.

March, 1984

The UJNR Panel on Earthquake Prediction Technology recognizes the critical importance of promoting prediction research in both countries. The Fourth Joint Meeting was extremely beneficial in furthering friendship and deepening understanding of the common research problems of both Japan and the U.S.

Technical sessions included presentation of 24 papers, including extensive discussion of national and agency programs, earthquake precursors, crustal strain and deformation, fundamental earthquake studies, and the 1983 Nihonkai-Chubu earthquake.

Discussion was extremely fruitful, and the Panel unanimously adopted the following resolutions:

1. One of the most important means of achieving joint progress is by the long-term exchange of researchers between our two countries. Since the First Joint Meeting such exchanges are already achieving extremely valuable results. Efforts should be made to cooperate on instrumental development and observations, data interpretation, and earthquake prediction experience, use of VLBI and laser ranging techniques, and rock mechanics.
2. We agree that exchanges of data and analysis methods are mutually beneficial and strongly encourage these activities. In particular, the Panel emphasized the importance of exchanging mutual experience in the area of automatic processing of seismic data, geodetic measurements,

precursory phenomena, and modelling techniques.

3. Cooperation in the application of space techniques to prediction research is already in progress. This cooperation should continue and should include exchange of data, sharing results from field experiments, development of techniques and instrumentation, and planning new experiments. It is noted that the Japanese geodetic satellite "GS-1" will be launched in the near future, providing a new resource for geodetic measurements by laser ranging, and that a Japanese transportable VLBI facility will be completed in 1985. Cooperative experiments using U.S. and Japanese laser ranging and VLBI facilities should be promoted.
4. The next joint meeting will be held in Japan tentatively in May, 1986.

STATUS OF EARTHQUAKE HAZARDS REDUCTION PROGRAM IN THE UNITED STATES

JOHN R. FILSON

Introduction

California and Alaska are well known for producing damaging earthquakes in the United States. Other regions of the country, however, such as the Puget Sound, the Great Basin, the Central United States in the Upper Mississippi Embayment and along the Atlantic Coast, also have nonnegligible earthquake risk. In an effort to mitigate the hazards associated with this risk and with the stimulous generated by the Alaskan earthquake in 1964 and the San Fernando, California, earthquake of 1971, an embryonic earthquake studies program was developed in the U.S. Geological Survey in the mid 1960's. Other agencies also had small scientific programs developing at this time that were investigating various aspects of earthquake occurrence. In 1978, the Congress of the United States passed the Earthquake Hazards Reduction Act which authorized a 3-year earthquake hazards reduction program. The program has been reauthorized by Congress every year from 1981 until the present; however, in 1984 the program was authorized for 2 years--1984 and 1985. The primary agencies involved in the national program are the Federal Emergency Management Agency, the National Science Foundation, the National Bureau of Standards, and the U.S. Geological Survey. Other agencies participate in developing techniques that can be applied to the earthquake problem, such as the National Geodetic Survey, the National Aeronautics and Space Administration, and the Nuclear Regulatory Commission. The objectives

that are outlined in the 1978 legislation establishing the earthquake program have not been changed since the law was originally passed. One of the primary objectives is the development of systems for predicting earthquakes and evaluating hazards in all areas of high or moderate seismic risk in the United States. This objective is the impetus and the justification used for pursuing earthquake prediction research under the authorizing legislation. Among the participating agencies, the Federal Emergency Management Agency has been designated the lead Federal agency for pursuing the objectives of the 1978 legislation. Its responsibilities are to plan and coordinate the Federal program in earthquake hazards reduction and to prepare and be involved in organization and planning for emergency response to earthquake occurrence. The National Science Foundation has the responsibility for fundamental research in earthquake processes, research in earthquake engineering, and research in societal response to earthquake warnings. The National Bureau of Standards tests and recommends improvements for proposed earthquake-resistant design and construction practices and develops and promotes the application of model building codes. Currently, the Geological Survey of the United States pursues five general areas in earthquake studies:

- Current Tectonics and Earthquake Potential of various earthquake-prone regions
- Earthquake Prediction Research
- Regional Assessments of Earthquake Hazards
- Earthquake Data and Information
- Engineering Seismology, primarily, strong motion seismology

The National Aeronautics and Space Administration conducts research under its geodynamics program on plate motion and the development of space techniques for application to the measurement of crustal deformation. The

National Geodetic Survey provides data for high-precision ground-leveling surveys and also develops regional techniques for measurement of crustal deformation. The Nuclear Regulatory Commission has responsibility for the siting of nuclear power plants in the United States.

In 1978 the total budget for the National Earthquake Hazards Reduction Program for the four principal participating agencies was about $53 million. In 1984 the addition of FEMA and slight increases in individual agency budgets brings the total being spent under the aegis of the Earthquake Hazards Reduction Program in the United States to about $65 million, a growth of about 20 percent from 1978. Of this total, the amount being spent by the Geological Survey is $35.4 million. Approximately $8.2 million is for Current Tectonics and Earthquake Potential, $14.2 million for Earthquake Prediction Research, $6 million for Regional Earthquake Hazards Assessments, $4 million for Earthquake Data Information Services, and $3 million for Engineering Seismology. The National Science Foundation budget, which totals about $26 million, consists of about $17 million for earthquake engineering studies and about $9 million for fundamental research. Most of the National Science Foundation funds are directed towards unviersities and private institutions. These monies are not spent within the Government. About 25 percent of the Geological Survey funds are directed towards grants and contracts for research to be carried out by private institutions and universities. Thus, the total of the National Science Foundation funding and that portion of the Geological Survey funding not spent within the Government is about $34 million, which is about one-half of the total national program.

Current Tectonics and Earthquake Potential Studies - The objectives of this element of the program are to: (a) delineate seismically active areas and the extent of seismic zones through monitoring with regional seismograph networks; (b) determine the geometry and structure of seismic zones through geologic mapping and geophysical analyses, and (c) use the geological and geophysical data obtained in the objectives above to estimate fault slip rates, maximum earthquakes, and recurrence intervals for active faults and seismogenic zones.

Substantial progress has been made in the past 5 years in estimating the long-term earthquake potential of various seismic zones in the United States. These estimates are based on detailed analyses of current tectonics of seismically active regions as interpreted from geological and geophysical observations. These studies have provided quantitative estimates of slip rates along active faults, earthquake recurrence intervals, and earthquake potential. They have also defined tectonic structures, heretofore unspecified, that give rise to the seismic activity.

Activities in this element include:

- Operation of regional seismograph networks in southern California, central and northern California, southern Alaska, the Puget Sound area, western Nevada, Yellowstone Park, central Utah, the central Mississippi Valley, and portions of the Northeastern United States. Earthquake catalogs and maps based on these data are completed on an annual basis.
- Geological and geophysical field work and fault excavation studies in southern and central California and central Utah. These studies give quantitative estimates of the earthquake potential of individual faults that the seismic monitoring efforts have identified as active.

o Studies of specific seismogenic features, including preshock-mainshock-aftershock sequences, to determine spatial and temporal characteristics of earthquakes and the geometry of crustal fault zones at seismogenic depths.

Earthquake Prediction Research includes field, laboratory, and theoretical investigations of earthquake mechanisms and of the physical characteristics of fault zones, with the goal of establishing the procedures and knowledge needed for the reliable prediction of the time, place, and magnitude of damaging earthquakes. These investigations have been focused on the central and southern California regions, Utah, Missouri, and in a few other selected areas of high seismicity around the world; the latter because frequent earthquakes are required to provide field observations and valid tests of possible earthquake precursors. Assessment of various possible geophysical precursors of earthquakes is emphasized in order to develop the analytical and instrumental capabilities for prediction. Reliable prediction depends on observing a variety of precursors, understanding their causes, and understanding the basic physics of the earthquake source. Thus, a prediction research program must be broadly based and its success will depend heavily on observations of precursors and earthquakes using a variety of densely spaced instruments.

The specific objectives of this element are to: (a) develop earthquake prediction methods and techniques to provide a rational basis for estimates of increased earthquake potential and short-term predictions; (b) evaluate in probabilistic terms the relevance of various geophysical, geochemical, and hydrological data to ensure accurate earthquake prediction; (c) develop theoretical and laboratory models of the earthquake process to guide observational experiments and to test empirical, predictive techniques; and (d) determine the physical mechanism for reservoir-induced seismicity and

develop techniques for predicting and mitigating this phenomenon.

Activities in this element include:

- The analysis, for prediction purposes, of the seismic data from nearly 500 seismograph stations in California and in other seismically active zones in the United States.
- The resurvey of 25 geodetic strain monitoring networks along the San Andreas fault and the eastern Sierras. These networks contain several hundred survey lines.
- The measurement of crustal deformation and fault offset at 250 sites along the San Andreas and other active faults.
- Recording of geophysical and geochemical data at 140 other sites along or near the San Andreas fault.
- Operation of prediction data and analysis centers in southern California (California Institute of Technology, Pasadena) and central California (Geological Survey, Menlo Park).
- Theoretical and laboratory research on crustal deformation and earthquake mechanisms. An earthquake model and rock mechanics laboratory is operated at Menlo Park, California.
- Based on the data collection and analysis and on the laboratory and theoretical studies described above, statistics are being developed on the relevance of various observed phenomena to earthquake occurrence.
- Contacts and scientific exchanges with earthquake prediction efforts in Japan, the People's Republic of China, and the Soviet Union.

In the past 5 years progress has been made in the understanding of the earthquake process and where the next ones are most likely to occur.

Highlights of the most noteworthy scientific advances of the past 5 years are:

- o Recurrence intervals for great earthquakes on plate boundaries can be specified rather accurately given certain information on the previous earthquake history and rates of tectonic deformation of that segment of the boundary.
- o Earthquake sequences occurring at the same place but decades apart may have nearly identical characteristics. The behavior of at least some faults appears to be surprisingly consistent for recent history, making short-term forecasting very promising.
- o The rate at which strain accumulates generally appears to be highly linear even in regions as large as southern California but may show sudden widespread pulses and, if for various other reasons, a large earthquake were expected, such a pulsation in the strain field could provide a warning.
- o Foreshocks appear, by variations in their focal mechanisms or by abruptly terminating, to give short-term warning of the impending mainshock in certain, but not all, geologic settings.
- o The probability for great earthquakes occurring along the San Andreas fault in southern California may be tested with an earthquake "instability" model that uses computer modelling of time-varying physical and fault strength data to calculate recurrence times.

Regional Earthquake Hazards Assessments - In addition to national and regional earthquake monitoring and earthquake potential estimates, hazards assessments in developed regions provide significant and useful results because of the exposure of population and property to damaging earthquakes. These results are built on earthquake potential and seismic monitoring studies described above. Regional hazard assessments require concentrated and specialized

attention to a specific area, and they require a synthesis of a wide variety of information. These studies form the foundation for analyses conducted on a city-by-city, street-by-street basis by State and local governments.

Because of the severity and frequency of ground shaking expected and the distribution of population, the hazards and risks due to earthquakes are greatest in the large urban centers of the western United States and Alaska. The program strategy consists of conducting investigations (using geological, seismological, geophysical, and geodetic techniques) to identify and map those geologic features near or within a given region that are most likely to be the source of damaging earthquakes and to estimate recurrence rates and maximum size of earthquakes that are likely to occur on these features. For the evaluation of the hazards from these earthquakes, regional-scale maps of the distribution, depth, and physical properties of surficial geologic units are combined with the predicted nature of the ground shaking to develop deterministic and probabilistic estimates of ground motion. Evaluations of the hazards that would be associated with earthquake-induced landslides, liquefaction, surface faulting, and coastal uplift or subsidence are made. Because of the relatively low earthquake occurrence rates in the East and because of the burial of the active geologic structures in some regions by younger sediments, specialized techniques such as detailed subsurface mapping are required to identify the sources of the earthquakes.

The specific objectives of this program element are: (1) based on current research results, prepare synthesis reports and maps that assess earthquake hazards in urban regions at risk to damaging earthquakes; (2) develop techniques for estimating strong ground shaking, ground failure, and other earthquake-related hazards in urban regions; (3) conduct research and specific studies to estimate more accurately potential losses due to

earthquakes; and (4) foster implementation of the results in terms of loss-reduction measures.

Activities in this element include:

- o Publication of work on an earthquake hazard assessment report and maps for the Los Angeles and San Diego region.
- o Conduct a joint effort with the State of Utah for an earthquake hazard assessment of the Salt Lake region. This effort is aimed at preparation of a comprehensive report in about 3 years time.
- o Special symposium in Los Angeles to deliver results of southern California studies to the local user community.
- o Completion of a joint effort with the State of Utah for an earthquake hazards assessment of the Wasatch Front region.
- o Joint planning effort with the State of Alaska to prepare an earthquake hazards assessment of the Anchorage region.

Data and Information Services - A key link in the development of a successful seismic hazards mitigation and disaster response program is the collection and transmittal of earthquake data for analysis and evaluation. The National Earthquake Information Center (NEIC) coordinates the rapid location and evaluation of earthquakes in the United States and large earthquakes that occur throughout the world. Within NEIC, the National Earthquake Information Service (NEIS) distributes , in a timely manner, earthquake information and data to the public and the scientific research community. NEIS also provides data support for the Tsunami Warning System of the National Oceanic and Atmospheric Administration and acquires fundamental data critical for seismic risk appraisal. Products of the NEIC include weekly, monthly, quarterly, and annual reports on earthquake activity, maps of earthquake distribution, and information services to the public. A 24-hour alert service is provided and

appropriate authorities are notified of any potentially damaging earthquakes within the United States. This service allows for the early inspection of dams and other critical facilities for possible earthquake damage.

To provide basic data for earthquake research, the Geological Survey supports the operation of the Worldwide Standard Seismograph Network and the Global Digital Seismograph Network. The data is used in studies of plate tectonics, Earth structure, and earthquake source mechanisms.

Effective transmission of technical information about significant earthquake hazards and warnings to State and local officials requires the development of established and knowledgeable points of contact. Points of contact in virtually all States have been established for geologic hazards. Meetings are held and background educational materials are routinely distributed to describe the nature and use of technical information about earthquakes.

Engineering Seismology - The measurement, analysis, and theoretical estimation of strong ground shaking near earthquake epicenters are used by engineers and architects in the design of structures and are extremely important in the siting, design, and construction of critical facilities. Theoretical and interpretative studies that explain the character of strong ground motion, and cast obervational data in forms more useful to the engineer, have been part of the Geological Survey Earthquake Hazards Reduction Program for several years. In FY 1983 responsibility for the National Strong Motion Network, a network of instruments designed specifically to record only severe earthquake ground shaking, was transferred to the Geological Survey from the National Science Foundation. The transferred observational responsibility and the existing analytical efforts have been combined to form the engineering seismology element.

The objectives of this element are: (1) Operate the National Earthquake Strong Motion Network and an associated data center. This network consists of some 500 specially designed instruments to record very strong ground motion on the ground and in structures near the source of damaging earthquakes. These instruments are located in seismically active regions of the United States. (2) Archive these data and disseminate them to engineers, designers, private institutions, and government agencies concerned with the siting, design, and construction of critical facilities and the establishment of building codes. (3) Develop techniques and standards for presenting the strong motion data in a more useful context than its raw form. The frequency content, average ground acceleration and velocity, duration of the ground shaking as well as the effects of local soil conditions, and the geometrical relationship of recording site to the earthquake source, if not taken into account, can yield misleading interpretations. (4) Conduct research on the estimation of the level and character of strong earthquake motion for application in engineering design in instances where no relevant data exist. (5) Conduct research on the physics of seismogenic failure including the dynamic processes controlling fault rupture and the seismic radiation field.

THE OUTLINE OF
THE FIFTH EARTHQUAKE PREDICTION PROGRAM OF JAPAN

Minoru Tazima

Geographical Survey Institute

Introduction

Earthquake prediction research in Japan has been conducted since fiscal year 1985 in accordance with the national program recommended by the Geodesy Council, Ministry of Education.

The Geodesy Council recommended the fifth five year program on earthquake prediction to the Prime Minister and the Cabinet ministers concerned on May 31, 1983. From 1984 fiscal year onward, observations and research related to earthquake prediction will be made according to the program.

The overall budget necessary for pursuing the program is not given in the program. However, the budget for 1984, the first fiscal year of the fifth program, is 5,800 million yen and the total budget spent up to the end of the fourth program amounts to about 81,000 million yen.

The fifth program consists of three parts. They are summarized in the following.

Review of the Work Done up to the Fourth Program Period

The first program which was put into practice from FY1965 to FY1968 was aimed at estalishing a system for obtaining data mainly from geodetic and seismological observations which were regarded as fundamental to research.

In the second program period from FY1969 to FY1973, the framework of the present day earthquake prediction system was established. The Coordinating Committee for Earthquake Prediction (CCEP) was organized in April, 1969, with

a view to exchanging information relevant to earthquake prediction research and for a forecast of seismic activity by putting various information together. The CCEP designated the areas of specific observation and intensified observation where the observations and research should be emphasized.

In the third program period from FY1974 to FY1978, much progress was made in observational techniques such as introduction of electro-optical distance measuring instruments in geodetic surveying, data telemetering techniques applied to seismological observation networks, establishment of more wells for underground water observations, and installation of ocean bottom seismometers and bore-hole strainmeters.

The system was developed so as to promote earthquake prediction. The observation networks and facilities were improved. The Earthquake Assessment Committee for Areas under Intensified Measures against Earthquake Disaster (EAC) was established. The importance of basic research was stressed and promoted.

Based on the results of intensified observations and research, unique phenomena preceding or accompanying earthquakes were recognized several times. But it was found that they appeared in various and complicated ways.

In the fourth program period (FY1979-FY1983), the following achievements have been made.

1. Intensification of nationwide observations for long-term prediction.

First order precise geodetic survey will be completed for the first time in the near future. Based on the results, the distribution of crustal strain throughout the country will be obtained. For each of the last two surveys, leveling over the whole land were completed in approximately six years. The data provided us with information about the vertical crustal movement over the

land.

Seismological observations of large, moderate, and small scale earthquakes have been improved in order to obtain reliable data quickly over the whole country. A system for microearthquake observations has been established which enables seismic activity over a wide area to be monitored with high reliability.

Ocean bottom seismometers that have a data transmitting coaxial cable which was installed off Omaezaki, are playing an important role in watching the seismic activity off the Tokai region. Using much improved ocean bottom observation techniques, crustal movements around the Japan trench have been defined more clearly. Meaningful results were also obtained in studying the relationship between geomagnetic variations and earthquake occurrence, verifying repeated fault movements by excavation and collecting historical records about earthquakes.

2. Concentrated observations for short-term prediction over the areas of intensified observation and other areas.

Existence of short-term precursory phenomena has been confirmed, including events found in the results of underground water and magnetic field observations which were newly introduced in anticipation of detecting short-term precursors. Good examples were found in a rapid change recorded by borehole strainmeters and an obvious change in radon content preceding the Izu-Oshima Kinkai Earthquake and associated foreshocks.

However, the precursors exhibit much complicated behavior and the precursor times are widely scattered. Although it is encouraging that various methods for earthquake prediction have been proven effective, still it has been recognized that it is important to make integrated analyses of various kinds of observations so as to detect anomalous premonitory effects with

certainty. It is also important to find suitable places for establishing observation stations.

3. Promotion of research for elucidating the earthquake occurrence mechanism

A rock-breaking experiment in a laboratory confirmed that anomalous deformation preceding the main rupture, as well as the distribution of microfractures, may be considered as precursors similar to those of natural earthquakes.

Various techniques for measuring crustal stress in the field have been introduced. They are much improved in reliability and have provided us with valuable data.

Based on explosion seismic experiments, the relation between the crustal structure and distribution of shallow earthquakes or anomalous crustal movements has been studied and the subduction of the Philippine Sea plate has been portrayed visually.

The test field observations at the Yamasaki fault succeeded in detecting precursory phenomena to some small earthquakes. The fracture zone of the fault has been extensively investigated.

These prove that every basic research subject included in the program plays an important role in earthquake prediction.

4. Improvement in the earthquake prediction system

Remarkable improvements have been made in the rapid analysis of large, moderate, and small scale earthquakes, owing to expanded efforts in establishing data acquisition and processing systems.

The detectability and observational accuracy of locations of microearthquakes have increased remarkably. Automatic and quick processing of data and establishment of data bases have made steady progress.

Associated with the promulgation of the Large-Scale Earthquake Counter-

measures Act, the EAC was established and the Tokai region was designated as the area under intensified measures against earthquake disaster. A system for monitoring the real-time records from the stations in the Tokai area throughout the day was established and expanded.

Policy for Planning

The general policy of the Japanese earthquake prediction program has been to designate important areas for research based on repeated observations and surveys over the whole land and secondly to concentrate various observations to obtain information about the time of earthquake occurrence.

The importance of basic research has been stressed in order to determine a scientific explanation for earthquake precursors. The fundamental way of thinking is summarized in the following. The fifth program is also based on it.

1) Observations and surveys over the whole land are the most effective means for long-term prediction. They are carried out with the hope of finding areas of anomalous crustal activity. In other words, their purpose is to locate an area where an earthquake might occur and to estimate its magnitude.

2) In an area where an anomaly is found, the observations and surveys for long-term prediction should be carried out more frequently to know the real condition of the anomalous phenomena. At the same time, intensified observations should be made there, including various methods for short-term prediction in order to investigate the phenomena in detail and to make an estimate of the time of earthquake occurrence.

3) There are many problems which must be solved in regards to the focal mechanism including the explanation of precursory phenomena. An important subject of research is to elucidate the mechanism in order to establish a scientific basis of earthquake prediction and in order to increase its

accuracy. Extensive research on the focal mechanism should be made while maintaining a close connection with observations and surveys for predicting location, magnitude and the time of earthquake occurrence.

Contents of the Program

1. Intensification of observations effective for long-term prediction

Long-term prediction is the basis of carrying out effective and concentrated observations for short-term prediction by clarifying long-term crustal movements in and around Japan and regional characteristics of seismic activity. For the purpose of increasing the accuracy of prediction of location and magnitude of possible earthquake occurrence, long-term crustal movements should be quantitatively determined and concentrated observations for investigating regional characteristics should be carried out as well as observations over the whole land. The merits and shortcomings of various techniques should be examined and efforts should be made to develop and introduce new techniques. Based on the improved techniques, geodetic surveys and earthquake observations over the whole land should be intensified.

In areas of intensified observation and specific observations, observations by mobile parties including ocean bottom observations, should be made. Investigations of active crustal structure and historical documents should be promoted to play an important part in evaluating characteristic crustal activities.

1) Observations over the whole land

A. Geodetic surveys

(a) Precise geodetic survey (GSI)

First order precise geodetic surveys and first order leveling surveys over the land are repeated every five years.

(b) Tide guage observations (GSI, JMA, HD)

Renewal of tide gauges as required and completion of data telemetering systems are desirable.

(c) Gravity and magnetic surveys (GSI, JMA, HD, Univ.)

Gravity and magnetic surveys over the land and continuous total force observations at fixed stations are conducted.

(d) Research and development of new techniques for geodetic surveys (GSI, JMA, HD, Univ., RRL)

Research on atmospheric corrections to leveling, development of multiwavelength EDM and application of space techniques for geodetic surveys such as satellite laser ranging and VLBI are made.

B. Seismological observations

(a) Large, moderate, and small scale earthquake observations (JMA)

The nationwide observation net is to be completed so as to be able to determine the location and magnitude of the earthquakes in and around Japan without omission.

(b) Microearthquake observations (Univ., NRCDP)

The observation net is to be improved by taking measures to meet changes for the worse in the observation environment and introducing new techniques including a system for transmitting and processing data quickly.

2) Observations in specific areas

A. Frequent repetition of geodetic surveys over a dense net (GSI, HD)

In areas of intensified observation and other areas, surveys such as precise strain measurements and leveling frequently made over dense nets.

B. Precise observations by mobile parties (Univ., NRCDP, JMA)

The mobile party observation system is to be completed so as to meet the need in a state of emergency. It includes seismological, geodetic, crustal movement, magnetic, gravity and geochemical observations.

C. Ocean bottom observations

(a) Ocean bottom seismological observations

(a-1) Ocean bottom seismological observations with data transmitted by coaxial cable (JMA)

In addition to the region off Tokai, equipment will be installed off the Boso Peninsula.

(a-2) Self-surfacing ocean bottom seismometer (Univ., NRCDP)

(b) Ocean bottom magnetic observations (Univ.)

A three-component ocean bottom magnetometer is installed to obtain information about sub-bottom electrical conductivity structure.

(c) Development of ocean bottom observation techniques

(c-1) Development of an ocean bottom seismological observation system applying a data telemetering device using a buoy (Univ.)

(c-2) Development of an ocean bottom crustal movement observation system (NRCDP, Univ.)

3) Basic investigations

A. Investigation of active crustal sturctures (GSJ, Univ., GSI, NRCDP, HD)

Investigation of active faults is made applying excavation, geophysical and geochemical techniques. Ocean bottom topography and geological structure are surveyed.

B. Investigation of historical documents (Univ., NRCDP)

2. Intensification of observations effective for short-term prediction

Short-term prediction plays an important part in earthquake prediction as well as long-term prediction. It is indispensable for making prediction practical. It is important for short-term prediction to be able to detect and examine precursory phenomena which take place immediately before the

earthquake occurs. As it has become more and more evident that precursors show complicated behavior, it is necessary to increase the observational accuracy so that really effective information can be discriminated. Developing a synthesized approach to prediction based on performing analyses of combined data from various kind of observations is required. It is important to have a more complete picture of the normal crustal movement, also taking local characteristics into consideration. In the Tokai region especially, improvement in the quality of observations and capability of collecting and processing data are required in view of intensifying the real-time monitoring system. The observation network should be made more dense as required. In the Tokyo Metropolitan area, observation facilities are to be completed and development and research on observational techniques are to be positively promoted aiming at putting prediction into practical use.

1) Continuous observation of crustal movement

Continuous observation of crustal movement is carried out to monitor crustal activity and is effective for detecting precursory phenomena. In order to distinguish precursors from various complicated phenomena, quick and synthesized analyses of observations are needed. Institutes concerned make efforts to increase the observation accuracy and data processing capability and conduct continuous observations of crustal movement by various methods.

A. Bore-hole strainmeter (JMA)

Bore-hole strainmeters are to be supplemented by a noise eliminating observation system. The real-time monitoring system is to be expanded as required.

B. Tilt- and extensometers (NRCDP, Univ., ILO, JMA, GSI)

Observations by tilt- and extensometers including bore-hole type tilt- and strainmeters are to be intensified. Data should be quickly processed.

C. Tidal observation (GSI, JMA, HD)

Combined with leveling results, sea level data from tidal stations are expected to provide information about anomalous vertical movements along coasts.

D. Synthesized array observation of crustal activity (Univ.)

Observation arrays in the areas of intensified observation and specific observations are to be completed so as to be able to make analyses on correlation among stations and various observation disciplines.

2) Gravity change measurements (GSI, Univ., ILO)

In order to investigate internal structure of the crust and its change, gravity measurments are to be repeated in areas of high crustal activity. The absolute measurement of gravity will also be carried out.

3) Seismological observations (JMA, NRCDP, Univ.)

Seismological observations are to be improved, using various possible techniques including installation of ocean bottom seismometers, establishment of arrays of observation systems and observation wells.

4) Geomagnetic and geoelectric observations

A. Magnetic observations (JMA, Univ.)

High-precision total field intensity observations are conducted in order to detect small short-term precursors.

B. Resistivity change observations (Univ., JMA, HD, GSI, NRCDP)

Crustal electrical resistivity observations are carried out applying geomagnetic and earth current observation techniques. The artificially applied electric current method and the specific resistivity meter are also used.

5) Observation of underground water and gas (GSJ, NRCDP, Univ.)

Underground water observations (water table, temperature, quality of

water and radon content observations) are recognized to be effective for detecting precursors. Underground gases are being monitored.

6) Research and technique development for prediction over the Tokyo Metropolitan Area and other urban areas

We are facing strong social demands for practical earthquake prediction over great urban areas, especially the Tokyo Metropolitan Area. At the same time, we are facing great difficulties in observations because of urban noises. Development of special techniques is highly desired.

3. Promotion of research into the elucidation of the earthquake occurrence mechanism

A successful approach to earthquake prediction with high reliability depends largely on elucidation of the series of processes that lend to the earthquake occurrence, especially of the complicated precursory phenomena taking place immediately before it. Basic studies are very important and should be promoted positively along with observations and research for long-term and short-term prediction.

Research consists of two main subjects. One is the study for direct clues to prediction. The other is the study of the state of the crust and its change which will be a great help in understanding precursors. A rock-breaking experiment which permits observations of precursory phenomena under controlled physical and chemical conditions and synthetic observations and experiments in test fields are included in the former subject. The latter one includes accurate measurements of crustal stress, detailed investigation of crustal structure, and measurement of seismic wave velocity.

1) Research to develop an understanding of the mechanism of precursors

A. Rock-breaking experiments (Univ., GSJ, NRCDP)

Explanation of the physical mechanism of earthquake precursors is to be

based on rock-breaking experiments which clarify the breaking process of rocks, especially various changes preceding the main rupture.

B. Synthesize observations and experiments in test fields (Univ., NRCDP, JMA)

Observations in the Yamasaki fault area and in the southwestern part of Ibaraki Prefecture are conducted in order to accumulate precursor examples and analyse them.

2) Research which serves to better understand the mechanism of precursors

A. Crustal stress measurements (Univ., NRCDP, GSJ)

Measurement of crustal stress is one of the fundamental subjects needed in order to estimate the amount of accumulated energy. The stress is to be examined in relation to the tectonics and recent crustal activity around observation sites and laboratory experiments.

B. Investigation of crustal structure (Univ., GSJ, HD, NRCDP, JMA)

Explosion seismic experiments and gravity and magnetic surveys are conducted in order to make an accurate determination of crustal structure.

C. Observation of seismic wave velocity changes (GSJ, NRCDP)

Reexamination of observational results so far obtained and observations with higher precision are carried out.

4. Intensification of earthquake prediction systems

For practical application of earthquake prediction, more synthetic and efficient systems are also to be established. In this respect, it is desired to intensify data processing systems, real-time monitoring systems and the organizations concerned. One should note that good results can be expected only if each organization fulfills its own proper function because earthquake prediction still largely depends upon future studies.

1) Intensification of data collecting and processing systems

The data processing system is to be completed so as to be able to collect and analyze a lot of data quickly and furnish them adequately to the EAC, the CCEP and other organizations which need them.

2) Intensification of real time monitoring systems

The prediction system for the Tokai earthquake should be completed including transmission of additional data as required other than those now telemetered. Also in the southern Kanto district, the data transmitting system is to be expanded.

3) Intensification of organizations concerned

4) Cultivation of researchers and specialists

5) Promotion of international cooperation

EARTHQUAKE PREDICTION MONITORING PROGRAM ALONG THE SAN ANDREAS FAULT

Mark D. Zoback
William L. Ellsworth

U. S. Geological Survey
Menlo Park, California 94025

Two major aspects of the earthquake prediction monitoring system are designed to provide real-time information on seismicity and crustal deformation along the San Andreas fault. This report highlights the current status and future directions of these parts of the Earthquake Prediction program.

Crustal Deformation

To supplement the relatively infrequent geodetic strain measurements being made along the San Andreas fault, a variety of continuously operating strain instruments are being used. The two primary instrument systems now being used are borehole dilatometers and creepmeters. Figures 1 and 2 show most of the currently operating dilatometers and creepmeters in California. Data from these instruments are now telemetered to Menlo Park at 10-minute intervals. Current plans call for increasing the dilatometer network two-fold in the next 2 years and gradually expanding the creepmeter network. A satellite telemetry system is now being installed which will make it possible to receive 10-minute data from the instruments without any use of telephone lines.

Other continuously operating strain sensitive instruments that are still being monitored include (1) shallow borehole tiltmeters, (2) surface strainmeters, and (3) magnetometers. However, relatively little effort is currently being expended on these instruments.

New instrument systems which are being developed include three-component borehole strainmeters, downhole tiltmeters, and ultrasensitive pore pressure monitors. A number of experiments have been conducted recently to test optimal sensitivity of dilatometer and pore pressure measurements. The tests show that sensitivities of 10^{-9}, or better, can be achieved in real-time by automatically correcting the data for responses to earth-tides and atmospheric pressure.

Our overall plan for fault zone monitoring calls for deployment of arrays of continuously monitoring downhole instruments to be co-located with a permanent two-color laser observatory. An example of this type of instrument array appears in Figure 3. We envision deploying similar arrays at frequent intervals along the major faults of the San Andreas system.

Seismicity Monitoring

An integrated and automated seismic monitoring system consisting of over 500 telemetered seismic stations now covers the entire length of the 100-km-long San Andreas system (Figure 4). Seismic monitoring for the southern half of the fault system is a cooperative effort by the California Institute of Technology and the U.S.G.S. in Pasadena, while the northern half is operated by the U.S.G.S. in Menlo Park.

At each center, dedicated on-line computer systems trigger storage of digital seismic traces whenever an earthquake occurs. Processing of these seismograms, including earthquake location and magnitude determination is typically completed within 24-48 hours. This provides a near real-time catalog of all earthquake activity and a seismogram data base for future analysis.

Real-time monitoring of activity is provided by alarm systems that automatically activate radio pagers, alerting duty seismologists that significant seismic activity is in process. In Menlo Park this system is fed by earthquake data provided by the real-time processing system which automatically times and locates all earthquakes in the region. A computer algorithm evaluates current seismic activity against pre-defined alarm criteria such as magnitude, location and event rate, and issues an alarm when thresholds are exceeded. This system can be easily reconfigured to use other alarm criteria, or to monitor specific regions with special alarm parameters.

When an alarm is issued, the duty seismologist can respond without coming to the office by logging into the computer from home, as all of the data are available on-line in real-time. Low-frequency data is also available on-line, which means that developments can be monitored by many scientists literally stationed throughout the country. This is particularly important for the issuance of short-term warnings, as the authority for making public statements resides with the Director of the U. S. Geological Survey in Reston, Virgina, and not at regional centers or field offices.

Although the monitoring capability of the existing seismic networks provides highly accurate information on an earthquake's location and magnitude within a few minutes of the event, its potential utility for monitoring and warning are just beginning to be explored. A new real-time processor system is currently being developed using loosely-coupled 32-bit microprocessors. This system is projected to have many times the processing power of the currently operating 8-bit processors, and is projected to eventually perform far more sophisticated and exhaustive

analysis of each earthquake than is currently possible. Prototype studies are also underway to evaluate the potential of the seismic network as a strong-motion early-warning system, based upon a real-time analysis of earthquake location, magnitude and projected ground motions.

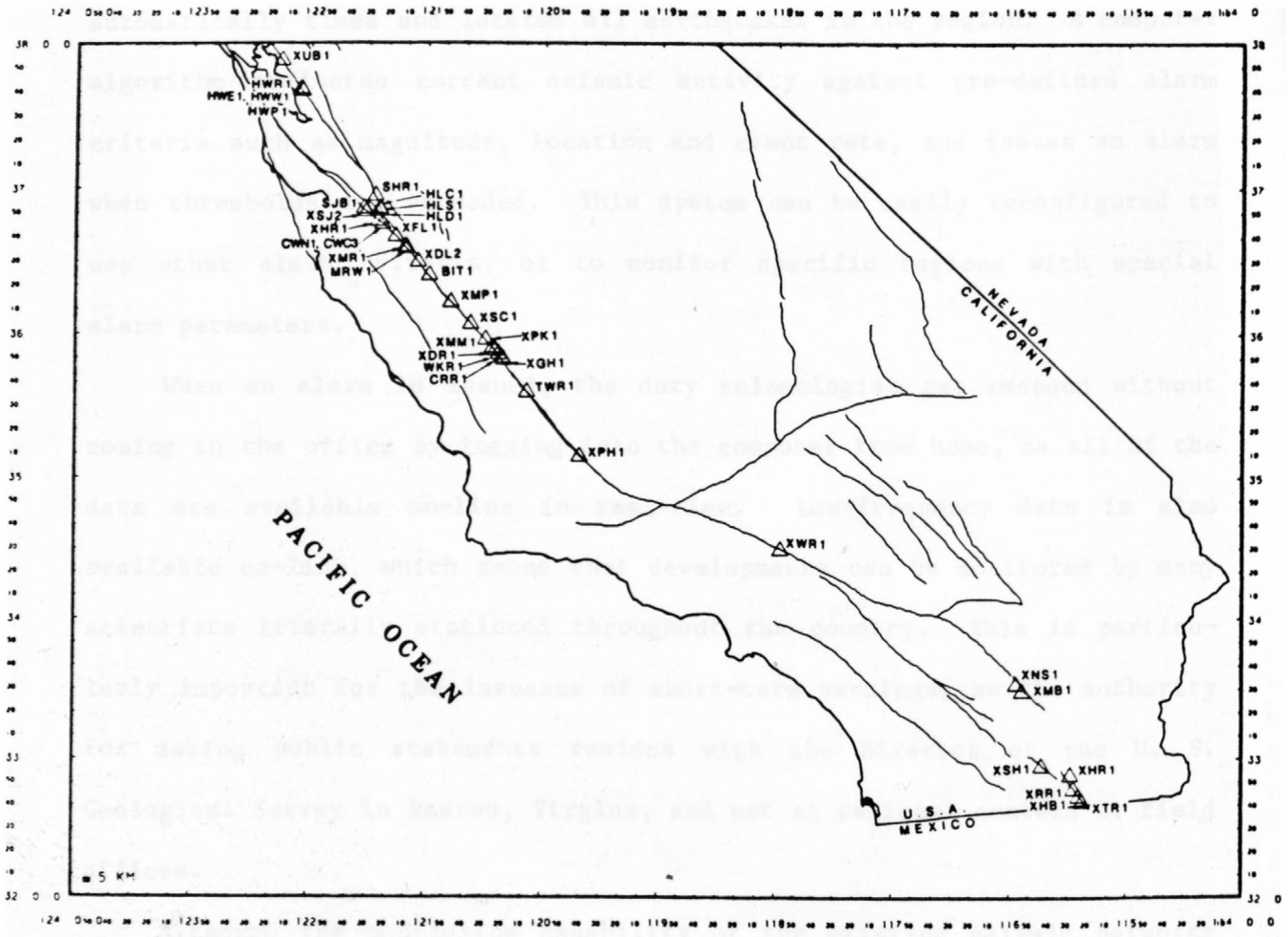

CREEPMETERS

FIGURE 1

Map showing the locations of creepmeters operated in central and southern California. The USGS operates 29 creepmeters in central California, USC operates 1 creepmeter in southern California and Caltech operates 7 creepmeters in southern California. The creepmeters are 10-20 meter long wires stretched through buried tubes crossing faults at angles of 22-45 degrees.

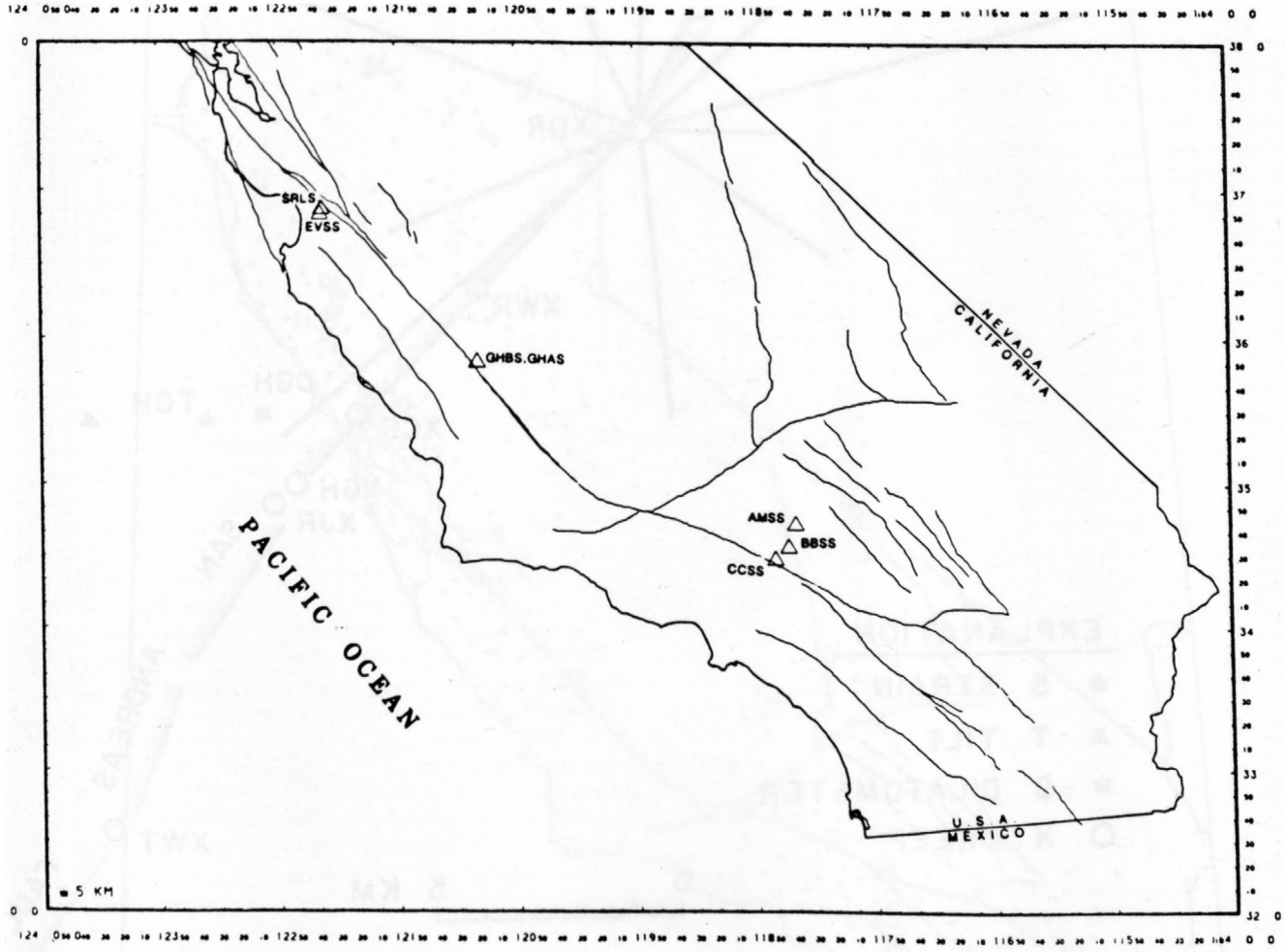

DILATOMETERS

FIGURE 2

Map showing Sacks-Evertson borehole volumetric strainmeters operated by the USGS in central and southern California. Two more instruments have been installed since this figure was prepared and three instruments are located at Pinon Flat observatory which are operated by Carnegie Institute.

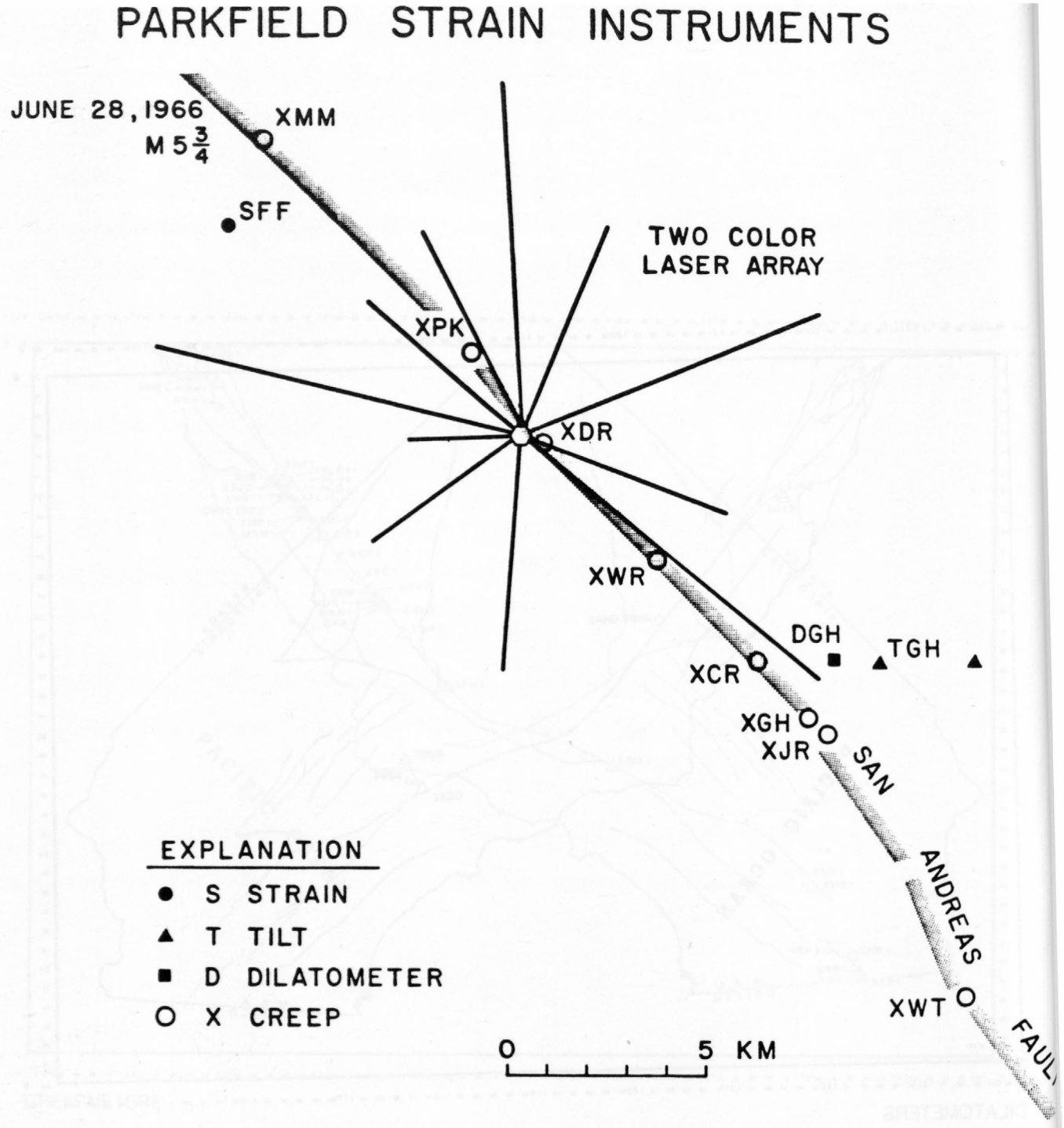

FIGURE 3

Crustal deformation array at Parkfield consisting of two-color laser observatory creepmeters, dilatometers, and surface strainmeters. Additional dilatometers will b installed near creepmeter XMM to be close to the expected hypocenter of the nex Parkfield earthquake.

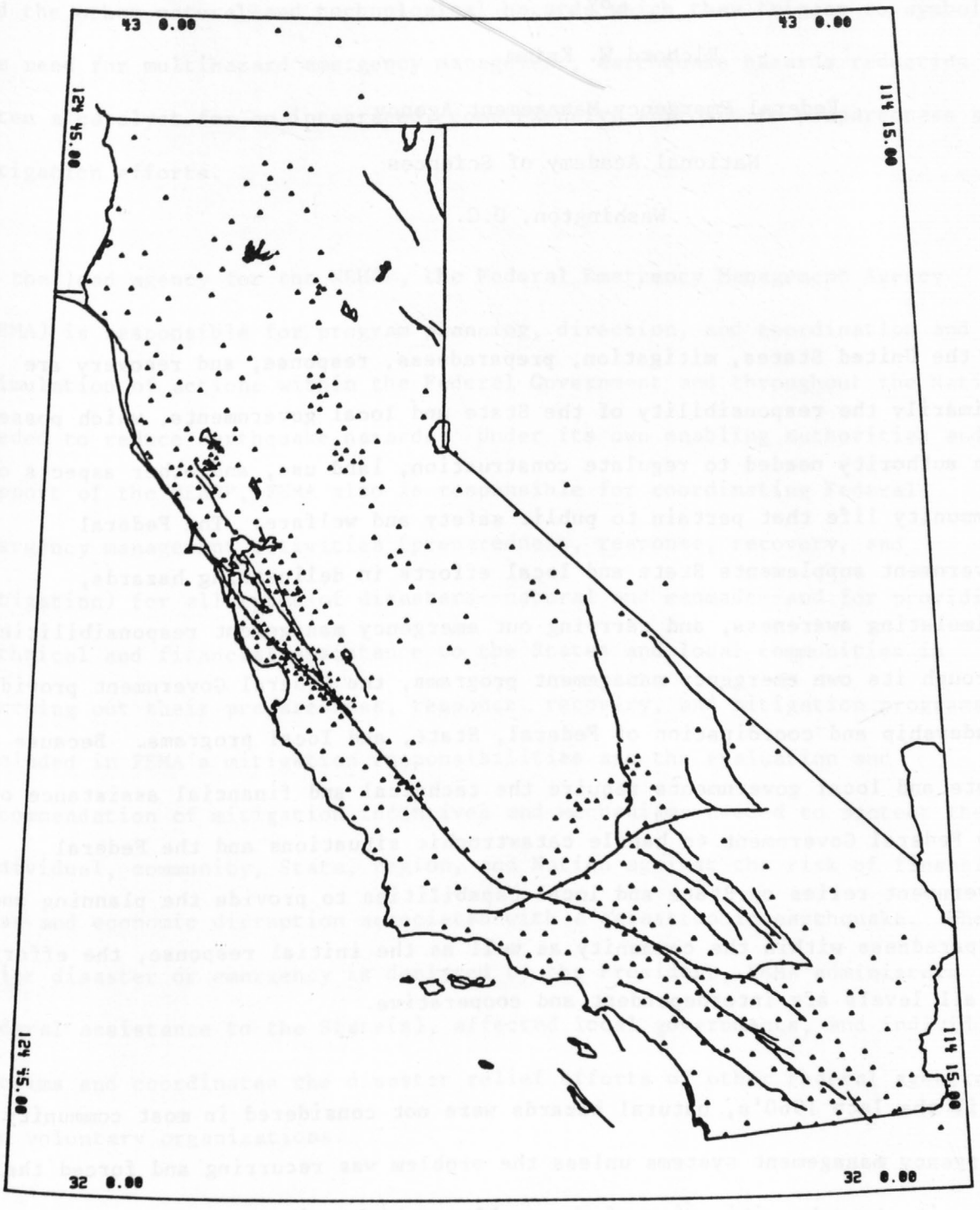

FIGURE 4

Map showing the locations telemetered seismic stations in California. The northern California network consists of 359 stations which telemeter data to Menlo Park. The southern California network consists of 192 stations operated jointly by the USGS and Caltech, and 27 stations operated by USC. The data for the USGS/Caltech stations are telemetered to the USGS office in Pasadena. Continuity of coverage is achieved by transmission of 8 stations from USC to Pasadena, 29 stations from Menlo Park to Pasadena and 20 stations from Pasadena to Menlo Park. Additional stations are shared between the University of Nevada, Reno and Menlo Park.

EARTHQUAKE PLANNING IN THE UNITED STATES

By

Richard W. Krimm

Federal Emergency Management Agency

National Academy of Sciences

Washington, D.C.

In the United States, mitigation, preparedness, response, and recovery are primarily the responsibility of the State and local governments, which possess the authority needed to regulate construction, land use, and other aspects of community life that pertain to public safety and welfare. The Federal Government supplements State and local efforts in delineating hazards, stimulating awareness, and carrying out emergency management responsibilities. Through its own emergency management programs, the Federal Government provides leadership and coordination of Federal, State, and local programs. Because State and local governments require the technical and financial assistance of the Federal Government to handle catastrophic situations and the Federal Government relies on State and local capabilities to provide the planning and preparedness within the community as well as the initial response, the efforts at all levels are interdependent and cooperative.

Until the late 1960's, natural hazards were not considered in most community emergency management systems unless the problem was recurring and forced the community to make mitigation of the problem a high priority. Since then, the initiation of several natural hazard programs at the Federal level has led to a significant increase in natural hazard preparedness and mitigation at the State and local levels. The National Earthquake Hazards Reduction Program (NEHRP)

has played a significant part in this change. Moreover, because earthquakes and the other natural and technological hazards which they trigger so symbolize the need for multihazard emergency management, earthquake hazards reduction is often a catalyst for an integrated, comprehensive approach to preparedness and mitigation efforts.

As the lead agency for the NEHRP, the Federal Emergency Management Agency (FEMA) is responsible for program planning, direction, and coordination and for stimulation of actions within the Federal Government and throughout the Nation needed to reduce earthquake hazards. Under its own enabling authorities and in support of the NEHRP, FEMA also is responsible for coordinating Federal emergency management activities (preparedness, response, recovery, and mitigation) for all types of disasters--natural and manmade--and for providing technical and financial assistance to the States and local communities in carrying out their preparedness, response, recovery, and mitigation programs. Included in FEMA's mitigation responsibilities are the evaluation and recommendation of mitigation incentives and mechanisms needed to protect the individual, community, State, region, and Nation against the risk of financial loss and economic disruption associated with a catastrophic earthquake. When a major disaster or emergency is declared by the President, FEMA administers Federal assistance to the State(s), affected local governments, and individual victims and coordinates the disaster relief efforts of other Federal agencies and voluntary organizations.

Based on a review of Federal emergency management programs, FEMA has embarked upon an improved method for implementing its programs--the Integrated Emergency Management System (IEMS). IEMS stresses an integrated approach to management

of emergencies across the full spectrum, including natural disasters, such as tornadoes, hurricanes, floods, and earthquakes; technological disasters, such as explosions, release of hazardous materials, accidents involving radiological materials, and possible nuclear powerplant accidents; resource shortages; and possible attack. It emphasizes the preparedness elements common to emergencies across the full spectrum, while at the same time recognizing elements unique to specific types of emergencies. IEMS therefore, provides for an integrated approach to preparedness for all emergencies, in line with FEMA's purpose and charter. The system builds on the foundation of existing emergency plans, systems, and capabilities and focuses on the integration of Federal preparedness programs, on improving coordination among the Federal agencies involved in the response to various emergencies, and on the linkage between Federal preparedness programs and State and local preparedness in such areas as resources management, continuity of government, and resource mobilization for major domestic and national security emergencies. By identifying opportunities to develop programs that support and complement each other, Federal, State, and local governments can more effectively and efficiently utilize available funds and resources.

The Earthquake Hazards Reduction Act of 1977, as amended, which established the NEHRP, stresses that natural and manmade hazards may not be independent of one another in any given disaster and that planning for and responding to different hazards have certain common elements. FEMA was directed to make maximum use of these commonalities and has developed several pilot studies to initiate a multihazard approach to preparedness and mitigation; for example, a dam safety, flood, earthquake project in Utah and a hurricane-earthquake project in Puerto Rico.

FEMA assistance to State and local earthquake preparedness programs focuses on the preparation of response plans that address the extraordinary problems caused by catastrophic earthquakes in high-risk, high-population areas. Projects are ongoing or planned in southern California (a five-county area around Los Angeles); San Diego (California); the San Francisco Bay Area; Puget Sound; Alaska (earthquake-tsunami hazards); Hawaii; Utah; a central United States regional project encompassing Illinois, Indiana, Kentucky, Tennessee, Missouri, Arkansas, and Mississippi; Charleston, South Carolina; upper New York State; and Boston, Massachusetts.

Each project follows a logical sequence of tasks. Initially, based on estimates of past and potential seismic activity in the area provided by the U.S. Geological Survey (USGS), vulnerability analyses (loss studies) are conducted to determine probable primary and secondary earthquake effects, estimates of possible casualties and injuries requiring hospitalization, and estimates of potential damage to critical/special facilities and lifelines needed for immediate response. Using the data from the analyses, FEMA assists State and local governments in determining the resources required for lifesaving and other emergency operations and to develop response plans. The plans include implementation measures, such as guidelines, procedures, and specific assignments. The final phase of the planning efforts consists of scheduled training exercises.

As Chair of the Interagency Coordination Committee's Subcommittee on Federal Earthquake Response Planning, FEMA coordinates the development of a national comprehensive plan for immediate Federal agency response to catastrophic

earthquake in any area of the country. A draft planning guide was issued in May 1983 and is serving as an interim operating plan for Federal response until the national plan is completed. Headquarters/regional forums are being held to discuss issues, problems, and next steps in this planning effort, which will be followed by exercises.

The Federal Interagency Committee on Seismic Safety in Construction and the non-Federal Building Seismic Safety Council are providing similar coordination and leadership in the mitigation aspects of earthquake hazards reduction. Although our preparedness efforts tend to focus primarily on removal of those at risk from the area of impending disaster and effective response measures to control the situation, locate and treat the injured, provide for the homeless, preserve and reestablish lifelines, and establish order, many lives can also be saved through another form of preparedness, which we distinguish as mitigation. Mitigation, lessening the impact of a hazard on property, reduces property losses and injury or loss of life resulting from falling debris and structural damage to residential or nonresidential structures, critical facilities, or lifelines. Unfortunately, mitigation at the State and local level is often the phase of emergency management most frequently viewed as a low priority item.

Part of FEMA's earthquake activities is directed toward public awareness in order to stimulate interest, cooperation, and participation in preparedness planning and implementation. During the past year, FEMA began discussions with USGS and the American Red Cross (ARC) concerning the development, review, and field-testing of informational materials. Educational materials developed around the country in both public and private sectors were reviewed. A series

of model materials designed for community use and adaptation were designed. This series includes brochures on home safety checklists, family earthquake drills, awareness posters, etc., which will be pilot-tested this year. Two portable exhibits have been developed for community outreach activities of regional, State, and local personnel. Work has begun on a cooperative production of television public service announcements with the ARC. FEMA also will be providing earthquake information along with information on other hazards in support of multihazard education programs, including a series of emergency information exchanges concerning the application of strategies at the state level; a grant to the Children's Television Workshop, producer of TV's Sesame Street for children; and a series of competitive challenge grants to stimulate local public information demonstration projects.

FEMA has established the framework for a community-oriented earthquake hazards awareness and education program to enhance the knowledge and understanding of various societal groups regarding earthquake phenomena and risks and to encourage adoption of hazard reduction measures by the community and individuals. During fiscal year 1983, program activities in this area focused on transferring information and experience gained from the Southern California Earthquake Preparedness Project (SCEPP) and incorporating information and recommendations provided by the societal research community regarding community outreach programs. Specifically, FEMA field-tested the first in a series of special-topic courses on earthquake hazards reduction (mitigation/preparedness) in the San Francisco Bay area. This course, entitled "Earthquake Hazard Mitigation for Utility Lifelines," provides city and county public works directors and engineers with information on how to assess the potential impact

of earthquakes on utility systems (gas, water, sewer, electric); lessen the effects of ground shaking on critical components of these systems; and develop procedures to hasten system recovery following an earthquake.

FEMA also awarded funds to support two pilot earthquake education centers in Memphis, Tennessee, and Charleston, South Carolina. These pilot centers--institutions which have been monitoring seismic networks and are viewed by the community, State and local emergency managers, the media, and the public as authoritative providers of earthquake information-- will provide a wide range of products and services to individuals, families, neighborhoods, schools, and businesses as well as offer opportunities for community members to participate in project development and implementation. These community-oriented education centers will recruit and train community outreach volunteers, modify existing products and develop new items to address seismic risk in the area, establish a speakers' bureau, maintain a collection of printed and audiovisual materials for volunteer and teacher use, and develop mechanisms for tracking product dissemination and evaluating the effectiveness of products and services.

SCEPP, one of the projects to which FEMA provides technical assistance and financial support, brought together some of the Nation's most prominent geologists and policy makers in the field of earthquake prediction for a three-day workshop in January. Local government and industry in southern California were represented as well as FEMA, the California Seismic Safety Commission and the Office of Emergency Services of California. This workshop led to recommended actions such as development of common criteria for making prediction decisions related to public policy; formal adoption of prediction

terminology; legislative changes to assure immunity of public entities for actions taken in the event of a prediction; development of a procedure for rescinding (or extending) a prediction; development of prediction response plans by all government entities in seismically hazardous areas; and inclusion of damage forecasting in a prediction system in a multigovernmental and multihazard context.

At present, U.S. preparedness planning at all levels is essentially response planning and for the most part will remain as such until an accurate prediction capability exists. Current preparedness activities include consideration of evacuation routes, shelters, supplies, medical facilities, etc.; however, the plans are prepared in the knowledge that the event will occur before the evacuation.

An accurate prediction capability, especially one providing a relatively short timeframe and a projected damage estimate, would enable all levels of government to broaden, refine, and implement their plans to meet the crisis rather that react to it. For example, communities could delay capital improvements, allocate additional funds, implement and test command and control procedures, establish special communications networks or protect existing ones, establish public information centers, shut off gas, store water and food, reroute transportation, divert supplies and shipments, and ultimately establish the temporary shelters and evacuate the endangered population.

For FEMA, an accurate prediction capability, ideally one providing a lead time of a least a year, would enable us to adjust program priorities to provide

greater technical and financial support to communities and State(s) affected. In and of itself, such a capability would enable greater integration of all preparedness programs and the application of capabilities used in preparing for other natural and manmade disasters.

The closest we have come to predicting a catastrophic earthquake in the United States is in California. No prediction has been issued; however, statements have been issued to the effect that a magnitude 8 earthquake has a 20-50% probability of occurring in southern California within the next 20 years. Both SCEPP's activities and statements of this kind, which can be taken as a warning to pending disaster, have increased earthquake hazards awareness in California. A recent poll by the Field Institute of California residents statewide indicates that 55% of the public believes that a major earthquake is extremely or very likely to occur in their area--up 14% since 1979. According to the survey, about three out of four California residents would take seriously a government scientist's prediction of an impending earthquake--the same as in 1979. Those who would take specific precautions if a major earthquake were predicted rose from 13% in 1979 to 32% in 1983. Most people (80%) would appreciate advance warning from scientists of a major, damaging earthquake. However, despite these increases, the degree to which the public worries about earthquakes, as indicated by the poll, shows less concern--55% do not worry at all, whereas 8% admit to worrying a lot.

The business community, with investments at stake, has been prompted by the statements of increasing probability to take action. SCEPP indicates that the southern California area is seeing a flurry of earthquake preparedness activity

within the private sector. In February, a recently formed group of downtown Los Angeles business and industry representatives involved in emergency preparedness discussed ways for companies to initiate seismic safety planning. It seems doubtful to me that without the perception of impending catastrophic losses, business would be evaluating its risk of loss and taking preparedness actions.

However, although we have made significant progress in public awareness and response planning throughout the United States and could easily incorporate preparedness activities prior to an event into current response plans, there remain many uncertainties associated with such preparedness activities in the event of a prediction, valid and invalid. These uncertainties, socioeconomic and legal, need to be addressed as we develop prediction capability in the United States. For example, when a community decides to take action, based upon a prediction, to clear and possible demolish unsafe buildings, the owners of those properties and the tenants relying on that space are adversely affected. Clearly, in any such actions by the community, legal issues arise. As indicated earlier, we still need to resolve legal issues related to liability for response actions; the legal ramifications of preparedness actions are areas of even greater dispute. Since no official predictions have been issued, we have never been in that situation before.

We are being conservative in the making of predictions partly because of the strong adverse legal and socioeconomic impacts of a false prediction--the other side of the coin. Throughout the process, scientists and planners must continue to work closely together to ensure that our capabilities develop in a deliberate, coordinated, and well orchestrated manner. Exchanges such as this

one are particularly beneficial to our planning efforts as well as to prediction efforts.

THE NIHONKAI-CHUBU EARTHQUAKE, 1983

Japan Meteorological Agency

Abstract

On 26 May 1983 at 1200 JST, a large earthquake of magnitude 7.7 occurred off Western Akita and Aomori prefectures, northern Honshu, Japan. The earthquake was felt in a broad area from Hokkaido to western Honshu. The maximum seismic intensity was 5 on the JMA scale in areas near the epicenter, such as Akita, Fukaura and Mutsu. The Japan Meteorological Agency (JMA) issued tsunami warnings, including a warning of the highest grade "great tsunami" 13-14 minutes after the occurrence of the earthquake.

Tsunamis occurred along the coastal areas of the Japan Sea for many hours. Around midnight the tsunamis began to subside and the tsunami warnings and tsunami advisories which had been issued for coastal areas were terminated from 2100 to 2330.

The maximum height of the tsunamis recorded with a tide gauge was 1.9 m above sea level at the port of Noshiro, Akita Prefecture. The maximum run-up height of the tsunami was 6.6 m according to field survey by JMA, though run-up heights higher than 10 m are described in other reports.

The loss of life and property due to the earthquake and the tsunamis was as follows:

1) 104 persons were killed.

2) 3049 houses were totally or partially destroyed.

3) 706 boats were lost.

The total amount of damage amounted to ¥ 150 billion ($700 million).

The disaster was characterized by the seriousness of the tsunamis that swept the coastal areas of eight prefectures producing 100 of the 104 deaths

that occurred during the earthquake. On the other hand, damage directly caused by the earthquake was mostly restricted to Akita and Aomori prefectures. Houses, buildings, highways, railroads and banks etc. were damaged by the earthquake. Liquefaction of ground occurred at many places, and made the damage more serious.

The occurrence of the more that 100 casualties due to an earthquake or a tsunami, is the greatest since the tsunami of the Chilean Earthquake in 1960, and the fourth highest in Japan since World War II. The issuance of the warning of a "great tsumani" was the second time in the history of the tsunami-warning service in JMA which started in 1949. The only previous issuance was the warning for the Boso-Oki Earthquake in 1953.

The earthquake was named "the Nihonkai-Chubu Earthquake, 1983" (the middle Japan Sea Earthquake, 1983) by JMA.

Introduction

A large earthquake of magnitude 7.7 occurred to the west of northern Honshu, Japan, on 26 May 1983. The earthquake produced a great impact not only on the science of seismology but also on studies of the prevention or mitigation of disasters caused by earthquakes.

The Japan Meteorological Agency (JMA) issued tsunami warnings to vulnerable areas 13-14 minutes after the occurrence of the earthquake. Nonetheless, 100 of a total of 104 deaths were caused by the tsunami.

JMA is trying to do its best to mitigate future disasters caused by earthquakes and tsunamis with cooperation with other governmental organizations and universities.

This paper is a brief summary of the earthquake and related phenoma, as well as procedures taken by JMA at and after the occurrence of the earthquake.

A complete report is given in the "Report on the Nihonkai-Chubu

Earthquake" (Technical Report of the Japan Meteorological Agency No. 106, 1984).

Focal Parameters

Focal parameters of the Nihonkai-Chubu Earthquake determined by JMA are as follows:

origin time	$11^h59^m57.5^s$	26 May 1983 (JST)
eipcenter	139° 04.6' E	40° 21.4' N
focal depth	14 km	
magnitude	7.7	

Seismic Intensity Distribution

The maximum seismic intensity was 5 on the JMA scale at Akita, Fukaura and Mutsu JMA stations. The most distant station where tremors were felt was Yonago Station, located 743 km from the epicenter. This distance is slightly shorter than the average felt distance for earthquakes of magnitude 7.7. On the other hand, the area of seismic intensity 4 or over is nominal. The pattern of seismic intensity distribution shows concentric circles in north-eastern Japan, while it is elongated to the west in the central and western Japan. The distribution pattern of the maximum amplitudes from strong-motion seismographs also shows westward elongation along the Japanese Islands (See Fig. 1).

Foreshock Activity

Though foreshock activity of the earthquake was not high, three foreshocks were located by JMA near the epicenter of the main shock. The largest foreshock has a magnitude of 5.0 and occurred at 2249 on 14 May. The other two shocks had magnitudes of 2.4 and 2.3 and occurred at 0452 and 2314 on 22 May, respectively. The Tohoku and Hirosaki University seismic networks for detecting microseismicity determined hypocenters of several tens of foreshocks.

Aftershock Activity

From 26 May to the end of September, 313 earthquake aftershocks occurred. The largest aftershock occurred on 21 June at the northern end of the aftershock area. It had a seismic intensity of 4 on the JMA scale and was observed at stations at Fukaura, Aomori, Esashi and Mori of JMA.

The decreasing rate of aftershock frequency can be expressed with the modified Omori's formula (Utsu, 1961) (See Fig. 2):

$$N = A (t + c)^{-p}$$

with p = 1.1. This means that the decrease of aftershocks is normal.

The hypocenters of 745 aftershocks from 26 May to 30 September were determined. The aftershock area covered about 180 km in the N-S direction and about 50 km in the E-W direction and formed an elongated "S"-shape distribution along the line of the 3,000 m isobath (See Fig. 3).

The sequence of occurrence of aftershocks revealed the following features:

1) Several large aftershocks occurred in places where a seismicity gap had formed in the aftershock area.
2) The secondary aftershock area of the largest aftershock formed in the area adjacent to the northern end of the aftershock area of the main shock.
3) A group of earthquakes which can be considered to be aftershocks in an indirect sense occurred west off the Oga Peninsula.

The aftershock area covered about 9×10^3 km^2. The area is a little larger than the one expected for a main shock of magnitude 7.7 according to the Utsu-Seki's formula (Utsu, 1961):

$$\log S = 1.02 M - 4.0$$

where M is the magnitude of the main shock, and S is the aftershock area expressed in km^2. It was found, however, that the aftershock area (less 2 x

10^3 km^2 which was the secondary aftershock area of the largest aftershock) was of a size expected for the magnitude of the main shock, according to above formula.

The Gutenberg-Richter statistical formula on the magnitude-frequency relation (Richter, 1958):

$$\log N = a - b M$$

where N is numbers of shocks of magnitudes between M and M + dM was applied to 368 aftershocks larger than or equal to M 3.9. The b value obtained was 1.0, which is normal for the seismicity for the Japanese Islands.

The precise determination of hypocenters of aftershocks was determined by means of the station correction method. The distribution of 277 relocated hypocenters of aftershocks suggests that a fracture due to the main shock was produced along the plane inclining to the east.

Focal Process

On the basis of the analysis of Japanese and foreign seismograms, it was found that the main shock was a multiple shock consisting of three events, a pre-event, main event 1, and main event 2.

The pre-event and the main event 1 have a reverse fault focal mechanism with compression in an E-W direction. The focal mechanism of the main event 2 has not been determined (See Fig. 4a and 4b).

A source model to explain the data of long-period body waves has been derived. The rise time was estimated to be about four to five seconds. The seismic moment of the pre-event was found to be $2.0 - 3.0 \times 10^{26}$ dyne.cm. The combined moments of both the pre-event and the main event 1 which occurred three seconds after the former, was found to be 1.5×10^{27} dyne.cm. The total moment of the main shock which includes the moment of the main event 2 occurring 26 seconds after the main event 1, was found to be 3.5×10^{27}

dyne.cm. This value is less than half of the moment obtained from data from long-period surface waves. This result suggests the possibility that a considerable part of the fault ruptured very slowly.

A source model has been derived to explain near field features of strong-motion seismograph records. The pre-event is estimated to have been generated by fault rupture which propagated westward with a velocity of 2.5-3.0 km/sec, and a total dislocation of 5-6 meters. The main event 1 is estimated to have been generated by fault rupture which propagated both southward and northward from a point near the epicenter of the pre-event. Total dislocation was 5-6 meters along the southern part and 3-4 meters along the northern part of the fault.

It was found that the largest aftershock was also a multiple shock which consisted of three events; a pre-event, main event, and post-event. The pre-event has a reverse fault focal mechanism with east-west compression. The seismic moment of the pre-event, the main event and the post-event was found to be 0.15×10^{26}, 1.5×10^{26} and 0.4×10^{26} dyne.cm respectively (See Fig. 4c).

Analysis of Records of Borehole Dilatational Strainmeters

The strain records of the main shock obtained from 31 borehole dilatational strainmeters in the Tokai and in southern Kanto areas, have been analyzed from various view points (See Fig. 5).

Initial motions of records from the short period component of the strainmeters show contractions at most stations. This motion is consistent with the above-mentioned focal mechanism. Theoretical seismograms derived from the source model show remarkable similarity to actual seismograms. Relative sensitivity derived from the amplitude ratio of theoretical seismograms to real seismograms at each station is compatible with the

relative sensitivity derived from the long-period surface waves from distant earthquakes or from earth tides.

Co-seismic step-like changes have been observed in the records of the long period component of strainmeters at most stations. Theoretical residual strains have been calculated from the source model, and compared with observed ones, but the expected regularity cannot be found in quantities and polarities of the steps in records of strain meters at some points do not express motions directly produced from the source process, but express local ground deformations near the observation points.

Observations from the Array System* of the Seismological Observatory of JMA

Hypocenters of 220 aftershocks were determined by the array system of the Seismological Observatory at Matushiro, Nagano Prefecture. The distribution of epicenters, located by the array system, shows similiar patterns to the one obtained by routine observation by JMA mentioned above, but deviates slightly to the south (See Fig. 6).

* The array system consists of six seismometers at the vertices of a hexagon with a diameter of 20 km and one seismometer at the center of the hexagon. Signals from the seven seismometers are analyzed by a computer on a real-time basis, in the Seismological Observatory of JMA at Matsushiro.

Geomagnetic Data

Records of total magnetic force by proton magnetometers in Japan have been analyzed as follows:

1) Difference between Kakioka and 19 observation stations in Japan (monthly average, 1977-1983).
2) Difference between Mizusawa and Oga (monthly average, 1977-1983).
3) Difference between Mizusawa and Oga (daily average, 1983).

Geomagnetic changes which exceed 1 nT were not found before or after the earthquake.

Seismicity in the Past

Data on major earthquakes near the coast of the Japan Sea in northern Japan, such as locations, their aftershocks, damage, and tsunamis, are summarized in figures and tables. Focal mechanism solutions of 26 former major earthquakes in the area are also summarized. The solutions show reverse fault or strike-slip fault motion associated with compression in a NW-SE direction or E-W direction. Reverse faults are common in the sea area and strike slip faults are common in the land area. The focal mechanism solution of the main shock and that of the largest aftershock are compatible with motion of past earthquakes (See Fig. 7 and 8).

Tsunami

Tide records of 74 tide gauge stations belonging not only to JMA but also to other organizations have been studied. Tsunami waves in the Japanese Sea, Okhotsk Sea, and the Pacific Ocean have been detected in records of 63 tidal stations. Arrival times, maximum heights and other elements have been closely analyzed on the records. The first wave reached Fukaura at 1207, Oga at 1208, Ryotsu at 1248, Saigo at 1333, and Izuhara at 1524. As the first wave began to fall at eight of the tide gauge stations near the source, it began to rise

at distant stations. This phenomenon suggests that subsidence of the sea bottom occurred in the eastern half of the source area of the earthquake.

Periods of the waves are 5 to 15 minutes in most records. The tsunami waves continued to be recorded the following day at most stations, and were even detected two days after the earthquake. The long duration of the waves were due to multiple reflection off the coasts on either side of the Japan Sea.

The maximum recorded height for a tsunami in this earthquake was 194 centimeters at Noshiro Port Tidal Station (the gauge malfunctioned during the arrival of the second wave). The second highest was 127 centimeters at Ryotsu Station and the third was 124 centimeters at Iwanai Station (See Fig. 9).

The tsunami source area estimated from the reversal transmission chart, was about 150 km long in the N-S direction and about 90 km wide in the E-W direction. Comparison between the tsunami source area and aftershock area reveals that the tsunami source area was wider than the aftershock area in the E-W direction and that it extended further to the east. This result suggests that gradual crustal movement took place co-seismically in the area east of the aftershock area (See Fig. 10).

Tsunami waves caused by the largest aftershock were recorded at 59 tidal stations. The first wave rose simutaneously at all the stations. The maximum height of the recorded tsunamis was 42 cm at Yoshioka in Hokkaido.

(12) Field Survey

Local Meteorological Observatories and Weather Stations of JMA dispatched survey parties to the coastal areas on the Japan Sea on 26 May. The parties interviewed residents from many cities and towns of the area concerning the earthquake and tsunami, measured run-up heights, and registered damage from the earthquake and the tsunami.

Damage caused by the earthquake was restricted to Hokkaido, Aomori, and Akita prefectures. Liquefaction produced heavy damage to roads, banks, harbors, houses, and crop fields at many places in Akita and Aomori prefectures.

Damage caused by the tsunami occurred over a broad area of eight prefectures: Hokkaido, Aomori, Akita, Yamagata, Niigata, Ishikawa, Kyoto, and Shimane. The fishing industry suffered great damage: 255 boats were sunk, 451 boats were washed away, 1187 boats were damaged, and many fishing implements were washed away. Houses were destroyed or inundated, and crop fields were flooded by the tsunami. Damage was as serious in Shimane Prefecture, far from the source, as in Akita and Hokkaido Prefectures, near the source.

The run-up height of the tsunami was measured at 170 points on the Japan Sea. It was high in Hokkaido, Aomori, and Akita prefectures. The maximum height measured by the JMA survey parties was 6.6 meters at the town of Hachiryu-cho in Akita Prefecture. Run-up heights higher than 10 meters were reported by other surveyers (See Fig. 11).

(12) Tsunami Forecasting Services

Sendai District Meteorological Observatory issued a tsunami warning "Oo-tsunami (great tsunami)" at 1214, Sapporo District Meteorological Observatory issued a warning "Tsunami" at 1214, and JMA in Tokyo, issued a warning "Tsunami" at 1213, for respective areas in their charge. The warnings were transmitted through networks of the Nippon Telegraph and Telephone Public Corporation, police forces, and prefectural offices to municipal authorities of the areas on the Japan Sea. The Japan Broadcasting Corporation (NHK) broadcast the warnings nationally at 1219.

Tsunamis repeatedly inundated areas along the Japan Sea and then began to

weaken late at night. The tsunami forcasting centers (Sapporo, Sendai, Tokyo, Osaka) terminated the warnings and advisories between 1058 and 2330.

References

Japan Meteorological Agency 1984, Report on the Nihonkai-Chubu Earthquake, 1983: Technical Rep. JMA, No. 106

Richter, C.F., 1958, Elementary Seismology: W.H. Freeman & Co.

Utsu, T., 1961, A statistical study on the occurrence of aftershocks: Geophys. Mag. 30, p. 521-605.

Figure Captions

Fig. 1. Epicenter of the main shock and the distribution of seismic intensities (1-5) on the JMA scale and maximum amplitudes of strong-motion seismographs (mm).

Fig. 2. Record of aftershocks.

Fig. 3. Epicentral distribution of aftershocks.

Fig. 4. Focal mechanisms of the main shock and the largest aftershock.

a. focal mechanism of the pre-event of the main shock.

b. focal mechanism of the main event 1 of the main shock.

c. focal mechanism of the pre-event of the largest aftershock.

Fig. 5. Co-seismic step-like changes in the records of the long period component of bore-hole strainmeters.

Fig. 6. Distribution of the epicenters of the main shock and aftershocks determined by the array system of the Seismological Observatory, JMA.

Fig. 7. Distribution of the epicenters of earthquakes during the period from 1926 to 1982.

Fig. 8. Types of focal mechanisms and the direction of pressure axes of major earthquakes during the period from January of 1926 to June of 1983.

Fig. 9. Distribution of wave heights (in centimeters) of the tsunami recorded with tide gauges.

Fig. 10. Tsunami source area estimated by the method of reversal transmission chart. Epicenter distribution of aftershocks up to 2400 of 26 May is also shown.

Fig. 11. Distribution of run-up heights of the tsunami surveyed by JMA.

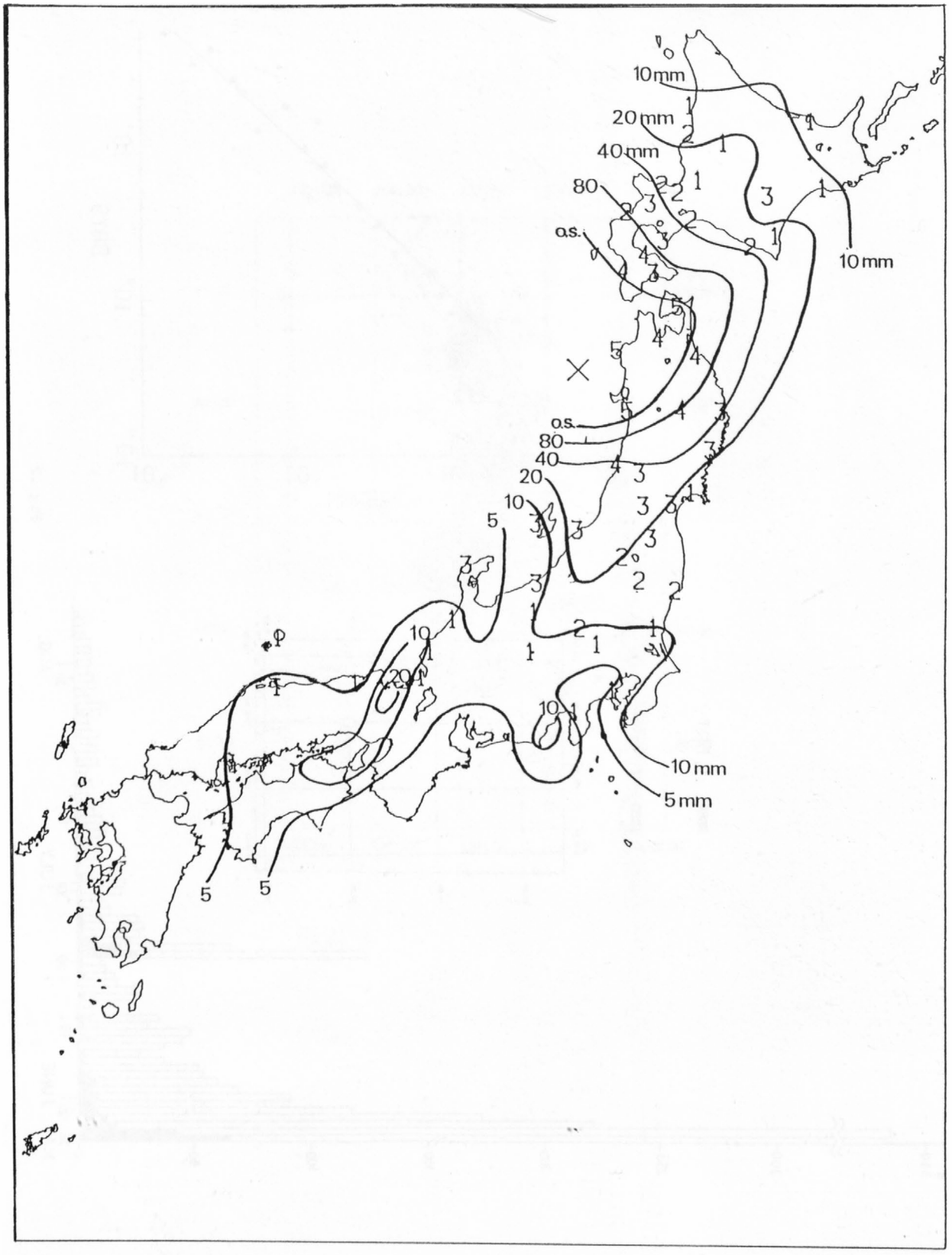

Fig. 1

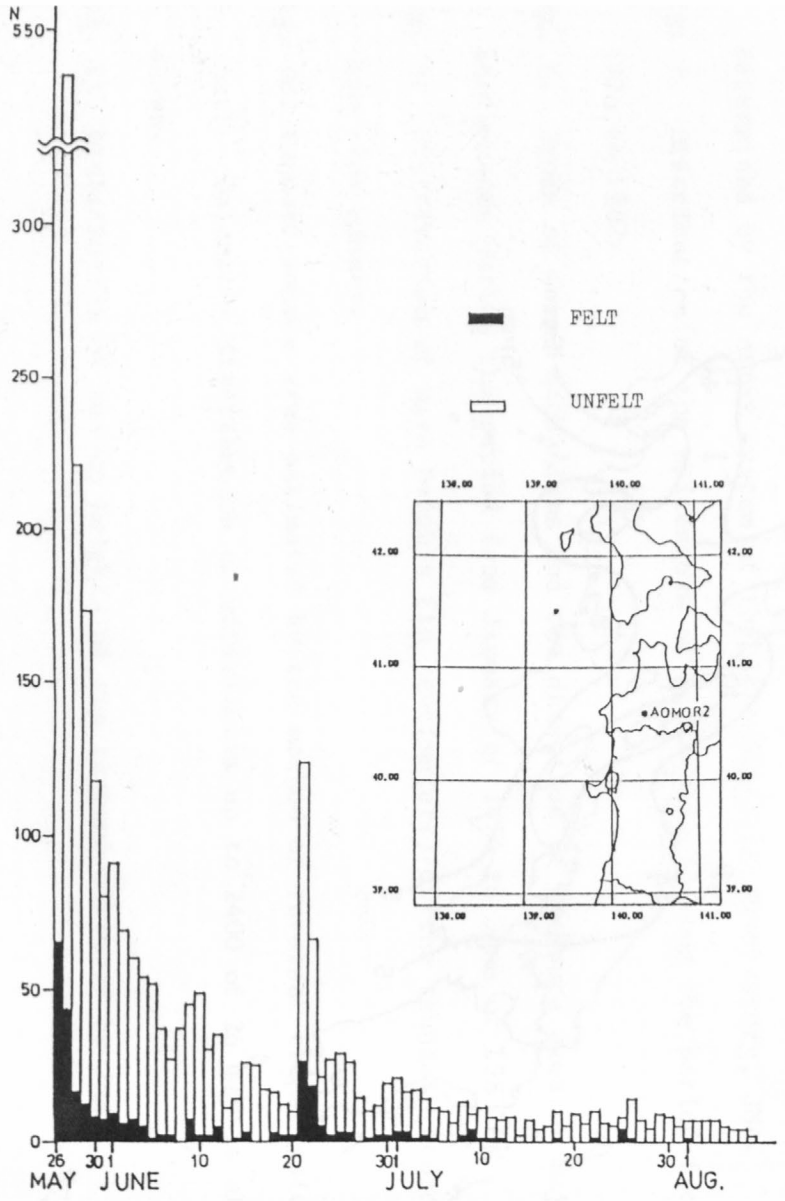
N
550
300
250
200
150
100
50
0
FELT
UNFELT
AOMOR2
26
30
1
10
20
30
1
10
20
30
1
MAY
JUNE
JULY
AUG.

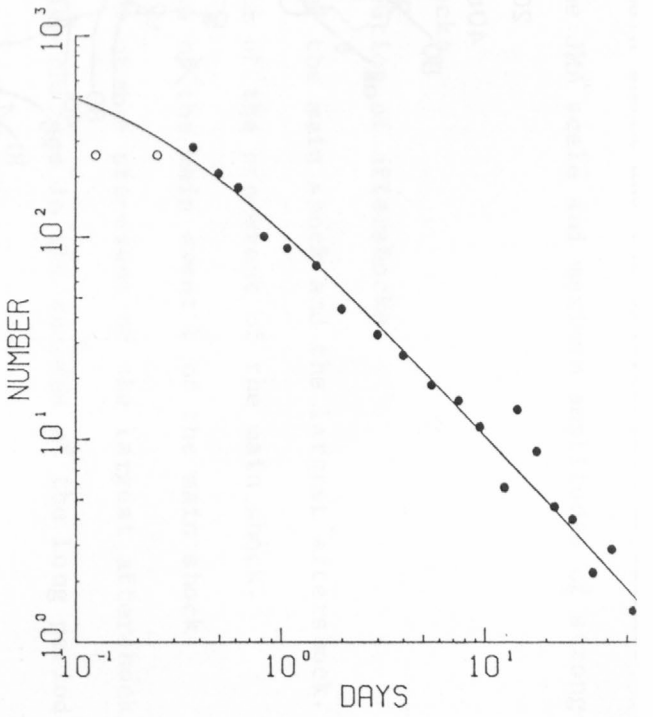
NUMBER
DAYS

Fig .2

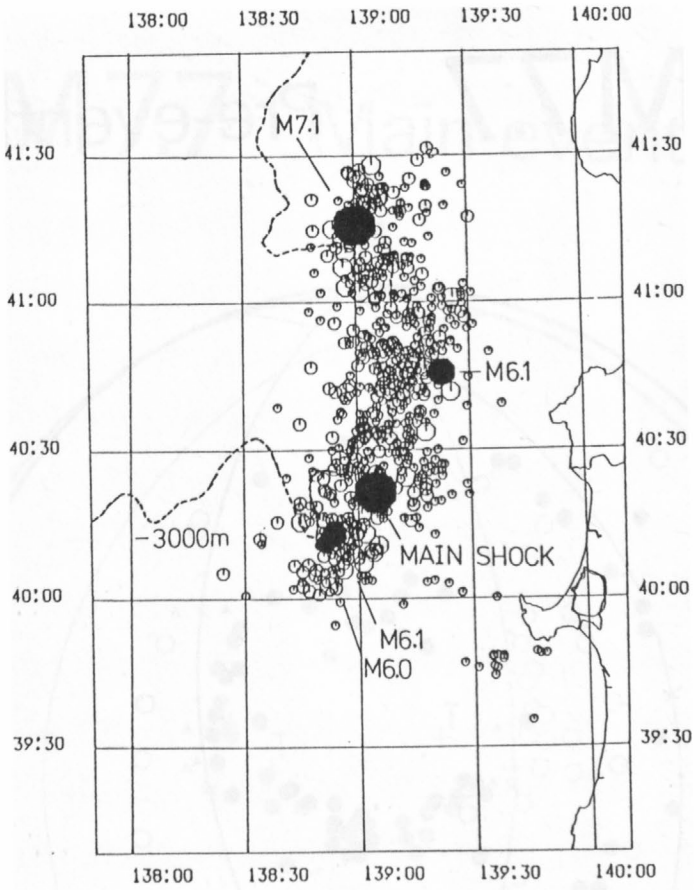
138:00
138:30
139:00
139:30
140:00
41:30
41:00
40:30
40:00
39:30
M7.1
M6.1
-3000m
MAIN SHOCK
M6.1
M6.0

Fig. 3

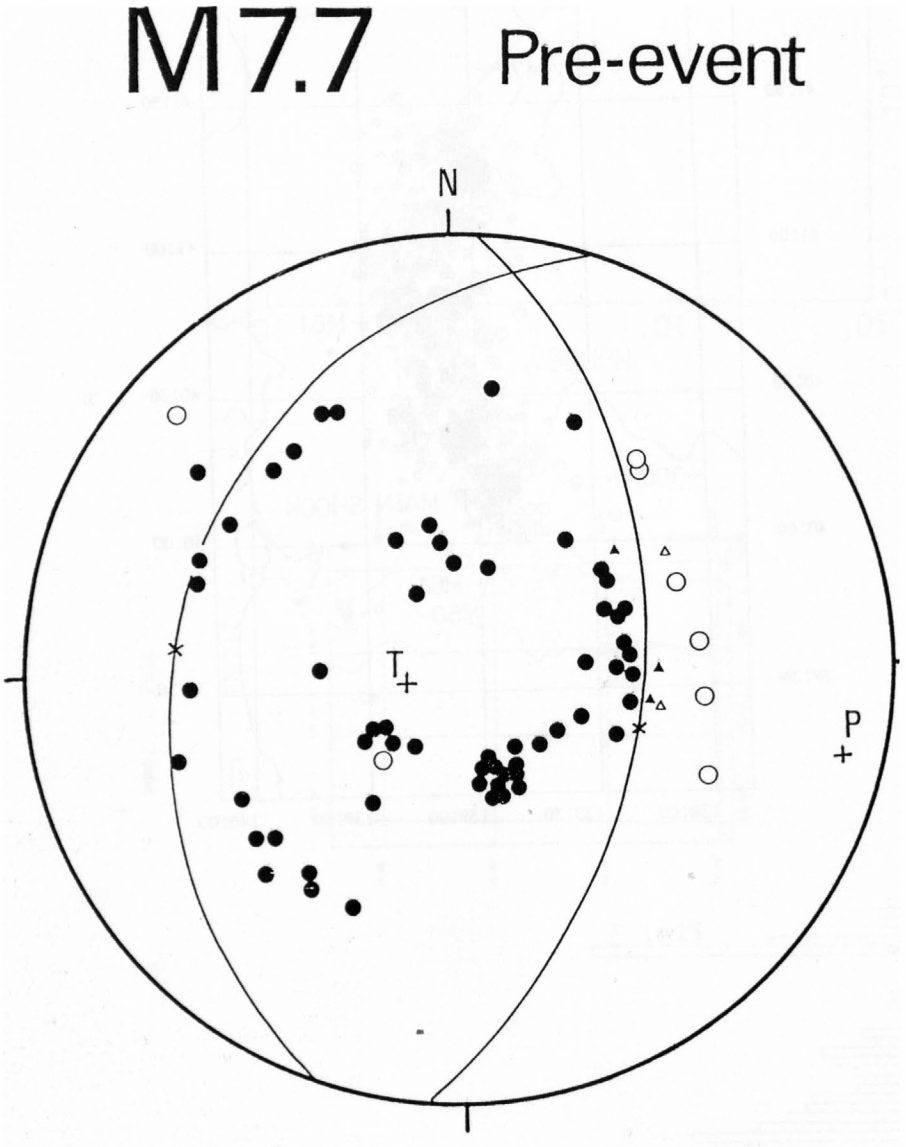

Fig. 4 a

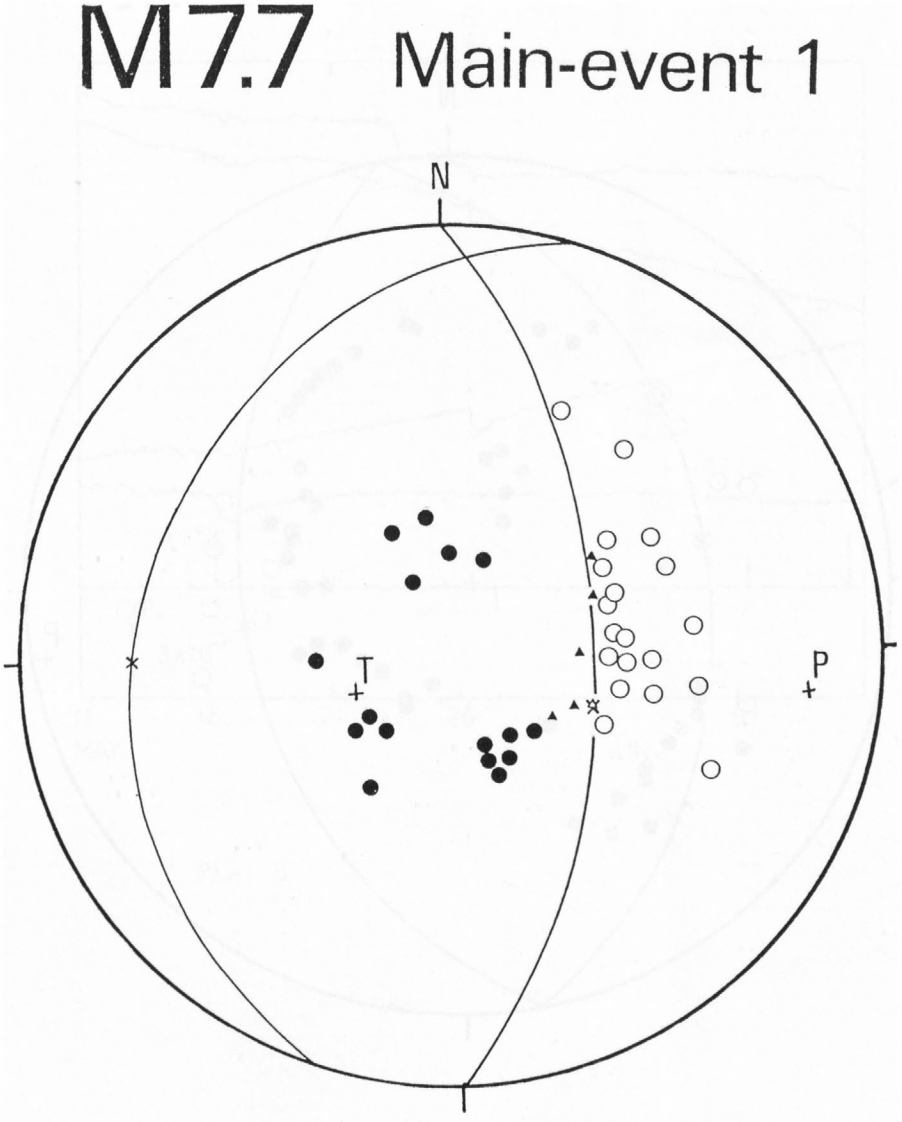

Fig. 4 b

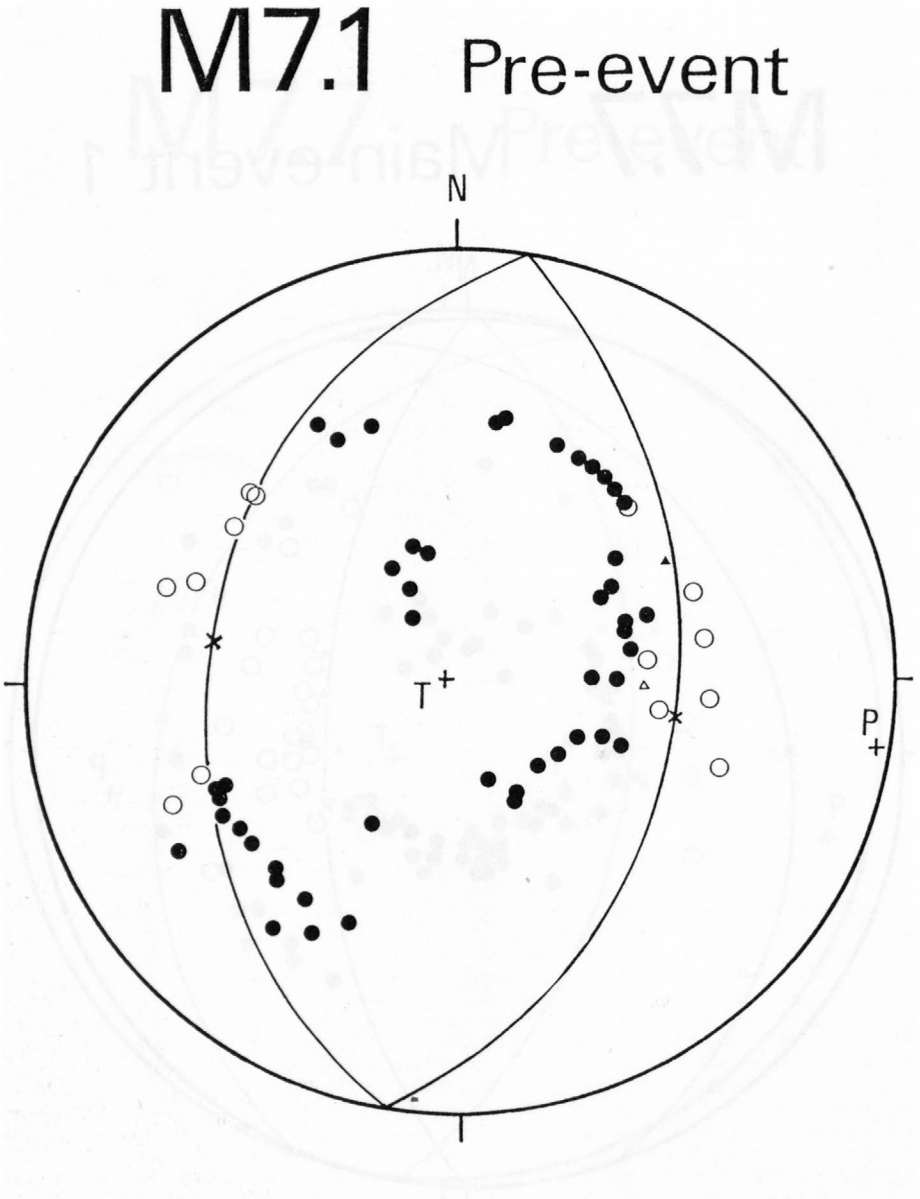

Fig. 4 c

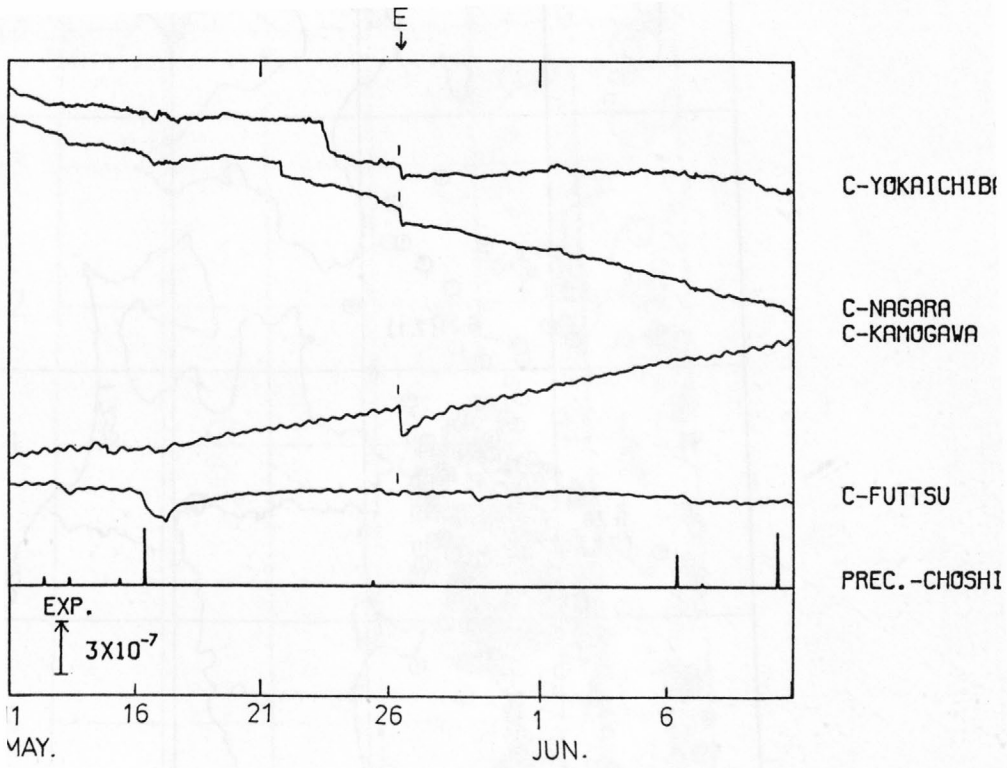
E
C-YOKAICHIBA
C-NAGARA
C-KAMOGAWA
C-FUTTSU
PREC.-CHOSHI
EXP.
3X10⁻⁷
1
16
21
26
1
6
MAY.
JUN.

Fig. 5

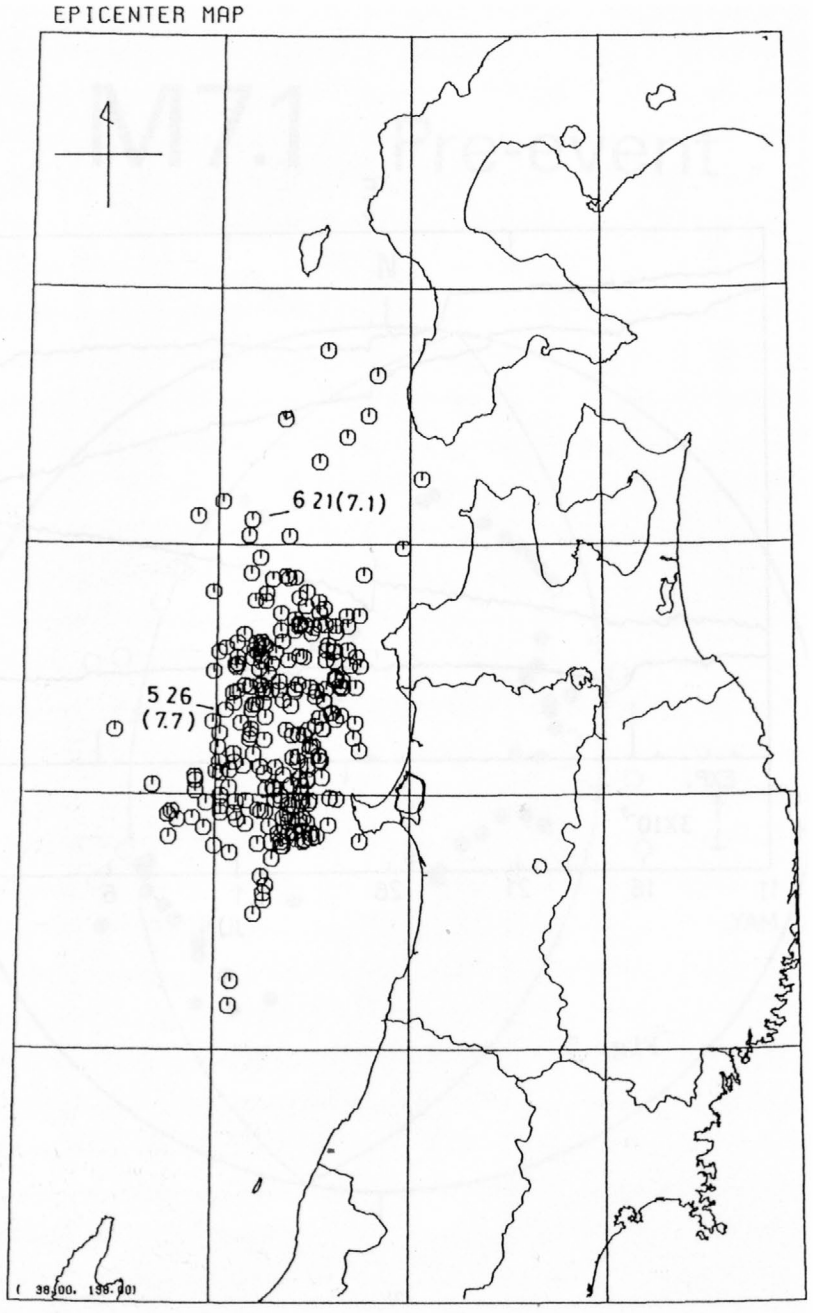

Fig. 6

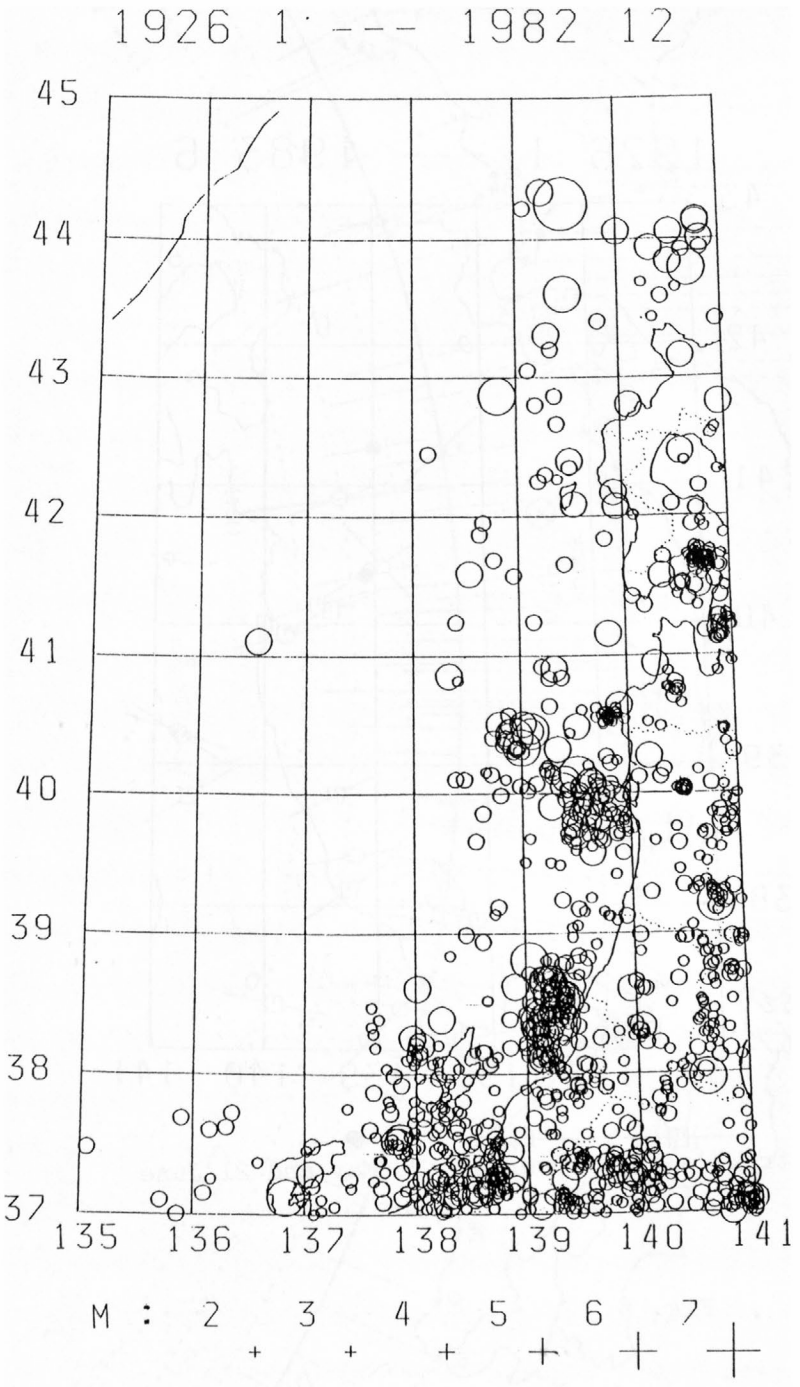
1926 1 --- 1982 12
45
44
43
42
41
40
39
38
37
135
136
137
138
139
140
141
M : 2 3 4 5 6 7

Fig. 7

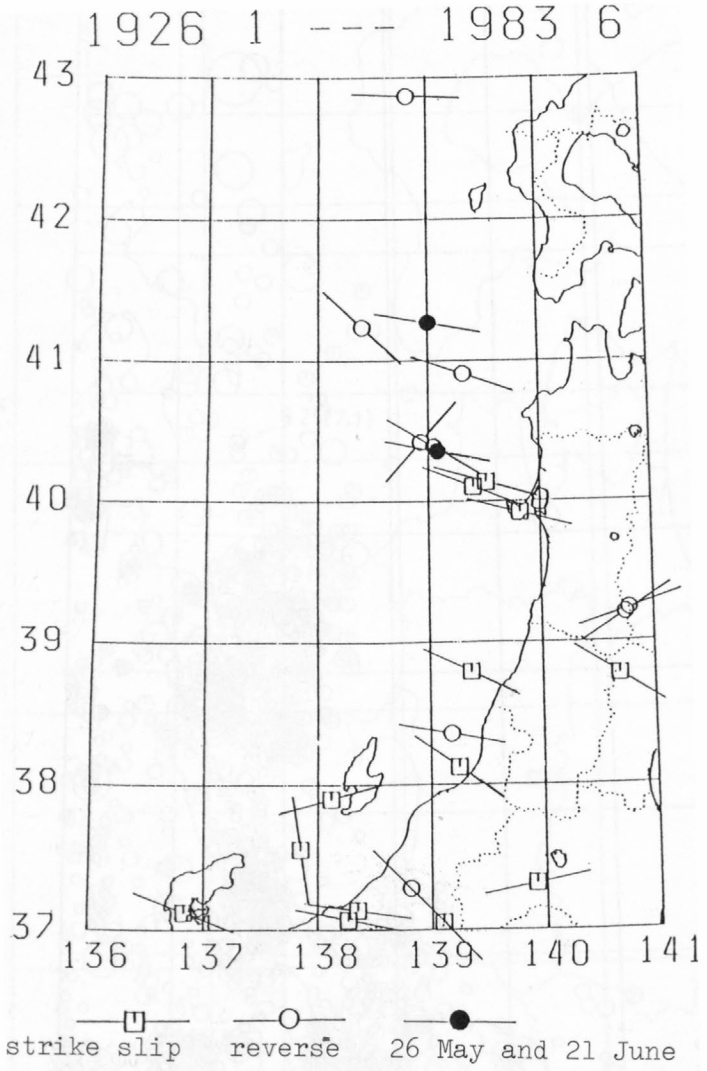
1926 1 --- 1983 6
43
42
41
40
39
38
37
136
137
138
139
140
141
strike slip
reverse
26 May and 21 June

Fig. 8

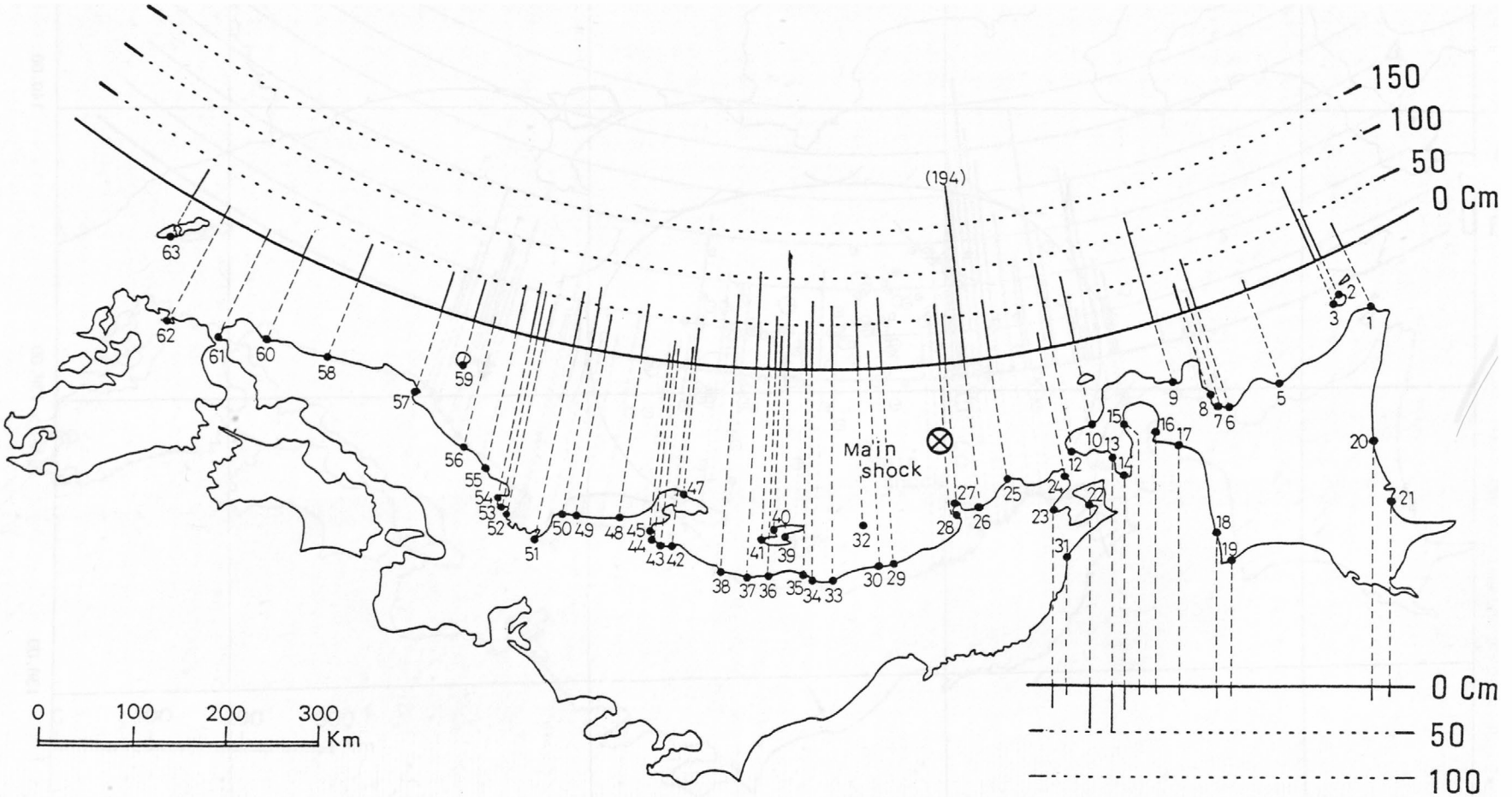

Fig. 9

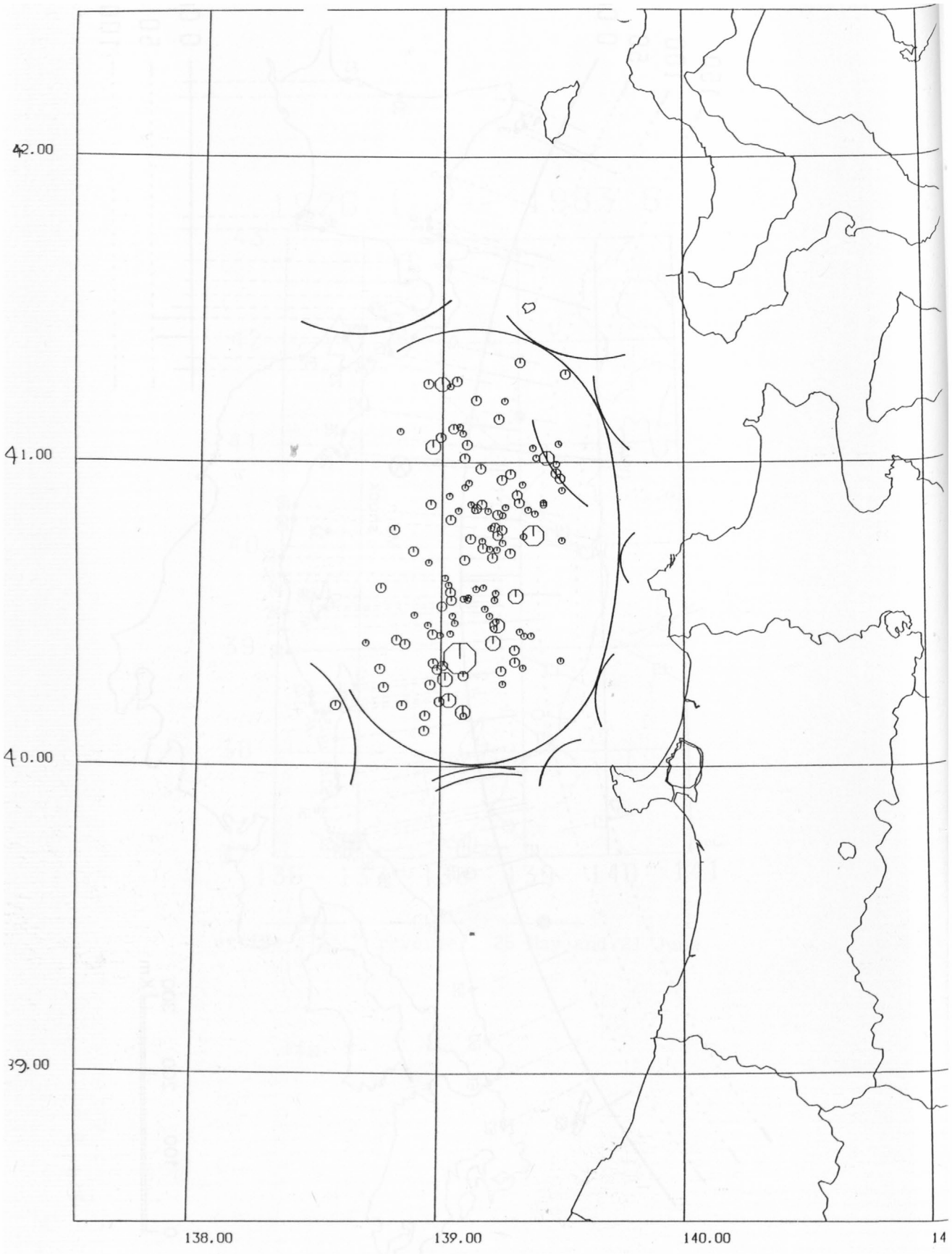

Fig. 10

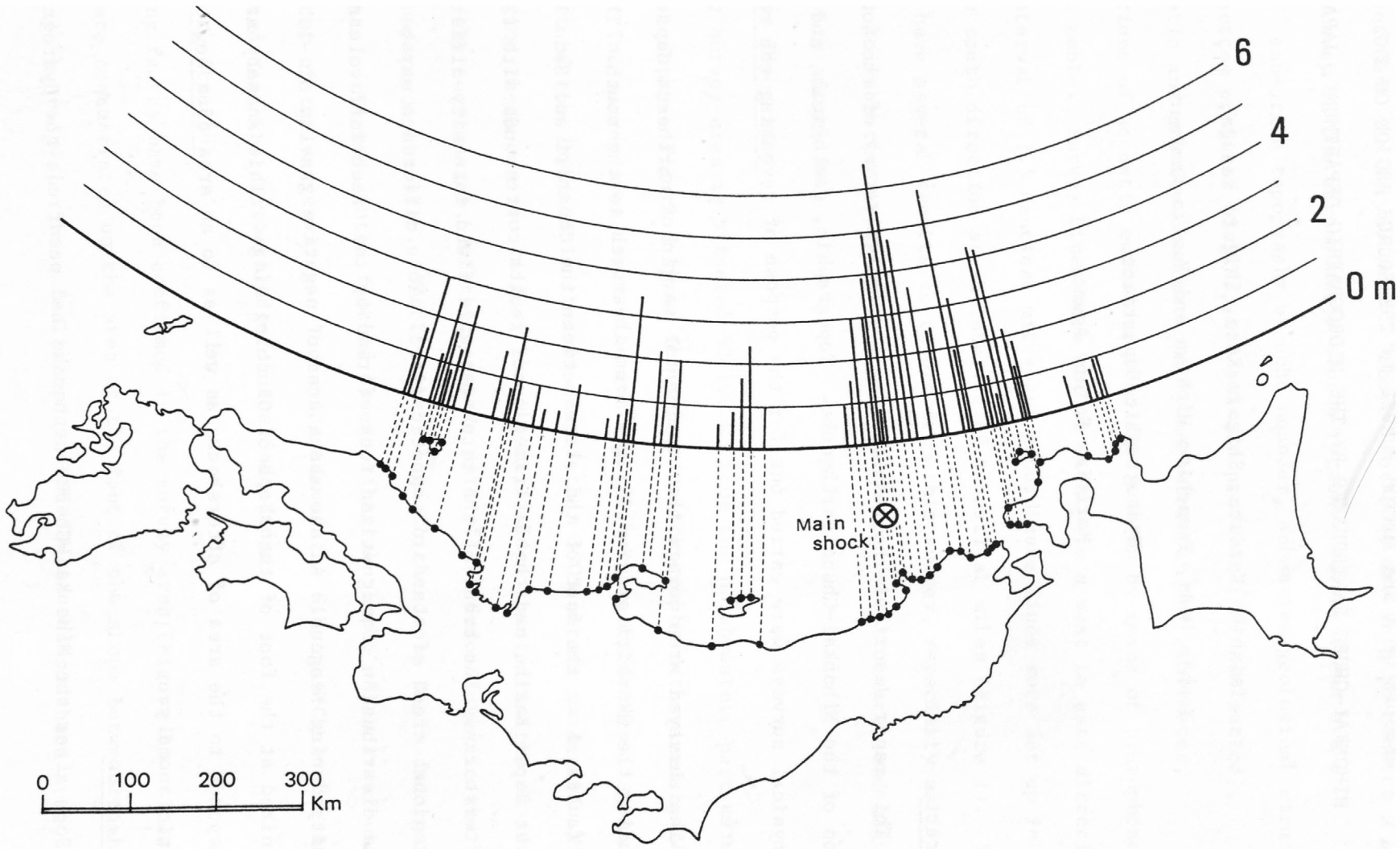

Fig. 11

RESULTS OF A SEA BOTTOM SURVEY IN THE SOURCE REGION OF THE NIHONKAI-CHUBU EARTHQUAKES BY THE HYDROGRAPHIC DEPARTMENT, JAPAN

Tadahiko Katsura, Shigeru Kato, Shigeru Kasuga,
Yoshio Ueda, Tsunehiro Hiraiwa and Yumiko Kamimura
Hydrographic Department
Maritime Safety Agency

Abstract

This paper describes the results of a sea bottom survey of the source region of the Nihonkai-Chubu earthquake. Topographic, geological, and geophysical surveys were carred out for the purpose of revealing the regional features.

The surveyed area covers the continental margin of northeast Japan including the Okushiri and Sado Ridges from the north to the south. There are many faults along the foot of the slope between the Okushiri and Sado Ridges and the Japan Basin, and the distribution of faults corresponds with the area of aftershocks. The trend of the total magnetic field intensity differs from the regional trend of standard magnetic field. This difference may be caused by the distribution of magnetized rocks formed by the Green Tuff volcanic activity during Neogene. An anomalous area of negative gravity of -10 mGal is recognized at the foot of the slope of Okushiri Ridge. This anomaly area corresponds to the area of aftershocks as well as to an area of a negative magnetic anomaly.

Introduction

Soon after the Nihonkai-Chubu earthquake had occurred, the Hydrographic

Department sent the survey vessel "Shoyo" for a 20 day trip to conduct a sea bottom survey in the earthquake's source region. Survey items are as follows: submarine topography by echo sounder, submarine geological structure by sub-bottom profiler (3.5kHz) and seismic profiler (air gun method), geomagnetic and gravity observations by magnetometer and gravimeter, observations of acoustic emissions from aftershocks by means of hydrophone streamer cable. Survey lines were set up mainly in a west to east direction at an interval of 1.5 nautical miles and subordinate lines were set up in a north to south direction at an interval of 8 nautical miles (Figure 1). The authors have several results to report from this survey, especially as it pertains to submarine topography, submarine geological structure, and magnetic and gravity anomalies.

Submarine Topography

The survey area is situated 50-100 km from the northwestern part of northeast Japan. Figure 2 shows the submarine topography determined by this survey. The survey area covers the continental margin of northeast Japan and that part of the Japan Basin that is deeper than 3000 meters in depth. Within this region there are two ridges, the Okushiri Ridge located in the eastern part of the survey area, and the northern part of the Sado Ridge, in the southern part of the area. Small valleys lead to the Japan Basin and small knolls are confirmed at the foot of the continental slope. They are found at the center of the survey area. The epicenter of the Nihonkai-Chubu earthquake is located near the northern edge of the Sado Ridge.

Geological Structure

Many faults have been confirmed in the survey area (Figure 3). These faults are concentrated on the area at the foot of the slope between the Japan Basin and two ridges. These faults extent NNE-SSW in the southern area, and

NW-SE in the northern area. Many of these faults have displacements down to the west. It is confirmed that grabens formed by pairs of faults. The length of these faults ranges from 10-20 kilometers to a maximum of 22 kilometers. The displacement along these faults is usually a few tens of meters. It seems that some of these faults, especially near the earthquake epicenter, have been displaced by the Nihonkai-Chubu earthquake occurrence. However, we cannot confirm this fact because of a lack of data. It is particularly interesting that the distribution of faults corresponds with the area of aftershocks.

Some projected events were recognized on the record of the sub-bottom profiler just above the fault scarp with the displacement of a few tens of meters (Figure 4). The cause of this record has been studied, but we do not have a conclusive explanation for it. The probable cause may be a peak of rocks, the spouting of gas or liquid, or other unexplained reasons.

A hypothesis has been proposed that the Nihonkai-Chubu earthquake was caused by movement of an east-dipping thrust fault which formed at an early stage of subduction of the Japan Sea plate beneath northeast Japan. We could not, however, find any evidence to resolve this problem.

Total Magnetic Intensity

Figure 5 shows the total magnetic intensity chart in the survey area. The regional magnetic field around the survey area is 48,500 - 49,000 nT in total force, and oriented in a NE-SW direction. However, the contour lines of Figure 5 are remarkably different from the regional distribution. The reason for this difference can be attributed to the complicated distribution of magnetized rocks which cause anomalies of short-wave length and which were formed by the Green Tuff volcanic activity during the Neogene. The amplitude of the anomalies ranges from about 200 - 300 nT. Some of these anomalies correspond to topographic features such as the Okushiri Ridge and others fall

at right angles to the strike of the topography. A negative anomaly is recognized in the area at the foot of the slope of the Okushiri Ridge which is the source region of the Nihonkai-Chubu earthquake. This anomaly suggests the existence of a basement depression beneath the sea bottom.

It has been ponted out that the magnetic anomaly of the Japan Basin is characterized by NE-SW or NNE-SSW directions. In addition, a negative anomaly of -250 nT is found at the margin of the survey area at latitude of 40° 41'N. Moreover, some anomalies with the same direction are recognized on the western slope of the Okushiri Ridge.

Free Air Gravity Anomaly

Figure 6 shows the free air gravity anomaly chart in the survey area. A positive gravity anomaly belt of 30-40 mGal is observed along the Okushiri Ridge in a north to south direction. In addition, a concave shape for the anomaly is recognized in the northeast margin of the survey area which is related to basement structure of the Nishi-Tsugaru Basin.

The negative anomaly area of -10 mGal exists at the latitude of 40° 50'N between the Japan Basin and the western slope of the Okushiri Ridge. This negative anomaly area is situated at the eastern side of the fault zone, and corresponds to the aftershock region as well as to the negative magnetic anomaly area.

The positive anomaly area of +20 to +30 mGal is recognized at the northern end of the Sado Ridge at the southwestern part of the survey area. The correspondence with the topography in this area is less distinct than in the case of the Okushiri Ridge area where relief and anomalies correspond well with each other.

Conclusion

1. Many faults were confirmed in the survey area.

2. Almost all of these faults are considered to have generated crustal movement during this earthquake. This movement caused tsunamis which produced serious damage in northeast Japan.

3. Several extraordinary hyperbola reflections were recorded on the profile of the sub-bottom profiler. They seem to be a out-of-plane reflection or a kind of emission from the sea bottom.

Caption of Figures

Figure 1 Track lines of the survey of the Nihonkai-Chubu earthquake.

Figure 2 Submarine topography in the survey area. Contour interval 100 meters.

Figure 3 Submarine geological structure of the survey area.

Figure 4 An example of projected events on the record of sub-bottom profiler.

Figure 5 Total magnetic intensity chart of the survey area. Contour interval 50 nT.

Figure 6 Free air gravity anomaly chart of the survey area. Contour interval 10 mGal.

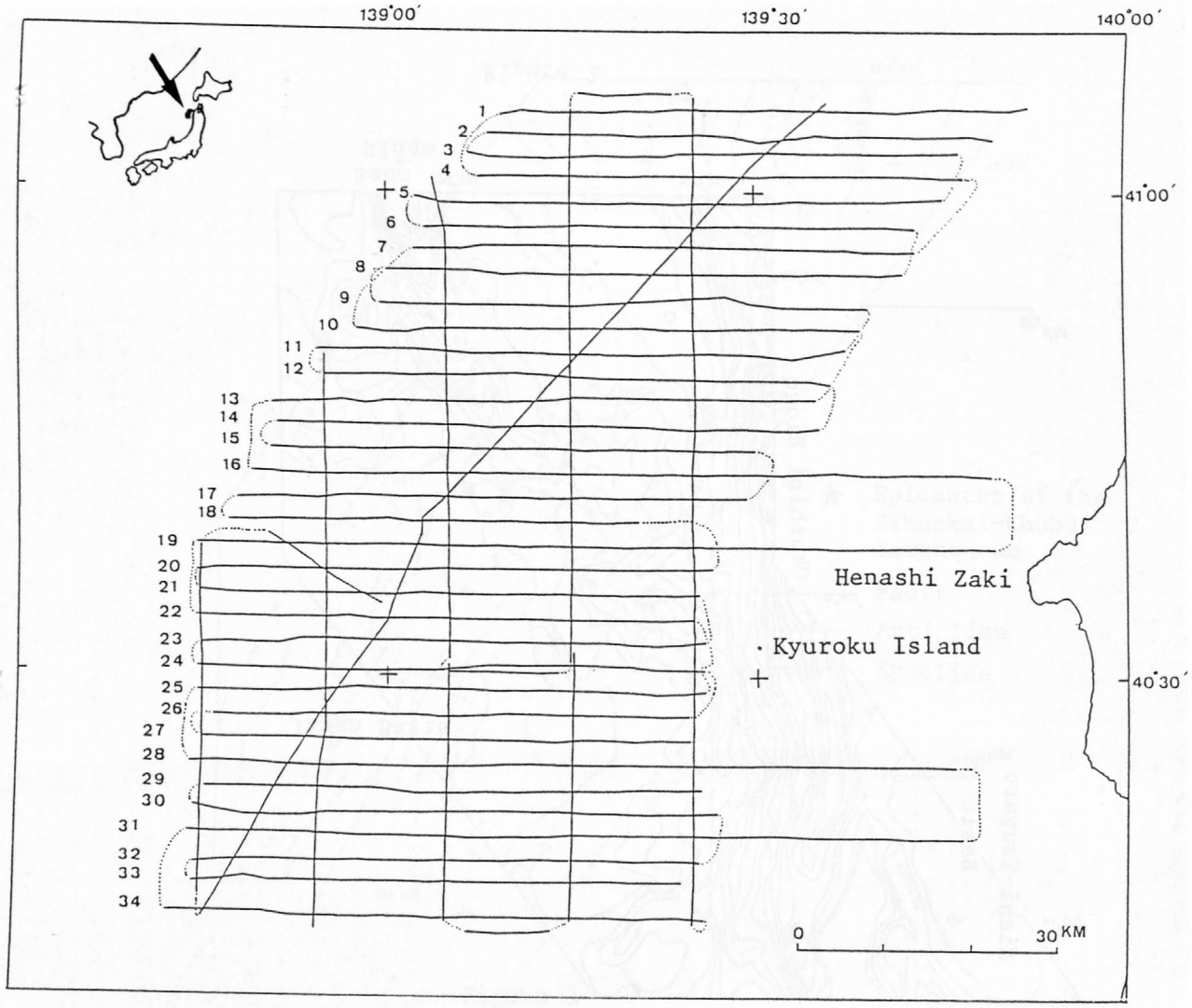
139°00′
139°30′
140°00′
41°00′
40°30′
1
2
3
4
5
6
7
8
9
10
11
12
13
14
15
16
17
18
19
20
21
22
23
24
25
26
27
28
29
30
31
32
33
34
Henashi Zaki
Kyuroku Island
0
30 KM

Figure 1

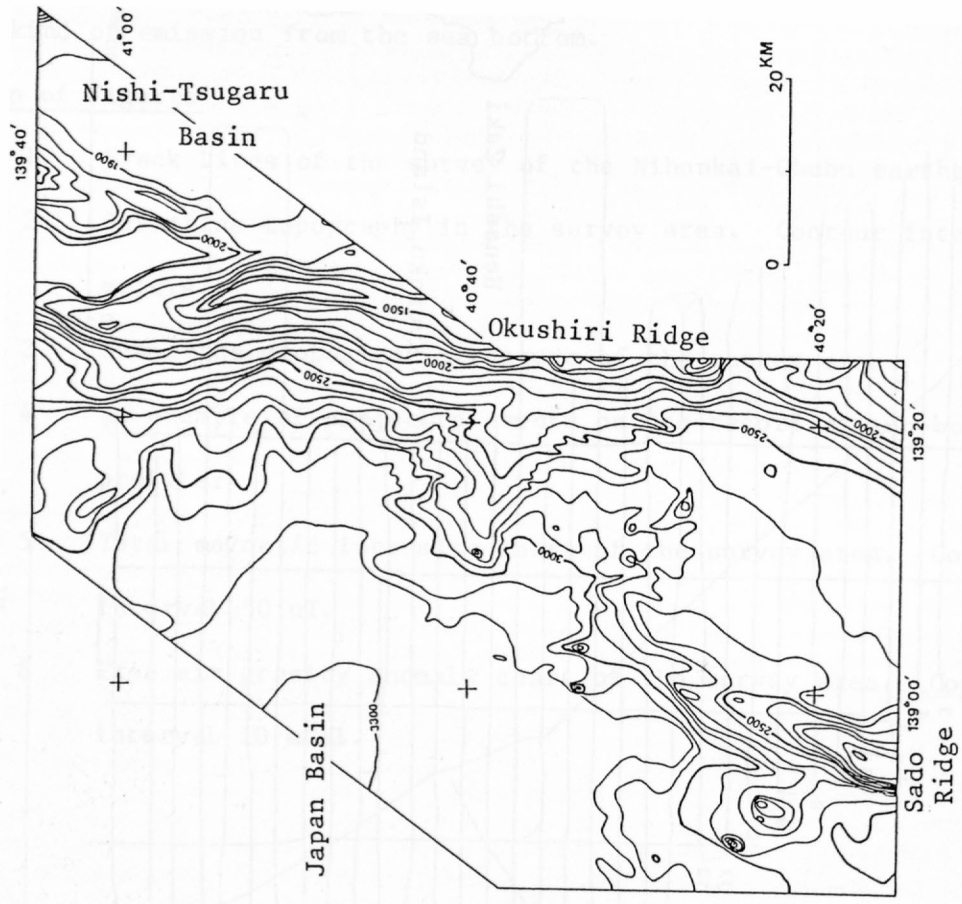
41°00′
Nishi-Tsugaru
Basin
139°40′
1900
2000
0
1500
40°40′
Okushiri Ridge
40°20′
20 KM
0
2000
2500
2000
139°20′
3000
2500
Japan Basin
3300
139°00′
Sado
Ridge

Figure 2

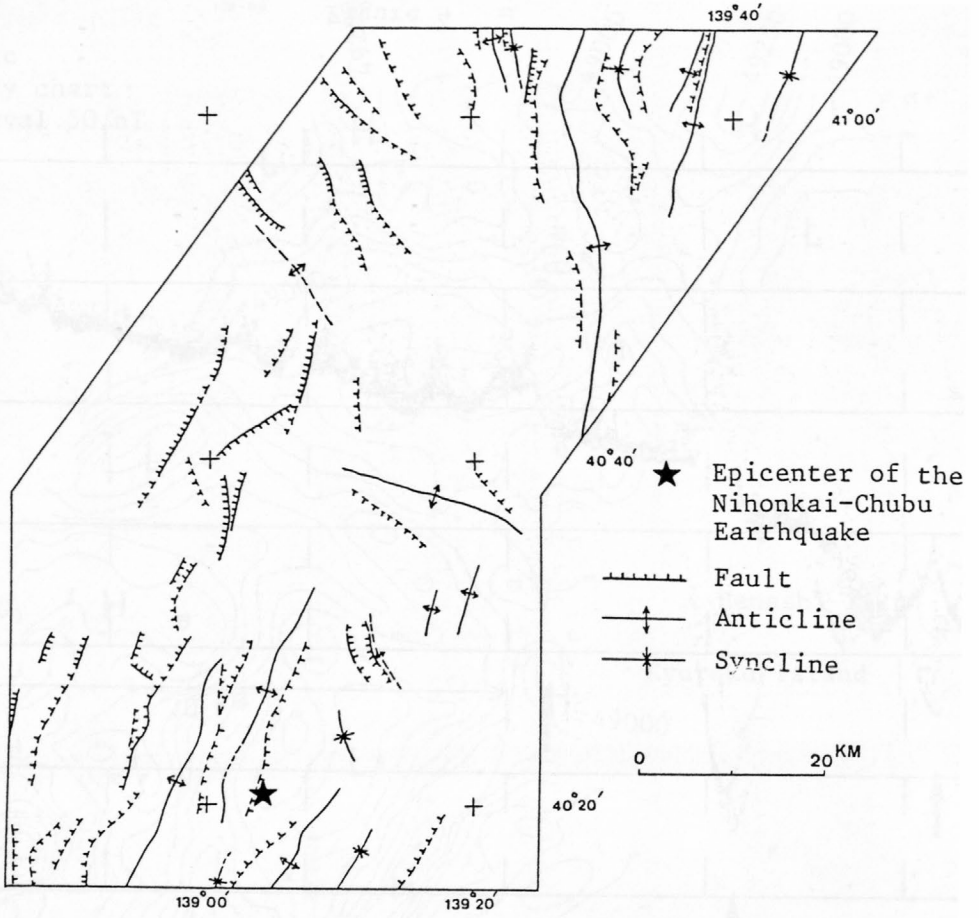
139°40′
41°00′
40°40′
40°20′
139°00′
139°20′
Epicenter of the Nihonkai-Chubu Earthquake
Fault
Anticline
Syncline
0
20 KM

Figure 3

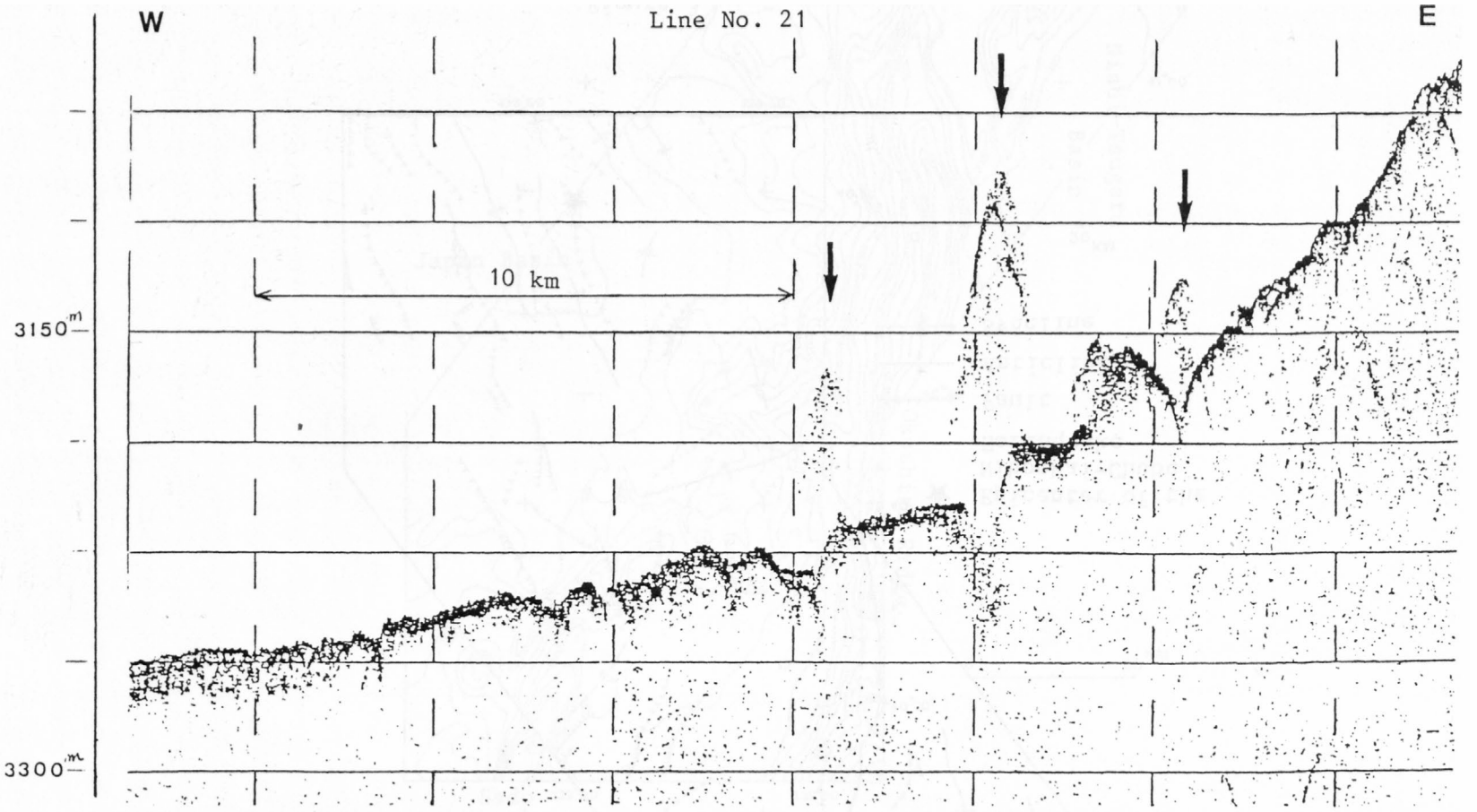

Figure 4

Total magnetic
intensity chart
Contour interval 50 nT
138°-40'
139°-00'
20'
140°-00'
41°-00'
40'
40°-20'
49250
49000
48500
48950
H
L
Henashi Zaki
Kyuroku Island

Figure 5

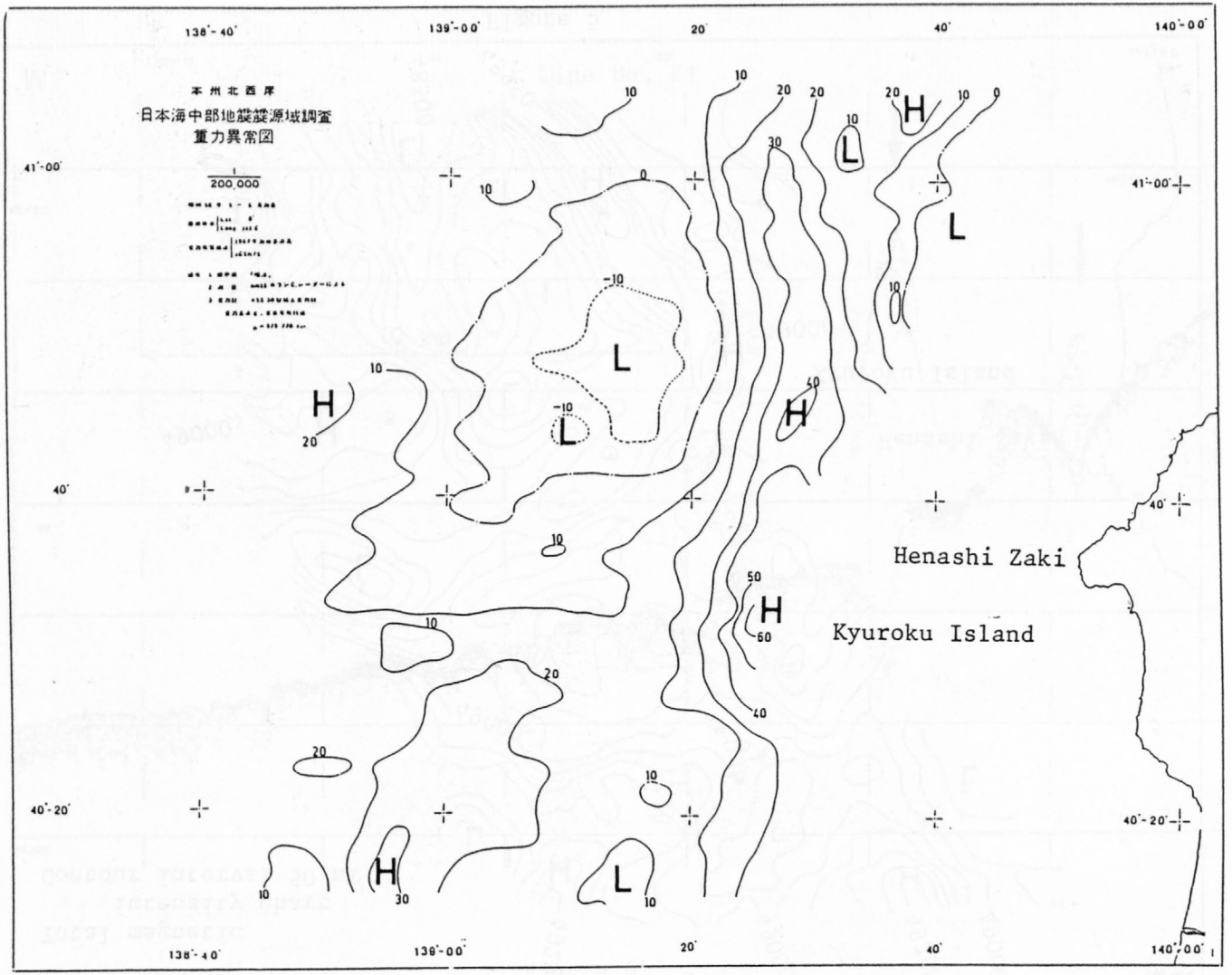
本州北西岸
日本海中部地震震源域調査
重力異常図
1/200,000
138°-40'
139°-00'
20'
40'
140°-00'
41°-00'
40°
40°-20'
Henashi Zaki
Kyuroku Island
H
L

Figure 6

THE 1983 AKITA-OKI EARTHQUAKE AND ITS IMPLICATIONS FOR PLATE KINEMATICS

TETSUZO SENO

INTERNATIONAL INSTITUTE OF SEISMOLOGY AND EARTHQUAKE ENGINEERING,

BUILDING RESEARCH INSTITUTE, MINISTRY OF CONSTRUCTION,

TSUKUBA, IBARAKI PREFECTURE, JAPAN 305

Abstract

The Akita-Oki earthquake of May 26, 1983 was unusual in two respects; it was large compared to other known historical earthquakes along the eastern margin of the Japan Sea and the time of occurrence was unexpected in terms of the spatio-temporal correlation between large interplate earthquakes along the Japan Trench and intraplate earthquakes in northern Honshu (Seno, 1979). However, this unusual occurrence can be explained if we interpret the event not as an intraplate earthquake but as an interplate earthquake following the new hypothesis that the eastern margin of the Japan Sea off northern Honshu constitutes an embryonic convergent boundary between the North American and Eurasian plates, which was recently proposed by Kobayashi (1983) and Nakamura (1983).

Seismic slip vectors from along the Japan and Kurile Trenches, the eastern margin of the Japan Sea, and south Kanto are examined to test the new hypothesis. Seismic slip vectors along the Japan Trench and eastern margin of the Japan Sea, including that of the 1983 Akita-Oki earthquake, do not contradict the idea that northern Honshu is part of the North American plate. However, seismic slip vectors and the strain pattern of recent horizontal crustal movements in southern Kanto indicate two major directions between Kanto and the Philippine Sea plate. One direction is from the relative motion between the North American and Philippine Sea plates, and the other from the motion between the Eurasian and Philippine Sea plates. These

movements suggest to us that northern Honshu does not behave simply as the North American plate but rather as a microplate independent from both the North American and Eurasian plates.

Introduction

The Akita-Oki earthquake of May 26, 1983 occurred along the eastern margin of the Japan sea. Its magnitude was determined as 7.7 by the Japan Meteorological Agency and its seimsic moment was determined as 4-8 x 10^{27} dyne-cm using long-period surface wave data by Ishikawa and others (1984), Shimazaki and Mori (1983) and Kanamori (1984). The epicenter is located about 60 km northwest of the Oga peninsula, Akita prefecture (e.g., Umino and others, 1983), which is the eastern edge of the deep marginal sea of the Japan Basin. Almost pure reverse faulting having a fault plane dipping shallowly to the east has been obtained as a focal mechanism solution (Shimazaki and Mori, 1983; Ishikawa and others, 1984; Kanamori, 1984; Tada, 1984). The aftershock activity of this event indicates that the width of the fault is about 40 km in an east-west direction, the length is about 100-130 km in a north-south direction, and the depth ranges from 0 to 20-25 km (Umino and others, 1983; Sato and other, 1984). The event was significant because it ruptured at least to the depth of bottom of the lower crust (Sato and others, 1984; Tada, 1984) in contrast to the intraplate seismicity in northern Honshu which is confined within the upper crust. Its magnitude and seismic moment are the largest among the earthquakes known along the eastern margin of the Japan Sea at least since the end of the last century. Apparently, the possible occurrence of an event of this size off the Japan Sea coast of northern Honshu had not been recognized by most Japanese seismologists prior to it taking place.

Shimazaki (1978) and Seno (1979) noticed a temporal correlation between the occurrence of large interplate earthquakes along the Japan Trench and

major intraplate earthquakes in northern Honshu for approximately the last 100 years. Seno (1979) also noted a spatial correlation between the location of rupture zones of large earthquakes along the trench and the area of high intraplate seismic activity. He contended that intraplate seismicity is high behind a rupture zone of an expected large interplate earthquake during a 50 year period before and during a 10 year period after the occurrence of the event. According to this theory, the area of high seismic risk at present is middle northern Honshu (Seno, 1979). However, the zone that ruptured during the Akita-Oki earthquake is not included in the expected high seismic area. Therefore the occurrence of the Akita-Oki earthquake appears to conflict with the hypotheses on the relation between large interplate earthquakes and intraplate seismicity proposed by Seno (1979).

However, a new hypothesis on the plate boundary around Japan, which has been developed since the fall of 1982 (Kobayashi, 1983; Nakamura, 1983; see detail Seno, 1984a), could explain the apparent breakdown of the Seno's theory. This hypothesis proposes that the eastern margin of the Japan Sea from west of southern Sakhalin to northern Honshu constitutes an embryonic convergent boundary between the North American and Eurasian plates (Fig. 1). It also proposes that the boundary continues to the south through Fossa Magna in central Honshu and joins to the margin of the Philippine Sea plate at the north of Izu Peninsula (Fig. 1). Previous work such as Chapman and Solomon (1976) assumed that the boundary between the Eurasian and North American plates passes from Sakhalin through central Hokkaido and joins with the junction between the Kurile and Japan Trenches. Instead, Kobayashi (1983) and Nakamura (1983) proposed that the boundary had jumped from central Hokkaido to eastern margin of the Japan Sea and Fossa Magna several million years ago. This was proposed mainly on historical seismicity and recent reverse faulting

along the eastern margin of the Japan Sea (Hatori and Katayama, 1977; Fukao and Furumoto, 1975). Quaternary faulting and folding off and on the Japan Sea coast of northern Honshu (Huzita, 1980; Research Group of Active Faults, 1980; Tamaki, 1984), and high rate of uplift in central Honshu at the west of Fossa Magna during the Quaternary (see Nakamura, 1983; Seno, 1984a). The occurrence of the Akita-Oki earthquake gave a large impact to this hypothesis because the occurrence of such a large event could not be explained by previous ideas on the plate boundary around Japan and the mode of faulting of the earthquake is conformable to the new hypothesis.

In this paper, I compare direction of seismic slip vectors along the plate boundary proposed by Nakamura (1984) and Kobayashi (1983) with the global plate motions determined independently from these seismic slip vectors (Minster and Jordan, 1978, 1979; Seno, 1977) in order to test this hypothesis. If northern Honshu is part of the North American plate, it is expected that seismic slip vectors along the Japan Trench and south Kanto may differ from those expected from the Eurasian-Pacific and Eurasian-Philippine Sea relative plate motions. I also examine slip vectors along the Kurile Trench and eastern margin of the Japan Sea to see whether they are consistent with the relative motions for the North American-Pacific and North American-Eurasian plates, respectively.

Seismic slip vectors

The Japan Trench

Azimuth of seismic slip vectors along the Japan Trench are plotted versus latitude of epicenters in Fig. 2. Only earthquakes of thrust type and with well-constrained slip vectors are plotted. The data source are from Seno

(1983). Different symbols indicate differenct authors of the mechanism solutions. If two solutions are available for one event, both are presented and connected by a vertical line in Fig. 2. The relative plate motions, Pacific-Eurasia and Pacific-North America, were calculated from the RM-2 geohedron of Minster and Jordan (1978) along the epicentral locations of the earthquakes; they are indicated by the solid and dotted lines, respectively, in Fig. 2. The errors in plate motions at 95% confidence level of RM-2 geohedron are indicated by the bars.

It is seen that the seismic slip vectors deviate systematically from the direction of the Pacific-Eurasian relative plate motion by about 10 degrees in a clockwise sense. On the contrary, the deviation from the Pacific-North America relative plate motion is not large, although there is still a few degrees systematic discrepancy. Note that the discrepancy from the Pacific-Eurasian motion is significant even if the error of the RM-2 geohedron is taken into account. If the focal mechanism solutions represent truely the differential motion between the Pacific and northern Honshu, this indicates that northern Honshu is not part of the Eurasian plate. However, a systematic bias might be introduced to the mechanism solutions due to anomalous velocity structure beneath the northern Honshu island arc and result in the apparent systematic deviation from the plate motion. Engdahl and others (1977) found a significant bias in fault plane solutions along the Aleutian arc. They found, in contrast, only a small bias for mechanism solutions along the Kurile Trench. Because the station-source geometry along the Japan Trench is similar to the Kurile Trench, the bias due to the heterogeneity in velocity structure beneath the northern Honshu arc would not be so large. However, the difference between the slip vectors and the relative plate motions are quite small and thus more precise estimation for the plate effect on the mechanism

solutions are necessary before concluding that the systematic deviation of Fig. 2 truly indicates that northern Honshu is not part of the Eurasian plate.

The Kurile Trench

Next we examine whether seismic slip vectors along the Kurile Trench are consistent with the North America-Pacific plate motion, in order to supplement the results along the Japan Trench. The azimuth of seismic slip vectors along the Kurile Trench is plotted versus latitude of epicenters of thrust type events in Fig. 3. Only well-constrained slip vectors are plotted. The slip vector directions are corrected for the oblique convergence along the Kurile Trench to represent motions on a horizontal flat plane (Minster and Jordan, 1978). The North America-Pacific relative plate motion calculated from RM-2 geohedron is indicated by the solid line; error bar is the same as in Fig. 2. In this figure, we see that the differential motion caused by earthquakes is almost consistent with the North America-Pacific plate motion. However, it should be noted that some seismic slip vector along the Kurile Trench were used to construct RM-2 of Minster and Jordan (1978) and thus these are not independent with each other. However, because only one solution out of those presented in Fig. 3 was used by Minster and Jordan (1978), the comparison is not meaningless. It indicates only that those solutions are consistent with previous solutions used by Minster and Jordan and that they are consistent with the North America-Pacific motion of RM-2 geohedron. It also should be noted that the deviation of the slip vectors from the Eurasia-Pacific plate motion along the Japan Trench is larger than the deviation of slip vectors from the North America-Pacific plate motion along the Kurile Trench, and in constrast, the deviation of the slip vectors from the North American-Pacific motion are similar between the Japan and Kurile Trenches. This indicates that if we regard the Kuriles as part of the

North American plate, northern Honshu also could be part of North American plate if the plate effect beneath both island arc is similar.

Eastern margin of the Japan Sea

Fig. 4 shows a plot of azimuth of slip vectors versus latitude of epicenters along the eastern margin of the Japan Sea from south of Sakhalin to northern Honshu. In this case, because the number of data is scarce, we include solutions of which slip vectors are not well-constrained. Further, easterly dipping nodal planes are assumed to be fault planes to interpret the mechanism solutions. The relative motion between North America-Eurasia is calculated from RM-2 along this margin and is indicated by the solid line in Fig. 4. The seismic slip vectors are almost consistent with the relative plate motion although their standard deviation from the plate motion is large; this is likely because we used events for which slip vectors are not well-constrained. It is noted that the slip vectors are not well-constrained. It is noted that the slip vector of the Akita-Oki earthquake is well-constrained (Ishikawa and others, 1984; Kanamori, 1984) and coincides almost with the relative plate motion.

South Kanto

The uncertainty in relative plate motion is most significant in south Kanto as suggested by the following two cases: (1) Kanto is part of the Eurasian plate, and (2) Kanto is part of the North American plate. Fig. 5 shows a velocity vector-space diagram between the Philippine Sea, Eurasia and North American at 35°N, 140°E in south Kanto. Seno's (1977) rotation vector for the Philippine Sea plate is used for the left figure and Minster and Jordan's (1979) for the right figure. Both give the same 20 degrees difference in relative plate motion between cases (1) and (2).

Seismic slip vectors and the crustal deformation pattern were examined to

see the relative motion between Kanto and the Philippine Sea. Only the slip vectors of events considered to represent the differential motion between Kanto and the Philippine Sea were used. They are the 1923 Kanto earthquake and its aftershocks, the 1968 Saitama earthquake, and the 1974 and 1983 southwest Ibaraki earthquakes. The data source for slip vectors are from Seno (1984b). The azimuth of these slip vectors is plotted versus time in Fig. 6 with different symbols for different authors. In addition to the seismic slip vectors, we also examined axes of horizontal crustal strain revealed by geodetic surveys in south Kanto conducted by Geographical Survey Institute. Seno (1980) calculated theoretical patterns of horizontal strain using a two dimensional finite-element modelling of the Japanese island assuming two alternative directions of plate contact, N30°W and N50°W in south Kanto. These directions correspond to the relative plate motion direction between the North America-Philippine Sea and between the Eurasia-Philippine Sea, respectively. If strain axes revealed by geodetic surveys in south Kanto match either of the theoretical strain patterns, we classified them into either of the two directions of plate contact. The directions thus interpreted from geodetic data are plotted by the lines in Fig. 6. The data include triangulations and more precise direct measurements of distance in the south Kanto precise geodetic net and Mitaka rhombus conducted by the Geographical Survey Institute since the great 1923 Kanto earthquakes. The data source is in Seno (1984b).

The plot in Fig. 6 shows that there is a large discrepancy in the slip vector of the 1923 Kanto earthquake among authors. It is also noted that the slip vectors of its aftershocks are also scattered between N30°W and N50°W. More recent data, both earthquake slip vectors and geodetic data, also indicate both the two directions. These suggest that there are apparently two

directions of plate contact in south Kanto.

Discussions and conclusions

The comparison of seismic slip vectors around northern Honshu with relative plate motions show that those along the Japan Trench and eastern margin of the Japan Sea are consistent with the idea that northern Honshu is part of the North American plate. However, the slip vectors and horizontal crustal deformation in south Kanto show two directions of plate contact, North America-Philippine Sea and Eurasia-Philippine Sea. Because the slip vectors along the Japan Trench differ from the Eurasia-Pacific relative plate motion, if south Kanto and northern Honshu are part of the same plate, those slip vectors in the two segments conflict with each other. Because there appears to be no possible plate boundary between south Kanto and northern Honshu, we have to seek other possibilities to resolve this apparent conflict.

First, we are reminded that there might be a systematic bias in the slip vectors along the Japan Trench due to the anomalous velocity structure beneath the island arc, a so called plate effect. If we assume about a five degrees clockwise bias in the slip vectors in Fig. 1 from the true ones due to the plate effect, those slip vectors come to lie on both of the relative motions, North America-Pacific and Eurasia-Pacific. This can resolve the above apparent conflict in slip vectors between the Japan Trench and Kanto because in this case both of the plate interactions, Pacific-Eurasia and Pacific-North America, are found along the Japan Trench. Assuming a 5 degree systematic bias is speculative and this should be substantiated by using a three dimensional ray-tracing method beneath the northern Honshu arc as Engdahl and others (1977) did beneath the Aleutians and Kuriles.

Next, there is a small possibility that the interpretation of seismic slip vectors and crustal deformation in south Kanto is not correct because of

the complexity in this region. South Kanto is located near the triple junction between the Japan, Izu-Bonin Trenches and the Nankai Trough, and three plates, Eurasia, Philippine Sea and Pacific plates, interact with each other beneath Kanto. In this complex tectonic setting, it is not easy to identify earthquakes as occurring at the plate interface between Kanto and the Philippine Sea. More studies are necessary to elucidate the plate interaction in the south Kanto region including determination of precise focal mechanisms and modeling of crustal deformation before permitting discussion of this possibility.

In this study, we prefer the first possibility, that there exists a systematic bias in the slip vectors along the Japan Trench because it is simpler and can resolve the problem within the fundamental premise of plate tectonics that plates are rigid. In this case, northern Honshu should be a microplate, behaving sometimes as the North American plate and other times as the Eurasian plate. Because this northern Honshu microplate does not have its own plate driving force such as downgoing slabs or spreading axes, it is very likely that the motion of this microplate is easily affected by interaction with the surrounding major plates. This conclusion also implies that the boundary in central Hokkaido is still active to some extent. The behavior of northern Honshu, as states above, will provide us a unique opportunity to observe how jumping of a plate boundary can take place.

References

Chapman, M.E. and S.C. Solomon, North American-Eurasian plate boundary in northeast Asia, J. Geophys. Res., 81, 921-930, 1976.

Engdahl, E.R., N.H. Sleep, and M.T. Lin, Plate effects in north Pacific subduction zones, Tectonophysics, 37, 95-116, 1977.

Fukao, Y. and M. Furumoto, Mechanism of large earthquakes along the eastern

margin of the Japan Sea, Tectonophysics, 25, 247-266, 1975.

Hatori, T., and M. Katayama, Tsunami behavior and source areas of historical tsunamis in the Japan Sea, Bull. Earthquake Pres. Inst., Univ. of Tokyo, 52, 49-70, 1977 (in Japanese).

Huzita, K., Role of the Median Tectonic Line in the Quaternary tectonics of the Japanese Islands, Mem. Geol. Soc. Japan, 18, 129-153, 1980.

Ishikawa, M. Takeo, N. Hamada, M. Katsumata, K. Satake, K. Abe, M. Kikuchi, K. Sudo, M. Takahashi, S. Kashiwabara, and N. Mikami, Source process of the 1983 Nihonkai-Chubu earthquake, the Earth Monthly, 6, 11-17, 1984 (in Japanese).

Kanamori, H., The 1983 Akita-Oki earthquake (Mw=7.8) and its implication for systematics of subduction earthquakes, Proc. US-Japan Seminar on Earthquake Predict., submitted, 1984.

Kobayashi, Y., Initiation of subduction, The Earth Monthly, 5, 510-514, 1983 (in Japanese).

Minster, J.B. and T.H. Jordan, Present-day plate motions, J. Geophys. Res., 83, 5331-5354, 1978.

Minster, J.B. and T.H. Jordan, EOS, Rotation vectors for the Philippine and Rivera plates, 60, 958, 1979.

Nakamura, K., Possible nascent trench along the eastern Japan Sea as the convergent boundary between Eurasian and North American plates, Bull. Earthquake Res. Inst., Univ. of Tokyo, 58, 711-722, 1983 (in Japanese).

Research Group of Active Faults, "Active Faults in Japan", Univ. of Tokyo Press, Tokyo, 1980 (in Japanese).

Sata, T., Kosuge, M., Tanaka, K., and Sato, H., Aftershock distribution of the Nihonkai-Chubu earthquake, abstract, Seismol. Soc. Japan, 1984 No. 1, 37, (in Japanese).

Seno, T., Intraplate seismicity in Tohoku and Hokkaido and large inbterplate earthquakes: A possibility of occurrence of a large interplate earthquake off the southern Sanriku coast, northern Japan, J. Phys. Earth, 27, 21-51, 1979.

Seno, T., Transient features of regional stress field, - and example of south Kanto, The Earth Monthly, 2, 146-154, 1980 (in Japanese).

Seno, T., A consideration on the "Japan Sea Subduction Hypothesis", Jisin, 36, 270-273, 1983 (in Japanese).

Seno, T., Earthquakes and tectonics along the eastern margin of the Japan Sea, The Earth Monthly, 6, 4-8, 1984a (in Japanese).

Seno, T., Is northern Honshu North American plate?, The Earth Monthly, 6, 49-54, 1984b (in Japanese).

Shimazaki, K., Correlation between intraplate seismicity and interplate earthquakes in Tohoku, northeast Japan, Bull. Seism. Soc. AM., 68, 181-192, 1978.

Shimazaki, K., and J. Mori, Focal mechanism of the May 26, 1983, Japan Sea earthquake, abstract, Seismol. Soc. Japan, 1983, No. 2, 15, 1983.

Tada, A., Nihonkai-Chuby earthquake and crustal deformation, The Earth Monthly, 6, 18-22, 1984 (in Japanese).

Tamaki, K., Structure and tectonics of the eastern border of the Japan Sea, The Earth Monthly, 6, 38-49, 1984 (in Japanese).

Umino, T., Matsuzawa, A., Ohara, K. Shimizu, H. Hasegawa, A., Takagi, A. Kosuge, M, Tanaka, K. Sato, T., and Sato, H., Distribution of aftershocks of the 1983 Nihonkai-Chubu earthquake, abstract, Seismol. Soc. Japan, 1983, No. 2, 4, 1984 (in Japanese).

Figure Captions

Fig. 1. Plate boundaries around Japan based on the new hypothesis that the eastern margin of the Japan Sea and Fossa Magna is an embryonic convergent plate boundary between the North American and Eurasian plates (after Nakamura, 1983; Kobayashi, 1983). The boundary previously proposed by Chapman and Solomon (1976) is indicated by the broken line.

Fig. 2. Azimuth of slip vectors along the Japan Trench plotted versus latitude of epicenters. Different symbols indicate different authors of mechanism solutions. Relative plate motions, Eurasia-Pacific and North America-Pacific, (RM-2, Minster and Jordan, 1978) are represented by the solid and dotted lines, respectively. Error bars indicate errors at 95% confidence level of RM-2. Data of slip vectors are from Seno (1983).

Fig. 3. Azimuth of slip vectors along the Kurile Trench plotted versus latitude of epicenters. North America-Pacific relative motion (RM-2, Minster and Jordan, 1978) is indicated by the solid line. Data of slip vectors are from Seno (1984b).

Fig. 4. Azimuth of slip vectors along eastern margin of the Japan Sea. North America-Eurasia relative plate motion (RM-2) is indicated by the solid line.

Fig. 5. Velocity-space diagram showing the relative motions between the Eurasian, Philippine Sea and North American plates, using the Philippine Sea rotation vector of Seno (1977), left, and Minster and Jordan (1979), right, respectively.

Fig. 6. Seismic slip vectors and direction of plate contact from crustal strain data plotted versus time in south Kanto. The different solutions of the same earthquake are connected by a vertical line. Directions revealed by the geodetic data are indicated by the horizontal lines. Data are from Seno (1984b).

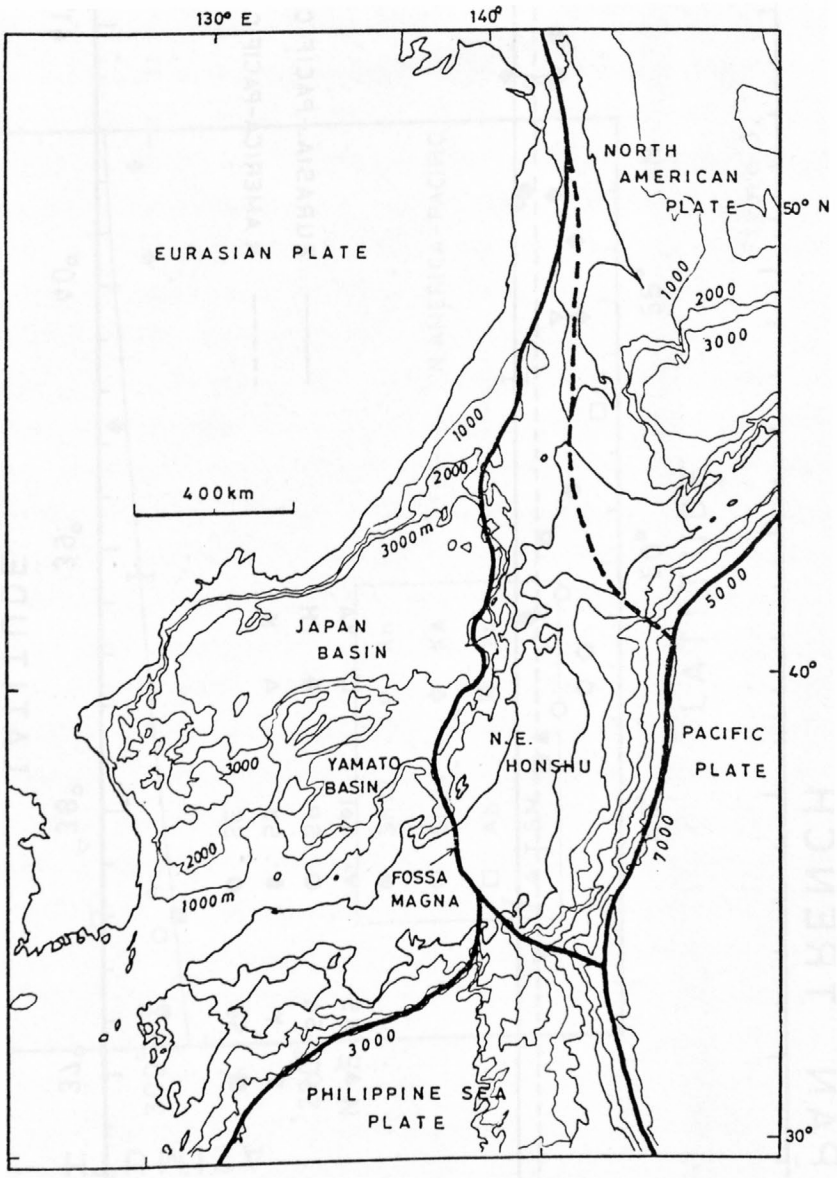
130° E
140°
NORTH
AMERICAN
PLATE
50° N
EURASIAN PLATE
1000
2000
3000
400km
1000
2000
3000m
5000
JAPAN
BASIN
40°
N.E.
HONSHU
PACIFIC
PLATE
YAMATO
BASIN
3000
2000
7000
1000m
FOSSA
MAGNA
3000
PHILIPPINE SEA
PLATE
30°

Figure 1.

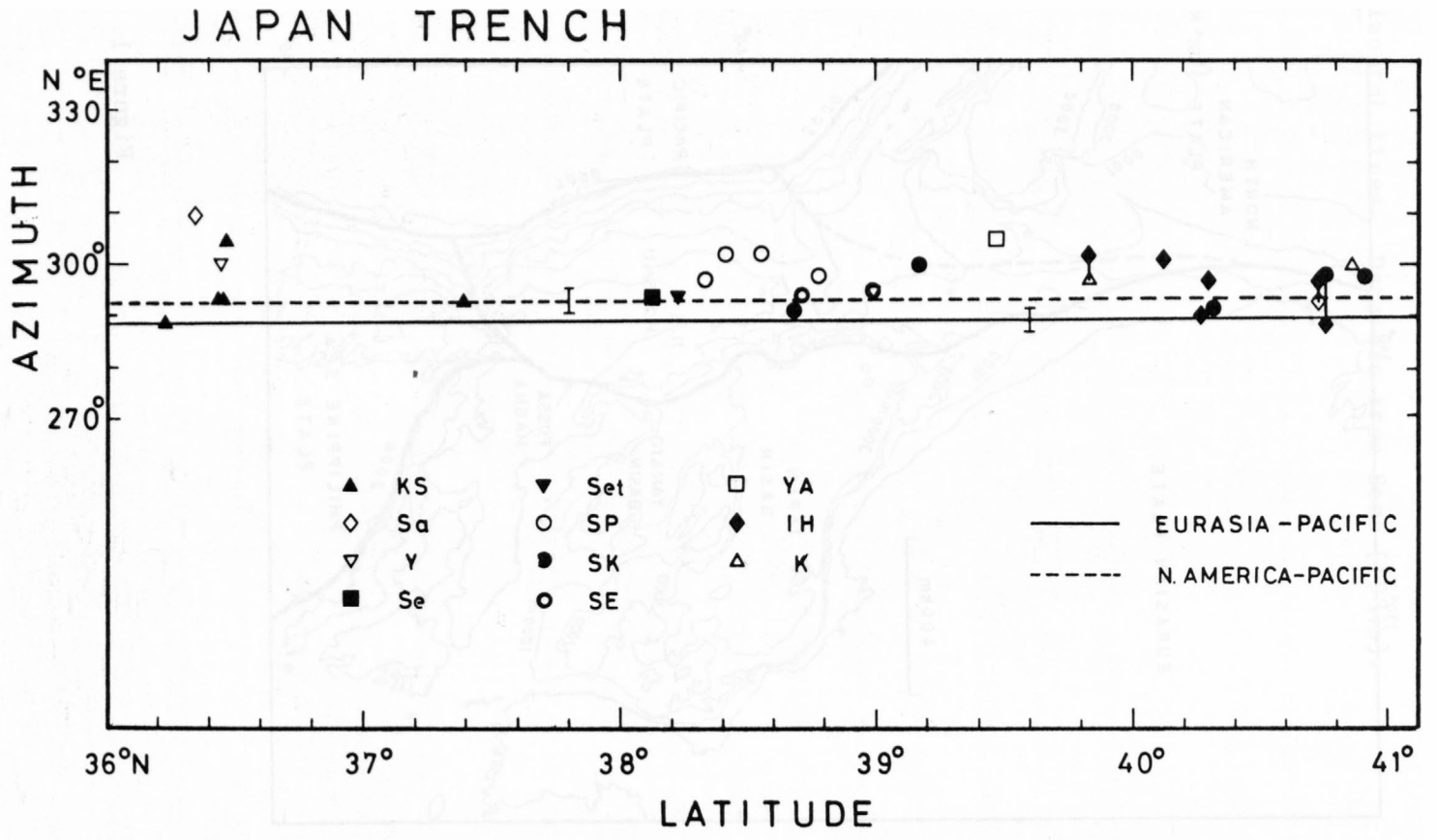
JAPAN TRENCH
N °E
330
300°
270°
AZIMUTH
KS
Sa
Y
Se
Set
SP
SK
SE
YA
IH
K
EURASIA - PACIFIC
N. AMERICA-PACIFIC
36°N
37°
38°
39°
40°
41°
LATITUDE

Figure 2.

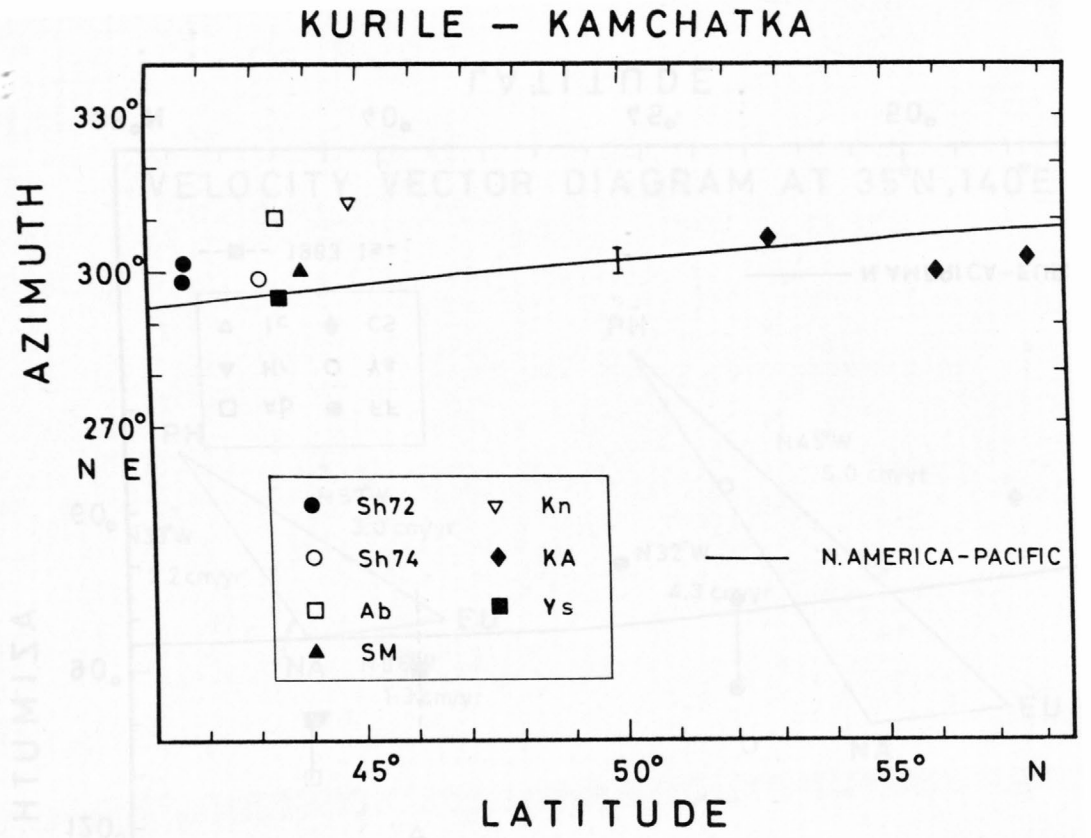
KURILE – KAMCHATKA
330°
300°
270°
AZIMUTH
N E
Sh72
Sh74
Ab
SM
Kn
KA
Ys
N. AMERICA-PACIFIC
45°
50°
55°
N
LATITUDE

Figure 3.

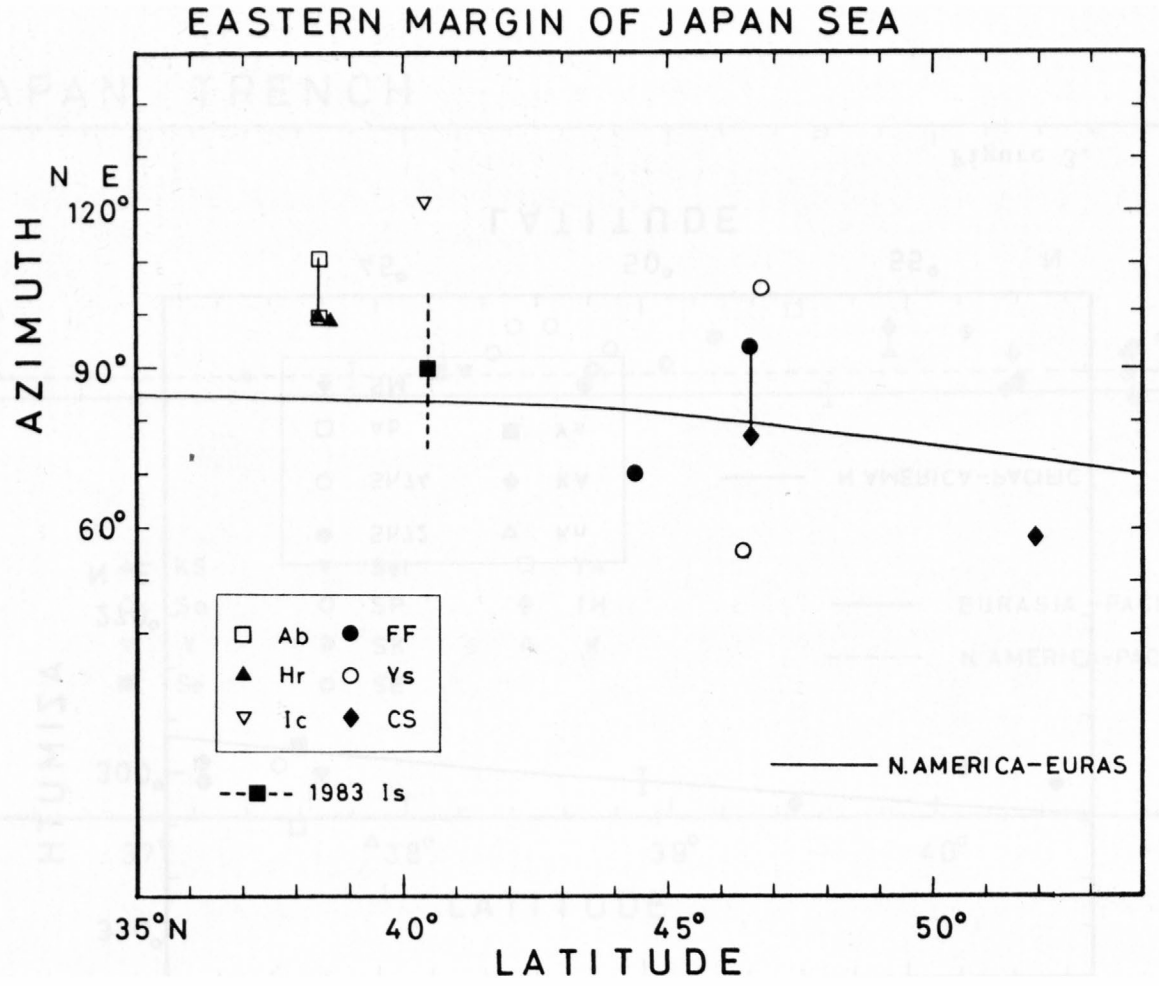
EASTERN MARGIN OF JAPAN SEA
AZIMUTH
N E
120°
90°
60°
35°N
40°
45°
50°
LATITUDE
Ab
FF
Hr
Ys
Ic
CS
1983 Is
N. AMERICA-EURAS

Figure 4.

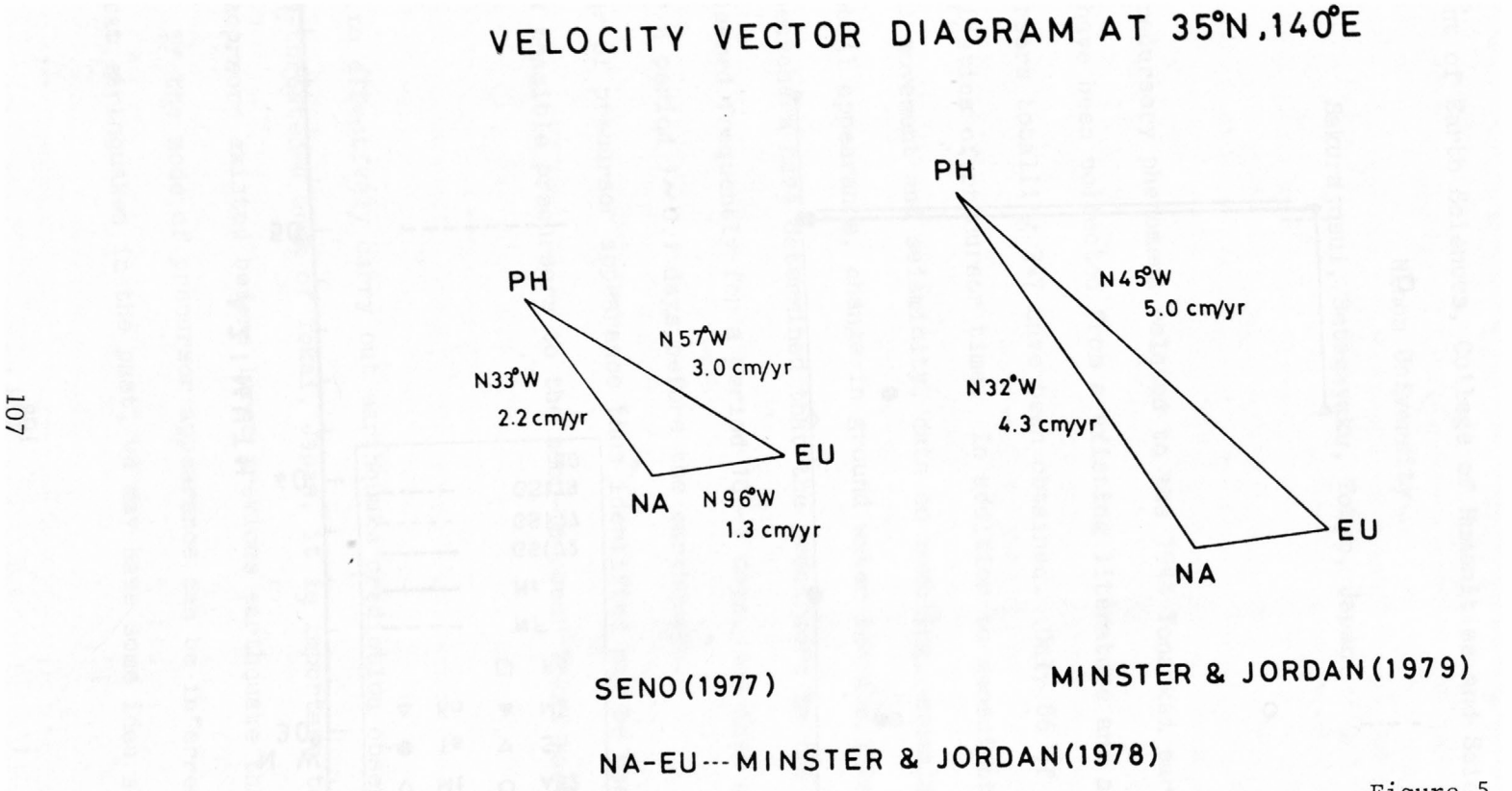
VELOCITY VECTOR DIAGRAM AT 35°N, 140°E
PH
N57°W
3.0 cm/yr
N33°W
2.2 cm/yr
EU
NA
N96°W
1.3 cm/yr
SENO(1977)
PH
N45°W
5.0 cm/yr
N32°W
4.3 cm/yr
EU
NA
MINSTER & JORDAN(1979)
NA-EU---MINSTER & JORDAN(1978)

Figure 5.

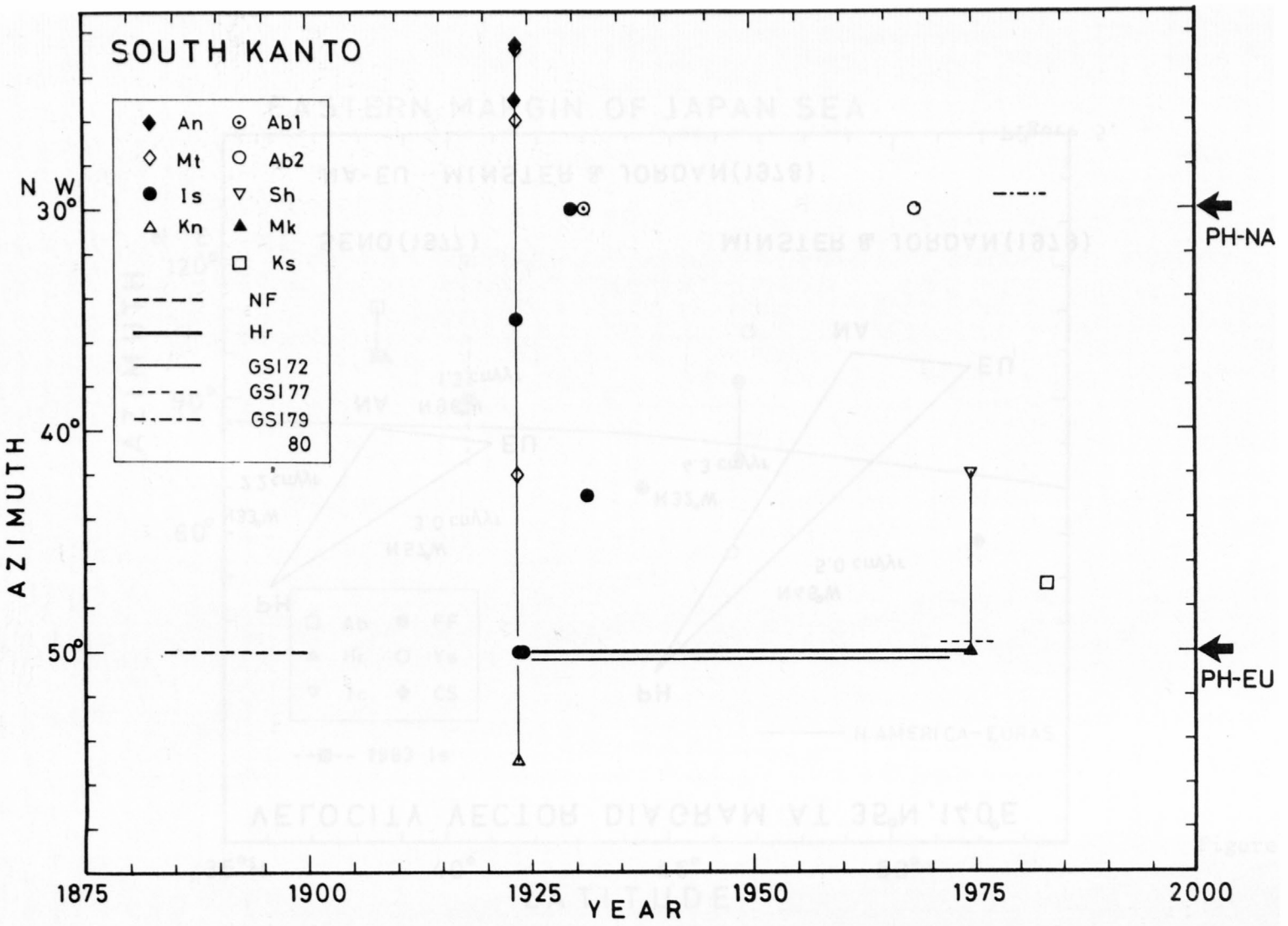
SOUTH KANTO
An
Mt
Is
Kn
Ab1
Ab2
Sh
Mk
Ks
NF
Hr
GSI 72
GSI 77
GSI 79
80
N W
30°
40°
50°
AZIMUTH
1875
1900
1925
1950
1975
2000
YEAR
PH-NA
PH-EU

Figure 6.

PRECURSORS TO THE 1944 TONANKAI EARTHQUAKE OF MAGNITUDE 7.9, JAPAN

Tsuneji Rikitake

Department of Earth Sciences, College of Humanities and Sciences,

Nihon University

Sakurajosui, Setagayaku, Tokyo, Japan

Abstract

Various precursory phenomena related to the 1944 Tonankai earthquake of magnitude 7.9 have been collected from a existing literature and a postcard search. Precursors totalling 347 have been obtained. Only 66 of the 347 can be used as statistics of precursor time. In addition to geoscientific data such as crustal movement and seismicity, data on rumbling, anomalous animal behavior, fireball appearance, change in ground water and the like have been obtained. Researchers have determined that the precursors to the Tonankai earthquake appeared frequently for a period 10~1 days, and then more frequently for a period 1~0.1 days before the earthquake.

The manner of precursor appearance thus identified may be useful for estimating how possible precursors to the soon-to-occur Tokai earthquake would occur.

Introduction

In order to effectively carry out earthquake prediction observation in the earthquake-threatened area of Tokai, Japan, it is important to know what earthquake precursors existed before large previous earthquake that occurred in this area. If the mode of precursor appearance can be inferred to some extent for great earthquakes in the past, we may have some idea about how

precursors would appear before a similar earthquake in the future, assuming that the physical mechanism of earthquake occurrence is approximately the same for these earthquakes.

The 1944 Tonankai earthquake, of which the magnitude was one time determined as 8.0 and recently revised as 7.9 by the Japan Meteorological Agency (JMA), occurred toward the end of the World War II when Japan was in a state of confusion. No accurate count of victims was made at the time due to the confusion immediately before the surrender of Japan. However, later it was estimated that 1000 people lost their lives. In addition, the military censorship for news media was so strict that no real damage could be publicized. Under the circumstances, information about the Tonankai earthquake was so limited that it is even called a "phantom earthquake".

Despite little recorded data on the Tonankai Earthquake, the Association for the Development of Earthquake Prediction (1982, 1983) undertook a major effort to collect precursor data related to the earthquake. It is believed that the pattern of precursor appearance in the Tonankai earthquake plays an important role in estimating possible patterns of precursor apperance for the Tokai earthquake.

Sources of Data

Precursor data for the Tonankai earthquake are taken from the following four sources:

(i) Existing literature

(ii) Seismic data by Central Meteorological Observatory (now JMA)

(iii) Inquiries by return post cards

(iv) Inquiries mainly made by volunteers at high and middle schools in Shizuoka Prefecture

1) Existing Literature

Every report on the Tonankai earthquake was under strict military control, so that no thorough investigation on various features of the earthquake could be made. Under the circumstances, very few reports on the earthquake was published soon after the earthquake. Some of them were classified as top secret.

2) Seismic Data

The numbers of felt and unfelt earthquakes at as number of weather stations in Central Japan have been examined for the period during 1938-1945 using the table published by JMA and the original records at the Owase and Tsu weather station.

The most outstanding feature revealed by the seismic data is the point that a large number of unfelt earthquakes having an S - P time of 2 - 3s were observed at Owase from the period August - September, 1944. Such activity was not observed at the neighboring stations, say Shionomisaki and Tsu. The locations of these and other neighboring stations are shown in Fig. 1. It is therefore certain that a swarm of small earthquakes occurred nearby the Owase station, which is the only station that registered the activity.

3) Return Post Card Inquiry

In view of the scarcity of precursor data found in existing literature, the Association for the Development of Earthquake Prediction (1983) undertook an inquiry survey by return post card. Inquiry post cards, of which the postal fare was prepaid, were sent to 2,000 people, who were middle school students at the time of the Tonankai earthquake, picking up their names from membership lists of alumni associations. Most of them were forced to work at factories or farms under the military control at the time of the earthquake. It was requested on the card to reply to the following questions:

1. Did you observe any anomalous phenomenon precursory to the Tonankai

earthquake?

2. If yes, please answer the following.

a) When?

b) Where?

c) What kind of phenomenon?

d) How much, how long, to what extent----etc.?

e) Was it experienced by yourself, or was it secondhand information?

610 people kindly replied to the questions. This number amounts to about 30% of the people poled. Some of the respondents replied with comments by their relatives and friends, so that the total number of respondents certainly exceeds 30% of the inquired people.

The number of people who recognized or noticed something unusual before the Tonankai earthquake amounts to 102. Among them, there are some people who pointed out more than one anomaly, so that there are 131 replies in total.

4) Volunteer Inquiries in Shizuoka Prefecture

A number of high and middle schools as well as a branch offices of the prefectural office made the inquiry survey about the Tonankai earthquake at a time when the fear of coming Tokai earthquake was stressed in the later half of the 1970's. These inquiries were mostly concerned with general aspects of the Tonankai earthquake, so that they did not particularly put much emphasis on precursors. Among 5,692 pages of inquiry, only 207 reply sheets contained some precursor-like phenomena. Only 6% of the precursor data can provide reliable precursor times.

Data

1) Data From Existing Literature

A number of data clearly indicates that Pt. Omaezaki had been subsiding before the earthquake and that the subsidence slowed down ten to several years

before the earthquake. The land at Pt. Omaezaki tended to uplift several days prior to the earthquake occurrence with an enormous acceleration several hours before the earthquake occurrence. It is fortunate that the transient crustal movement immediately before the occurrence of this great earthquake was monitored by a levelling survey which was being conducted over the deformed area by coincidence. Fig. 2 shows the precursory uplift of a levelling bench-mark near Kakegawa as estimated by Mogi (1982).

It is extremely interesting that the bubble of a levelling apparatus swayed side to side, so that no measurement could be performed a few minutes before the earthquake occurrence as reported by Koshiyama (1976). The reported ground instability is supported by other observations brought to light by the return post card inquiry which will be presented in the following section.

Most reports on earthquake noise suggest that rumbling took place at almost the same time that the earthquake occurred. This is quite a contrast to the reports on the Ansei Tokai earthquake (Association for the Development of Earthquake Prediction, 1982) which stated that rumblings had been heard from about 100 days prior to the main shock.

2) Data From Post Card Inquiry

As stated in the last section, the return post card inquiry provided the most reliable data set. Among crustal movement and earthquake data, we have a number of reports that suggest that the ground became unstable several minutes prior to the earthquake occurrence. The ground seems likely to have tended to sway with a period of several seconds. Such a view matches with the report which describes the sway of the bubble of a levelling apparatus several minutes prior to the earthquake occurrence.

Rumblings and foreshocks were relatively few for the Tonankai earthquake

although some were reported.

It appears to the author that the reports on anomalous animal behavior as described in a number of reports are typical for animal precursors to a large earthquake.

It is not quite clear whether or not earthquake light is a phenomenon preceding an earthquake. It is interesting, however, that in two reports which are independent from one another, it was described that a fire ball appeared. In view of the fact that many fire balls were observed prior to the Songpan-Pingwu earthquakes (M=7.2, 6.7, 7.2, 1976) in Sichuan Province, China (Rikitake, 1982), it cannot be ruled out that the reported fire ball might have something to do with the earthquake occurrence.

Not many reports on underground water are available. Fig. 3 shows the spots where precursor-like phenomena was observed.

3) Volunteer Inquiries in Shizuoka Prefecture

These inquiries were mainly concerned with earthquake damage rather than with premonitory effects, so that little data can be used for inferring precursor time.

There is one report that strange rumblings were heard a few times a day, 4-5 days before the earthquake. Several reports on foreshocks were collected. The precursor times range from several months to a few minutes. The data for anomalous animal behavior include crows, pheasants and eels. A few reports on fireballs are available, although no precursor time is known.

It is interesting to note that a report from Kakegawa indicates that noises were received by a radio set before the earthquake. The reporter wrote that the earthquake was predicted because of radio noise.

Characteristics and Statistics of Precursors

The data preceding the Tonankai earthquake are summarized in Table 1.

There were a total of 347 observations. It is possible, however, to estimate the approximate precursor time only for 66 of the observations.

It is difficult to evaluate the accuracy of these precursory data. In the following analysis of precursory statistics, it is presumed that the data are all correct because there is no other way of analyzing the data.

1) Characteristics of Precursors

a) The ground around Pt. Omaezaki had been subsiding before the Tonankai earthquake. The subsidence slowed down about 10 years before the earthquake, and it appears that the land there tended to uplift several years prior to the earthquake. The uplift seems likely to have accelerated several hours before the earthquake.

b) A swarm of unfelt earthquakes, that lasted about two months, occurred near Owase, Mie Prefecture about 100 days prior to the main shock.

c) Most of the earthquake noise occurred at the same moment the main shock occurred. However, a number of reports indicate that rumblings took place several days prior to the earthquake. In contrast to the Ansei Tokai earthquake, no rumblings preceded the main shock of the Tonankai earthquake by more than several months.

d) There are reports which strongly support the fact that the ground became unstable several minutes before the main shock. They are as follows;

(i) The bubble of a levelling apparatus swayed from side to side, so that no measurement could be made.

(ii) A machine tool stand for determining the center of a metal rod mounted on a lathe became unstable at a factory.

(iii) A chain hanging beside an electric furnace at an aircraft factory started to make a sound as a result of slow swaying

just before the earthquake.

(iv) Centering of an object attached to a lathe at an airplane factory was impossible.

(v) It was difficult to cut a duralumin plate along a straight line with scissors at a factory.

(vi) A young man lying on the ground in an air-raid shelter felt some sway as if someone was stamping on top of the shelter. This report was from an airplane factory destroyed in the earthquake.

(vii) Middle school students, who were working in a factory, suddenly felt dizzy. While they were talking to each other about the strange feeling, the great shock took place.

Most of the above reports were reported by people who were handling precise instruments and machine tools. It seems quite likely that the ground began to sway with a period of a few seconds immediately prior to the main shock occurrence.

e) Precursor times are identified for 20 instances of anomalous animal behavior. As for the species involved, there was mosquitos, rats, mantis, grasshopper, leech, catfish, dog, crow, chicken, pheasant, horse, --- etc.

f) Among the reports on earthquake lights and fire balls, there are two independent reports that a fire ball appeared.

g) Prior to the earthquake, the seismicity in a broad area around the epicenter of the coming earthquake became high, forming a so-called "doughnut phenomenon". In contrast, the epicentral area was forming a seismic gap. During the 20-year period preceding this earthquake, the activity of deep-focus earthquakes in the Chubu and Kinki districts

was high.

2) Statistics of Precursor Time

In order to make statistical studies on precursor times which range from a few minutes to several years, precursor time T is measured in units of days and the frequencies of $\log_{10} T$ are counted with an interval of 1.0 for each range. Fig. 4 is the histogram of frequency distribution of logarithmic precursor times for the total data set. The shaded columns in the figure indicate the geoscientific data.

Looking at the figure, we observe that peaks of precursor times appear for $\log_{10} T = 0 \sim 1$ and $-1 \sim 0$. It may be said, therefore, that the frequency distributions of animal, light and geoscientific precursors are more or less the same. That is, the precursors to the Tonankai earthquake appeared most frequently in the period $10 \sim 1$ days before the earthquake, and the next most frequent occurrences were for a period $1 \sim 0.1$ days before the earthquake.

According to Weibull distribution analyses, the mean precursor times are estimated as 0.73, 0.50 and 1.0 days for the total, animal and geoscientific data. It may be said that there are no conspicuous differences in precursor times between the three data sets.

Concluding remarks - Possible appearance of precursors anticipated for the earthquake suspected to occur in the Tokai area in the near future

One of the main purposes of collecting and analyzing precursors to the Tonankai earthquakes was to identify the possible types of precursors that might precede the anticipated future great earthquake in the Tokai area. As the physical mechanism producing the anticipated earthquake may be approximately the same as that for the great earthquakes in the past, there is good reason to presume that the precursors, if any, would occur in a fashion similar to those for the past earthquake.

It is therefore intended to describe herein the possible types of precursors that might occur before the hypothetical great earthquake expected in the Tokai area. The assumption is made that the pattern of precursor appearance noted in the cases of the Ansei Tokai and Tonankai earthquakes will repeat themselves.

Summarizing what was stated in this paper along with the study on the precursors to the Ansei Tokai earthquake, a likely precursor appearance may be as follows;

1) About 20 years before the earthquake: Seismicity in the Kinki, Chubu and Kanto areas will become high. Moderately large earthquakes, including magnitude 6~7 events, will tend to occur frequently.
2) About 10 years before: Ground subsidence at Pt. Omaezaki will slow down and the ground will tend to uplift several years before the earthquake.
3) Several months before: Noises will be heard in Mie, Aichi and Shizuoka Prefectures.
4) About 100 days before: Swarms of small earthquakes will occur near the epicentral area.
5) About 10 days before: The number of precursory phenomenon including anomalous animal behavior will increase. Fire balls may be observed. The precursors will be observed over a wide area from Izu to Kii Peninsulas. The land uplift at Pt. Omaezaki will accelerate.
6) Several hours before: The uplift of land at Pt. Omaezaki will accelerate even more.
7) Several minutes before: The ground will become unstable and start to sway.
8) A few seconds before or at the same time: Terrific rumbling will occur.

What is written above is of course fictitious. But the author believes that

the probability of observing premonitory effects of a roughly similar kind would be high, should the anticipated earthquake occur in the Tokai area.

References

Association for the Development of Earthquake Prediction, Precursors to the Ansei Tokai and Tonankai Earthquakes, 106 pp, 1982 (in Japanese).

Association for the Development of Earthquake Prediction, Precursors to the Tonankai Earthquake with Supplements to the Ansei Tokai Earthquake, 204 pp, 1983 (in Japanese).

Koshiyama, T., Kokudo Chiriin Koho, Spec. Vol., No. 100, 7-8, 1976 (in Japanese).

Mogi, K., Temporal variation of the precursory crustal deformation just prior to the 1944 Tonankai earthquake, Zisin (J. Seismol. Soc. Japan), (ii), 35, 145-148, 1982 (in Japanese).

Rikitake, T., Earthquake prediction work in Sichuan Province, China with special reference to the Songpan-Pingwu earthquakes, Chinese Geophys., Am. Geophys. Un., 2, 139-156, 1982.

Figure Captions

Fig. 1 The epicenter of the Tonankai earthquake and the nearby weather stations.

Fig. 2 Change in the height of a levelling bench mark near Kakegawa prior to the Tonankai earthquake of which the occurrence time is shown by an arrow (Mogi, 1982).

Fig. 3 Spots where precursors were observed before the Tonankai earthquake. The data are taken from the result of post card inquiries. The numerals indicate respective precursor types: (1) earthquake, (2) crustal movement, (3) rumbling noise, (4) anomalous animal behavior, (5) underground water and hot spring, (6) anomalous weather, (7) supernatural power and (9) anomalous sea condition, although disciplines (6) and (7) are excluded from the statistics of precursors.

Fig. 4 Histogram of logarithmic precursor time in units of days for the entire Tonankai earthquake precursor data set. The interval of each range is 1.0. Shaded columns represent the frequency of geoscientific data.

Table 1. The numbers of precursors to the Tonankai earthquake for various disciplines.

Discipline	Total data	Data for which approximate precursor time is estimated
Crustal movement	18	8
Rumbling noise	208	10
Earthquake	46	13
Anomalous animal behavior	34	20
Earthquake lights and fire ball	26	10
Underground water	13	4
Anomalous sea condition	2	1
Total	347	66

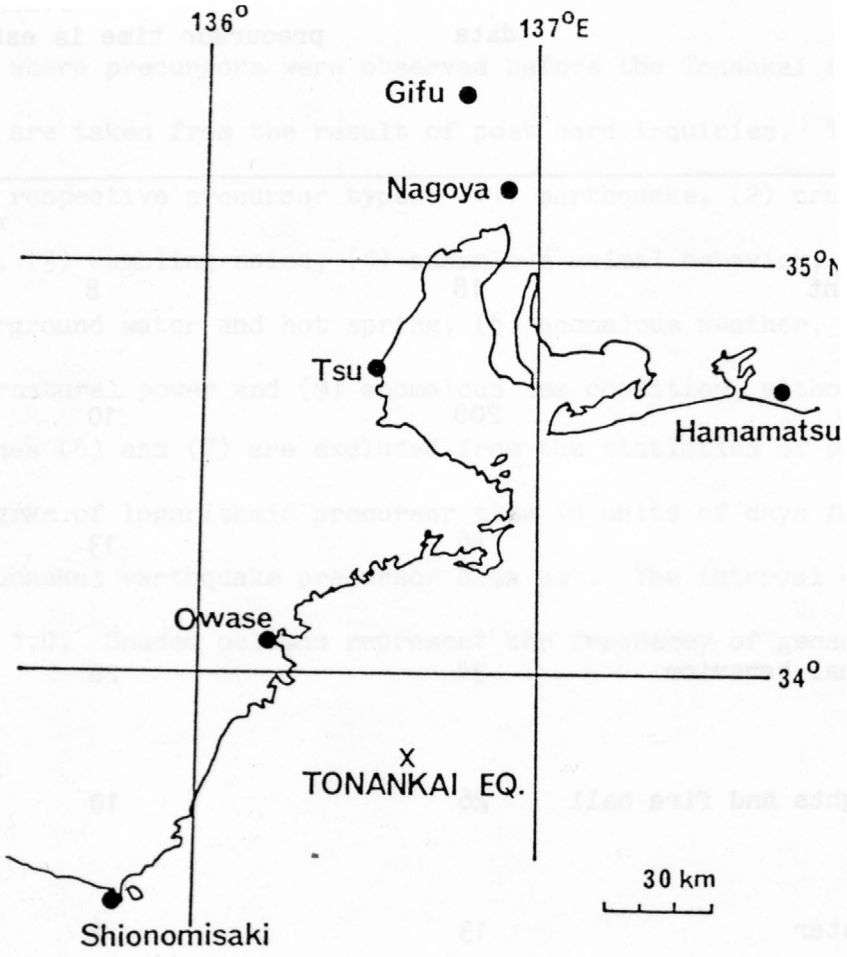
136°
137°E
Gifu
Nagoya
35°N
Tsu
Hamamatsu
Owase
34°
X
TONANKAI EQ.
30 km
Shionomisaki

Figure 1.

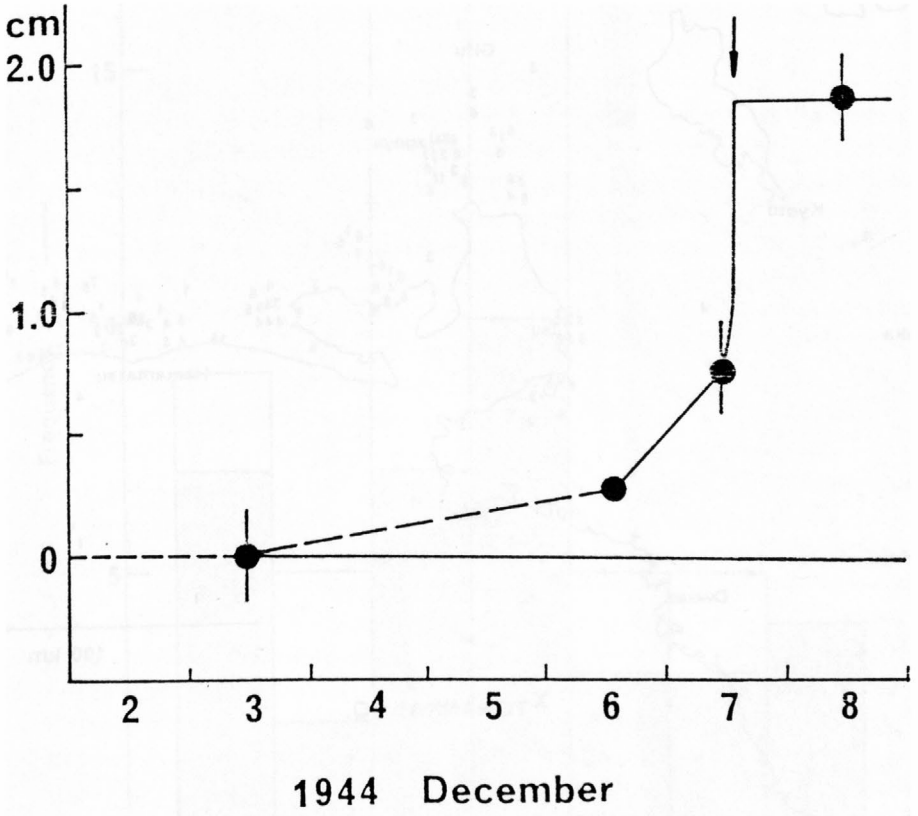

Figure 2.

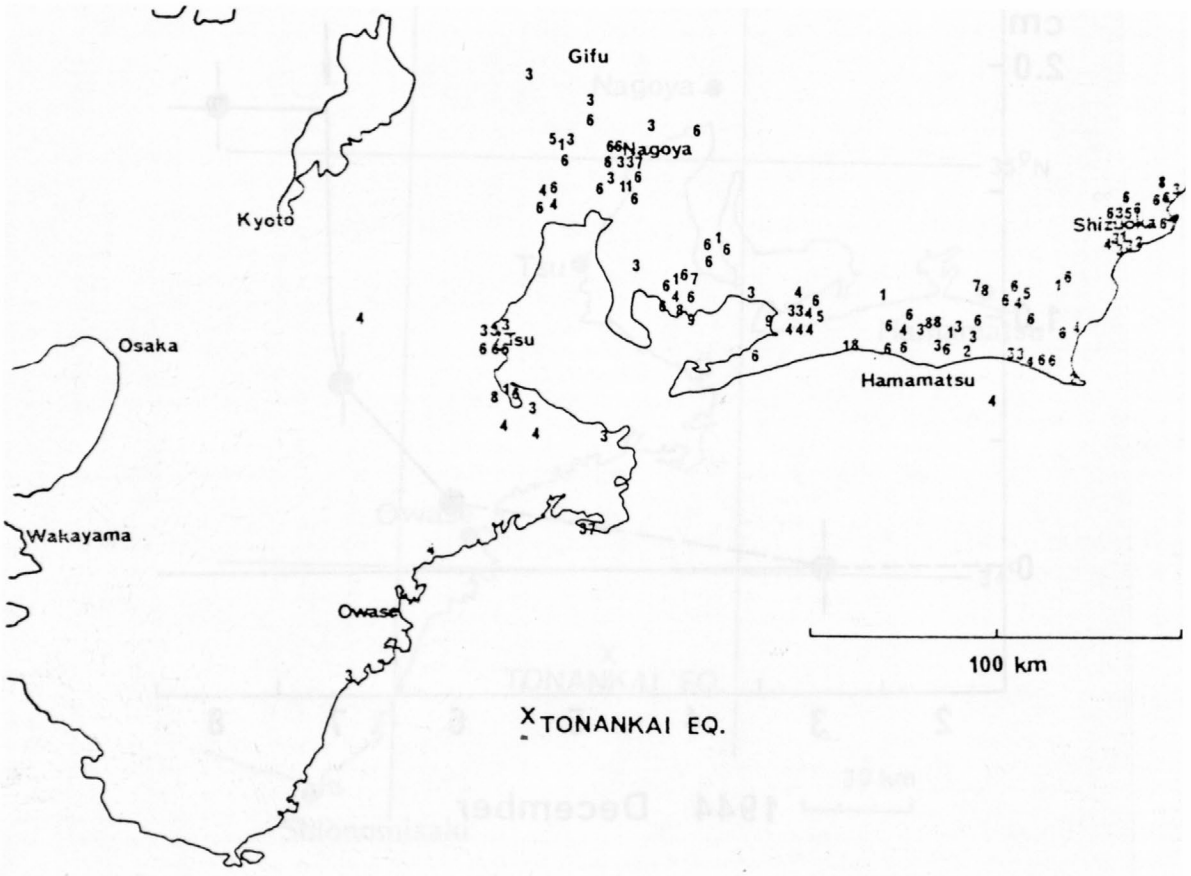
Gifu
Nagoya
Kyoto
Osaka
Wakayama
Owase
Hamamatsu
100 km
TONANKAI EQ.

Figure 3.

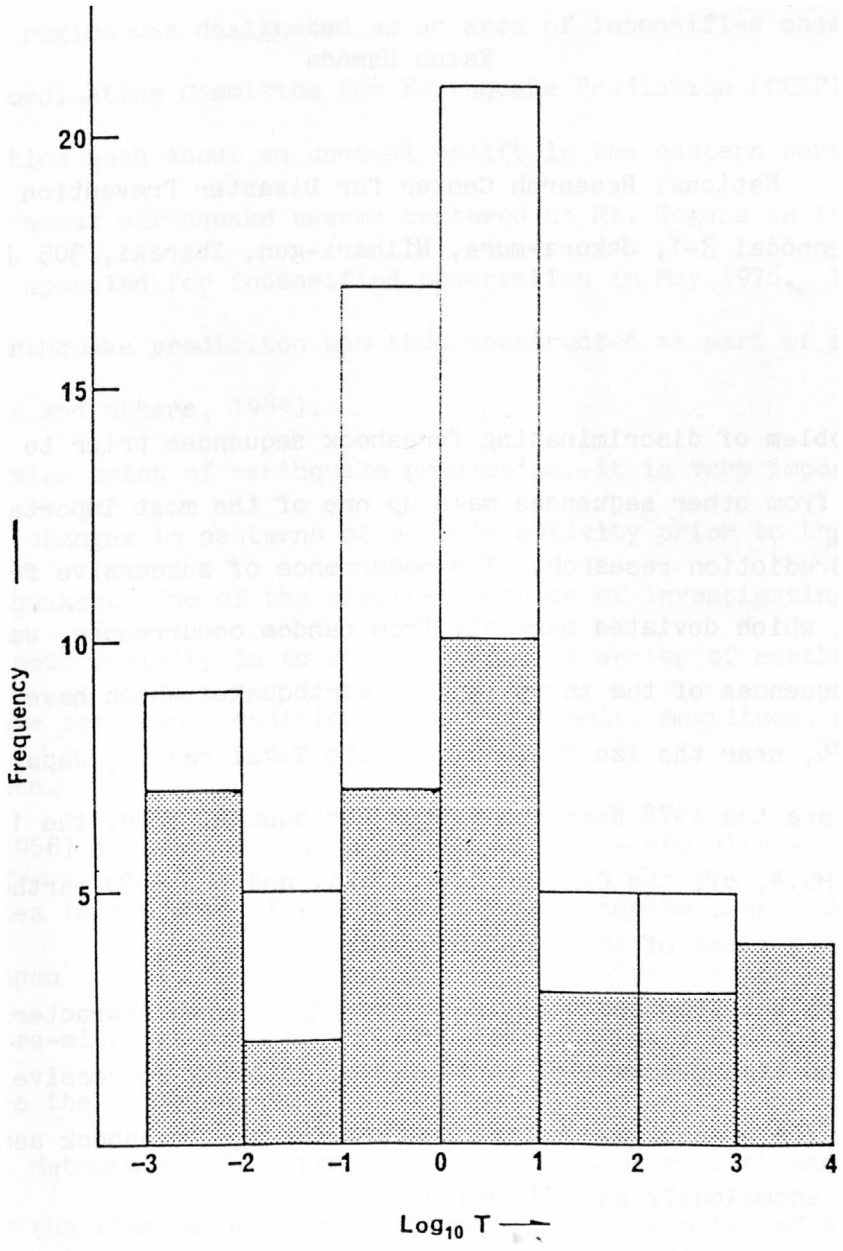

Figure 4.

THE FEATURE OF SUCCESSIVE OCCURRENCES OF FORESHOCK SEQUENCES SEEN IN RECENT MAJOR EARTHQUAKES NEAR THE IZU PENINSULA, TOKAI REGION, JAPAN

Kazuo Hamada

National Research Center for Disaster Prevention

Tennodai 3-1, Sakura-mura, Niihari-gun, Ibaraki, 305 Japan

Abstract

The problem of discriminating foreshock sequences prior to major earthquakes from other sequences make up one of the most important aspects of earthquake prediction research. The occurrence of successive foreshock occurrences, which deviated markedly from random occurrences, was found in the foreshock sequences of the three largest earthquakes which have occurred since December 1976, near the Izu Peninsula in the Tokai region, Japan. These three earthquakes are the 1978 Near Izu-Oshima Earthquake, M7.0, the 1978 earthquake, M5.4, off the Cape of Kawanazaki, and the 1980 earthquake, M6.7, off the eastern coast of the Izu Peninsula.

Matsumura has proposed a new parameter, ν , which characterizes the pattern of the time sequence of earthquakes, as being successive, random, or periodical. The present successive feature for the foreshock sequences is indicated by anomalously small ν values.

The present results lead to the suggestion that foreshocks occur and have a triggering effect at a critical stress level of breakage. The ν value seems to be one of the useful parameters for the discrimination of foreshocks in the Izu area in the Tokai region, Japan.

The seismic data analyzed were obtained by the NRCDP (National Research

Center for Disaster Prevention) network covering the Kanto-Tokai region.

Introduction

The Tokai region was designated as an area of intensified observation in 1974 by the Coordinating Committee for Earthquake Prediction (CCEP). The CCEP issued information both about an unusual uplift in the eastern part of the Izu Peninsula, and about earthquake swarms centered at Mt. Togasa in the Izu Peninsula, and appealed for intensified observation in May 1976. The NRCDP network for earthquake prediciton was thus constructed as part of a national program (Hamada and others, 1984).

From the view point of earthquake prediction, it is very important to try to detect some changes in patterns of seismic activity prior to the occurrence of major earthquakes. One of the simplest methods of investigating the pattern of seismic activity is to analyze the time series of earthquakes selected by some pertinent conditions, such as domain, magnitude, amplitude of seismograms, etc.

Hamada (1968) analyzed the time series of micro- and ultra-microearthquakes in the area of the Matsushiro earthquake swarm, Nagano Prefecture, Japan, and found that characteristic features prior to major micro- and ultra-microearthquakes occurred both intensely and intermittently a few days before the major shocks.

Recently, Matsumura (1982) proposed a new parameter which characterizes the pattern of the time sequence of earthquakes, as a monitor of some changes in seismic activity. This parameter, ν, which is closely related to apparent interaction among successive earthquakes, represents the pattern of earthquake occurrence: $\nu = 0.5$ for random occurrence, and $\nu \lesssim 0.5$ for successive and periodic occurrences, respectively. Matsumura analyzed microearthquake data observed at the Iwatsuki deep borehole observatory located at a depth of 3500

m below the surface, near Tokyo, by using the parameter ν. The results are as follows: The time sequence of the microearthquakes shows a successive pattern in terms of gross, and the ν value tends to deviate from the mean level before and after major earthquakes with a magnitude of 4 or greater. The remarkable decrease in ν started about twenty days prior to the earthquake with M6.1, which occurred on 25 September 1980.

This paper describes the time series analysis of microearthquakes recorded by the NRCDP network covering the Izu Peninsula, which was made by using the parameter ν . Features of successive occurrences indicated by anomalously small ν values such as 0.22, 0.05, and 0.06 were found before the three largest earthquakes, with M7.0, 5.4, and 6.7, respectively, which have occurred near the Izu Peninsula since the commencement of observation at the Nakaizu station (JIZ) as a part of the NRCDP network.

According to recent knowledge on seismic sources, there are many cases where a large earthquake is not simply a single event but multiple events triggered by an initial break (e.g. Kikuchi et al., 1982; Zhou et al., 1983). The Near Izu-Oshima Earthquake, M7.0, can also be separated into an initial rupture and the main rupture 6 seconds later (Shimazaki and Somerville, 1978). Therefore, successive occurrences as defined by interaction with triggering effects between successive earthquakes, might be an indication of an approaching large shock which is a multiple event.

Overview of the recent seismic activities near the Izu Peninsula

In accordance with plate tectonics, the Izu Peninsula is thought to be situated at the northern end of the Philippine Sea plate near the triple junction of the Pacific, the Asian (Eurasian) and the Philippine Sea plates, one of the most seismically active zones in and around Japan (e.g. Kasahara and Hamada, 1981). Figure 1 illustrates the long-term seismic activities

around the Izu Peninsula and the Izu Islands. There is an apparent trend of directional migration before and after a quiet period: a southwards migration occurred from 1930 to 1945, followed by a quiet period up to 1955, then by a northward migration from 1956 to the present. The most recent high seismic activities near the Izu Peninsula began with the Off Izu Peninsula Earthquake, M6.9, in 1974, breaking the relative quiescence of several tens of years after the 1930 Kita-Izu Earthquake M7.0. Figures 2 and 3 illustrate in more detail the seismic activities in and around the Izu Peninsula which have occurred since 1974 and 1980, respectively.

Data and methods of analysis

The seismic data analyzed here was recorded at the Nakaizu station (JIZ) and other stations surrounding the area which were equipped with a three-component set of velocity-type seismometers of 1 Hz (see Fig. 2). Data selection was made by a threshold level of the maximum amplitude of the seismogram, the S-P times at stations JIZ and NSI, and hypocenter locations as given in Table 1. Because the routine work of hypocenter determination of microearthquakes was started in July 1979 for the Kanto-Tokai area, data selection was made based on locations of shocks which occurred after that.

Matsumara (1982) proposed the ν value as a parameter showing the patterns of seismic activities. The following Weibull distribution is often adopted as a mathematical model of earthquake occurrence.

$$f(\tau) = \mu\tau^{p-1}\exp(-\mu\tau^{p}/p) \qquad (1)$$

Where, f is the probability of appearance of $\tau, \tilde{\tau}$ time intervals of successive earthquakes, μ a constant parameter showing seismic activity and p a parameter showing the pattern of seismic activity. According to the moment method, if the number $\tilde{\tau}$ is large, the following is derived from the equation (1).

$$\{\Gamma(1/p + 1)\}^2 / \Gamma(2/p + 1)$$
$$= (\bar{\tau})^2 / \overline{\tau^2} \equiv \nu \qquad (2)$$

The ν, which can be calculated very easily from the observed time intervals, corresponds to the p in the Weibull distribution of formula (1), as illustrated in Fig. 4. The patterns of earthquake occurrences are classified into three categories: successive, random, and periodical, corresponding to three ranges of ν, $0 < \nu < 0.5$, $\nu = 0.5$, and $0.5 < \nu < 1.0$, respectively. The present method of analysis is the calculation of ν values based on formula (2), that is, the ratio of square of the mean τ to the mean of squared τ, where τ is the time inteval between successive earthquakes selected by certain conditions.

Variation of the ν value prior to major earthquakes

The Near Izu-Oshima Earthquake, M7.0, of 14 January 1978, is the largest event ever observed by the present NRCDP network near the Izu Peninsula. The ν value and the number of earthquakes before and after this event were examined and illustrated in Fig. 5.

There are remarkable foreshocks which started at 8:00 a.m. 4 hours before the main shock, as seen in Fig. 5-C. An anomalously small ν value was found for this foreshock sequence, as seen in Fig. 5-A. The ν value was calculated according to formula (2), using the number of shocks counted at station JIZ in the Izu Peninsula about 30 km from the foreshock zone, which is located at the east end of the aftershock zone near the Izu-Oshima Island, as illustrated in Fig. 2. The foreshock sequence is illustrated in more detail with an extended time scale in Fig. 6, where black circles represent small or medium sized shocks reported from JMA and magnitudes are shown by numerals. White circles represent primarily the microearthquakes counted at station JIZ, which were used for the calculation of ν value of the foreshock sequence.

The number of the foreshocks per unit time interval was examined by comparing them with those in the case of the random model. The seismic data shown in Fig. 6 was also used for this examination. It is well known that if the earthquake occurrence is random, the distribution of the number of shocks per unit time interval shows a Poisson distribution.

Figure 7 shows the results of the comparison of the foreshocks. As seen in the figure, foreshock occurrences are intermittent and concentrated in comparison with random occurrences. The number of cases in which the number of shocks is zero per 5 minutes is 4 times that expected from random occurrences. Simultaneously, the number of cases in which the number of shocks is 7 or more per 5 minutes is about 10 times that expected from random occurrence. Such an earthquake occurrence pattern is quantitatively indicated by one paramater of 0.224. Such a small ν value is certainly meaningful. Matsumura (1982) made a numerical experiment to examine the ν value distribution for random occurrences. According to his experiment, the number of cases out of 10,000 in which ν is less than 0.3 is zero when earthquake occurrence is random and ν value is calculated from 100 shocks.

An earthquake swarm commenced on November 14, 1978 off the Cape of Kawanazaki, about 20 km east from the nearest station JIZ, and lasted until the end of December, 1978. The largest earthquake in this sequence, the Kawanazaki-Oki Earthquake, M5.4, occurred on December 3, 1978. It is the third largest shock ever observed by the present NRCDP network.

Calculated ν values before and after the above sequence are illustrated in Fig. 8. The ν value was calculated from 50 successive shocks. Using the window method with 25 successive shocks, calculated values were plotted at the time of the last event that was used for the calculation. After the commencement of the swarm, the moving window was used for 50 shocks because of

the large number of shocks. The number of time intervals between successive shocks is constant, accordingly the total time intervals are not constant. The average total time interval for 50 shocks was about 10 days until the middle of November, and a few days or within one day only after the commencement of the swarm. The mean value of all ν is 0.339 with a standard deviation of 0.138. An anomalous decrease down to 0.05 in ν value ws found at the beginning of the swarm and then ν values fluctuated largely between 0.1 and 0.6 before the main shock of M5.4. Such a quick decrease in ν value followed by a large fluctuation before the main shock are characteristic features of this swarm.

An earthquake swarm commenced on June 25, 1980, off the eastern coast of the Izu Peninsula, and lasted until September, 1980, including the main event, the Izu-Huanto-Toho-Oki Earthquake, M6.7, on June 29 (see Fig. 2). This M6.7 event is the second largest one ever observed by the present NRCDP network.

Recent ν values up to the present, including the M6.7 event above, were examined and the results are illustrated in Fig. 9. The NRCDP started the routine work of hypocenter determination in July, 1979. Accordingly, hypocenter data was used for the calculation of ν value in Fig 9 under the conditions of data selection given in Table 1. The ν value in the figure was calculated from 50 shocks. Moving the window by 5 shocks, calculated ν values were plotted at the time of the last event. There are two remarkable earthquake sequences in June-September, 1980 and January, 1983. The largest shocks are the M6.7 event in the former sequence, and the M4.4 event in the later one, as shown in the figure. There are remarkable decreases in ν value at the beginning of the two earthquake sequences which are followed by major shocks and large fluctuations of ν value. Rapid decrease in ν value also appears in May and September, 1982, corresponding to small swarms off the Cape

of Kawanazaki which do not include major shocks of M4 or above.

Figure 10 shows the number of earthquakes per hour counted at station NSI in the Izu Peninsula (see Fig. 2) and the ν value calculated from these events prior to the Izu-Hanto-Toho-oki Earthquake in 1980. An unusually small ν value of 0.05 before the major event is consistent with the anomalously small ν value in the same period as shown in Fig. 9.

Conclusion

Patterns of seismic activities in the Izu Peninsula area in the Tokai region, Japan were examined by using the ν value proposed by Matsumura (1982). Events from 1977 through 1983 were used with particular interst in the three largest events: the 1978 Near Izu-Oshima Earthquake M7.0, the 1978 Kawanazaki-Oki Earthquake M5.4, and the 1980 Izu-Hanto-Toho-Oki Earthquake M6.7. Concluding remarks are as follows:

1) The above three major shocks were accomplished by obvious foreshocks or precursory earthquake sequences which occurred 4 hours to 9 days before the major shocks.

2) These foreshocks and precursory sequences hve a particular feature: successive characteristics indicated by anomalously small ν values.

3) Anomalous decrease in ν value was found 6 times from October, 1977 through October, 1983. In 4 of the 6 cases, earthquakes with M4.0 and above occurred within 9 days from the commencement of the unusual decrease.

References

Hamada, K. (1968). Ultra mirco-earthquakes in the area around Matsushiro, Bull. Earthq. Res. Inst. 35, 271-318.

Hamada, K. M. Ohtake, Y. Okada, S. Matsumura, and H. Sato (1984). A high quality digital network for microearthquake and ground tilt observations in the Kanto-Tokai area, Japan, presented at the US-Japn

Seminar on Practical Approaches to Earthquake Prediction and Warning held in Tokyo and Tsukuba, Japan in 1983, and submitted to ERP earthquake prediction research.

Kasahara, K., and K. Hamada (1981). A plate model consistent with the tectonics of the Kanto-Tokai area, Japan, Proceedings of the 2nd Joint Meeting the U.J.N.R. Panel on Earthquake Prediction Technology, U.S. Geological Survey Open File Rep. 82-180, 85-97.

Kikuchi, M. and H. Kanamori (1982). Inversion of coupled body waves, Bull. Seism. Soc. Am. 72, 491-506.

Matsumura, S. (1982). One-parameter expression of earthquake sequence and its application to earthquake prediction, J. Seism. Soc. Japan Second Series 35, 65-76.

Shimazaki, K. and P. Somerville (1978). Sumary of the static and dynamic parameters of the Izu-Oshima Kinkai earthquake of January 14, 1978, Bull. Earthq. Res. Inst. 53, 613-628.

Zhou, H., C. R. Allen, and H. Kanamori (1983). Rupture complexity of the 1970 Tahghai and 1973 Luhuo earthquakes, China, from P-wave inversion, and relationship to surface faulting, Bull. Seism. Soc. Am. 73, 1583-1597.

Figure captions

Fig. 1. Long-term seismic activities around the Izu Peninsula and the Izu Islands. Hypocenter locations and magnitudes are taken from the JMA bulletin.

M: earthquake magnitude, H: focal depth.

Fig. 2. Epicenters of major earthquakes, aftershock area, and swarm area after the Off Izu Peninsula Earthquake of 1974 (after JMA). Black circles denote seismic stations of the NRCDP net.

X: epicenters of major earthquakes

1. Off Izu Peninsula Earthquake, 1974, M6.9
2. Kawazu Earthquake, 1976, M5.4
3. Near Izu Oshima Earthquake, 1978, M7.0
4. Earthquake swarm off the Cape of Kawanazaki, 1978, M5.4 *Kawanazaki-Oki Earthquake)
5. Earthquake swarm off the eastern coast of the Izu Peninsula, 1980, 1980, M6.7 (Izu-Hanto-Toho-Oki Earthquake)

Fig. 3. Recent seismic activities in and around the Izu Peninsula. Hypocentral locations and magnitudes are taken from the NRCDP bulletin. Detection capability was not constant but inreased during this period, according to the establishment of additional stations. N: number of earthquakes plotted.

Fig. 4. Relation between ν value and p value. The Earthquake occurrence pattern is classified into three categories: periodical, random, and successive, corresponding to three rangs of p value, $p>1$, $p=1$, and $p<1$, respectively. When the data is finite, such as n=50 or 100, the mean of ν value becomes slightly higher than that calculated from equation (2) (after Matsumura, 1982).

Fig. 5. The ν value calculated from seismic records at station JIZ and the number of shocks befor and after the 1978 Near Izu Oshima Earthquake M7.0.

A: ν values and the number of shocks n nused for the calculation are as follows:

Oct, 1977	=.348	n=103	
Nov, 1977	.437	129	
1 Dec 1977 - 13 Jan 1978	.492	80	
8:00 - 12:00 a.m. 14 Jan 1978	.224	132	Open circle
0:00 - 5:00 a.m. 16 Jan 1978	.419	150	Solid circle
1-21 Mar 1978	.335	241	

B: Daily number of shocks counted at station JIZ. The daily number is omitted for the period Jan 14 through the end of February because the shocks were countless.

C: Number of felt shocks every 10 minutes reported from the JMA Oshima Weather Station. Numerals indicate intensity on the JMA scale. Pronounced foreshocks occurred from 8:00 a.m. 4 hours before the main shock at 12:24 14 Jan 1978.

Fig. 6. Foreshock sequence of the 1978 Near Izu-Oshima Earthquake counted at station JIZ. One white circle denotes one earthquake. Black circles with magnitudes indicated by numerals aretaken from the JMA bulletin.

Fig 7. Distribution of the number of the foreshocks of the 1978 Near Izu-Oshima Earthquake in 5 minutes, compared with the Poisson distribution of the random model. The data shown in Fig. 6 was analyzed here.

X: number of the foreshocks in 5 minutes for 8:00 - 12:25 14 Jan 1978.

N: frequency of x

Expected frequencies are calculated, assuming Poisson distribution. It

is clearly seen that the foreshock occurrence is intermittent and concentrated.

Fig. 8. The ν value calculated from seismic records at station JIZ. The ν value was calculated from 50 shocks. Moving the window by 25 shocks, calculated values were plotted at the time of the last event that was used for the calculation. After November 25, the window was moved by 50 shocks because of the large number of shocks which occurred off the Cape of Kawanazaki.

Fig. 9. The ν value calculated from hypocentral data in the NRCDP bulletin. The ν value was calculated from 50 successive shocks which occurred within the limited domain as given in Table 1. Moving the window by 5 shocks, calculated ν values were plotted at the time of the last event that was used for the calculation. The mean ν value is 0.323, with a standard deviation of 0.150.

Fig. 10. Number of shocks per hour and ν values calculated from seismic records at station NSI before the Izu-Hanto-Toho-Oki Earthquake, M6.7. The number of shocks after the main event is omitted because the shocks were countless. An anomalously small ν value of 0.05 is consistent with that in the same period shown in Fig. 9.

Table 1. List of data used for the ν value calculation.

Number	Period	Conditions for data selection
1	October 1977-March 1978	1. S-P times at JIZ $<$10 sec 2. The maximum amplitude at JIZ $>$ 4 mm p-p(107μkine)
2	July-December 1978	1. S-P times at JIZ $<$ 10 sec 2. The maximum amplitude at JIZ $>$ 4 mm p-p(107μkine)
3	July 1979-October 1983	Hypocenter locations are taken from the NRCDP bulletin regardless of magnitudes under the following conditions. 1. $34.5° \leq$ LA $\leq 35.3°$N 2. $138.7° \leq$ LN $\leq 139.5°$E 3. $0 \leq$ H ≤ 30 km Where,LA,LN,and H are latitudes, longitudes, and depths of hypocenters, respectively.
4	June 1980	1. S-P times at NSI $<$ 10 sec 2. The maximum amplitude at NSI $>$ 4 mm p-p(142μkine)

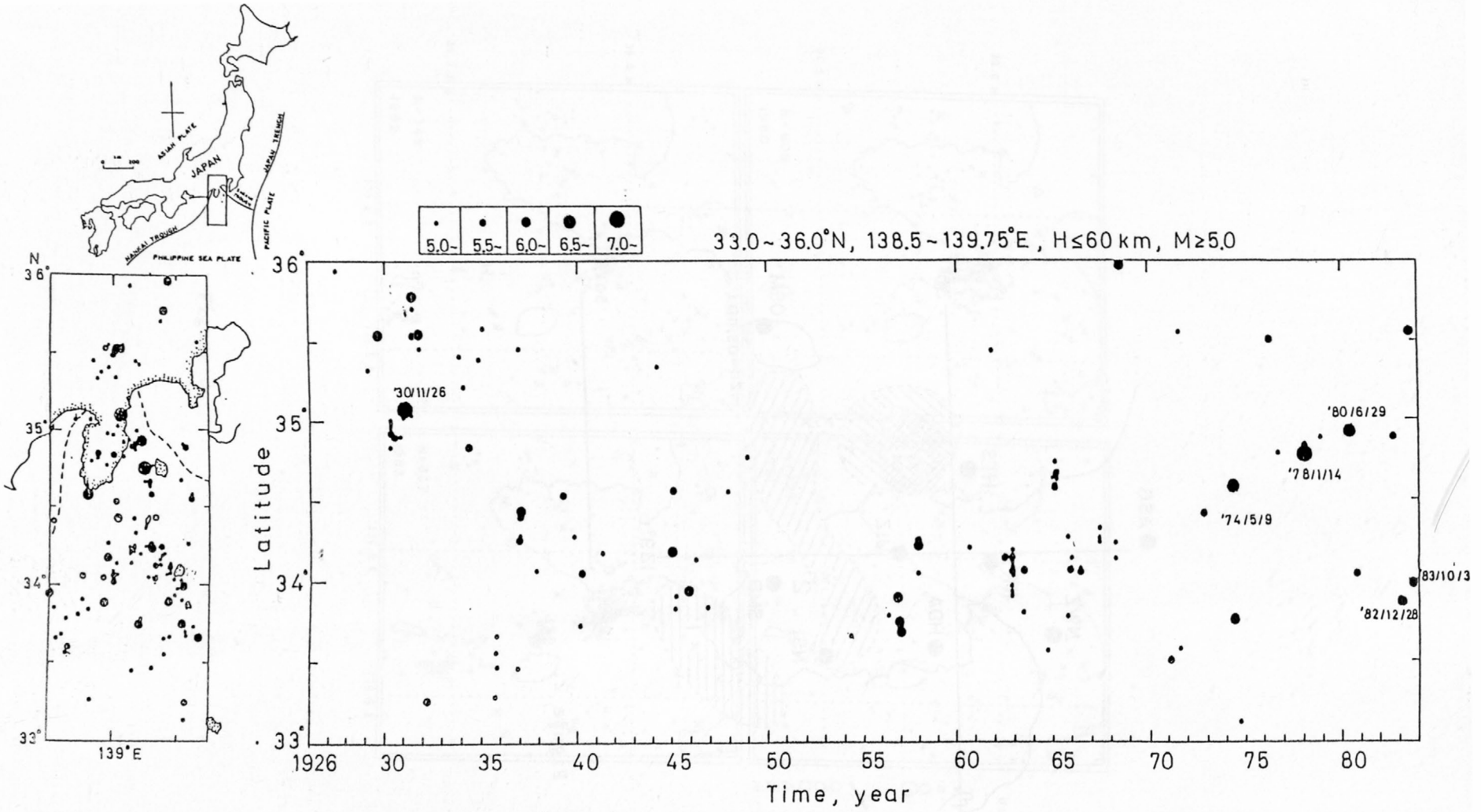

FIG. 1

Figure 1.

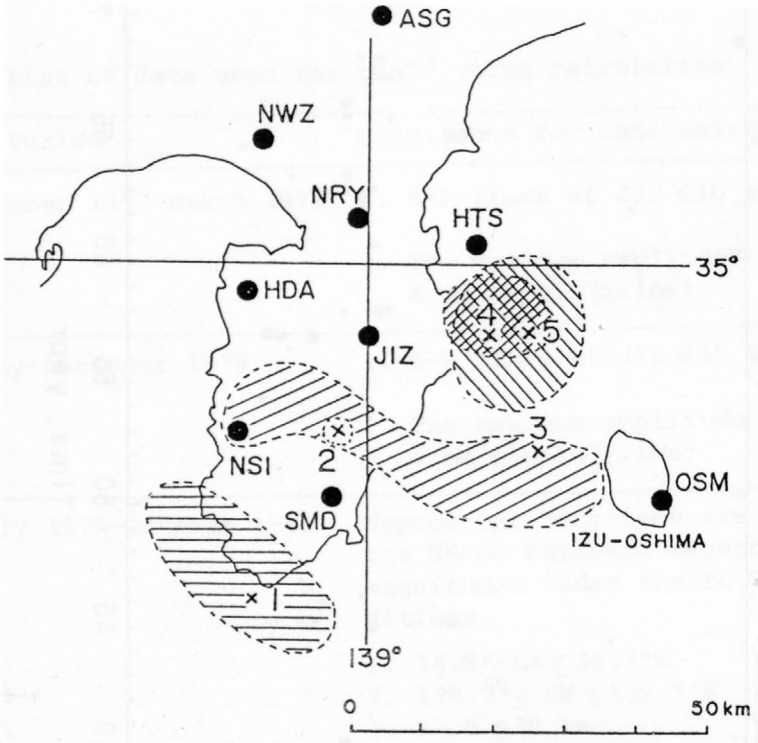
ASG
NWZ
NRY
HTS
35°
HDA
JIZ
4
5
3
NSI
2
OSM
SMD
IZU-OSHIMA
1
139°
0
50km

Figure 2.

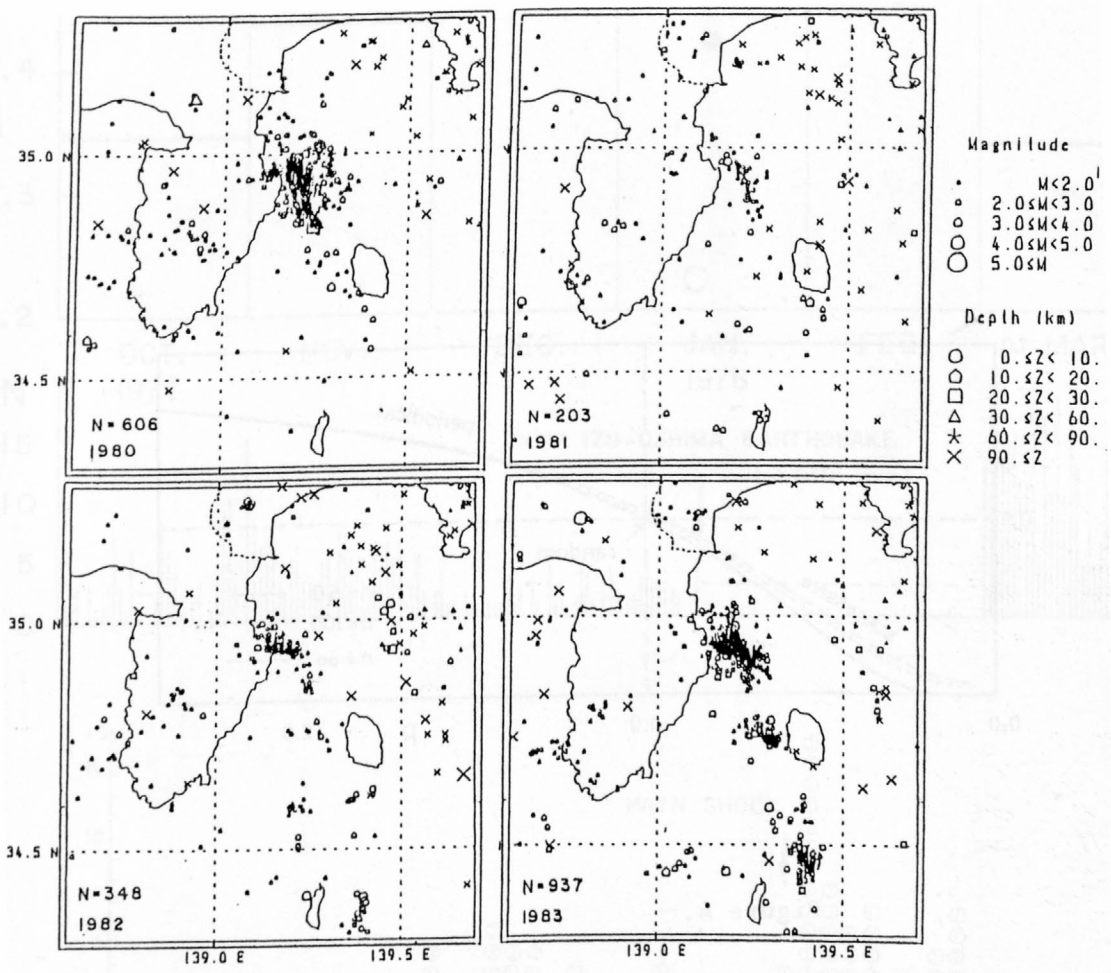
35.0 N
34.5 N
N=606
1980
N=203
1981
N=348
1982
N=937
1983
139.0 E
139.5 E
Magnitude
M<2.0
2.0≤M<3.0
3.0≤M<4.0
4.0≤M<5.0
5.0≤M
Depth (km)
0.≤Z< 10.
10.≤Z< 20.
20.≤Z< 30.
30.≤Z< 60.
60.≤Z< 90.
90.≤Z

Figure 3.

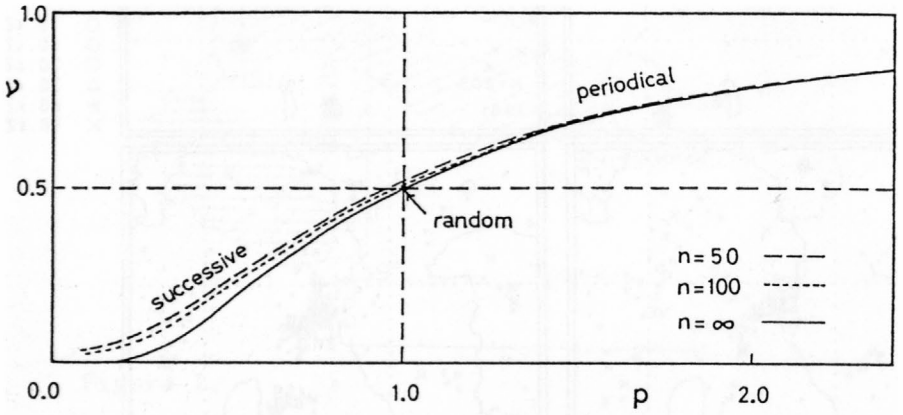

Figure 4.

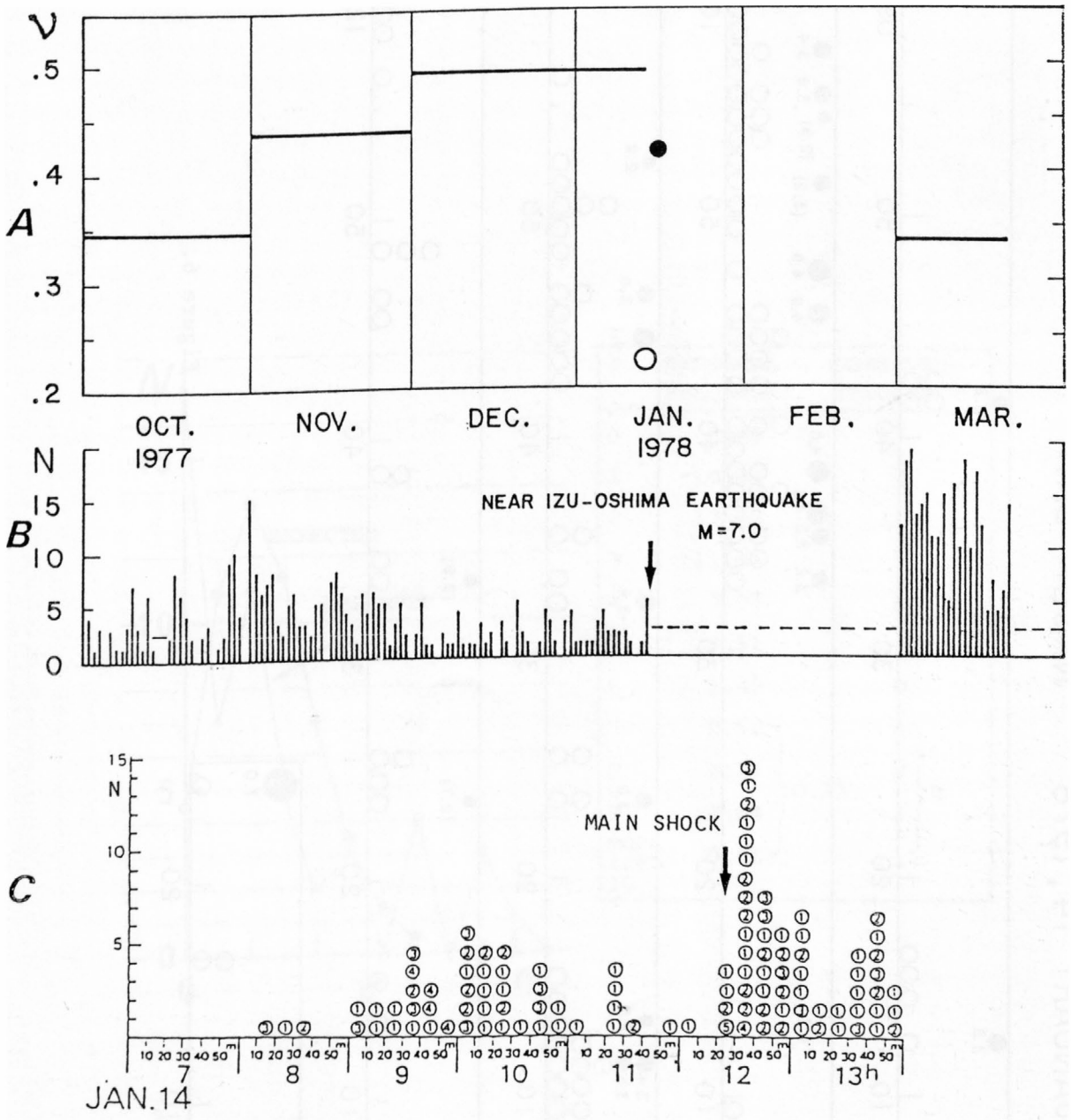
A
ν
.5
.4
.3
.2
OCT.
1977
NOV.
DEC.
JAN.
1978
FEB.
MAR.
B
N
15
10
5
0
NEAR IZU-OSHIMA EARTHQUAKE
M=7.0
C
15
N
10
5
MAIN SHOCK
7
8
9
10
11
12
13h
JAN.14

Figure 5.

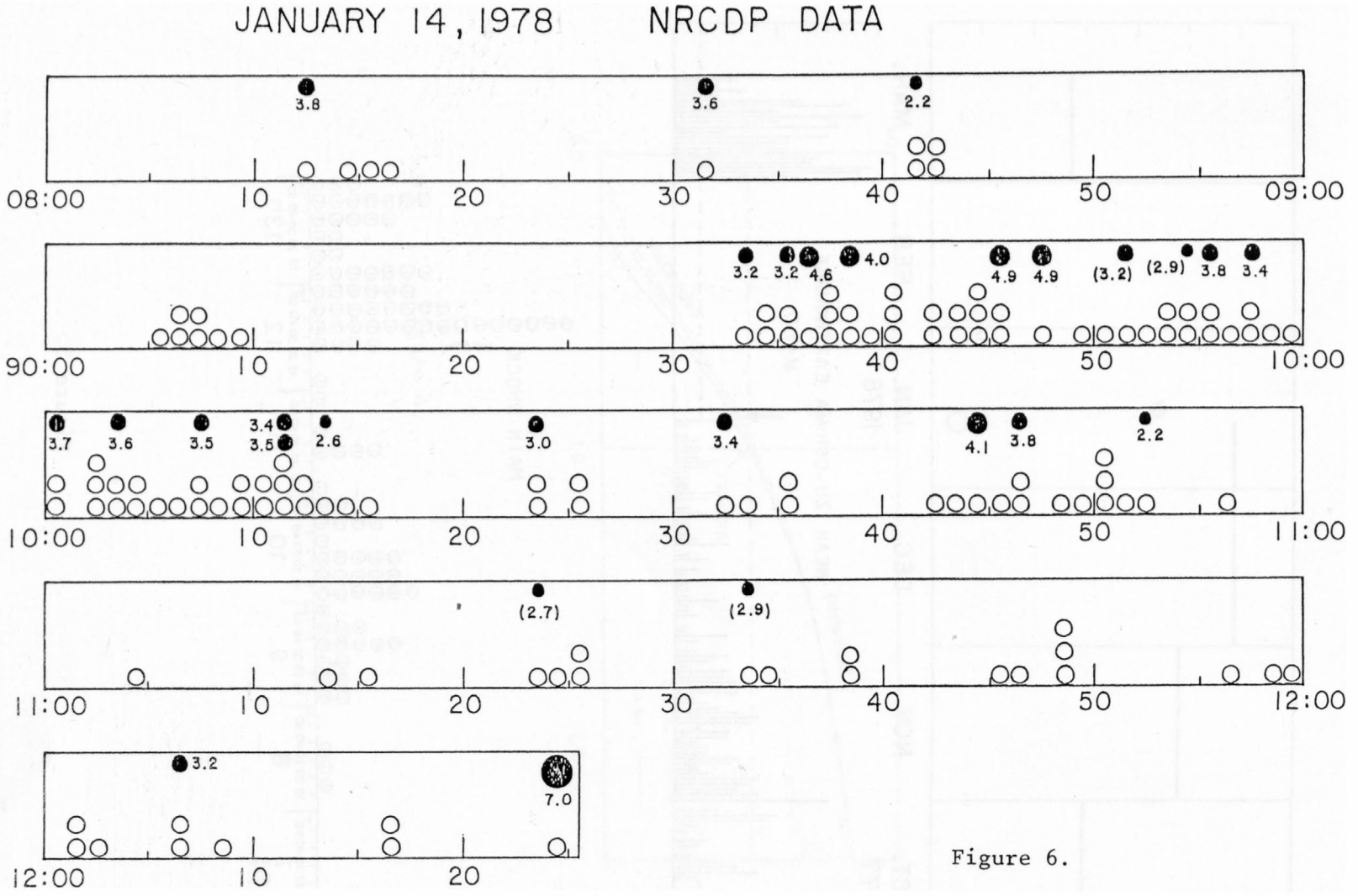
JANUARY 14, 1978 NRCDP DATA
3.8
3.6
2.2
08:00
10
20
30
40
50
09:00
3.2
3.2
4.6
4.0
4.9
4.9
(3.2)
(2.9)
3.8
3.4
90:00
10
20
30
40
50
10:00
3.7
3.6
3.5
3.4
3.5
2.6
3.0
3.4
4.1
3.8
2.2
10:00
10
20
30
40
50
11:00
(2.7)
(2.9)
11:00
10
20
30
40
50
12:00
3.2
7.0
12:00
10
20

Figure 6.

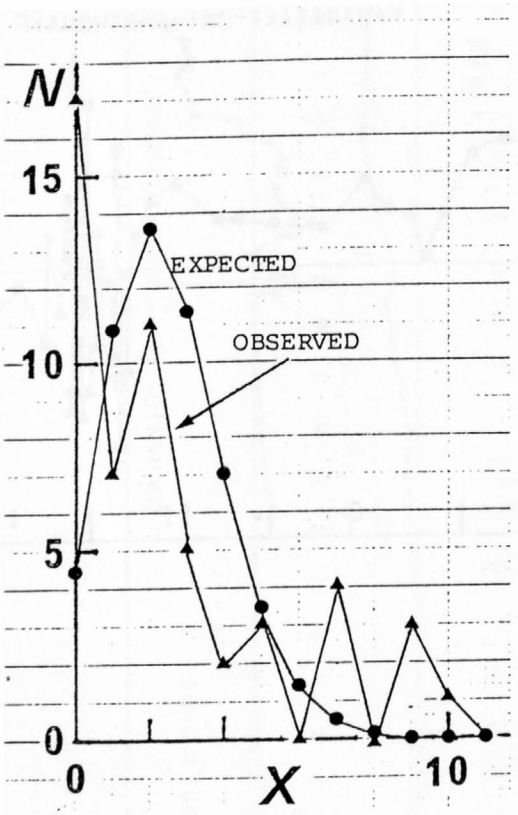

X	EXPECTED FREQUENCY		OBSERVED FREQUENCY	
0	4.39		17	
1	10.94		7	
2	13.62		11	
3	11.31		5	
4	7.04		2	
5	3.51		3	
6	1.45		0	
7	0.52		4	
8	0.16	0.73	0	8
9	0.04		3	
more than 10	0.01		1	

Figure 7.

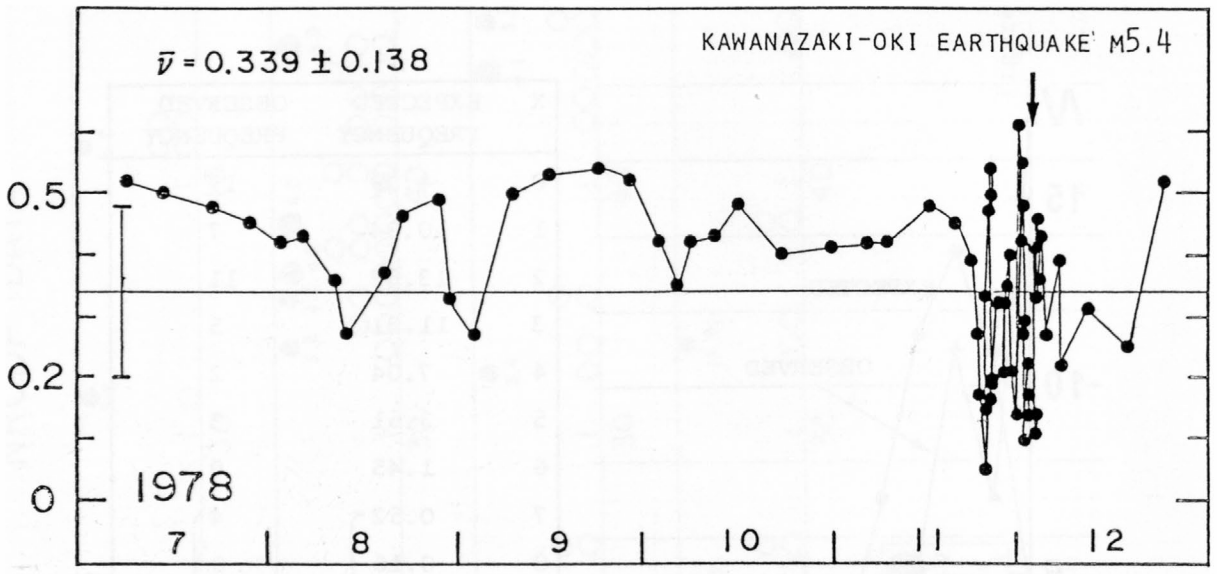
$\bar{\nu}$ = 0.339 ± 0.138
KAWANAZAKI-OKI EARTHQUAKE M5.4
0.5
0.2
0
1978
7
8
9
10
11
12

Figure 8.

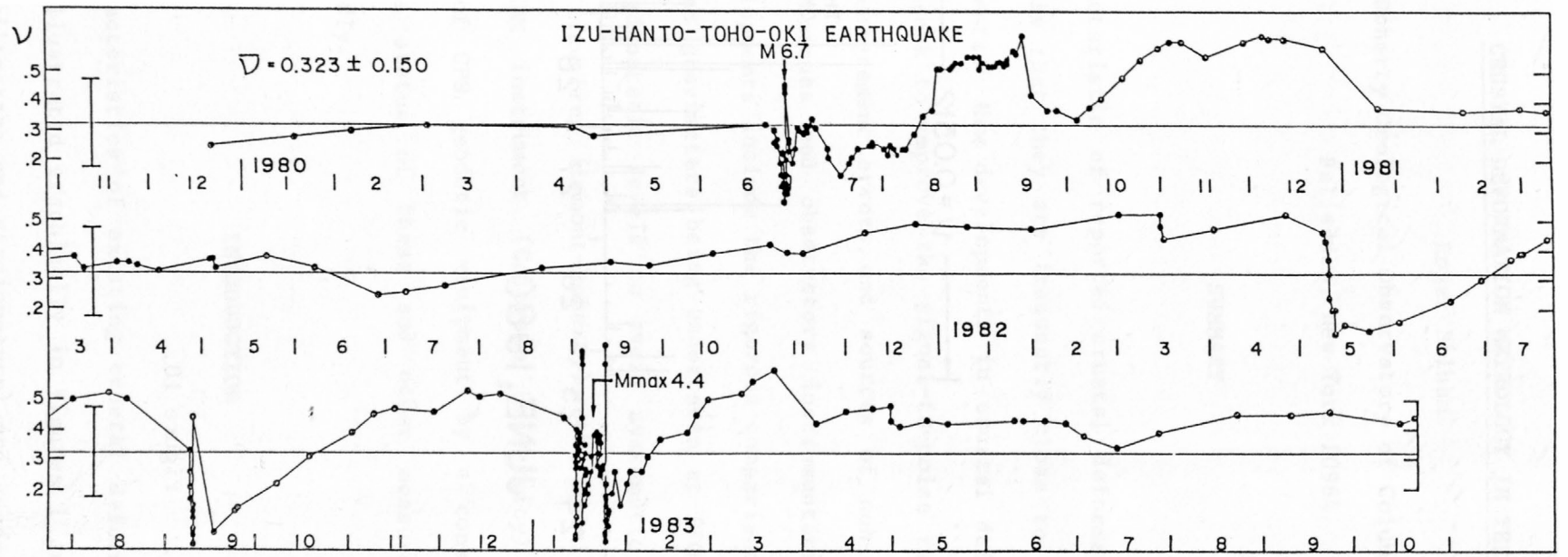
ν
IZU-HANTO-TOHO-OKI EARTHQUAKE
M6.7
$\bar{\nu}$ = 0.323 ± 0.150
.5
.4
.3
.2
1980
1981
1982
1983
Mmax 4.4

Figure 9.

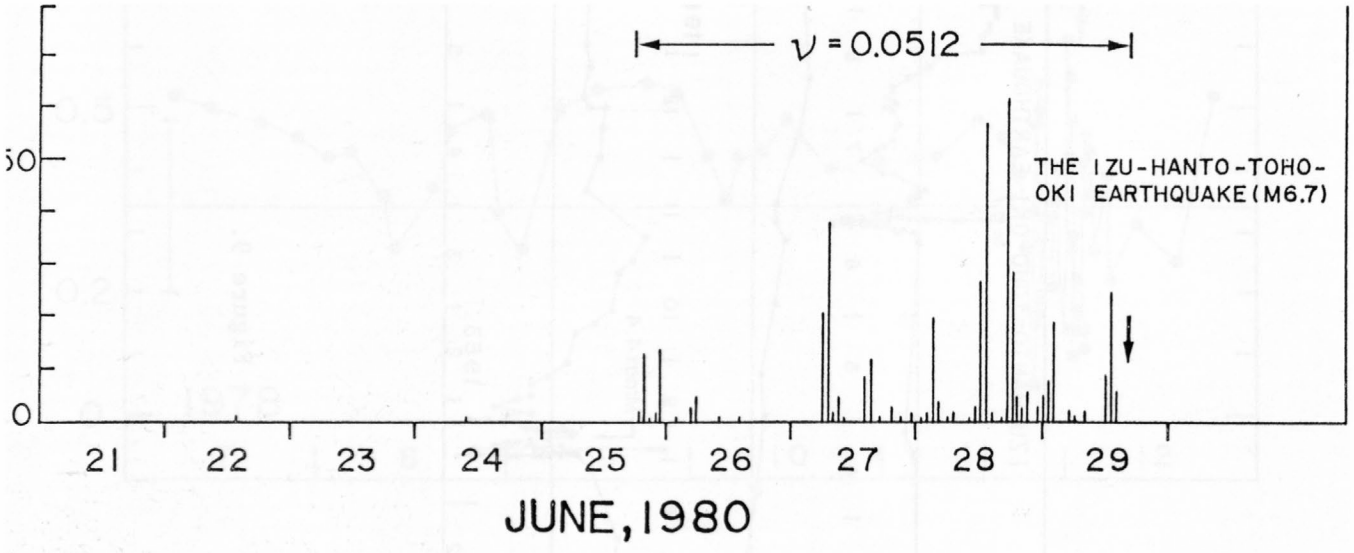
ν = 0.0512
THE IZU-HANTO-TOHO-
OKI EARTHQUAKE (M6.7)
50
0
21
22
23
24
25
26
27
28
29
JUNE, 1980

Figure 10.

CRUSTAL DEFORMATION METROLOGY IN THE U.S.

Roger Bilham

Lamont-Doherty Geological Observatory of Columbia University

Palisades, New York 10964

SUMMARY

A characteristic of reported crustal deformation precursors to earthquakes is that they are frequently close to the noise level in the measurements. New developments in crustal deformation metrology in the U.S. seek to improve the signal-to-noise ratio by suppressing systematic measurement errors and sources of non-tectonic signal in geodetic techniques and observatory instrumentation. Examples of current developments include the rigorous comparison of extensometers, tiltmeters and gravimeters being undertaken at PFO (IGPP), the development of hydrostatic levels to avoid systematic errors associated with optical leveling (Lamont-Doherty), the development of a three wavelength EDM instrument (Colorado University) and the planned acquisition of GPS geodetic equipment by a consortium of universities. The status of these and other measurement systems are reviewed briefly.

INTRODUCTION

The characteristics of existing crustal deformation measurement systems are illustrated graphically in Figures 1 and 2. Observatory instruments (tiltmeters and strainmeters) and geodetic techniques are

plotted as a function of observation baseline and resolution under optimum conditions (independent of measurement period). Note that short baseline instruments measure long wavelength signals but that the reverse is not possible without spatial aliasing of the signal. This observation forms the basis of perhaps the single most important method for suppressing short-wavelength signals of non-tectonic origin. Short wavelength signals are known to be large in the near-surface and instruments in such locations tend to be most successful if they are several hundreds of meters long. Experiments designed to quantify the dependence of instrument noise level on baseline length are difficult to conceive that are not also site dependent. A significant series of experiments are being undertaken at Pinon Flats Observatory in California in which extensometers and tiltmeters of different design, baseline length and depth of burial are being intercompared. The observatory is operated by the University of California, San Diego (IGPP) but the site has recently become a proving ground for new instrumentation developed by many other investigations (Wyatt and Agnew, 1984). Of the numerous instruments being investigated the most stable at present are the 530 m long Michelson waterpipe tiltmeters and the 800 m laser strainmeters (Berger and Lovberg, 1974). Using these as "best-case" instruments it is possible to plot the performance of observatory instruments on diagrams similar to Figures 1 and 2 with the inclusion of estimates of noise-level/frequency dependence. Figure 3 shows a composite plot where the noise levels of tilt and strain instrumentation on the left-hand side of the diagram are estimated at hourly, daily and yearly periods. Clearly such estimates are approximate but they do illustrate some of

the basic difficulties encountered in monitoring earthquake related signals with amplitudes of the order of a part in 10^{-7} or less.

It is evident from Figure 3 that the precision of the most advanced geodetic measurement systems and the most stable observatory installations for the measurement of crustal deformation are approximately equivalent at periods around one year. At shorter periods, water-tube tiltmeters, laser extensometers and cryogenic gravimeters exhibit superior resolution and at longer periods space-based geodetic methods, absolute measurements of the acceleration due to graivity, electromagnetic multiwavelength distance measurements and first-order leveling provide superior long term stability. Wyatt and Agnew (1984) have recently derived numerical estimates for equivalent noise levels for geodetic and instrumental data at PFO that provide a quantitative justification for the temporal noise estimates in Figure 3.

Also plotted on Figure 3 are regions typical of coseismic strains anticipated from the rupture of crustal materials and typical annual strain signals anticipated from linear interseismic strain accumulation. An important assumption in earthquake prediction studies is that the seismic process is non-linear with time since otherwise tectonic signals would be inaccessible to observatory instruments. It is evident that non-linear strain accumulation must occur in order to account for the numerous large amplitude strain precursors reported in the literature (Bilham, 1981). These strain precursors lie between the extremes of coseismic and interseismic strain, in many cases close to the noise level of existing crustal deformation measurements.

The marginal signal-to-noise ratio of reported strain precursors has stimulated a number of investigators to examine the possiblility

of improving the basic tools available to the earthquake prediction community. A number of specific developments are summarised in the following pages.

TILTMETERS

There are three principal developments in tiltmeter instrumentation occurring presently in the U.S. Long baseline tiltmeters are being tested by IGPP (Wyatt and Agnew, 1984) and LDGO (Bilham et al., 1979) at Pinon Flats Observatory, borehole tiltmeters based on mechanical pendulums are being tested by Colorado Uninversity (Levine, Meertens and Harrison, 1981) and improved methods of implanting bubble-tiltmeters are being actively pursued by St. Louis University (Morrisey, 1983) and the USGS, Menlo Park. Present borehole tiltmeter developments are concentrating on 30 m deep or shallower deployment.

Although the results from deep borehole implantation of mechanical pendulums are encouraging, data from such installations have yet to demonstrate stabilities comparable to that exhibited by long baseline instruments. Analysis of recent data from the two Michelson tiltmeters at PFO shows that the instruments track to within a few tenths of a microradian at periods of less than 15 months (Figure 4a). The signal-to-noise ratio close to tidal periods is greater than 40 db for deep borehole tiltmeters (Levine, personal communication) and for the PFO Michelson tiltmeters (Wyatt and Agnew, 1984). An innovative form of tiltmeter using a central-pressure transducer (Horsfall and King, 1979) that shares the same end mounts as the LDGO tiltmeter exhibits similar long term stability but much reduced

signal-to-noise ratio at tidal periods largely due to a significant temperature dependence of uncertain origin.

The 532 m long tiltmeters at PFO are referred to 26 m deep layers below each measurement pier using vertical extensometers. Despite the fact that end measurement piers are excavated into a granite subsurface the effects of rainfall are significant and unpredictable. Figure 4b illustrates the observed surface vertical displacement signal relative to the base of the 26 m boreholes following heavy rain, a signal that has been removed from the data shown in Figure 4a.

Of more concern is the discovery reported by Evans and Wyatt (1984) that borehole fluid pressurisation can cause widespread deformation at PFO. The discovery was noted during the pressurised purging of boreholes for volume dilatometer deployment. A fractured zone encountered at 100 m depth is held responsible for a bladder-like distension that resulted in surface elevations of tens of microns in addition to horizontal displacements, tilts and vertical strains extending to distances of more than 100 m from the borehohle. Should such fractures be common it may be necessary to employ much deeper end-reference extensometers in future installations in order to avoid certain types of hydraulic noise.

The Michelson tiltmeters at PFO both use interferometric sensors that provide good precision but require frequent attention. New mechanical water-height sensors are being tested to provide systems for remote unattended deployment.

LASER EXTENSOMETERS

There is little doubt that the use of stabilised lasers in evacuated paths provides the most stable form of extensometer presently available for surface deployment. The observed stability and noise levels of these instruments approach those exhibited by deep quartz-tube extensometers (Beavan and Bilham, 1979). Additions to the PFO extensometers by IGPP personnel have lead to some striking improvements in the attachment of the extensometer and mounts to deeper, presumably more stable lithology. A seasonal strain signal of the order of 0.5 microstrain is superimposed on much of the data acquired at PFO despite the correction of the data for surface displacements in the upper 25 m. The long term signals monitored by the extensometers are of the order of 0.1 microstrain per year in approximate agreement with geodetic data in the region (Wyatt and Agnew, 1984). The observed improvement in data corrected for near-surface noise suggests that deeper end-reference piers might suppress residual noise signals further.

CARBON-FIBER EXTENSOMETERS

Wire strainmeters using carbon-fiber length standards (King and Bilham, 1976) have met with limited application in the U.S. due to the comparative rarity of suitable underground sites in areas of tectonic interest. A network of 20 m long carbon-fiber extensometers have been operated for a number of years by USC (Leary, 1983) in abandoned gold mines in the mountains north and east of Los Angeles. The shallow

depth of these mines result in annual thermoelastic signals of a few microradians. An array of water-filled carbon-fiber extensometers was installed in the Yakataga seismic gap following the St. Elias earthquake of 1979. Noise levels in the 2 m deep surface excavations were found to be far too high for reliable monitoring of precursory signals. The long term stability of carbon-fiber extensometers is thought to be better than 1 microstrain per year.

Considerably more successful has been the installation of carbon-fiber extensometers in fault-crossing observatories in the PRC. In Figure 3 a region of precursory deformation is highlighted of short wavelength and comparatively large signal strength. This region represents observations reported by Chinese (Wu and Han, 1981) and Soviet scientists concerning large precursory signals observed across block-boundary faults at remote distances from the epicenter. Measurements across fault zones demand less instrument stability than those within homogeneous stiffer materials where tectonic signals are diminished in amplitude (Bilham and Beavan, 1979). Fault zones appear to behave as "strain telescopes".

The PRC experiments conducted by LDGO in conjunction with the State Seismological Bureau, Beijing, are aimed at improving their existing quartz-tube extensometers through side-by-side comparison with carbon-fiber extensometers in the same site. We have made considerable progress in suppressing thermoelastic and thermal signals in long period data from two sites (Niuguyou and Dahuichang) by the expedient of using data acquired in the early morning only. Although this limits the bandwidth of the data it enables valuable existing long period data from these and similar sites to be reprocessed in studies of the major earthquakes of the last two decades.

BOREHOLE STRAINMETERS

Borehole dilatometers (Sacks, 1978) and borehole strainmeters designed by Gladwin (University of Queensland) have been installed in PFO for evaluation against the long-baseline instrumentation. Initial results indicate settlement drift on both types of borehole instrument of more than 3 microstrain per year. The shear strain components derived from the three component Queensland extensometers show relatively low drift compared to the dilatation signal. The symmetrical drift-rates exhibited soon after installation by all three components of the strain tensor show this to be a promising new tool for monitoring crustal shear in deep boreholes.

LEVELING

First-order leveling is potentially one of the most useful methods to monitor crustal deformation since the distance between benchmarks (1-5 km) reduces the spatial aliasing of deformation signals. Its usefulness is marred by known systematic errors in leveling mountainous terrain and by the relatively high cost and slow rate of traverse compared to other geodetic techniques. Empirical methods to correct for height dependent errors have met with partial success (Holdahl, 1983), but the errors associated with measurements in regions of high relief can exceed several cm per vertical km. LDGO personnel are developing a hydrostatic level that avoids systematic height-dependenet errors by thermally-controlling the density of the measurement fluid to one part per million (Figure 6). Using water

close to its maximum density demands that the temperature of the system must be maintained to within 0.3°C of 3.98°C (Figure 6). Height measurements are made by determining the pressure developed at each end of the fluid tube. Since no fluid flow occurs within the measurement-tube the measurement process is rapid and, given a 100 m-300 m long measurement-tube, we anticipate that hydrostatic leveling will be faster as well as more accurate than optical leveling.

In the prototype 10 m long device we have developed a suitable counter-flow heat exchanger system that enables us to maintain the temperature of the fluid tube well within the prescribed temperature requirements. Analytical models demonstrate that the same system applied to a 150 m tube will be able to retain adequate thermal control given 50°C outside temperatures. The measurement system in the prototype is controlled by a portable computer that logs ambient conditions and internal parameters continuously.

We have obtained accuracies of several tenths of a mm in repeatability tests over vertical ranges of up to 2 m, which is substantially worse than our design goal of 50 microns accuracy over a 5 m range. The source of these errors appears to be hysteresis in the Paroscientific measurement transducers, whose dynamic range is being exploited to the limit in this application. An unexpected source of noise is that the instrument is very sensitive to movement of the pressure tube during measurement. If this problem cannot be overcome it might exclude the level from being used to transfer vertical datums across river bridges, one of the potential applications of a successful hydrostatic level. Given present single set-up accuracy

limitations, a field-operational level might have to be several hundred meters long in order to compete in accuracy with optical-leveling. In these circumstances the cumulative random errors introduced per km by the two leveling techniques appear to be comparable. We are continuing to examine ways of improving accuracy in the prototype prior to construction of a longer device.

UNIVERSITY GPS CONSORTIUM

Seven university groups have recently submitted a major proposal to the National Science Foundation to acquire instruments suitable for receiving signals from the Global Positioning Satellites in order to measure surface deformation over baselines of the order of 30-200 km. The anticipated precision of the system will provide 1 cm horizontal measurement accuracy and 2 cm vertical accuracy. These values are somewhat superior to the accuracy of VLBI and LRS techniques whose principal value is perceived to be in the measurement of considerably longer baselines (Flynn, 1984).

An important feature of the University Consortium instruments will be the presence of water vapour radiometers at each of the three initial GPS receiver sites. The radiometers will be built at the University of Colorado as portable versions of a successful radiometer system operated by NOAA in meteorological studies. The radiometers are required to suppress errors caused by uncertainties in atmospheric water-content. The use of dual-wavelength GPS receivers reduces uncertainties caused by fluctuations in the ionosphere. If funded the system will be first used in tectonic studies in 1986.

TRILATERATION

The use of single wavelength geodimeters with line-of-sight correction for refractive index (Savage and Prescott, 1973) and dual wavelength devices (Slater and Huggett, 1976) provide data with measurement accuracies of the order of 0.1 microstrain. Dual wavelength measurements have limited range (5 km) compared to single wavelength measurements (30 km) and the instrumentation has not been as easy to reproduce as current geodimeters. A three wavelength instrument that is expected to provide increased range (>60 km) and resolution (.05 microstrain) is currently being tested at the University of Colorado (Levine, 1978).

SEA LEVEL

The use of sea level as a reference datum to monitor vertical motions in coastal regions is being investigated by LDGO. The accuracy of an array of tide gauges spaced 40 km apart in the Shumagin Islands appears to be of the order of 4 cm over periods of days (equivalent to first-order leveling precision). Shelf waves with 28-120 minute periods and amplitudes of less than 3 mm are routinely observed by the array. We are optimistic that further reduction in sea level noise may attend correction for sea current, wind and temperature effects. The data are transmitted via satellite (Bilham, Beavan and Hurst, 1982).

The destruction of sea level records by epicentral tsunamis has focussed attention on instruments designed to "capture" the few hours

preceeding and following a great earthquake. A tsunami surge-recorder is presently being developed that will be inserted into holes in harbour structures and rock beaches to record pre-seismic, co-seismic and post-seismic sea level transients with cm accuracy with a range of more than 10 m (Bilham, 1984).

GRAVIMETRY

Absolute g measurement is presently achievable with better than 10 μgal accuracy using the portable apparatus developed at the University of Colorado (Zumberge et al., 1982). This provides approximately 2-3 cm height resolution given a typical surface gradient of 3 μgal per mm of vertical height change. Cryogenic gravimeters presently achieve 10 μg stabilities over periods of considerably less than a year (Goodkind, 1979). There is reason to believe that improvements to both types of instrument may occur in the next few years.

DISCUSSION

The above review is necessarily brief and omits much that is of interest. The following paragraphs discuss foreseeable limits to accuracy in some of the techniques discussed.

Geodetic measurement methods are noise-limited by uncertainties in atmospheric paths and by benchmark instabilities. It is probable that improvements in instrumentation will not greatly change the 10^{-7} precision attainable from dual-wavelength EDM devices. It appears at present that 10^{-8} accuracy (1 mm per 100 km) may be attainable

either using three-wavelength EDM devices or GPS receivers with radiometers.

The stability of the water-tube tiltmeter datum is inherently better than that of the most-stable laser extensometers although in practice the stability of the instrument itself is not a limiting factor in the measurement. To realise the potential stability of a Michelson tiltmeter requires low-noise, reliable sensors and, in surface locations, a satisfactory solution of attaching the instruments to deep stable lithology. The noise level in data from surface-installed long-baseline extensometers may be reduced by suitably indexing the ends of the instruments to deep layers. It is reasonable to suppose that suitably installed water-tube tiltmeters and laser strainmeters may attain RMS noise levels of several parts in 10^8 in future years with stabilities of similar magnitude.

Leveling accuracy is likely to improve in regions of considerable relief through the application of precise algorithms for the removal of thermal gradients in optical techniques. The accuracy that vertical height changes may be measured is likely to be limited to 1 mm per vertical km both in hydrostatic and optical leveling.

CONCLUSIONS

A significant number of development programs are currently providing improved accuracy and stability in crustal deformation instrumentation. In some cases present instrumentation is adequate to provide the stability and sensitivity requird to monitor earthquake mechanisms but sources of local noise mask tectonic signals of

interest. Progress in identifying these noise sources and suppressing their effects is slow but rewarding. It is possible that we may see the noise level in geodetic and observatory instrumentation fall by an order of magnitude in the next decade.

REFERENCES

Beavan, J. and R. Bilham, Long series of strain observations from an aseismic area, EOS, Trans. AGU, 60, 316, 1979.

Beavan, R. J., R. Bilham, and K. Hurst, Installation of sea level monitors to detect vertical motion and tilt in Alaskan seismic gaps, EOS, Trans. AGU., 45, 1053, 1982.

Berger, J., and R. H. Lovberg, Earth strain measurements with a laser interferometer, Science, 170, 296-303, 1970.

Bilham, R., Delays in the onset times of near-surface strain and tilt precursors to earthquakes, Earthquake Prediction - An International Review, Maurice Ewing Series, Vol. 4, pp. 411-421, D. W. Simpson and P. G. Richards, eds., AGU, 1981.

Bilham, R., Vertical geodesy without slope dependent errors - A proposed hydrostatic level using water at 4°C, Tectonophysics, 97, 337-349, 1983.

Bilham, R., and J. Beavan, Tilts and strains on crustal blocks, Tectonophysics., 52, 121-138, 1979.

Bilham, R., R. Plumb, and J. Beavan, Design considerations in an ultra stable long baseline tiltmeter - results on a laser tiltmeter, Proc. Conf. Terrestrial and Space Techniques in Earthquake Prediction Research, Strasbourg, Sept. 1978, Vieweg Verlag Wiesbaden/FRG, pp. 235-254, 1979.

Evans, R., J. Beavan, R. Bilham, and G. King, A survey of earth strain tides in Great Britain, Geophys. J. Roy. astron. Soc., 57, 119-135, 1979.

Goodkind, J., Continuous measurements with the superconducting gravimeter, Tectonophysics, 52, 99-105, 1979.

Horsfall, J. A. C., and G. C. P. King, A new geophysical tiltmeter, Nature, 274, 675-676, 1978.

Levine, J., Observation of nearly duirnal resonance of the Earth using a laser strainmeter, Proc. 9th GEOP Conf., Int. Symp. Appl. Geodesy to Geodynamics, 1978, Dept. of Geodetic Science Rept. No. 780, Ohio State Univ., pp. 333-339, 1978.

Morrissey, S.T., Tiltmeter and earthquake prediction program in S. California and at Adak, AK, U.S. Geol. Surv. Open-File Rept 83-918, pp. 369-376, 1983.

Sacks, I. S., Borehole strainmeters, U.S. Conf. on Measurement of Ground Strain Phenomena Related to Earthquake Prediction, Carmel, Sept. 7-9, 1978.

Savage, J. C., and W. H. Prescott, Precision of geodolite distance measurements for determining fault movements, J. Geophys. Res., 78, 6001-6008, 1973.

Slater, L. E., and G. R. Huggett, A multi-wavelength distance-measuring instrument for geophysical experiment, J. Geophys. Res., 81, 6299, 1976.

Wyatt, F., and J. Berger, Investigations of tilt measurements using shallow borehole tiltmeters, J. Geophys. Res., 85, 4351-4362, 1980.

Wyatt, F., K. Beckstrom, and J. Berger, The optical anchor - A geophysical strainmeter, Bull. Seismol. Soc. Am., 72, 1701-1715, 1982.

Wyatt, F., D. C. Agnew, A. Linde, and I. S. Sacks, Borehole strainmeter studies at Pinon Flat Observatory, Carnegie Inst. Wash. Ybk, 82, in press.

Wyatt, F., G. Cabaniss, and D. C. Agnew, A comparison of tiltmeters at tidal frequencies, Geophys. Res. Lett., 9, 743-746, 1982.

Zumberge, M. A., R. L. Rinker, and J. E. Faller, A portable apparatus for measurements of the Earth's gravity, Metrologia, 18, 145-152, 1982.

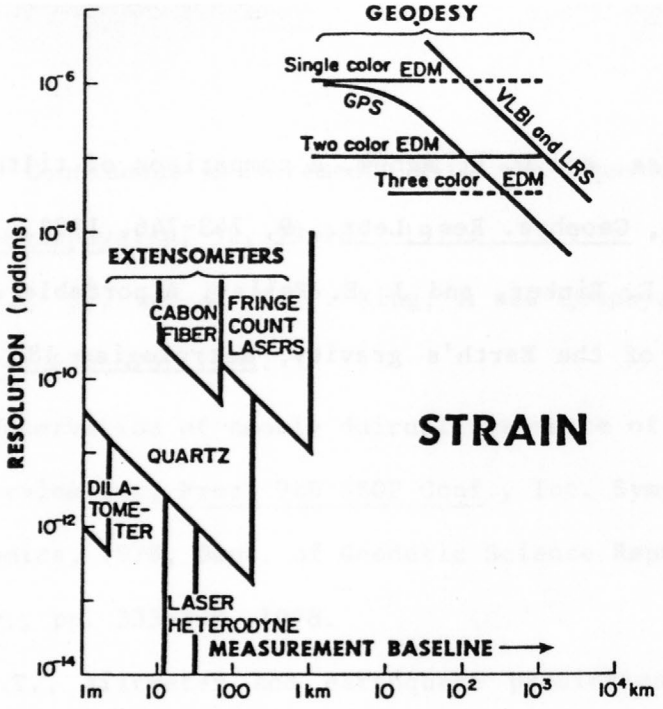

Figure 1. Strain resolution vs baseline for observatory and geodetic methods.

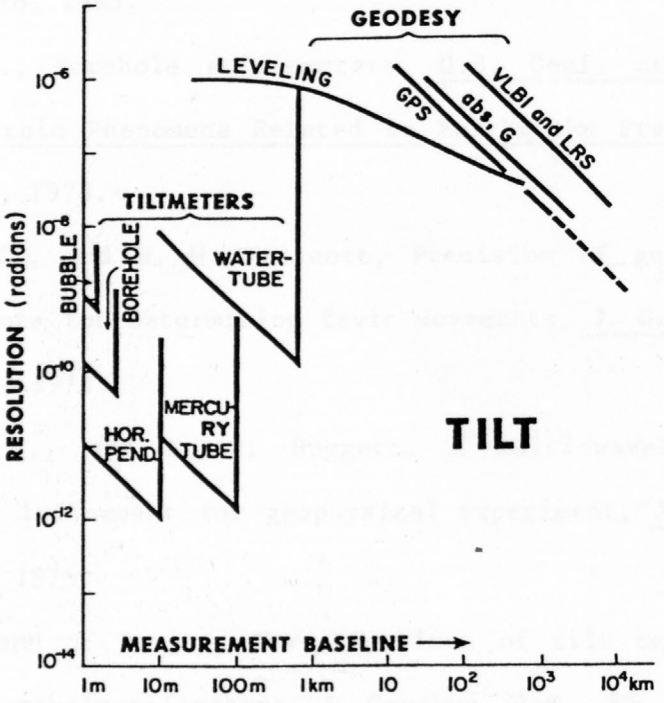

Figure 2. Tilt resolution vs baseline for observatory and geodetic methods.

The noise level of Observatory instrumentation is frequency dependent and at long periods the useful resolution is significantly reduced from the values shown in the figures. At periods close to a year most observatory instruments have noise levels similar or greater in magnitude than geodetic measurements of longer baseline. Geodetic measurement precision is noise-limited by the atmosphere and to a lesser degree by bench-mark instability.

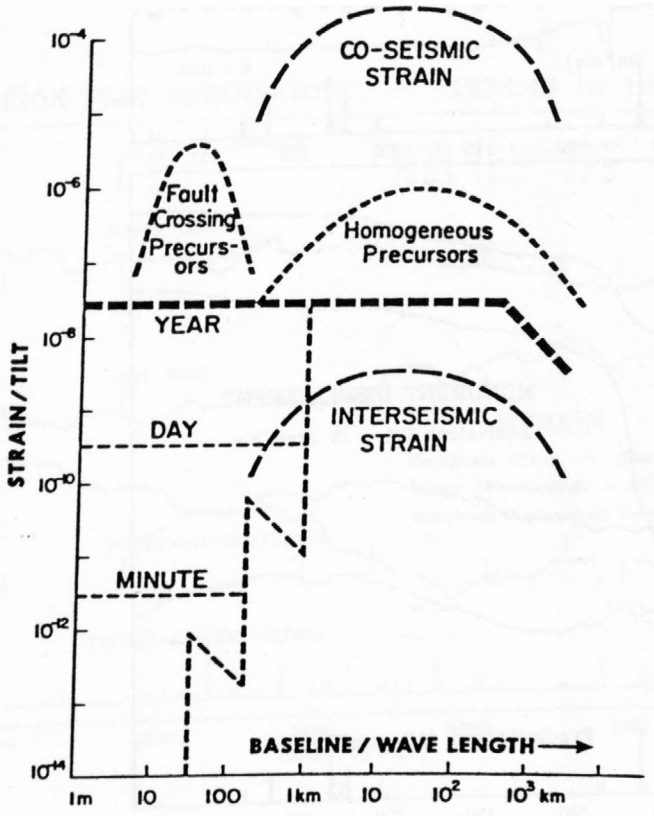

Figure 3. Strain and tilt instrumentation with baseline lengths up to 1km occupy the left-hand side of the figure with noise-levels depicted schematically for the periods indicated. Neither geodetic methods nor observatory instrumentation are presently useful for observing signals with strain rates less than 3×10^{-8}/year except at very long baselines.

Also depicted in the figure are magnitudes of typical epicentral co-seismic strain and minimum anticipated annual inter-seismic strain. Observed precursory strain signals are indicated for fault-crossing observatories and for observatories away from known zones of low compliance.

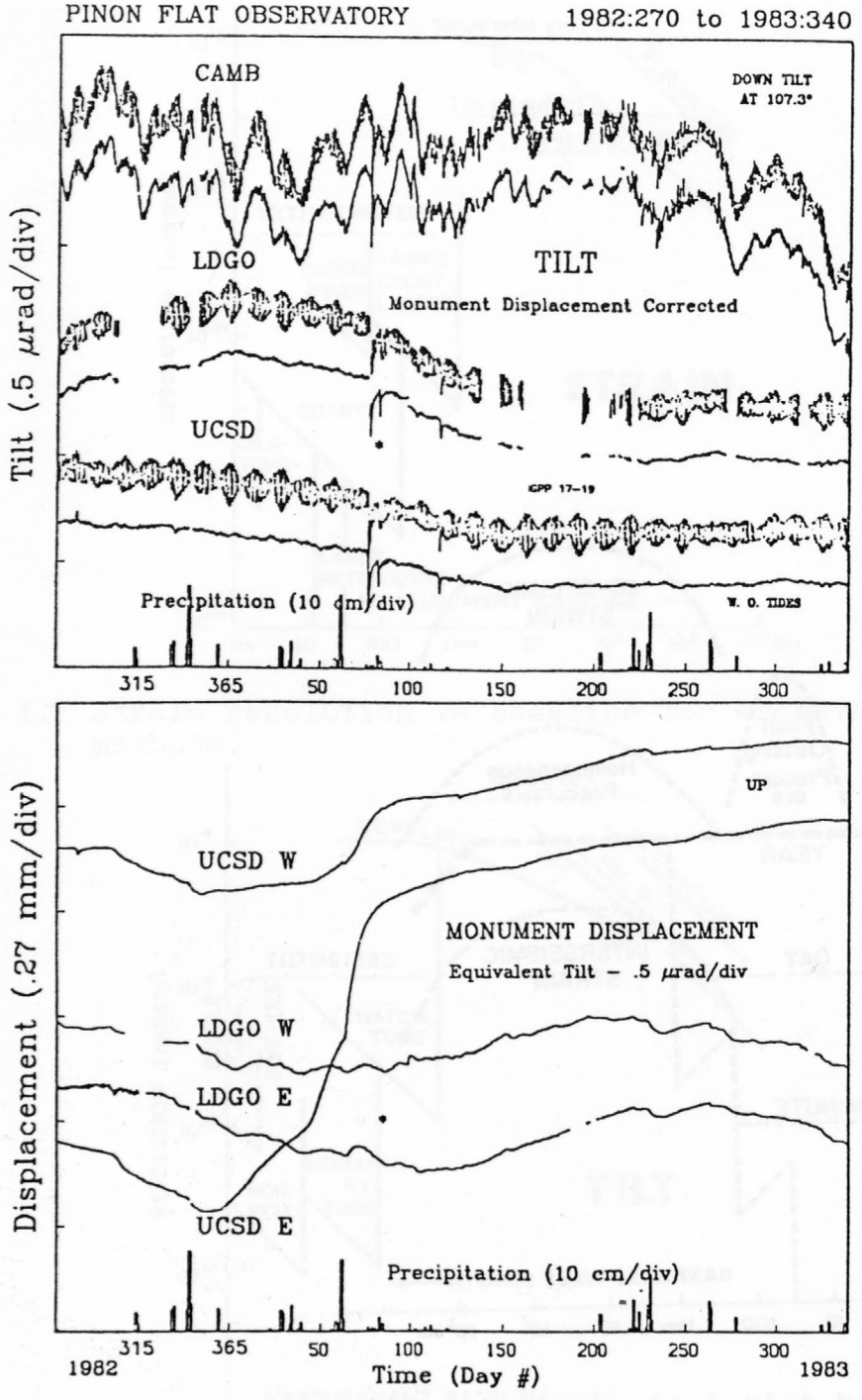

Figure 4a (above) represents 15 months of raw data and data from which tides have been filtered, from three 532m long tiltmeters at Pinion Flats Observatory. The LDGO and UCSD tiltmeters are both half-filled, water-tube tiltmeters with interferometric sensors. Figure 4b (below) shows vertical displacement data measured by 26m long vertical extensometers beneath each of the surface monuments. These signals have been removed from the tilt data in the Figure 4a plot. Note that the tiltmeters track to within several tenths of a microradian per year. (From Wyatt & Agnew, 1984).

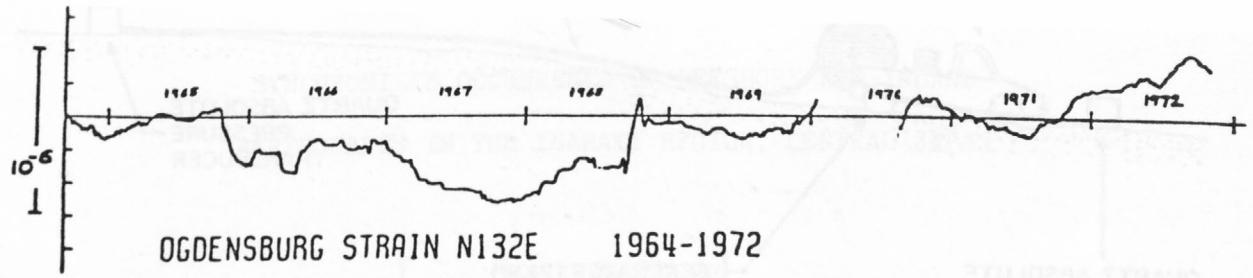

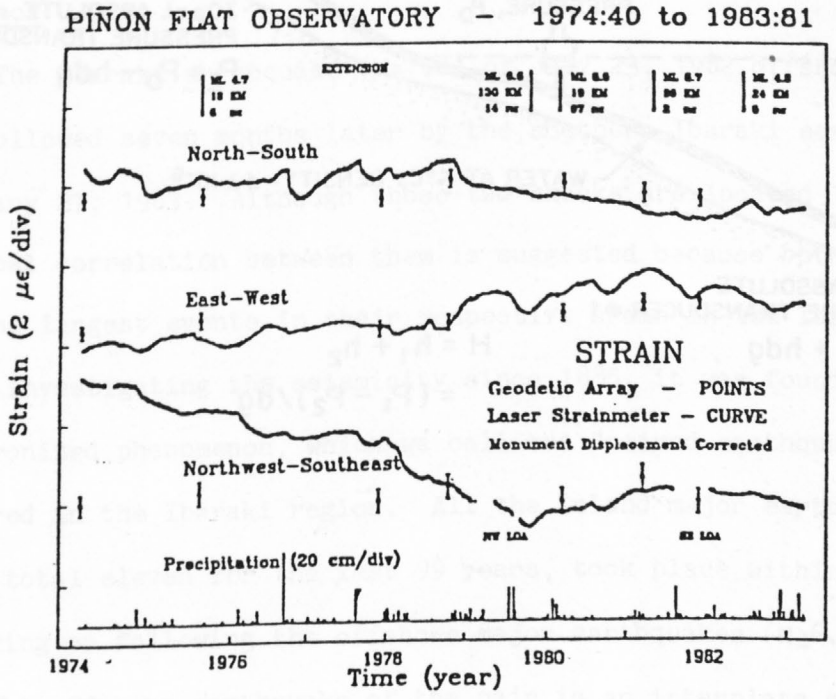

Figure 5. Strain data from one of four 650m deep quartz extensometers at Ogdensburg Seismic Observatory N.J., (Beavan & Bilham 1979) and from the Pinion Flat Observatory, Ca (Wyatt & Agnew 1984). The Ogdensburg data are contaminated by local strains due to mining in the vicinity of the observatory (seen as impulsive events at irregular intervals in the data). A 2.6 microstrain extension in 1970 caused by stope excavation within 20m of the instrument has been omitted from the record. The Pinion Flat data are contaminated by near-surface thermal and hydraulic noise.

The two sites have similar RMS noise and long term drift.

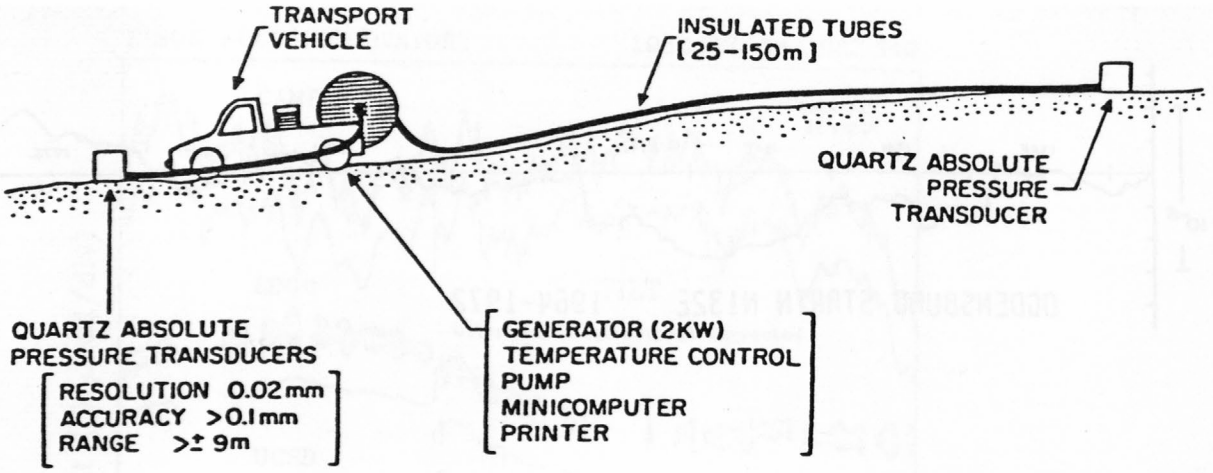

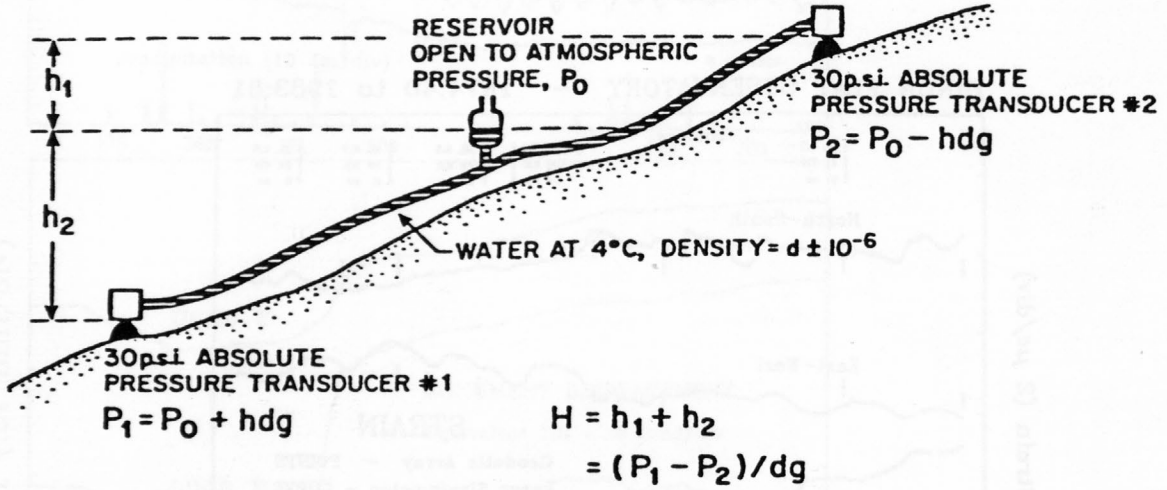

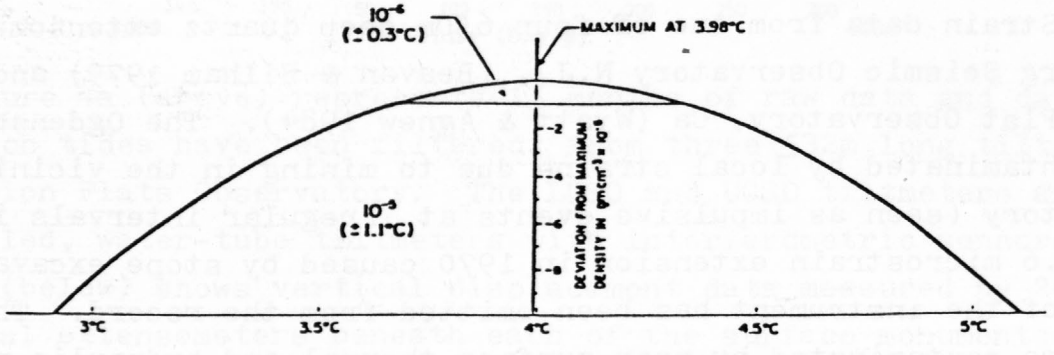

DENSITY VARIATION OF WATER AT TEMPERATURES CLOSE TO 4°C

Figure 6 Schematic views of the hydrostatic pressure level being developed for use in precision leveling.

SYNCHRONIZED OCCURRENCE OF OFFSHORE AND INLAND EARTHQUAKES IN THE IBARAKI REGION, CENTRAL JAPAN

Masakazu Ohtake

National Research Center for Disaster Prevention

3-1 Tennodai, Sakura-mura, Niihari-gun, Ibaraki, Japan

Abstract

The Ibaraki earthquake (M=7.0) of July 23, 1982 offshore of central Japan was followed seven months later by the southern Ibaraki earthquake (M=6.0) of February 27, 1983. Although these two shocks are located 160 km apart, a physical correlation between them is suggested because both of the earthquakes are the largest events in their respective areas in the last forty years. While investigating the seismicity since 1885, it was found that similar synchronized phenomenon, which we call the "paired earthquakes", repeatedly occurred in the Ibaraki region. All the inland major earthquakes ($M \geq 6.0$) which total eleven for the last 99 years, took place within 1.5 years preceding or following the offshore major earthquakes ($M \geq 6.5$).

The offshore earthquake of the pair is an interplate earthquake associated with the subducting Pacific plate, while the inland one is interpreted as a slab-slab collision of the Pacific plate and the Philippine Sea plate at the depth of about 70 km beneath Ibaraki Prefecture. The paired earthquake phenomenon occurs because rupture of the plate edge during the first earthquake causes an accelerated subduction of the Pacific Plate.

Introduction

On July 23, 1982, a shallow earthquake of magnitude 7.0 took place off

the east coast of Ibaraki Prefecture in central Japan. The offshore earthquake was followed by an inland earthquake of magnitude 6.0 which occurred at a depth of 72 km beneath southern Ibaraki on February 27, 1983. The lag time was seven months. Locations of those shocks are shown in Fig. 1. They were the largest events in the respective areas in the last forty years.

Although those two shocks are separated by 160 km in horizontal distance, the coincidental occurrence of remarkable events suggests that some physical correlation may exist between them. We have investigated past seismicity of the Ibaraki region for about one hundred years to determine whether or not the synchronized occurrence of offshore and inland earthquakes is an accidental phenomenon.

Seismicity of the Ibaraki Region

The southern part of Ibaraki Prefecture is one of the most seismically active areas in Japan. The seismicity, however, is rather deep in the crust with most of the earthquakes occurring at depths of 50-70 km. Recent studies on three-dimensional distribution of microearthquakes and focal mechanisms have revealed that the deep-seated seismicity is generated by the slab-slab interaction of the Pacific plate and the Philippine Sea plate which are converging beneath the Kanto District (KASAHARA, 1980, 1984; MAKI et al., 1980).

The Sea area to the east of the Ibaraki Prefecture is also subject to frequent earthquakes. Those earthquakes are distributed at shallow depths (0-40 km) to the west of the Japan Trench and are attributed to the westward subduction of the Pacific plate. The seismicity, however, is not as high as in the Tohoku region to the north of Ibaraki, and an earthquake exceeding magnitude 7.5 has not been registered. The off-shore seismicity does not

extend to the coast line but almost vanishes abruptly near longitude 140.8°E. A zone of low seismicity runs along the coast line as shown in Fig. 1. Therefore, seismicity in the Ibaraki region is clearly separated into the offshore (Region A) and inland (Region b) groups.

The contrast between the offshore and inland seismicity distinguishes the Ibaraki region from adjacent regions. To the south, a cluster of subcrustal earthquakes appears again at a depth of 70-80 km beneath northern Chiba (around 35.7°N, 140.2°E), but offshore seismicity is much weaker. To the north, dense seismic activity is not found beneath the crust. It should be noted that north-south trending contour lines of the deep seismic zone associated with the subducting Pacific plate bulge toward the west around 36°N in latitute (e.g., UMINO and HASAEGAWA, 1982). The Ibaraki region is located at this particular area.

Data

The trapezoidal area in Figs. 1 and 2 shows the Ibaraki region of the present study; the north and south boundaries are 36.6°N and 35.8°N, and the west and east boundaries are 139.8°E and the trench axis, respectively. The area includes seismic clusters in southern Ibaraki and is separated spatially from nearby seismicity. The study area is divided into Regions A and B as shown in the figure for classifying offshore and inland earthquakes.

Major earthquakes, $M \geq 6.5$ for Region A and $M \geq 6.0$ for Region B, from 1885 to 1983 are listed in Table 1 based on the UTSU's (1982) earthquake catalog and the Seismological Bulletin of the Japan Meteorological Agency for 1981-1983. The number of major earthquakes thus defined is eighteen for Region A and eleven for Region B. The epicentral distribution of those shocks is shown in Fig. 2.

The threshold magnitudes are chosen so as to provide uniform data for the

whole period since 1885. For earthquakes prior to the 1960's, the hypocenter coordinates and focal depths in particular, are subject to considerable uncertainty due to poor coverage of the observation net. For example, the Ishibashi study (1973) determined that the 1921 earthquake was located 30 km to the north of the epicenter originally sited. Most of the inland major earthquakes, however, are judged to have occurred in the deep cluster (about 70 km in depth) based on the distribution of seismic intensity and three-dimensional pattern of micro-seismicity (OHTAKE and KASAHARA, 1983).

Paired Earthquake Phenomenon

Figure 3 is the magnitude-time plot of major earthquakes in Regions A and B. This figure demonstrates that seismic activities in those regions tend to occur simultaneously. For instance, the magnitude 7.2 earthquake of 1895 (which was the largest event in Region B since 1885) was followed by the 1896 offshore earthquake of magnitude 7.5 with a lag time of only one year. During the following two decades, both the regions were quiet until remarkable activity started around 1920. Synchronized occurrences of earthquakes in Regions A and B are also seen in the 1920's, 1930's, and 1980's. We refer to such a synchronization of earthquake occurrence as the "paired earthquake phenomenon."

It is seen in Table 1 that all of the major earthquakes in Region B took place in pairs within $\pm$ 1.5 years of occurrence of major earthquakes in Region A. Periods of 1.5 years preceding or following major earthquakes in Region A are indicated by shaded portions in Fig. 3. The shaded zone, totaling 38.6 years, shares 39.0% of the whole period of 99 years so that 4.3 shocks out of 11 in Region B are expected to occur under the assumption of stationary random process. The number of observed shocks is 2.6 times larger than the statistically expected number.

The probability that n or more shocks out of N take place by chance in a specified period t is given by

$$p = \sum_{k=n}^{N} \left[{}_{N}C_{N} \, (t/T)^{k} \, (1-t/T)^{N-k} \right] \qquad (1)$$

where T is the total period. Substituting N=n=11 and t/T=0.39 into (1), we obtain $p=3.2 \times 10^{-5}$. However, the small value of P may not guarantee the non-accidental nature because the time series of major earthquakes apparently does not show random distribution (see Fig. 3). In order to eliminate the effect of swarm-like occurrences, we group the shocks occurring at intervals of less than 1.5 years into one event, consolidating eleven shocks of Region B into five events and eighteen shocks of Region A into nine events. The resulting probability is much increased but is still as small as 0.9×10^{-2}, and the null hypothesis that synchronized occurrence of earthquakes between Regions A and B is accidental is rejected at the 99% significance level.

Major earthquakes in Region B are always paired with major earthquakes in Region A, but the converse is not true. Among five events of Region B, three cases preceded and two cases followed major events of Region A with time intervals of less than 1.5 years. For the major events of Region A, such a correlation is not seen for four cases out of nine. Referring to Fig. 3, such companionless earthquakes of Region A are found in 1918-1919 (two shocks), 1938, 1961 (three shocks) and 1965.

Among the four companionless events, the largest one is the swarm activity of 1961 which includes magnitude 6.8, 6.5 and 6.6 earthquakes. Although the corresponding major earthquake ($M \geq 6.0$) is not registered, we note tnat a shock with magnitude 5.7 ($\phi=35^{\circ}59'N$, $\lambda=140^{\circ}02'E$, H=60 km) took place in Region B on January 14, 1960, one year preceding the offshore swarm. We further note that the 1938 event (M=6.5) was preceded by a

magnitude 6.1 inland earthquake which was located very near to the southern margin of Region B (June 6, 1938, ϕ=35°46'N, λ=140°24'E, H=50 km). The lag time was 3.5 months. Thus, two of the four cases of unpaired events in Region A may be correlated with inland seismicity.

For the paired earthquakes, the magnitude of the offshore shock M_A is always larger than the inland shock M_B, the difference being 0.5 on average. Figure 4 shows the relation between M_A and M_B, where the two possible cases of paired events mentioned above are also included. In instances where two or more shocks are grouped into one event, the largest shock is plotted. In Fig. 4, positive correlation is found between M_A and M_B, the correlation coefficient being 0.73. The existence of positive correlation strongly suggests that the paired earthquake phenomenon is not a statistical accident but is goverened by some physical process.

Dynamics of the Paired Earthquakes

According to Ohtake and Kasahara (1983), the southern Ibaraki earthquake of 1983 was a thrust-type earthquake in which the fault plane dips 31° toward N82°W, and the fault dimension is 5 km x 3 km. The southern Ibaraki earthquakes of 1943 and 1960 were also thrusts with the maximum compression axis oriented in an east-west direction (ICHIKAWA, 1971). The east-west compression is predominant, even for smaller events of magnitude 4 class which belong to the earthquake cluster of southern Ibaraki (MAKI and others, 1980) Those focal mechanisms are consistent with the relative motion between the Pacific and Philippine Sea plates, which are colliding beneath Ibaraki Prefecture.

Figure 5 illustrates the tectonic setting with expected faults of inland earthquakes (B) and offshore earthquakes (A) on an east-west striking cross section. The subducting Pacific plate is coupled with the adjacent plates at

two locations with the continental plate at the shallow portion A, and with the Philippine Sea plate at deeper portion B. Therefore, when the plate interface A is ruptured by an offshore earthquake, an increase of shear stress at B is expected to occur by accelerated subduction of the Pacific plate. This stress increase triggers another rupture at B, and vice versa.

The dynamic model proposed above predicts a positive correlation with magnitudes of paired earthquakes because larger displacement by the earthquake at A(B) must be balanced by larger displacement at B(A). However, magnitude of the inland earthquake at B may not exceed a certain limit which is controlled by the contact area between the two plates.

The portion in contact is roughly estimated as L=20 km along the down-dipping plate interface based on the three-dimensional distribution of microearthquakes (OHTAKE and KASAHARA, 1983). Assuming the maximum fault area as S=L x 2L, the maximum value of seismic moment, Mo, is estimated at 10^{26} - 10^{27} dyne.cm for a stress drop of 10-100 bars referring to the S-Mo diagram of KANAMORI and ANDERSON (1975). The corresponding earthquake magnitude is 6.7-7.3 based on the scaling of AKI (1972);

$$\log Mo = 1.5 M_S + 16.0 \qquad (2)$$

where M_S is the surface wave magnitude.

This rough estimate is in approximate agreement with the largest earthquake of the last 99 years in Region B, M-7.2 (see Table 1). A reliable estimation of the upper limit of the earthquake size is of great value for establishing earthquake disaster countermeasures.

Conclusions

In an investigation of past seismicity in the Ibaraki region of central Japan, a significant synchronization of occurrence time was found between offshore and inland earthquakes. All the major inland earthquakes ($M \geq 6.0$)

which total eleven in the last 99 years, took place within 1.5 years preceding or following major offshore earthquakes ($M \geq 6.5$). Among the eighteen major shocks in the sea area, at least eleven correlated to the inland major shocks in the same manner. We name this synchronization of seismicity as the "paired earthquake phenomenon." Magnitudes of the pairing offshore and inland earthquakes are found to be positively correlated. These statistical results may be used for forecasting the "next earthquake" when a major earthquake occurs in the Ibaraki region.

The paired earthquake phenomenon is explained by a model where the subducting Pacific plate is coupled with the continental plate at a shallow depth (0-40 km), and with the Philippine Sea plate at a deeper depth (around 70 km) beneath Ibaraki Prefecture. When one plate interface is ruptured by the preceding earthquake, shear stress increases at the other interface, and an earthquake follows. The double-couple plate model predicts that an earthquake belonging to the southern Ibaraki cluster will not exceed magnitude 7.3.

Thus, the paired earthquake phenomenon in the Ibaraki region is interpreted as a consequence of the peculiar tectonics of slab-slab collision. Similar phenomena are also reported for shallow and deep earthquakes along the deep seismic zone (MOGI, 1973; UTSU, 1975), and for nearby earthquakes in the crust (OIKE, 1980). However, the present model is not applicable to those cases since the tectonic circumstances are different. Studies on paired earthquakes in various tectonic conditions will contribute substantially to the understanding of lithosphere dynamics as well as to earthquake prediction.

References

Aki, K., Scaling law of earthquake source time-function, Geophys. J. R. Astr. Soc., 31, 3-25, 1972.

Ichaiawa, M., Reanalyses of mechanism of earthquakes which occurred in and near Japan, and statistical studies on the nodal plane solutions obtained, 1926-1968, Geophys. Mag., 35, 207-274, 1971.

Ishibashi, K., Relocation of the remarkable Ryugasaki earthquake of 1921 - In relation to the fault-like lines discovered by ERTS-I - (preliminaries), Zisin (J. Seismol. Soc. Japan), Ser. 2, 26, 3620367, 1973 (in Japanese).

Kanamori, H., and D.L. Anderson, Theoretical basis of some empirical relations in seismology, Bull. Seismol. Soc. Am., 65, 1073-1095, 1975.

Kasahara, K., Patterns of earthquake occurrences in the Kanto District, Abstr. Ann. Meet. Seismol. Soc. Japan, No. 2, 66, 1980 (in Japanese).

Kasahara, K., Patterns of crustal activities in the Kanto-Tokai region three plates converging, 1984 (in preparation).

Maki, T., I. Kawasaki, and A. Horie, Earthquake mechanisms associated with the conjunction of the sinking plates beneath the Kanto District, central Japan, Bull. Earthq. Res. Inst., 55, 577-600, 1980.

Mogi, K., Relationship between shallow and deep seismicity in the western Pacific region, Tectonophysics, 17, 1-22, 1973.

Ohtake, M. and K. Kasahara, Paired earthquakes in the Ibaraki region, central Japan, Zisin (J. Seismol. Soc. Japan), Ser. 2, 36, 643-653, 1983 (in Japanese).

Oike, K., Earthquake swarms in the patterns of the earthquake activity, J. Analytical Researches of Data on Natural Disaster, 7, 61-66, 1980 (in Japanese).

Umino, N. and A. Hasegawa, A detailed structure of the deep seismic zone and

earthquake mechanism in the northeastern Japan arc, Zisin (J. Seismol. Soc. Japan), Ser. 2, 35, 237-257, 1982 (in Japanese).

Utsu,T., Catalog of large earthquakes in the region of Japan from 1885 through 1980, Bull. Earthq. Res. Inst., 57, 401-463, 1982 (in Japanese).

Utsu, T., Correlation between shallow earthquakes in Kwanto region and intermediate earthquakes in Hid region, central Japan, Zisin (J. Seismol. Soc. Japan), Ser. 2, 28, 303-311, 1975 (in Japanese).

Fig. 1. Study area projected on the seismicity map for 1982 ($H<100$ km) by the National Research Center for Disaster Prevention. The major earthquakes of 1982 and 1983 are shown by large stars. See the text for Regions A and B.

Fig. 2. Epicenters of major shallow earthquakes ($H<100$ km) which occurred in Region A ($M\geq 6.5$) and Region B ($M\geq 6.0$) for the period from 1885 through 1983.

Fig. 3. Magnitude-time plot of major earthquakes in Regions A and B. Shaded protions indicate the $\pm$ 1.5 year range of occurrence time of a Region A earthquake.

Fig. 4. Diagram comparing the magnitude of paired earthquakes. M_A and M_B are magnitudes of major earthquakes which occurred in pairs in Region A and Region B, respectively. Broken lines indicate the $\pm$ 0.5 deviation range of M_B from the regression line.

Fig. 5. Tectonic model to interpret the paired earthquake phenomenon.

Table 1. Major earthquakes in the Ibaraki region (H < 100 km) for the period from 1885 through 1983.

Date (JST) Y M D	Epicenter (°N)	(°E)	Depth (km)	Magnitude	Region
1895-01-18	36.1	140.4		7.2	B
1896-01-09	36 1/2	141		7 1/2	A
1918-07-26	36.2	142.3		6.7	A
1919-08-04	36	142 1/2		6.7	A
1921-12-08	36.0	140.2	63*	7.0	B
1922-05-09	36.0	140.0		6.1	B
1923-01-14	36.1	139.9		6.1	B
1923-06-02	35.9	142.0		7.3	A
1923-06-02	36	142		7.1	A
1923-09-01	36	140		6	B
1924-01-15	36.2	140.5		6.0	B
1924-08-15	36.2	141.6		7.1	A
1924-08-15	36.3	142.2		6.7	A
1924-08-17	36	142 1/2		6.6	A
1924-08-25	36.2	142.0		6.7	A
1924-09-18	36.3	140.2		6.6	B
1930-06-01	36.57	140.62	30	6.5	B
1931-06-23	36.47	141.05	10	6.6	A
1938-09-22	36.40	141.02	30	6.5	A
1942-11-16	36.37	141.12	20	6.5	A
1943-04-11	36.35	141.45	10	6.7	A
1943-07-01	36.03	140.17	50	6.0	B
1944-06-16	35.97	140.18	50	6.1	B
1961-01-16	36.03	142.27	40	6.8	A
1961-01-16	36.22	141.98	20	6.5	A
1961-01-17	36.15	142.13	40	6.6	A
1965-09-18	36.32	141.47	40	6.7	A
1982-07-23	36.18	141.95	30	7.0	A
1983-02-27	35.93	140.15	72	6.0	B

Magnitude threshold is 6.5 for Region A and 6.0 for Region B.

* After ISHIBASHI (1973).

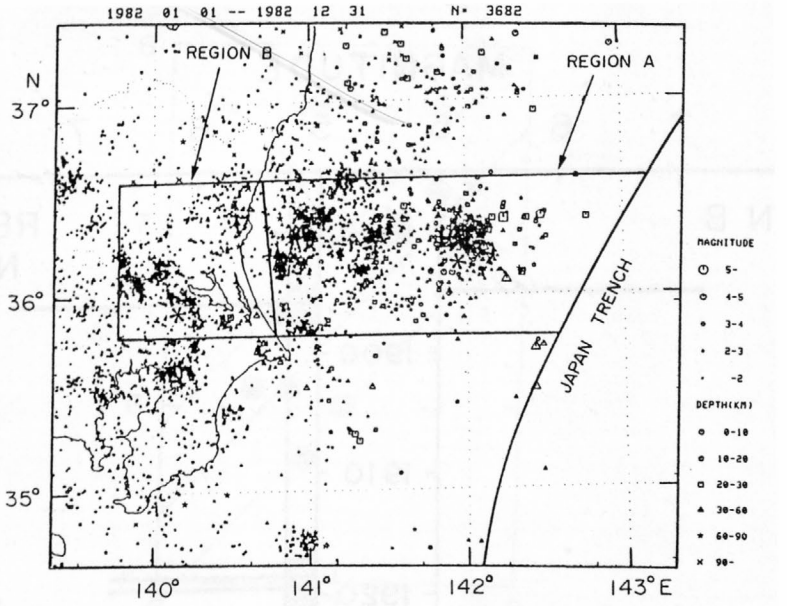

Fig. 1. Study area projected on the seismicity map for 1982 ($H < 100$ km) by the National Research Center for Disaster Prevention. The major earthquakes of 1982 and 1983 are shown by large stars. See the text for Regions A and B.

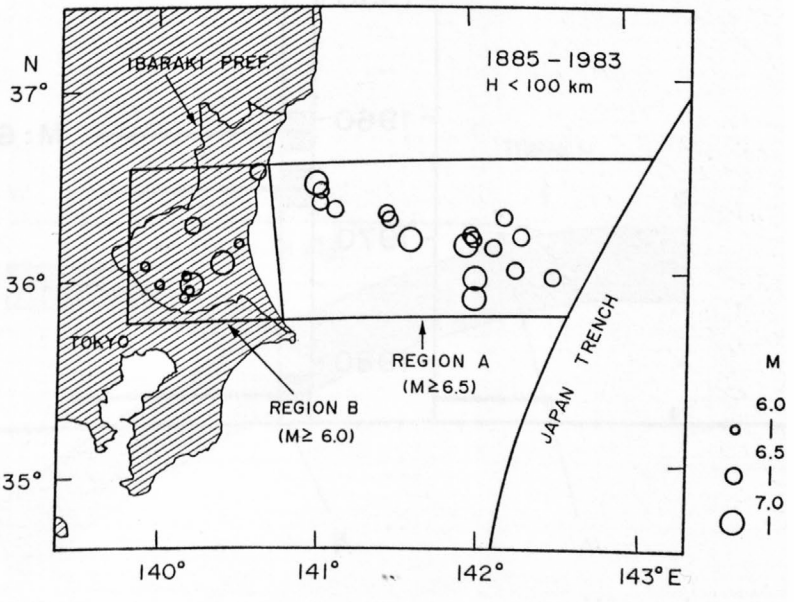

Fig. 2. Epicenters of major shallow earthquakes ($H < 100$ km) which occurred in Region A ($M \geq 6.5$) and Region B ($M \geq 6.0$) for the period from 1885 through 1983.

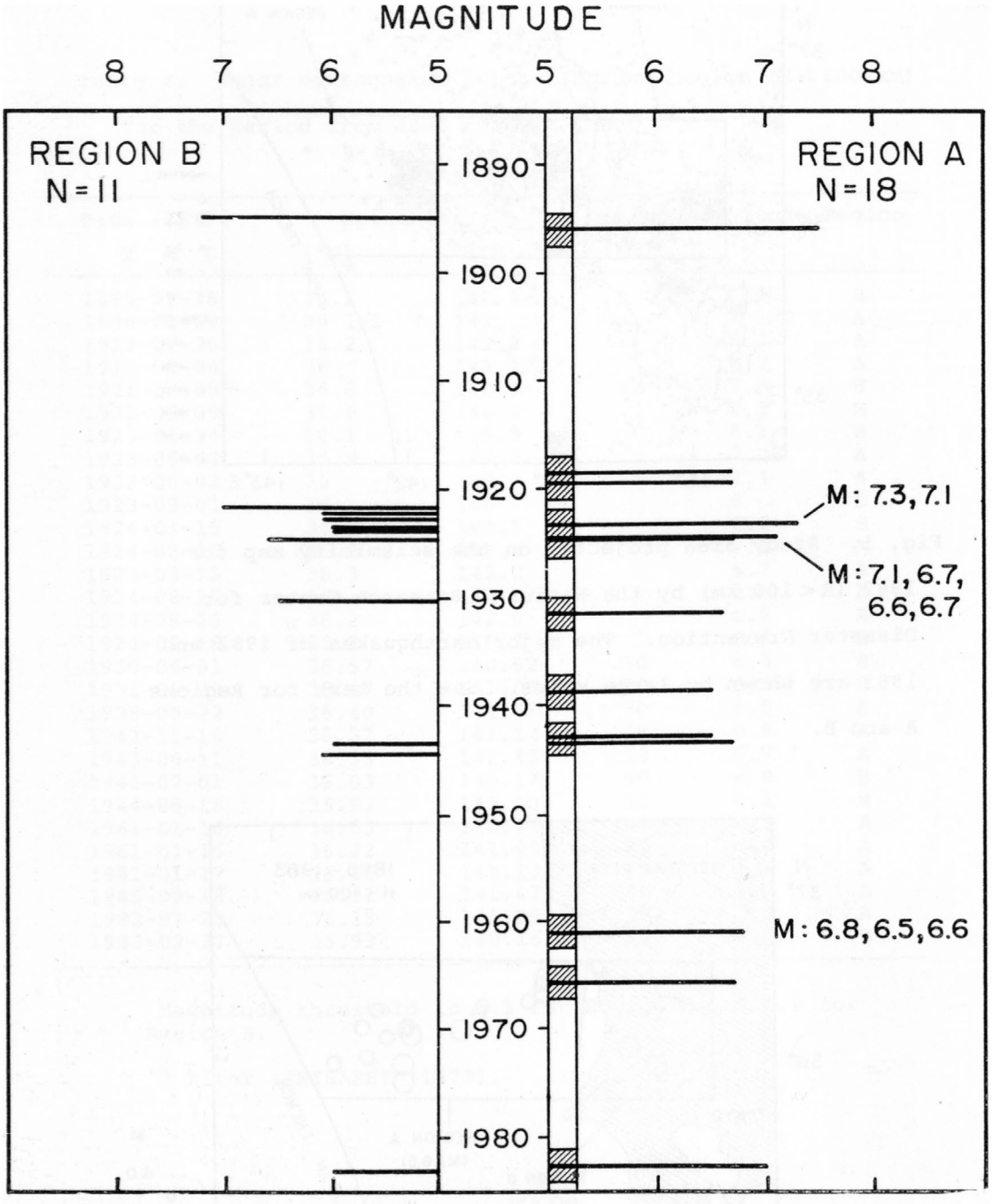

Fig. 3. Magnitude-time plot of major earthquakes in Regions A and B. Shaded portions indicate the ±1.5 year range of occurrence time of a Region A earthquake.

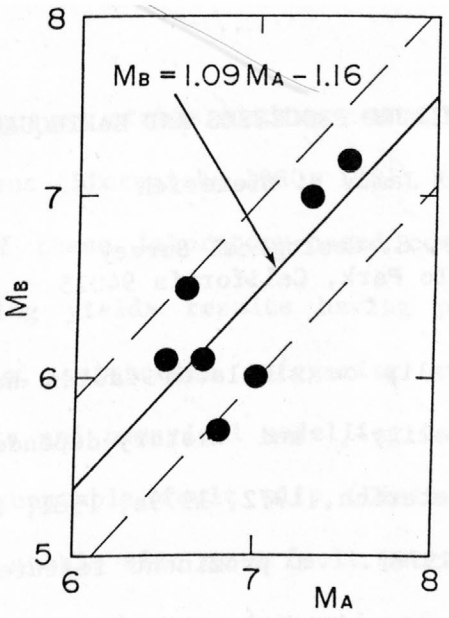

Fig. 4. Diagram comparing the magnitude of paired earthquakes. M_A and M_B are magnitudes of major earthquakes which occurred in pairs in Region A and Region B, respectively. Broken lines indicate the ±0.5 deviation range of M_B from the regression line.

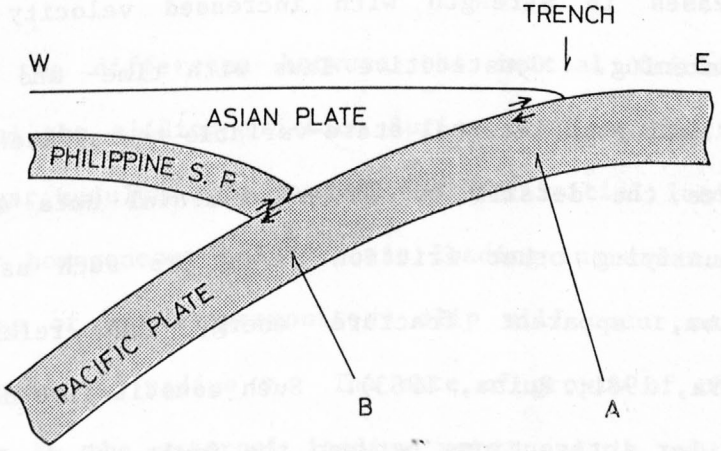

Fig. 5. Tectonic model to interpret the paired earthquake phenomenon.

HISTORY DEPENDENT FAILURE PROCESSES AND EARTHQUAKE PREDICTION

James H. Dieterich

U. S. Geological Survey
Menlo Park, California 94025

Laboratory study of slip on simulated faults has demonstrated the existence of time-, velocity-, and history-dependent processes that perturb fault strength (Dieterich, 1972, 1979a, 1981; Scholz and Engelder, 1976; Teufel and Logan, 1978). A prominent feature of the laboratory observations is displacement weakening at the onset of slip if the fault is previously stationary or if a slipping fault undergoes accelerated slip. The characteristic displacement, d_c, over which weakening occurs depends on the characteristics of the surfaces and varies from a few microns for polished surfaces to 200 microns for roughened surfaces separated by a thin layer of gouge. Other features of the experimental observations are increasing fault strength with time of contact and transient increases in strength with increased velocity followed by displacement weakening. Constitutive laws with time- and displacement-dependence that employ an internal state-variable to represent the history effects reproduce the details of the experimental data and provide a framework for unifying other friction parameters such as: static and sliding friction, apparent fracture energy and relaxation creep (Dieterich, 1979a, 1981; Ruina, 1983). Such constitutive laws when used in computations for interactions between the fault and loading apparatus have yielded results for mode of slip that appear to be in good agreement with observations. Unstable slip (stick-slip) with premonitory creep and

afterslip, creep events or stable sliding can all occur depending upon the experimental conditions (Dieterich, 1980, 1981; Ruina, 1983).

Extrapolation of these laboratory-based constitutive laws to models of earthquake faulting yields results having possible implications for earthquake nucleation, earthquake triggering and precursory processes. Laboratory experiments and numerical modelling indicate that two phases of stable slip precede unstable fault slip (Dieterich, 1979b). The first phase is a period of stable slip on a fault patch that expands with time. The second phase is a shorter interval of accelerating slip that culminates in unstable slip. The first phase of stable slip appears to arise as a direct consequence of the displacement weakening: unstable slip can nucleate only on a fault patch that is equal to or greater than some minimum size. For a circular patch the radius of the patch, r, must be equal to or greater than a critical radius, R, give approximately by:

$$R = 0.21\ \mu \frac{d_c}{\tau}$$

where τ is the difference between the initial friction (prior to instability) and the sliding friction during the instability and μ is the elastic shear modulus. In general, if the initial loading stress or the friction is homogeneous and tectonic loading increases monotonically, an initial phase of stable premonitory slip will occur as the slipping fault patch expands to radius r. The rate of growth of the stable slip patch is driven by the external loading rates and is controlled by the magnitdue of the stress/strength inhomogeneity.

The second phase of accelerating creep and the triggering of earthquake slip has been explored with the aid of a numerical model of the

nucleation zone of the earthquake source. The model assumes that the zone of slip does not expand during the interval covered by the computations and that average slip rates and average shear stresses on the slipping zone are sufficient to characterize the problem. The computations employ a time-marching procedure to follow the acceleration of slip on the patch. For patches $r >> R$ any initial stress, τ_i, above a critical stress, τ_c, results in accelerating slip leading to instability. For models employing representative constitutive parameters the logarithm of the time to instability following a step in stress, $\Delta\tau = \tau_i - \tau_c$, decreases in a nearly linear fashion as $\Delta\tau$ increases over a range of times from 1 second to 10^7 seconds. The displacements during the accelerating slip are proportional to d_c but the duration of slip is independent of d_c. Using parameters representative of the laboratory results, premonitory displacements during the accelerating creep phase are approximately 5 d_c. The time to instability depends additionally on the magnitude of the parameter controlling the direct velocity-dependence in the constitutive law. Model simulations in which the direct velocity parameter was varied show a linear scaling of the time to failure and the magnitude of the velocity dependence. As the velocity dependence goes to zero the constitutive law becomes simply a displacement dependent law and there is no delay between the time the critical stress is reached and the onset of unstable slip. Consequently, for constitutive laws without velocity dependence, triggering of earthquakes by tidal stresses should be apparent. The absence of a strong correlation of earthquakes with earth tides can therefore be used to establish limits on the velocity-dependence of earthquake producing faults. The magnitude of the velocity-dependence observed in

laboratory experiments appears to be sufficient to inhibit triggering by tidal stresses.

A principal uncertainty for application of internal state-variable constitutive laws to the problem of earthquake faulting is the magnitude of the displacement weakening parameter d_c. Laboratory experiments indicate that d_c is sensitive to the characteristics of the fault surfaces and several orders of magnitude variation have been observed. Unless d_c for earthquake faults in nature is significantly larger (in the range of a few milimeters to a few centimeters) than that observed on simulated faults in the laboratory, the size of the nucleation zone of stable slip and the premonitory displacements on that zone may be too small to detect directly using current strain observation methods. Estimates of fracture energy for earthquakes, if reliable, suggest that d_c for some earthquake faults may be as large as a few centimeters.

REFERENCES

Dieterich, J.H., 1972, Time dependent friction in rocks: J. Geophys. Res., 76, 20, 3690-3697.

Dieterich, J.H., 1979a, Modelling of rock friction, Part 1. Experimental results and constitutive equations: J. Geophys. Res., 84, B5, 2161-2168.

Dieterich, J.H., 1979b, Modelling of rock friction, Part 2. Simulation of preseismic slip: J. Geophys. Res., 84, B5, 2169-2175.

Dieterich, J.H., 1981, Constitutive properties of faults with simulated gouge, in: Geophysical Monograph 24, Mechanical Behavior of Crustal Rocks, American Geophysical Union, 103-120.

Ruina, A.L., 1983, Slip instabilities and state variable friction laws: J. Geophys. Res., in press.

Scholz, C.H., and J.T. Engelder, 1976, The role of asperity indentation and ploughing in rock friction, I, Asperity creep and stick-slip: Int. J. Rock Mech. Mining Sci. Geomech. Abstr., 13, 149-154.

Teufel, L.W., and J.M. Logan, 1978, Effect of shortening rate on the real area of contact and temperatures generated during frictional sliding: Pure Appl. Geophys., 116, 840-865.

Modeling of Seismic Cycles for Earthquake Prediction

Gerald Mavko
U.S. Geological Survey, Menlo Park, California 94025

Many theoretical models have been proposed to describe portions of major earthquake cycles. For example, elastic dislocation models have been particularly sucessful in explaining static coseismic deformation, as well as many features of observed aseismic deformation, including postseismic transients and steady strain accumulation. In contrast, a number of authors have modeled aseismic deformation as the viscoelastic response to some prescribed slip. In general, most models that predict coseismic slip, either from assumptions about fault strength or from fits to geodetic data, do not predict interseismic behavior; those that describe transients or steady strain accumulation usually do not predict coseismic slip. Generally some sort of resetting is required with these models to study successive earthquake cycles.

In this paper I present a theoretical fault model that predicts repeated complete large-scale earthquake cycles. An important feature of the model is the use of a fault zone constitutive law that has been inferred from laboratory sliding experiments. Unlike most previous models, the fault slip history throughout the entire cycle is computed as a direct consequence of the specified remote displacements, the material properties, and the sliding law.

Fault Zone Constitutive Law

The fault zone constitutive law used in the modeling was developed by Dieterich (1979, 1980, 1981) and Ruina (1980, 1983) to explain a number of laboratory friction experiments on both clean and gouge-filled sawcuts in

granite. One of the simplest forms describes the fault strength as a coefficient of friction $f = \tau / \sigma_n$, the ratio of shear stress to normal stress acting on the fault:

$$f = A_1 + \theta + A_2 \ln (v/V_o) \quad (1)$$

$$\dot{\theta} = -\frac{v}{d} \left(\theta + A_3 \ln (v/V_o)\right) \quad (2)$$

where A_1, A_2, A_3 and d are material constants, V_o is an arbitrary constant introduced for correct dimensions, v is the sliding velocity, and θ is a state variable that describes the evolution of friction with sliding. The constant A_1 in equation (1) is the nominal value of coefficient of friction, of the order ~0.5. All of the other terms describe fairly small (<10% perturbations about A_1. The last term in equation (1) describes a direct velocity dependence, somewhat like a viscous term; an increase in slip velocity causes an immediate increase in strength. In contrast, θ describes an indirect velocity dependence; an increase in velocity causes a negative rate of change of θ.

The direct and indirect effects are illustrated by the hypothetical sliding experiment in Figure 1 after the observations of Dieterich (1979, 1980, 1981). For sliding governed by equations (1) and (2), if we switch abruptly from an initial steady slip rate of V_1 with friction f_1 to a higher steady rate V_2, we would observe first an abrupt increase in friction, $\Delta f = A_2 \ln (V_2/V_1)$, from the direct velocity dependence. This would be followed by a gradual decay to a lower strength, $f_2 = f_1 - (A_3 - A_2) \ln (V_2/V_1)$, that occurs

only after a finite amount of slip, characterized by parameter d, has occurred.

The Model

The model consists of a thick homogeneous linear elastic slab with a vertical through-going cut, simulating the lithosphere near a strike-slip plate boundary (Figure 2). The plates are driven by a steady prescribed antiplane velocity of 3.5 cm/yr at the remote boundaries. The lithosphere is assigned a shear modulus 3.7×10^5 bar and a thickness L = 64 km. The base of the plate is made traction-free, as a numerical convenience. All of the calculations presented assume two-dimensional, antiplane motion, i.e., only displacements parallel to the fault-trace are nonzero.

The normal stress across the fault is specified to increase linearly with depth at 300 bar/km. This lithostatic gradient is the only spatially variable input in the shallow lithosphere. The fault zone in the deeper lithosphere is treated differently. Along the San Andreas fault, brittle earthquakes are seldom observed deeper than 15 km. The brittle-ductile transition at the base of the seismogenic zone is generally thought to result from increased temperature and pressure (Brace and Byerlee, 1970). To simulate the brittle-ductile transition in the numerical model, the velocity weakening constant A_3 is decreased below 15 km such that slip on the lower fault is always stable. A_3 is kept fixed above 15 km. All other friction law parameters and material parameters are kept spatially constant in each simulation.

Simulations

A simulation of a system with an unstable seismogenic zone is shown in Figures 3 through 8. Each curve in Figure 3 represents cumulative fault slip versus depth at one instant in time, where slip is measured relative to a steady state solution. Four complete earthquake cycles are shown. The shaded regions show slip during the simulated coseismic events. In this example, the earthquake ruptures the surface, although the maximum coseismic slip of 8 m occurs at a depth 10 km. The simulated instability lasts only a few seconds. The slip during the next several hundred days occurs primarily below the rupture zone at depths of 15-30 km. Slip in the seismogenic zone is remarkably low during the 215 years after the earthquake while the fairly steady slip in the lower lithosphere gradually accumulates the 8 m of displacement for the next event. The recurrence time of the events shown is about 245 years, equal to the slip per cycle divided by the average plate speed.

A plot of slip rate versus depth is shown in Figure 4. The first point to go unstable, the hypocenter, (dotted curve) is at 10 km depth and the rupture subsequently expands both upward and downward. Following the rupture, the slip rate below 15 km remains relatively high for 5 years as accelerated postseismic slip diffuses downward. Thirty-one days after the rupture, the slip rate at 20-30 km depth is still 100 times faster than the long-term plate rate. In the seismogenic zone ($\leq$15 km) the slip rate following the rupture falls off gradually, decaying to the average plate rate of 156 days, and the fault becomes essentially locked (more than a factor of 10 slower than the plate rate) by 5 years. Finally, ~30 years before the next event, accelerated slip is evident at seismogenic depths, reaching the average plate speed over the entire seismogenic zone by ~165 days before the eartquakes, 100 times the

plate speed (at the hypocentral depth) a few hours before the earthquake, and finally accelerating into the next hypocenter.

Slip versus time at 2 km and 10 km depth are shown in Figure 5. Both depths exhibit long periods of essentially locked fault with precursory increases in slip rate before each event. The locking is less pronounced and the increase in rate more pronounced at the shallower depth.

Fault shear stress versus time at a depth of 10 km is shown in Figure 6. The stress is relative to the steady value, which for σ_n(10 km) = 3000 bars is of the order 1500 bar. The stress drop for each event is ~138 bar. An important feature of the Dieterich-Ruina frictions laws is that the stress drop is a small fraction of the total stress, in this case ~9%. After the rupture, the stress accumulates at a variable rate until the next event. During the first quarter cycle, the strain rate is rapid and gradually decreases as the postseismic slip below the rupture decays away. During the last quarter of the cycle, the rate appears to increase again, primarily because the slip rate above and below the locked seismogenic zone gradually begins to increase and transfer load to the locked patch. Peak stress is reached a few years before the earthquake, followed by a small gradual stress drop leading into the main event.

Slip rate versus time in the seismogenic zone (10 km) is shown on log-log scales in Figure 7. The slope during the first 5-10 years after the earthquakes is very nearly -1; therefore the slip rate and energy dissipation rate (stress times slip rate) in the rupture zone fall off as t^{-1} during the postseismic period, similar to the observed decay of aftershocks.

The surface tensor shear strain versus time averaged over 16 km about the fault trace is shown in Figue 8 for the fourth earthquake cycle. Following the strain drop of the earthquake, the strain rate is relatively high for

40-50 years due to the rapid postseismic slip below 15 km. The strain continues to accumulate at a decaying rate to a peak strain a few years before the next event. Qualitatively, the reversal in strain rate appears to correspond to the unpinning of the central seismogenic zone, when the fault velocity at the hypocentral depth meets the average plate speed and becomes larger than velocity both above and below (Figure 4).

Discussion

The two-dimension simulation in Figures 3-8 resembles much of what is known about the northern half of the 1857 rupture along the San Andreas fault, particularly in the Carrizo Plain. There, Sieh (1979) estimated the surface slip to be ~8 m. The recurrence time has been estimated to be 228 years (Lindh, 1983) assuming a geologic slip rate of 3.5 cm/yr. The good agreement with the model suggests that the stress drop in the Carrizo Plain was about 10^2 bar and that the rupture tapered off sharply below about 15 km depth. Different combinations of stress drop and depth can also produce the same observed displacement.

Surface coseismic slip for the 1906 earthquake was observed to be somewhat smaller, averaging about 4 m but locally more than 6 m (Lawson, 1908, Thatcher, 1975). Thatcher (1975) found that geodetic data indicated a larger average slip of ~5 m extending to a depth of 10 km. Along about 70 km of fault near Tomales Bay the geodetic slip was nearly 7 m. The simulations, therefore, appear to describe fairly well the Tomales Bay section of fault, but have to be scaled down (for example, choosing a shallower brittle ductile transition at 12 km) to better describe the average slip.

Thatcher (1983) cites evidence that strain rates near the San Andreas fault have decreased with time since the previous great earthquake. These are plotted in Figure 9 with the strain rates predicted by the model simulations. The model strain rates fall off faster than the observed, but qualitatively account for the decay. Thatcher (1983) has already shown that postseismic slip below the rupture can explain the observations. The difference, however, is that Thatcher specified an ad hoc distribution of postseismic slip to explain the observations while in the present work the slip is predicted by the model as a natural consequence of a stable (nonlinear) viscous fault zone responding to the abrupt coseismic stress redistribution.

Possibly the most important feature of the model is that it predicts precursory deformation. Fault slip accelerates in the upper 15 km before each simulated earthquake, following hundreds of years of quiescence during which the fault may appear to be essentially locked. The preseismic slip rate for the simulations shown is predicted to become large enough to be easily detected with fault-crossing geodetic lines and creepmeters, but the precursor time is model dependent. For the simulation shown, the surface creep reaches 1 cm/yr about 28 years before the earthquake; for more unstable faults, the precursor size and duration decreases.

The fault stability depends on the effective elastic stiffness and only two quantities from the friction law: (A_3-A_2) which measures the difference between velocity-weakening and velocity-strengthening, and d, which is the characteristic slip. For the simulations studied, it appears that the stress drop, coseismic slip, and recurrence time depend primarily on (A_3-A_2) and only weakly on d. In contrast, the size and duration of the precursory slip depends primarily on d. Therefore, it appears that observations of coseismic and postseismic slip do not help calibrate our prediction of precursors.

Preliminary work on more unstable models suggests, however, that small deep events that nucleate near the hypocenters of great earthquakes may give an indication of the fault stability.

REFERENCES

Brace, W. F., and J. D. Byerlee, California earthquakes: Why only shallow focus, Science, 168, 1573-1575, 1970.

Dieterich, J. H., Modeling of rock friction 1. Experimental results and constitutive equations, J. Geophys. Res., 84, 2161-2168, 1979.

Dieterich, J. H., Experimental and model study of fault constitutive properties, ASME Appl. Mech. Div., Solid Earth Geophysics and Geotechnology, ed. S. Nemat-Nasser, ASME, New York, 21-29, 1980.

Dieterich, J., Constitutive properties of faults with simulated gouge, Mechanical Behavior of Crustal Rocks, Monograph 24, eds. N. L. Carter, M. Friedman, J. M. Logan, and D. W. Stearns, American Geophysical Union, 103-120, 1981.

Lawson, A. C., The California earthquake of April 18, 1906, Report of the State Earthquake Investigation Commission, 2 vol., 641 pp., Carnegie Institution of Washington, Washington, D.C., 1908.

Lindh, A. G., Preliminary assessment of long-term probabilities for large earthquakes along selected fault segments of the San Andreas fault system in California, Open-File Report 83-63, U.S. Geological Survey, 1983.

Ruina, A., Friction Laws and Instabilities: A Quasi-static Analysis of Some Dry Friction Behavior, Ph.D. Thesis, Brown University, 1980.

Ruina, A., Slip instability and state variable friction laws, J. Geophys. Res., 1983.

Sieh, K., Slip along the San Andreas fault associated with the great 1857 earthquake, Bull. Seismol. Soc. Amer., 68, 1421-1448, 1979.

Thatcher, W., Strain accumulation and release of the 1906 San Francisco earthquake, J. Geophys. Res., 80, 4862-4872, 1975.

Thatcher, W., Nonlinear strain buildup and the earthquake cycle on the San Andreas Fault, J. Geophys. Res., 88, 5893-5902, 1983.

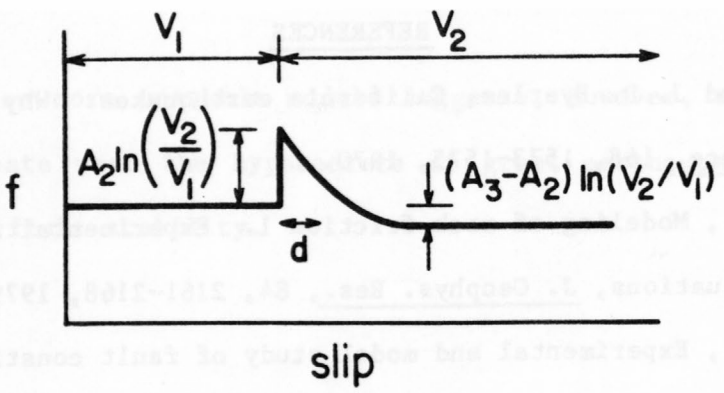

Figure 1. Friction coefficient versus slip in hypothetical sliding experiments, after the observations by Dieterich (1979, 1980, 1981). When the steady slip rate is switched abruptly from V_1 to V_2, we observe an instantaneous increase in friction followed by a gradual decay.

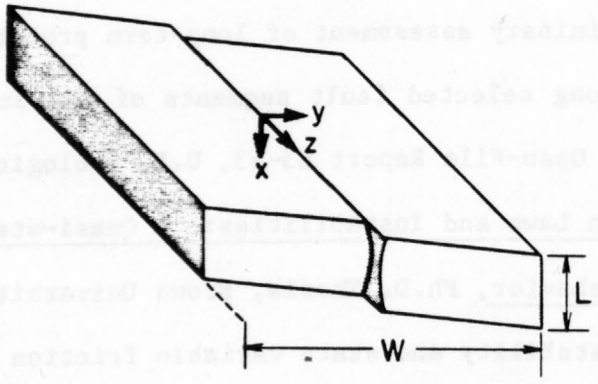

Figure 2. Two-dimensional antiplane fault model.

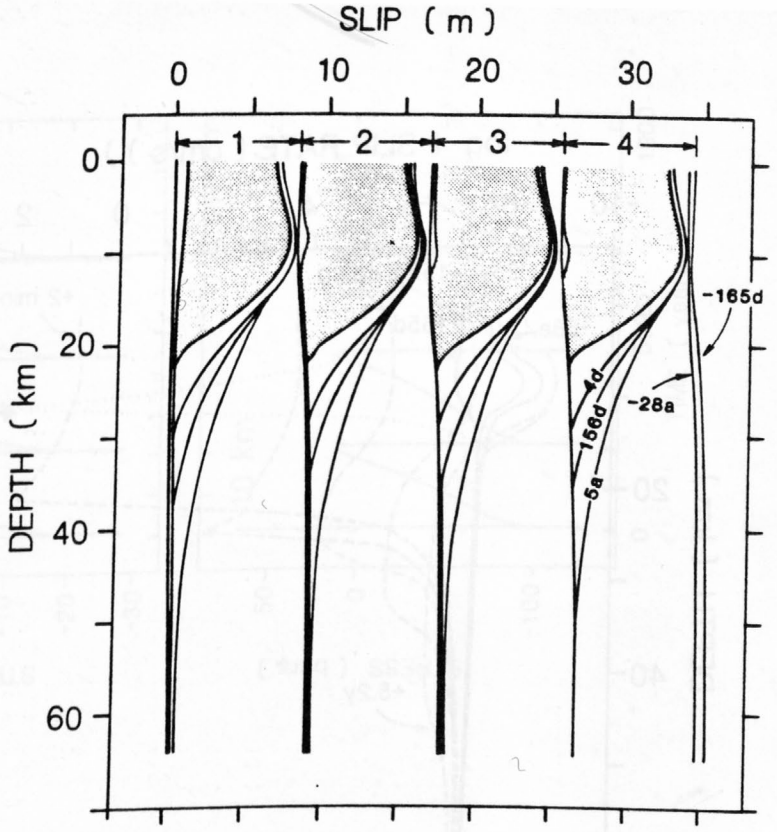

Figure 3. Two-dimensional simulation in a system with unstable seismogenic zone (parameter d = 10 cm). Each curve is cumulative slip versus depth at subsequent times through four earthquake cycles. Shaded regions show coseismic slip. Postseismic slip profiles labeled in days (+d) and years (+a) since the earthquake. Preseismic slip labeled in days (-d) and years (-a) before the next earthquake.

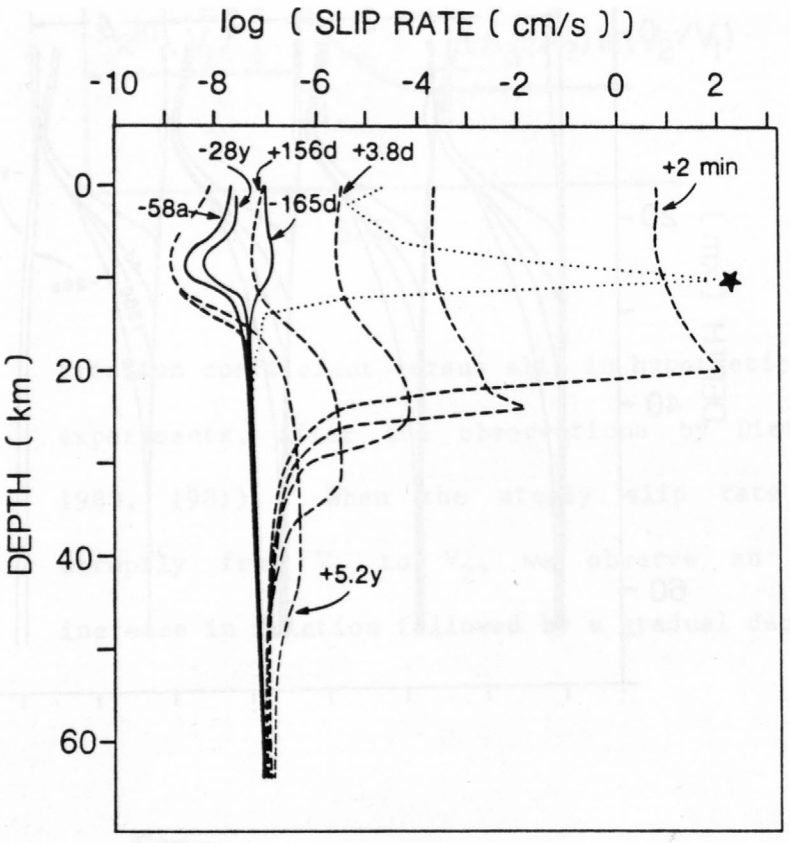

Figure 4. Log (slip rate) versus depth at subsequent times during the 4th cycle. Dotted curve shows slip rate profile at onset of earthquake with hypocenter (first point to go unstable) marked with a star. Selected postseismic velocity profiles shown with dashed lines and labeled in days (+d) or years (+a) since the earthquake. Preseismic curves shown in solid lines and labeled in days (-d) or years (-a) before the next earthquake.

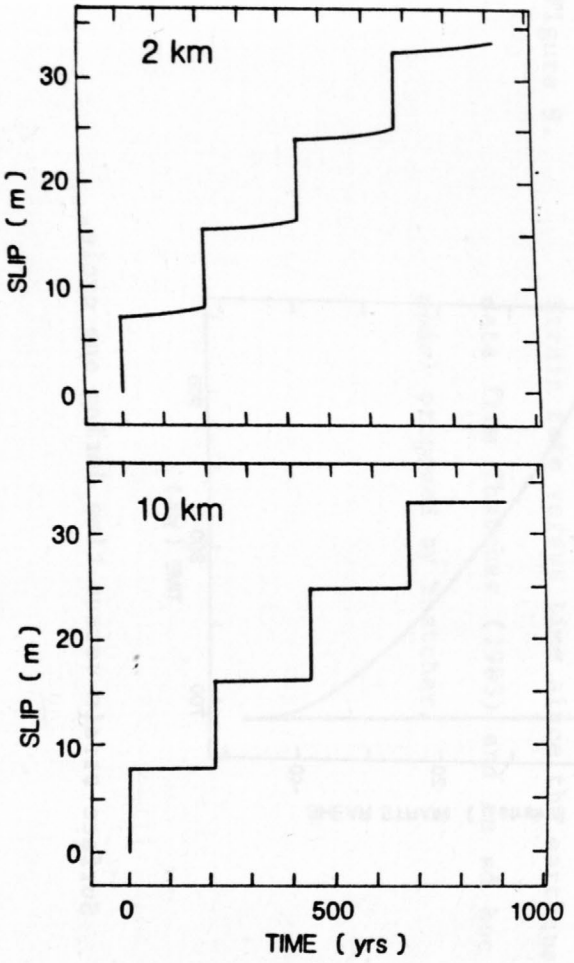

Figure 5.

Slip versus time at 2 km and 10 km depths.

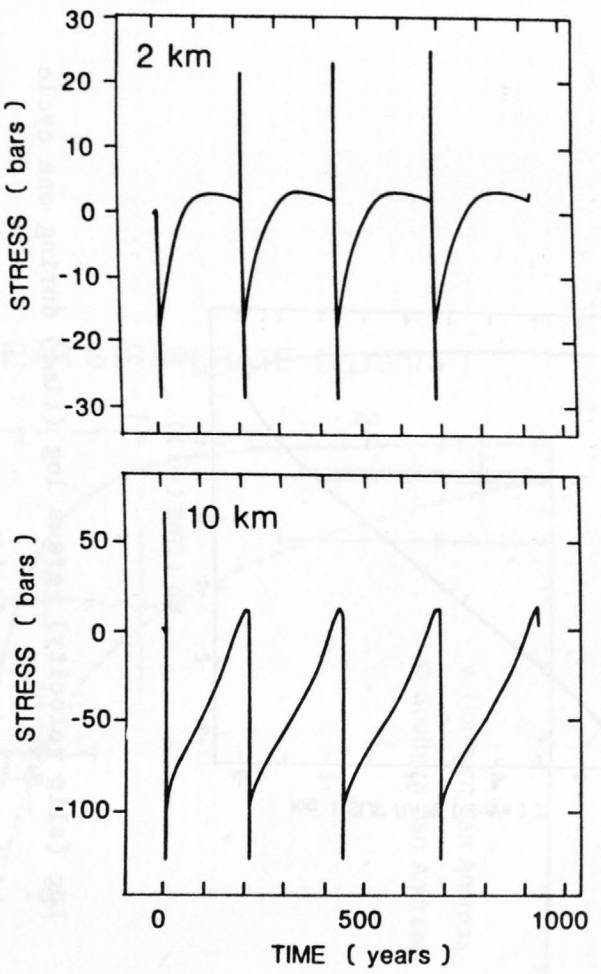

Figure 6.

Stress change (relative to the steady state value) versus time at 2 km and 10 km depths.

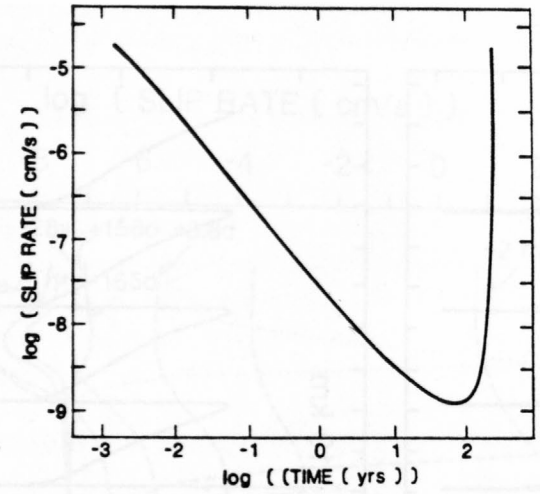

Figure 7. Log (slip velocity) versus log (time) during one cycle showing t^{-1} decay of slip rate.

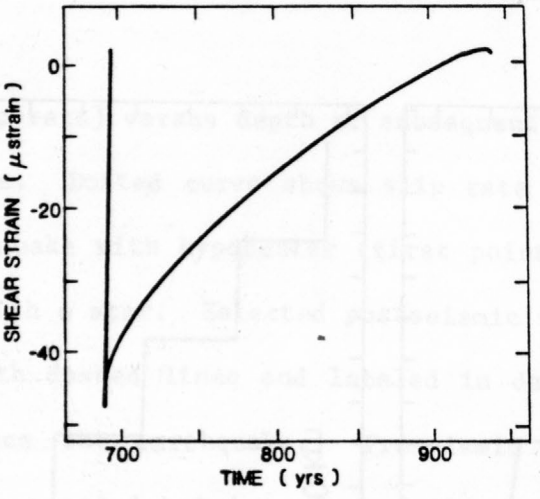

Figure 8. Surface strain versus time during one cycle.

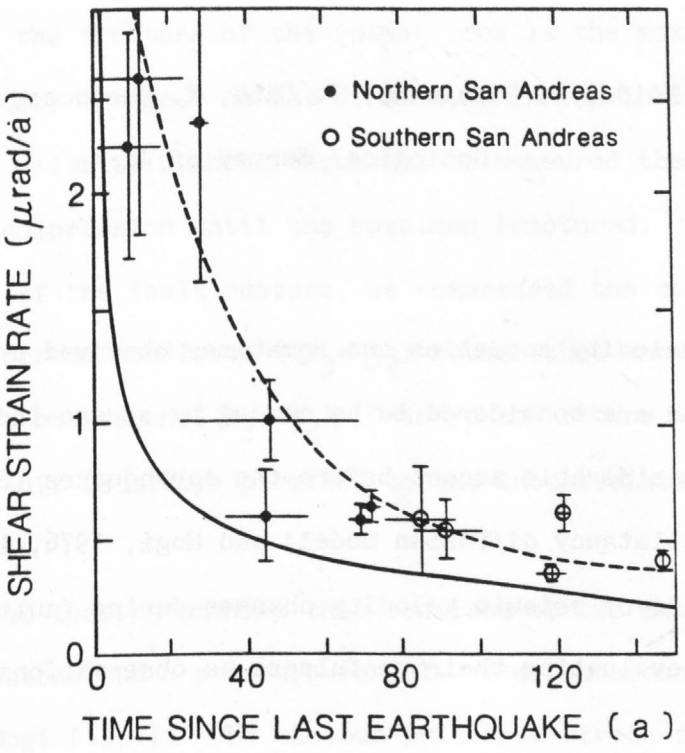

Figure 9. Strain rate versus time since the earthquake compared with data from Thatcher (1983) and an ad hoc postseismic slip model proposed by Thatcher.

THE EFFECT OF FAULT FORMATION ON VELOCITY AND ATTENUATION OF P-WAVE IN MARBLE UNDER GENERAL TRIAXIAL COMPRESSION

H. Koide, O. Nishizawa, T. Sato, K. Kusunose, and K. Ono

Geological Survey of Japan

Introduction

Seismic velocity anomalies are sometimes observed prior to large earthquakes and are considered to be caused by stress-induced fractures that increase in considerable amount before the earthquakes (Scholz and others, 1972, in the dilatancy diffusion model; and Mogi, 1976, in dry dilatancy model). Studies of seismic velocity changes during fault formation are thus important for evaluating their usefulness as observations for earthquake prediction.

The effect of faulting on seismic wave velocity and attenuation can be studied experimentally, if observations of the waves in an intact rock are made throughout the macroscopic fault-formation process. To clarify the effect of faulting on seismic waves, waves have to be monitored with relation to the size and the location of the individual fault. Spetzler and others (1981) and Sondergeld and others (1980) measured seismic velocities in pyrophyllite until a macroscopic fracture was formed. They measured the waves that propagated parallel to the fault plane. The velocity of this direction is expected to be a function of distance from the fault. Wang and others (1975) measured cross-fault P and S velocities during stick-slip motion. Though they failed to detect a velocity change, the investigation of velocity change in this direction is very important because we will predict earthquakes from seismic waves that cross the fault plane. The stress drop occurring

during the fracture of intact rock is some ten times bigger than that for stick-slip (i.e. for previously fractured rocks). So, the velocity change just before and after the fracture of the intact rock is the maximum expected value of seismic velocity change. As the first step in the investigation of the change in seismic velocity with earthquakes, we measured the elastic waves of intact rock under compression until the specimen fractured. In order to control the direction of the fault rupture, we compressed the specimen under the general triaxial stress condition ($\sigma_3 = \sigma_2$) rather than under the so-called triaxial stress condition ($\sigma_3 \neq \sigma_2$) (Granryd and others, 1983). Under this condition, the fault is always parallel to the intermediate-stress axis.

Experiment

We used a triaxial testing machine that consists of two mutually orthogonal loading pistons and a pressure vessel. The fundamental design is the same as that of Mogi (1971). The minimum principal stress is applied by oil, and for the other two principal stresses, by steel pistons. Load and pressure are servo-controlled. The axial displacement of each piston was monitored by LVDT. Rectangular prisms (35x35x70mm) of marble (location; Yamaguchi Prefecture, Japan) were used as test pieces.

We took 20MPa as the minimum stress, 80MPa as the intermediate stress, and the maximum stress was applied as the axial strain rate of 1×10^{-6}/sec. From our experience, under this stress condition, the fault plane always propagates between diagonally opposite edges and splits the specimen into two blocks, as illustrated in Figure 1.

Piezo-electric transducers (2 MHz resonance frequency) were attached to the specimen's surfaces (A, B) of the minimum principal stress and to the bottom end piece (EP). The elastic waves were radiated from EP and A transducers and the velocities of A-B, EP-A, and EP-B pass were monitored by

A,B transducers.

As the specimen was too small to set piezo-elastic transducers together, the strain was monitored using another specimen under the same stress and strain-rate conditions. For the strain parallel to the maximum and the intermediate-stress axes, cross-type gauges were directly pasted onto the specimen's surfaces subjected to the minimum stress. All surfaces parallel to the minimum stress direction were in contact with the steel pistons, so that the direct measurements along the minimum stress direction were impossible to make. Consequently, a metal cantilever-type displacement meter was used for this direction (Figure 1). This meter measures the displacement of the minimum stress direction from the elastic bending of the cantilever.

At the present stress and strain-rate condition, the marble was deformed as shown in Figure 2. $\varepsilon_1, \varepsilon_2, \varepsilon_3, \varepsilon_v$ indicate the maximum, the intermediate, the minimum, and the volumetric strain, respectively. The specimen yields at 180 MPa of the maximum stress, and then shows ductile deformation until the fault formation, where ε_1 and ε_2 reach -1.0 and 2.5 percent, respectively.

Figure 3 shows the variation of P-wave velocity of the minimum stress direction with respect to the axial strain during the deformation. Fifty percent velocity decrease was observed until the fault formed. Figure 4 shows the stress drop and the strain discontinuity caused by the fault formation. ε_1 and ε_2 recovered 0.5 and 0.15 percent, respectively, while ε_3 increased more than 0.6 percent after the failure.

Figures 5, 6, and 7 show the change of elastic wave forms caused by the fracturing. In Figure 5, we see that the arrival time of the A-B path became faster after the fault formation. As the ε_3 discontinuity in Figure 4 shows, the A-B path became longer after the fault formation. This arrival time change is not caused by the path shortening but by the increase of velocity.

The velocity recovery of the A-B path was about 6 percent relative to the velocity ratio at the time of faulting (Figure 8). Stress drop-velocity change relationships will be obtained from series of experiments of this type. The high frequency components (1-2 MHz) of the elastic waves through the EP-A path attenuated drastically after the failure, while those of the EP-B path did not (Figure 6, 7). Because the only difference between these two paths is that the EP-A path crossed the fault, the resulting high attenuation of the EP-A waves was caused by the fault plane.

References

Granryd, L., I. C. Getting, and H. Spetzler, 1983, Path dependence of acoustic velocity and attenuation in experimentally deformed Westerly granite, Geophys. Res. Letters, 71-74.

Mogi, K., 1971, Fracture and flow of rocks under high triaxial compression, J. Geophys. Res., 76, 1255-1269.

Mogi, K., 1974, Zairyo (in Japanese), 23, 320.

Scholz, C. H., L. R. Sykes, and Y. P. Aggarwal, 1973, Earthquake prediction: A physical basis, Science, 181, 803-810.

Sondergeld, C. H., I. C. Getting, H. A. Spetzler, and G. A. Sobolev, 1980, Velocity changes associated with generalized triaxial deformation of pyrophyllite, PAGEOPH, 118, 975-989.

Spetzler, H. A., G. A. Sobolev, C. H. Sondergeld, B. G. Sobolev, I. C. Getting, and A. Koltov, 1981, Surface deformation, crack formation and acoustic velocity changes in pyrophyllite under polyaxial loading, J. Geophys. Res., 86, 1070-1080.

Wang, C., R. E. Goodman, and P. N. Sundaram, 1975, Variation of V_p and V_s in granite premonitory to shear rupture and stick-slip sliding: Application to earthquake prediction, Geophys. Res. Letters, 2, 309-311.

Figure Captions

Figure 1. Schematic diagram of sample assemblage viewed from the intermediate stress direction. Left: Locations of piezo electric transducers. Labels 1 and 3 denote the maximum and minimum stress. Right: Assemblage of strain measurement; 1) metal strip, 2) strain gauge for detecting σ_3 displacement, 3) copper foil, 4) cross-type strain gauge for measuring in σ_1 and σ_2 directions. The specimens were jacketed by silicon rubber.

Figure 2. Stress-strain relations during the deformation.

Figure 3. P-wave velocity change during the deformation with respect to the axial strain.

Figure 4. Stress and strain discontinuity during the ultimate fracture.

Figure 5. Waveforms of A-B path, before and after the ultimate fracture.

Figure 6. Waveforms of EP-A path, before and after the ultimate fracture.

Figure 7. Waveforms of EP-B path, before and after the ultimate fracture.

Figure 8. Velocity change in A-B path, before and after the ultimate fracture.

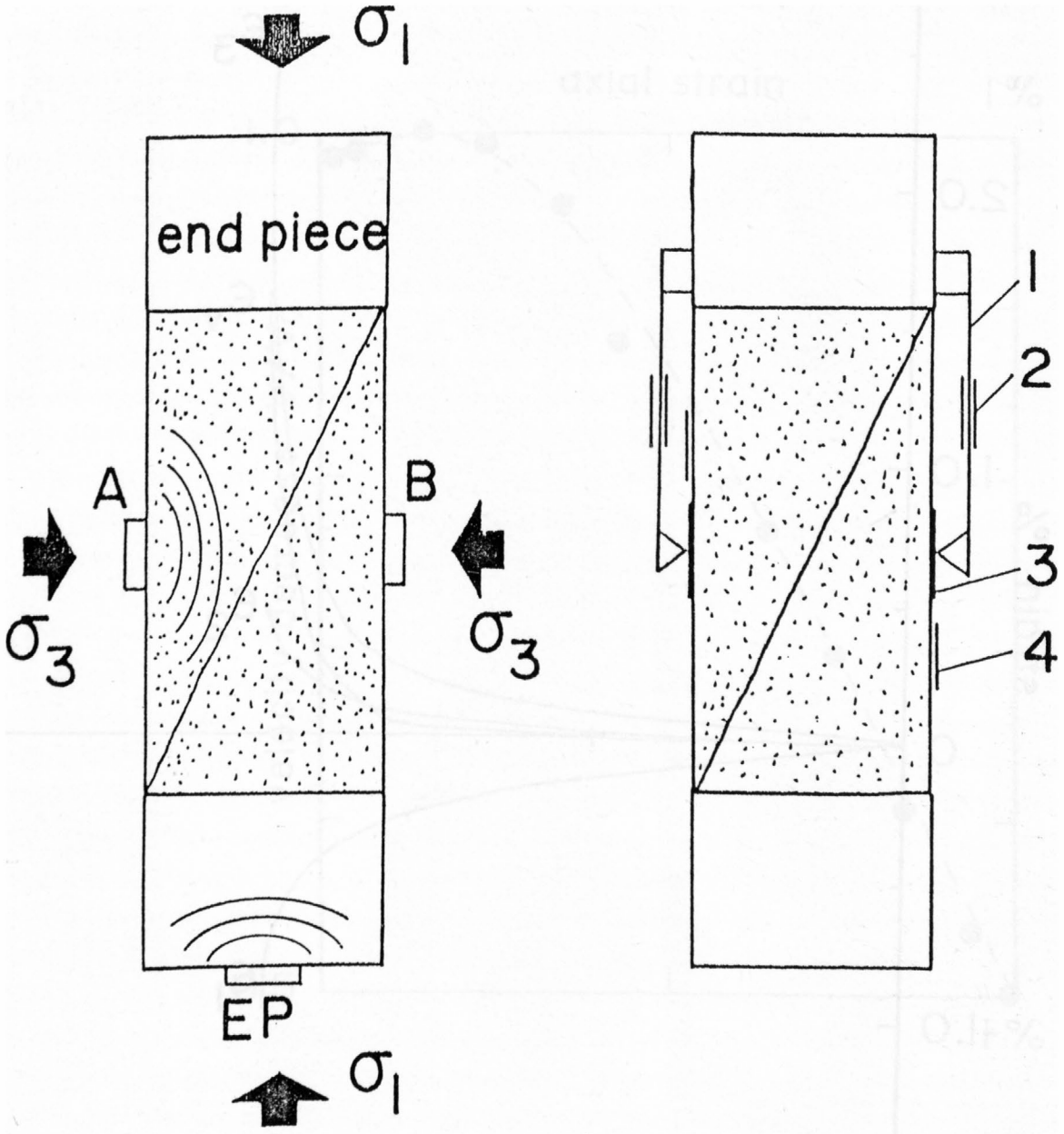

Figure 1.

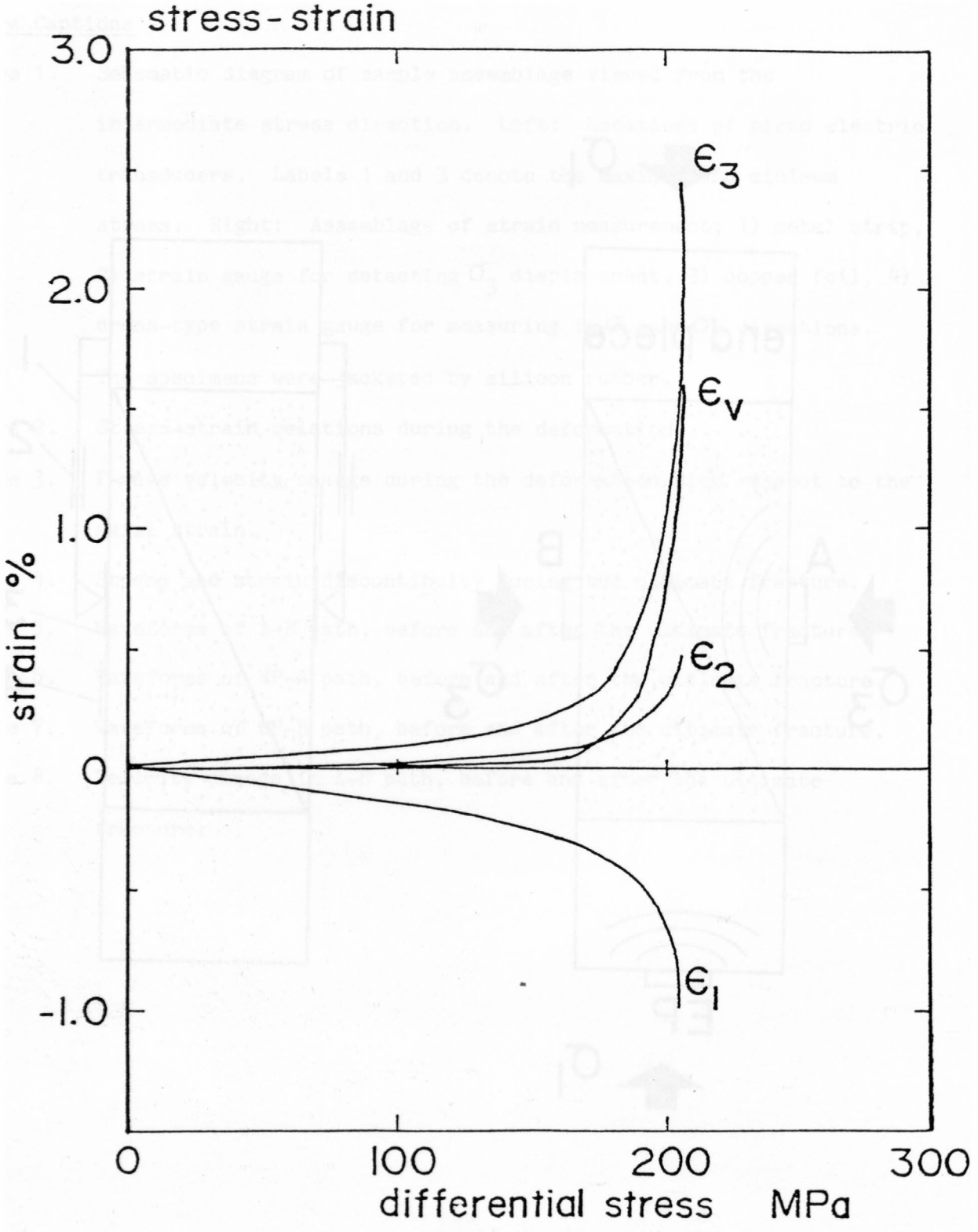
stress - strain
3.0
2.0
1.0
0
-1.0
strain %
ϵ_3
ϵ_v
ϵ_2
ϵ_1
0
100
200
300
differential stress MPa

Figure 2.

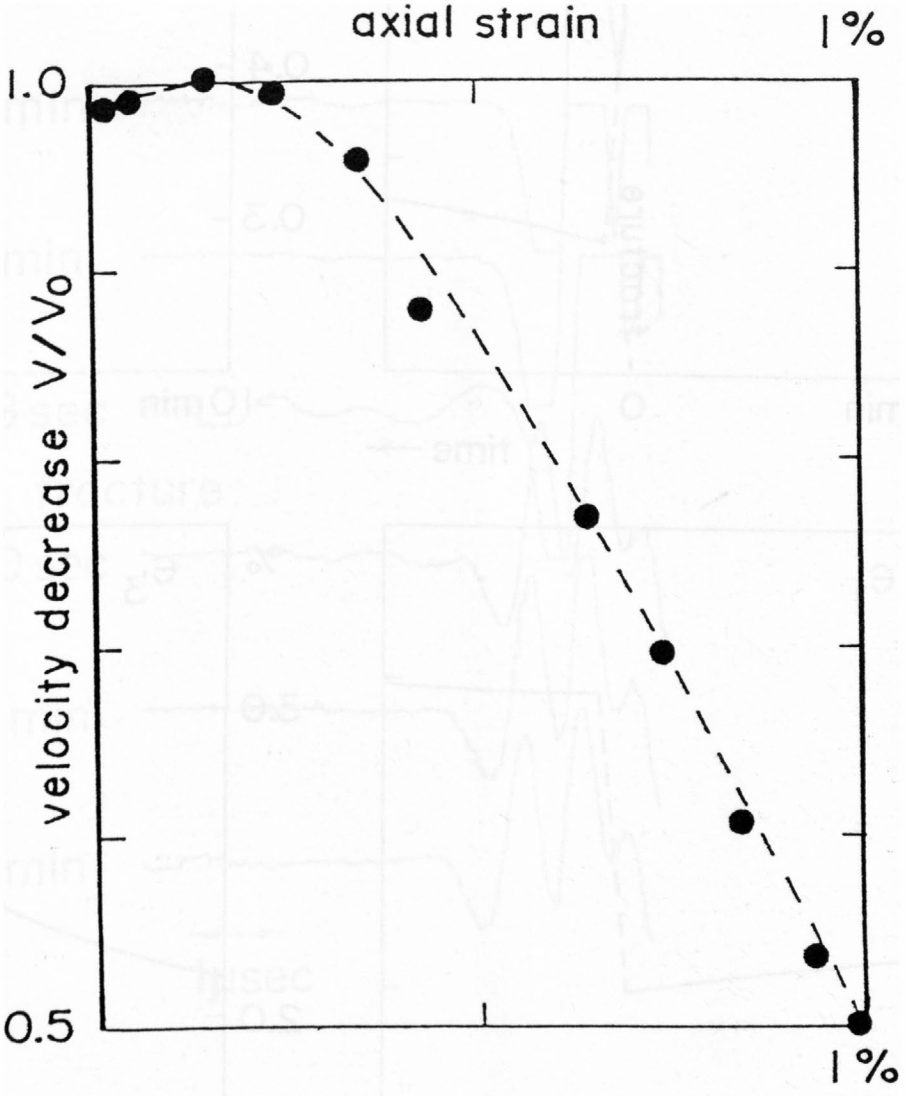

Figure 3.

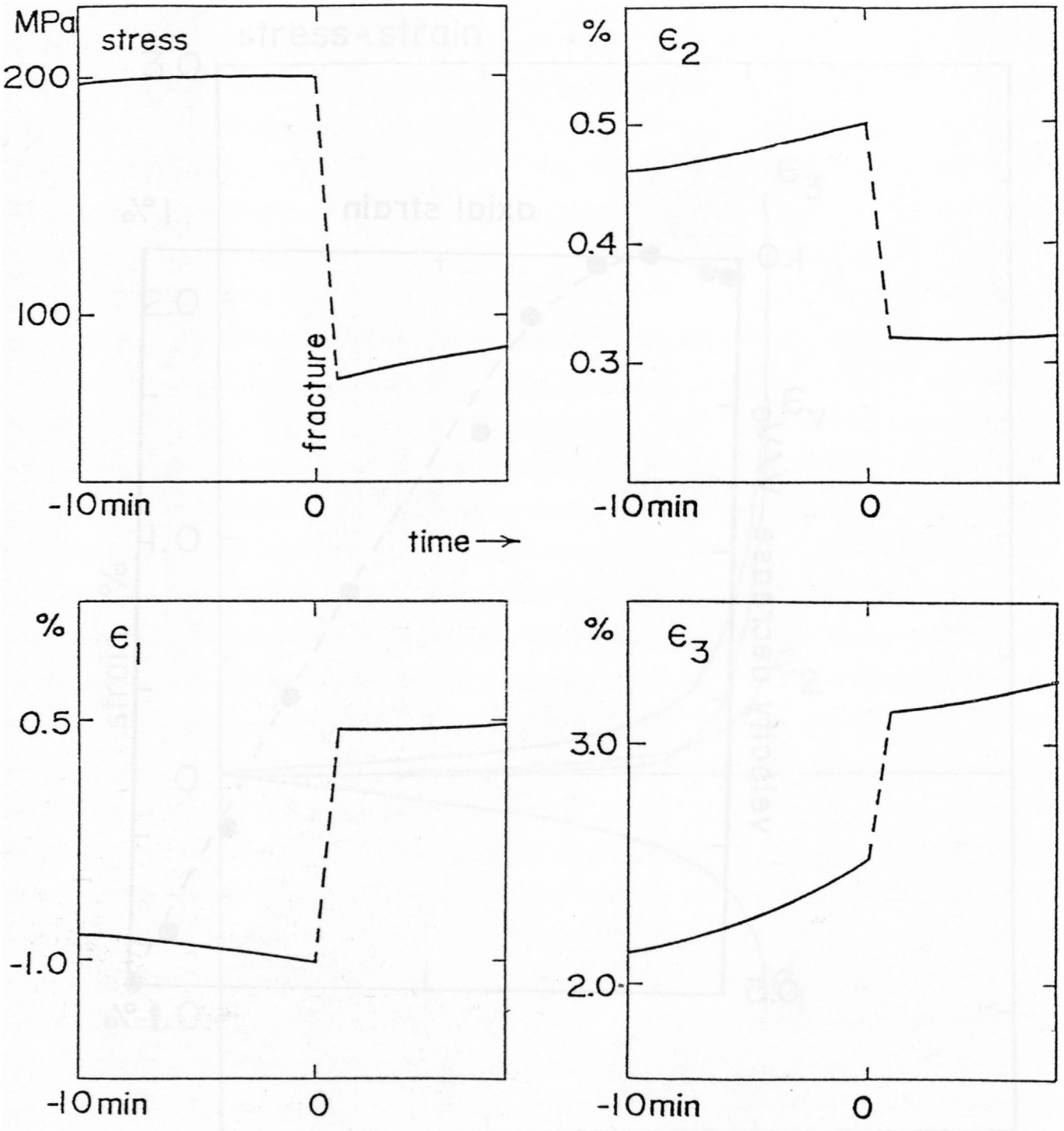
MPa
stress
200
100
fracture
-10min
0
time →
%
ϵ_2
0.5
0.4
0.3
-10min
0
%
ϵ_1
0.5
-1.0
-10min
0
%
ϵ_3
3.0
2.0
-10min
0

Figure 4.

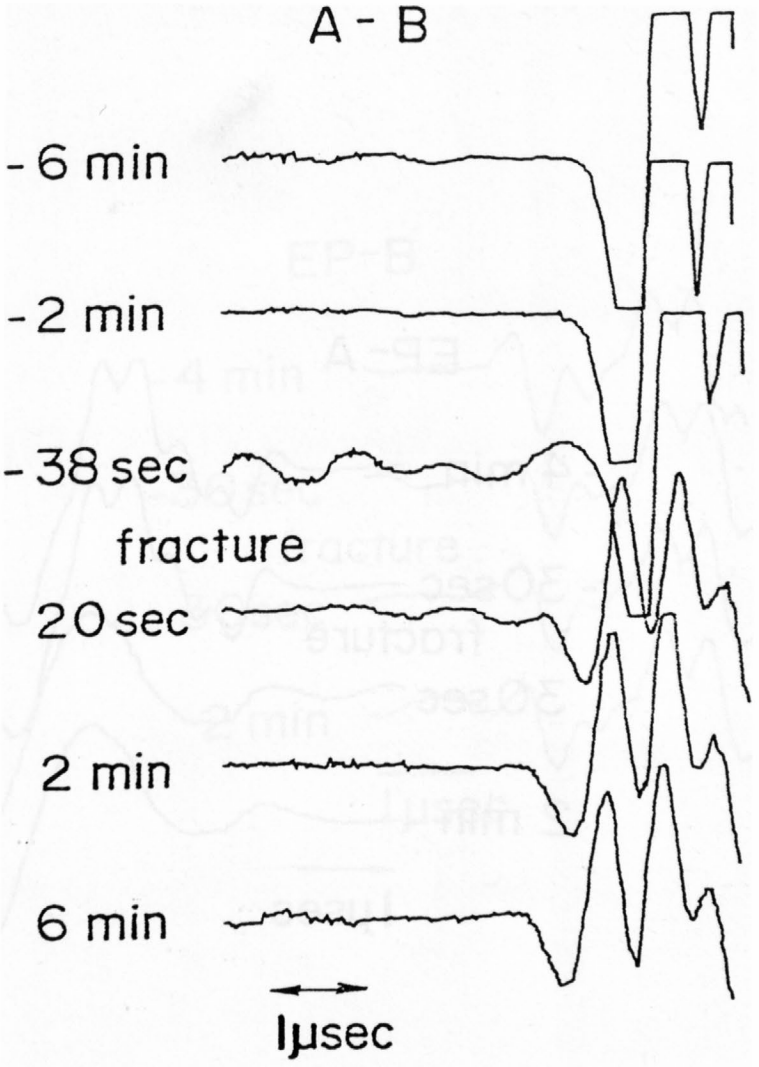

Figure 5.

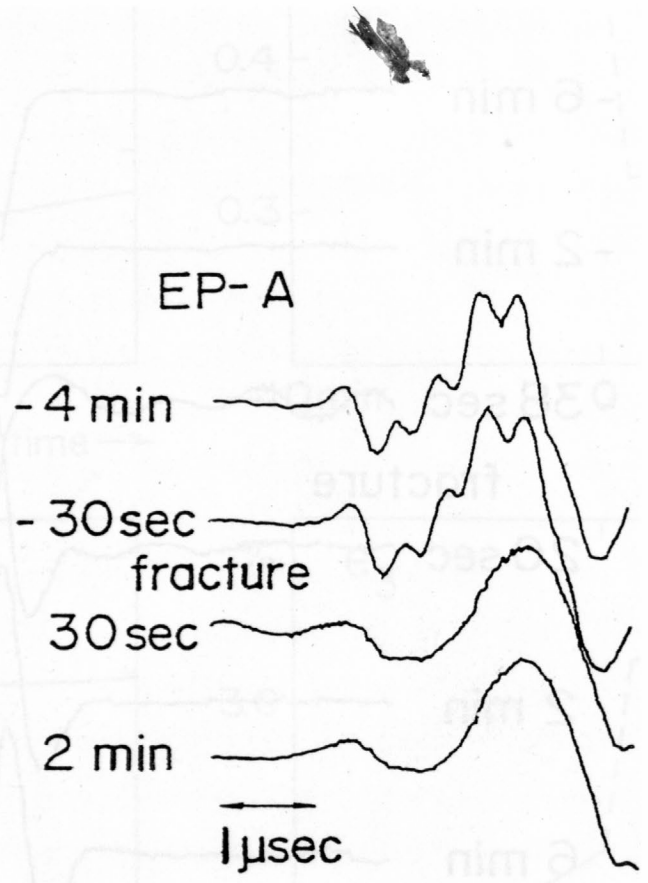

Figure 6.

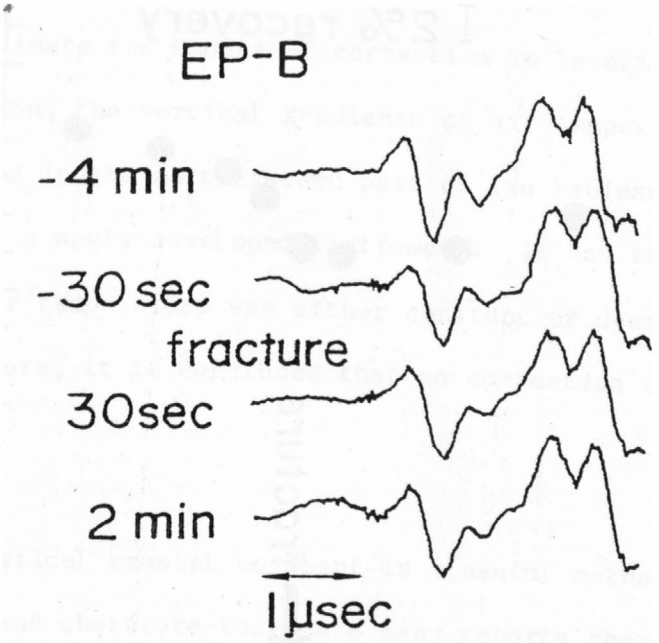

Figure 7.

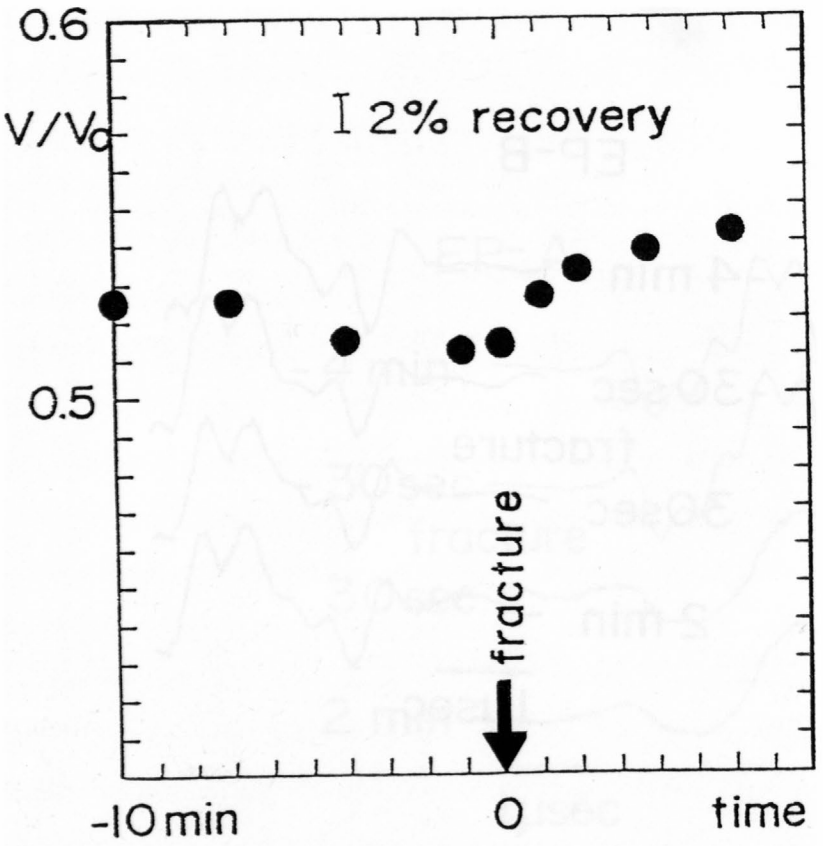

Figure 8.

REFRACTION CORRECTION IN LEVELING

Hitoshi Haruyama and Takashi Tada

Geographical Survey Institute

Abstract

In order to estimate the amount of correction in leveling caused by atmospheric refraction, the vertical gradients of air temperature near ground surface were measured in the northeastern part of Izu Peninsula, central Japan in December, 1983 by a newly-developed instrument. It has been revealed that in most cases the air temperature was either constant or decreased linearly with height. Therefore, it is concluded that no correction of refraction is necessary in winter.

Introduction

Detection of vertical crustal movement is a useful method for earthquake prediction research and therefore there are many reports about anomalous vertical crustal movement observed before earthquake occurrence. However, it is very difficult to judge whether the observed anomalous vertical crustal movement is a precursor related to the earthquake occurrence or is an apparent phenomenon caused by the errors of leveling because the amount of precursory vertical crustal movement is rather small. Therefore, the accurate estimation of errors of leveling becomes very important for earthquake prediction research.

Among errors of leveling, refraction error caused by the vertical distribution of air temperature near the ground surface is the most serious one. In particular, the accumulation of this error in mountain areas becomes

so large that it can not be neglected. For this reason, many theoretical studies about the refraction error have been carried out[1) 2)]. Nevertheless, the results of these studies were not previously applied to leveling in Japan because the magnitude of refraction correction was considered small, and extra equipment was required to measure air temperature variation with height near the ground surface.

We have attempted to measure accurate air temperature variations with height near the ground surface at the same time as leveling using a newly-developed apparatus and to calculate the precise refraction correction.

Observation

A new instrument has been developed in order to measure the vertical distribution of air temperature near the ground surface. A platinum resistance thermometer is used for the thermosensor. It is mounted in coaxial double tubes with many air holes. Inner walls and outer walls of the tubes are painted black and white, respectively. Fig. 1 shows one sensor. A hood can be mounted above a sensor to prevent direct sunlight when it is necessary.

The instrument consists of six sensors mounted on a pole three meters long, as shown in Fig. 2. The setting positions of the six sensors are changeable. An amplifier, an A-D converter, a digital recorder and a power supply are mounted on the pole also. Total weight of the instrument is about 14 kg. Deviation of each sensor is found to be less than 0.1°C by calibration using a thermoregulator and a crystal standard thermometer.

Observations were carried out in December, 1983 in the northeastern part of Izu Peninsula where the terrain is steep and anomalous crustal uplift has continued since 1974. Fig. 3 shows the location map of the test site and the leveling route. The length of the route is about 7 km and the maximum height

difference along the route is about 300 m. The total number of observation points was about 350.

The instrument was placed near the level and the air temperature and scale reading were measured at the same time. Fig. 4 shows a photograph of the observation set up.

Results

Fig. 5 shows time variation of air temperature at 0.3 m and 2.7 m from ground surface during the observation. The difference between air temperatures at both heights was small, 0.2-0.5°C. Some examples of vertical distribution of air temperature are shown in Fig. 6. Examples of constant, linear gradient, reverse and exponential distribution types are shown in Figs. 6-a, -b, -c and -d, respectively. According to the Kukkamaki's function[1], air temperature T was assumed as follows:

$$T = A + B * Z^{C},$$

where Z was height from ground surface and A, B and C were constants. A, B and C were calculated by the least-square method using the observed data. The results are listed in Table 1. Only for about 33% of the observations could the constant C be determined. The frequency distribution of calculated C is shown in Fig. 7 and the average value of calculated C is 0.971. In those cases where the constant C could not be calculated, vertical gradients of air temperature were almost zero and it leads to the result that C is equal to 0. The result that the mean value of calculated C is about 1.0 indicates that the vertical distribution of air temperature is able to approximate a linear equation of height in the observed range, not an exponential function.

This result, C = 0 or 1.0, leads to the following important conclusion that no correction of refraction is necessary in winter from the Kukkamaki's formula for the refraction correction,

$$R = -10^{-5} * \gamma * (s/50)^2 * \Delta t * d$$

where R is a correction value, s is sight distance, d is height difference, t is the temperature difference between Z = 0.5 m and Z = 2.5 m, and

$$\gamma = \{5.95/(250^C - 50^C)\} * \{200 * 150^C + (50^{C+1})/(C+1)\}$$

For reference, the correction values of refraction in the cases of C = -0.1 and C = -0.33 are listed in Table 2. The correction values in these cases are negligibly small, so no correction is necessary in winter, even when C is not equal to 0 or 1.0.

Conclusions

It has been revealed that in winter, C is nearly equal to 0.0 or 1.0; i.e., T is constant or varies linearly as Z. Therefore, we conclude from the observations described above that the correction of refraction is not necessary in winter.

However, the crustal movement shown in Fig. 8-b, which was obtained by the comparison between the results of November, 1982 and June, 1982, correlates to the terrain profile in Fig. 8-c. A preliminary observation of air temperature last summer suggests that the amount of correction of refraction is considerably larger than that in winter, so this crustal movement is probably a phenomenon caused by refraction error.

Therefore, it is necessary to study the detailed distribution of air temperature in summer and further observations will be carried out. Furthermore, a comparison between the observation results and the theoretical treatment based on the Holdahl theory will be studied.

References

Kukkamaki, T. J., Uber die nivellitische refraktion, Publ. 25, 48 pp., Finn. Geod. Inst., Helsinki, Finland, 1938.

Holdahl, S. R., Recomputation of vertical crustal motions near Palmdale,

California, 1959-75, preprint for presentation to the General Meeting of the IAG, Tokyo, Japan, May 7-20, 1982.

Tanaka, M., et al., in preparation.

Figure and Table Captions

Fig. 1 Photograph of sensor.

Fig. 2 Photograph of instrument.

Fig. 3 Location map of test site and leveling route.

Fig. 4 Photograph of observation state.

Fig. 5 Time change in air temperature at heights of 0.3 m and 2.7 m.

Fig. 6 Examples of vertical distribution types of air temperature. a: constant, b: linear, c: reverse, d: exponential

Fig. 7 Frequency distribution of determined C value.

Fig. 8 Recent vertical crustal movement in the northeastern part of Izu Peninsula.

Table 1 Result of calculation of C.

Table 2 Refraction correction values for C = -0.100 and C = -0.333.

Table 1

	a.m.	p.m.	total
determined	75 (30 %)	42 (42 %)	117 (33 %)
undetermined	117 (70 %)	58 (58 %)	235 (67 %)
sum	252	100	352

Table 2

section	distance	height diff.	correction	
			C=-0.100	C=-0.333
10004-10003(1)	947 m	-102.1156 m	-0.127mm	-0.135mm
10003-10004(2)	946	102.1170	0.176	0.190
mean	947	102.1163	0.152	0.163
10003-10002(1)	1033	-58.9626	0.025	0.027
10002-10003(2)	1040	58.9621	0.355	0.381
mean	1037	58.9624	0.165	0.177
10002-10001(1)	1449	-136.1425	-0.336	-0.355
10001-10002(2)	1458	136.1443	0.583	0.612
mean	1454	136.1434	0.460	0.484
total	3438	297.2230	0.777	0.824
corr./100m			0.261	0.277

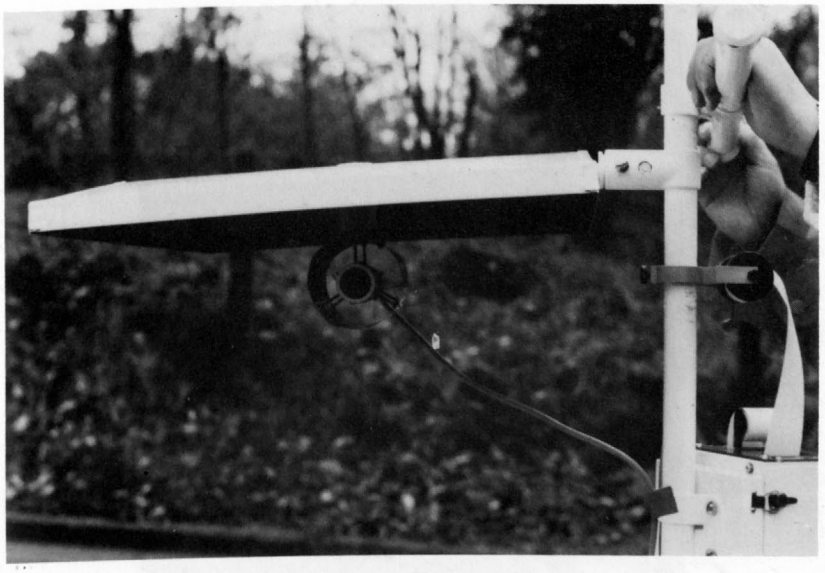

Figure 1.

Figure 2.

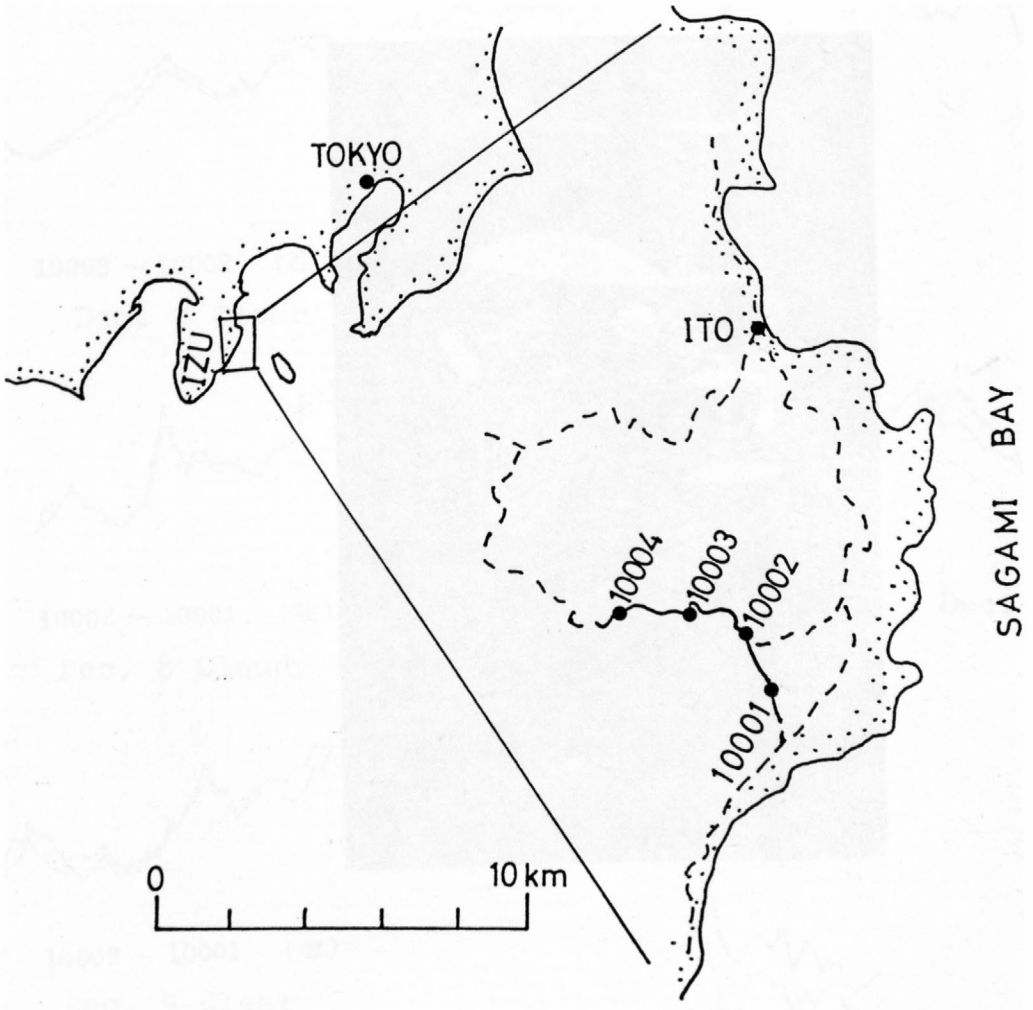

Figure 3.

Figure 4.

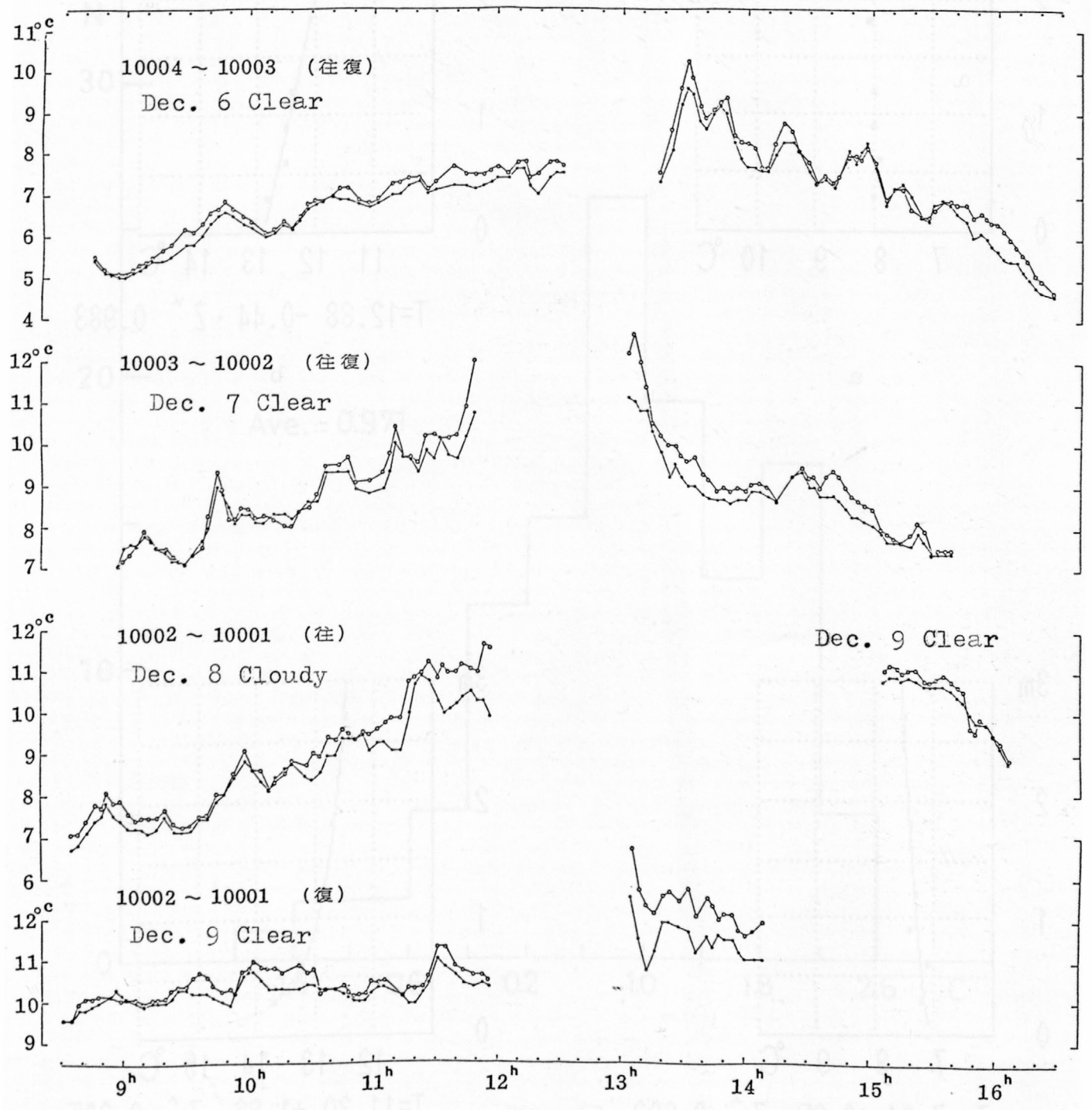
sensor No. 1, H:2.7 m
sensor No. 6, H:0.3 m
10004 ~ 10003 (往復)
Dec. 6 Clear
10003 ~ 10002 (往復)
Dec. 7 Clear
10002 ~ 10001 (往)
Dec. 8 Cloudy
Dec. 9 Clear
10002 ~ 10001 (復)
Dec. 9 Clear
°c
9h
10h
11h
12h
13h
14h
15h
16h

Figure 5.

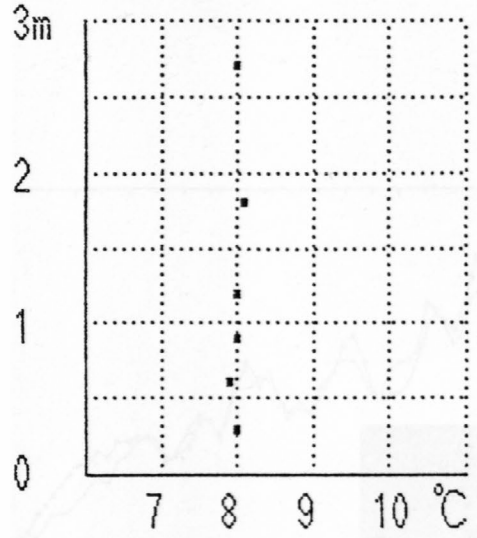

a

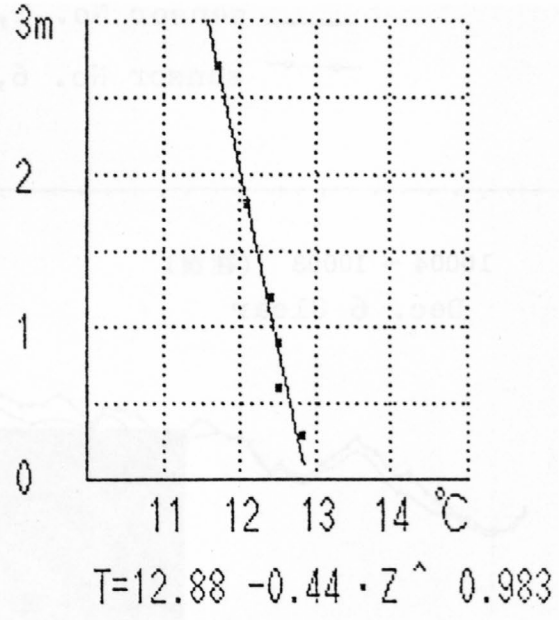

b

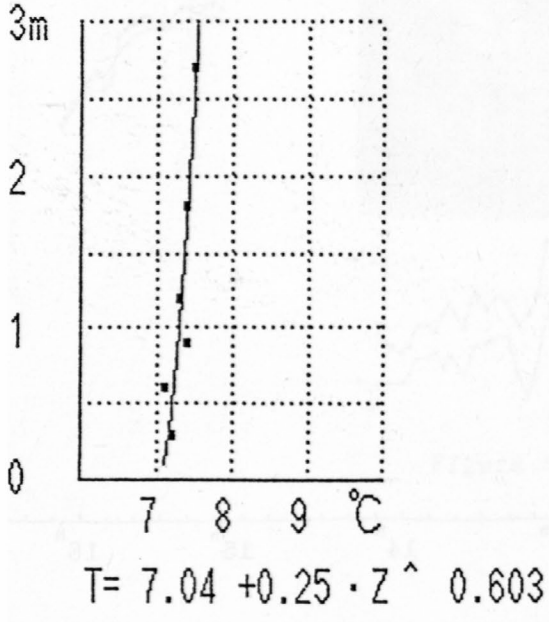

c

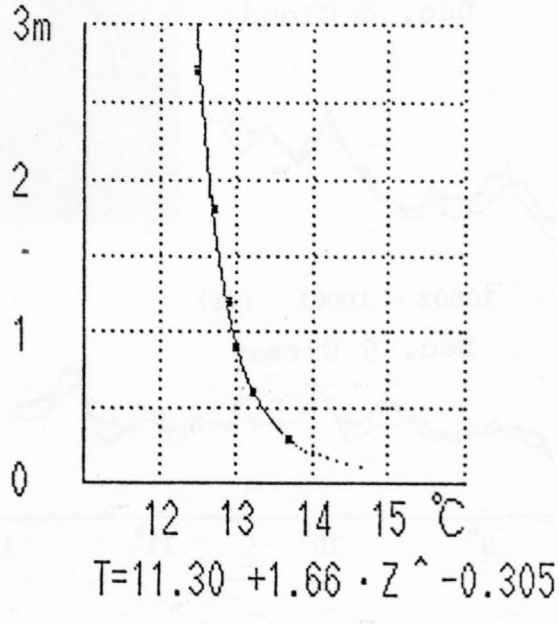

d

Figure 6.

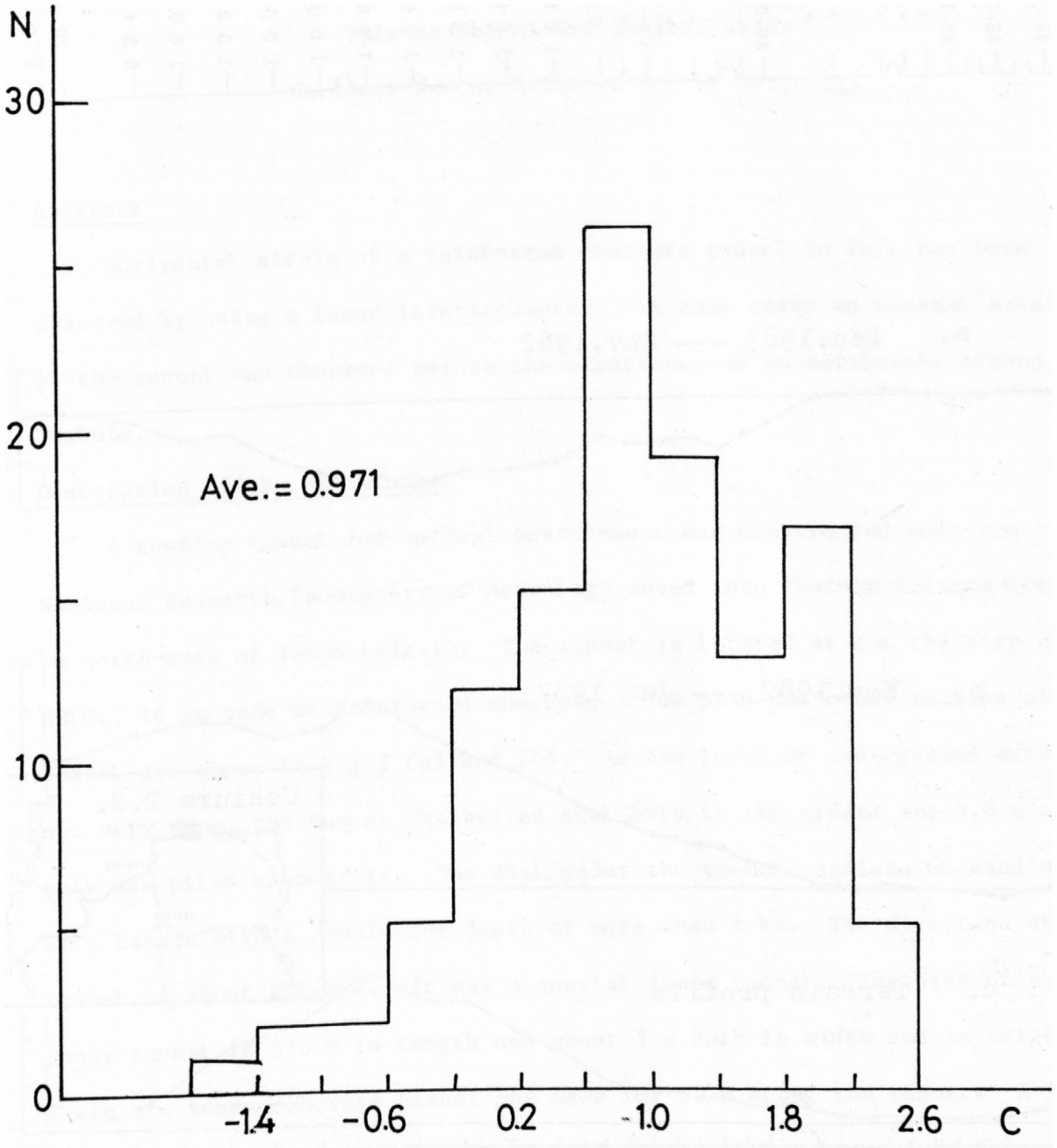

Figure 7.

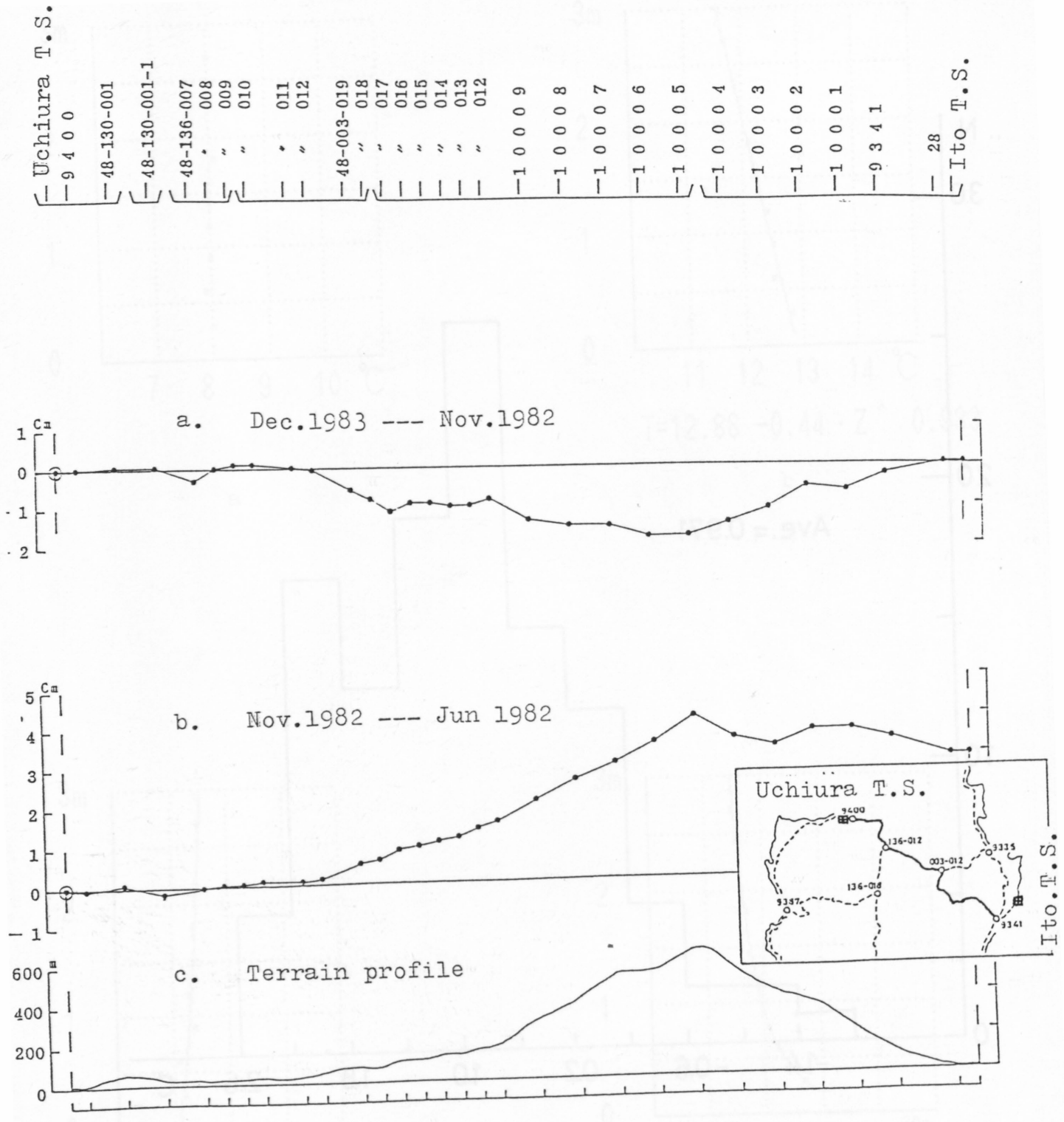
Uchiura T.S.
9400
48-130-001
48-130-001-1
48-136-007
" 008
" 009
" 010
" 011
" 012
48-003-019
" 018
" 017
" 016
" 015
" 014
" 013
" 012
10009
10008
10007
10006
10005
10004
10003
10002
10001
9341
28
Ito T.S.
a. Dec.1983 --- Nov.1982
Cm
1
0
-1
-2
b. Nov.1982 --- Jun 1982
5
4
3
2
1
0
-1
Uchiura T.S.
9400
136-012
3335
003-012
136-018
9387
9341
Ito.T.S.
c. Terrain profile
m
600
400
200
0

Figure 8.

STRAIN MEASUREMENT OF A CONCRETE TUNNEL IN THE SOIL USING LASER INTERFEROMETER

Tadanao Ohishi and Shoichi Seino

National Research Laboratory of Metrology

Abstract

Horizontal strain of a reinforced concrete tunnel in soil has been observed by using a laser interferometer. In some cases an unusual extension of the tunnel was observed before the occurrance of an earthquake around Tsukuba.

Description of the NRLM Tunnel

A testing tunnel for optical measurement was constructed when the National Research Laboratory of Metrology moved into Tsukuba Science City, 60 km north-east of Tokyo (Fig.1). The tunnel is located at the the site of NRLM. It is made of reinforced concrete. The plan and cross section of the tunnel are shown in Fig.2 (a) and (b). As the level of underground water is not very deep, the tunnel was buried shallowly in the ground and 3.5 m thick soil was piled up over it. The soil under the tunnel consists of sand and silt layers with a cumulative depth of more than 1 km. The direction of the tunnel is about ENE-WSW. It has a coaxial inner tunnel. The size of the inner tunnel is 310 m in length and about 3 m both in width and in height. There are seven concrete bases: one base for 50 m along the tunnel. A 54 m long optical bed for measurement of a 50 m span with a laser interferometer was installed near one end of the tunnel. The interferometer for measurement of tunnel strain was installed on the floor near the third base, 120 m apart from one end of the tunnel. Its span is 25 m with evacuated steel tube.

Initial Deformation and Yearly Strain Change of the Tunnel

The tunnel was constructed in the autumn of 1979. Fig.3 shows the strain of the tunnel between August 1980 and December 1981. The curve is not perfect; many discontinuities were observed in a period between October and December of 1980. From Fig. 3 we made estimations as follows:

(1) Initial extension of the tunnel had lasted until the midst of December of 1980.

(2) Since 1981 the tunnel has had ordinary conditions of strain through the year.

(3) The hatched portion in Fig.3 is the initial deformation of the tunnel.

Deformation of the tunnel just after construction was not observed. But it is estimated by extrapolating the initial deformation shown in Fig.3 that the tunnel expanded for almost one year, and the secular extension is estimated to be about 2×10^{-5} (Fig.4).

Yearly variation on the tunnel strain forms a fairly smooth sinusoid with its amplitude of about 8×10^{-6}. The main cause of the variation is estimated to be temperature change of the soil around the tunnel. The temperature change outdoors and in the tunnel are shown in Fig.5. On one hand the amplitude of the outdoor temperature change is 25 °C and on the other hand the tunnel temperature varies only 2.5 °C. The timing of the temperature change in the tunnel is delayed about three months compared with that outdoors. The phase of the tunnel strain change is delayed about three months compared with that of the temperature change in the tunnel. A clear explanation has not been made of the effect. The short-term change of tunnel strain is shown in Fig.6. On five days prominent extensions were observed. But temperature changes corresponding to these extensions were not observed. So it is

supposed that the strain force caused by the extension of the surface part of the soil makes the tunnel lengthen. It is obvious that some other factors and not temperature cause the tunnel strain. The factors may be rainfall, atmospheric pressure, underground water level and so on.

Effect of Rainfall

Tunnel strain and precipitation are shown in Fig.7 (a)-(d). It seems that rainfall causes shrinkage of the tunnel. But this correlation is not clear.

Strain Before Earthquakes

Fig.8 shows an example of unusual extension of the tunnel before the occurrance of an earthquake. But in the case shown in Fig.9, any unusual extension was not observed before earthquakes. It seems that these examples do not have any common meaning. However, it is found that by comparing the curves with the broken lines, both of these curves have rising components. The broken lines are smoothed by the long term secular strain model of the tunnel.

Tunnel strain changes before earthquakes are shown in Fig.10-Fig.14. These curves have not been examined in detail. At least in some cases, unusual extensions of the tunnel before earthquakes were found. It would be interesting if they are precursors. Examination from different angles is necessary.

FIG.1 LOCATION OF THE NRLM TUNNEL

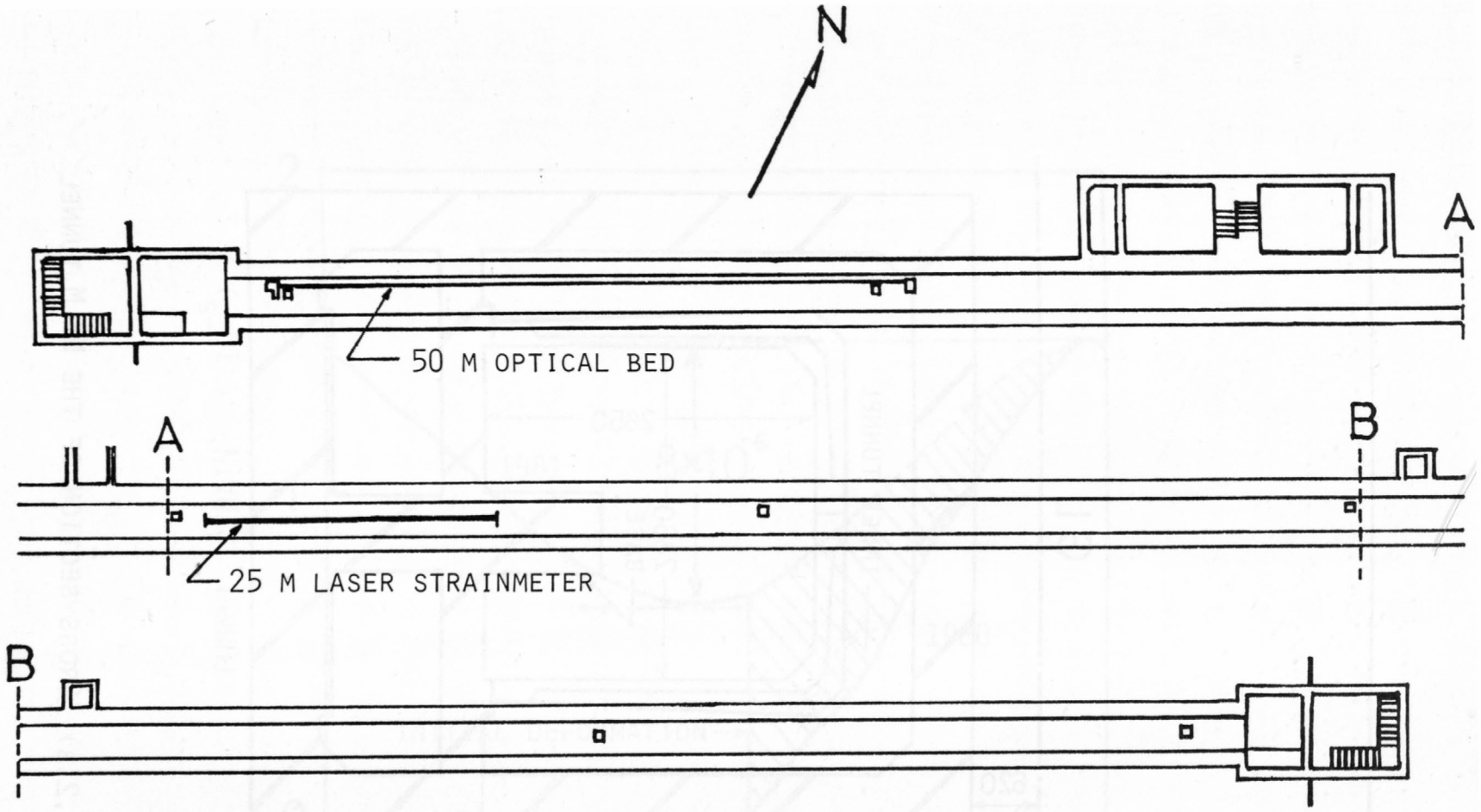

FIG.2(A) PLAN OF THE NRLM TUNNEL

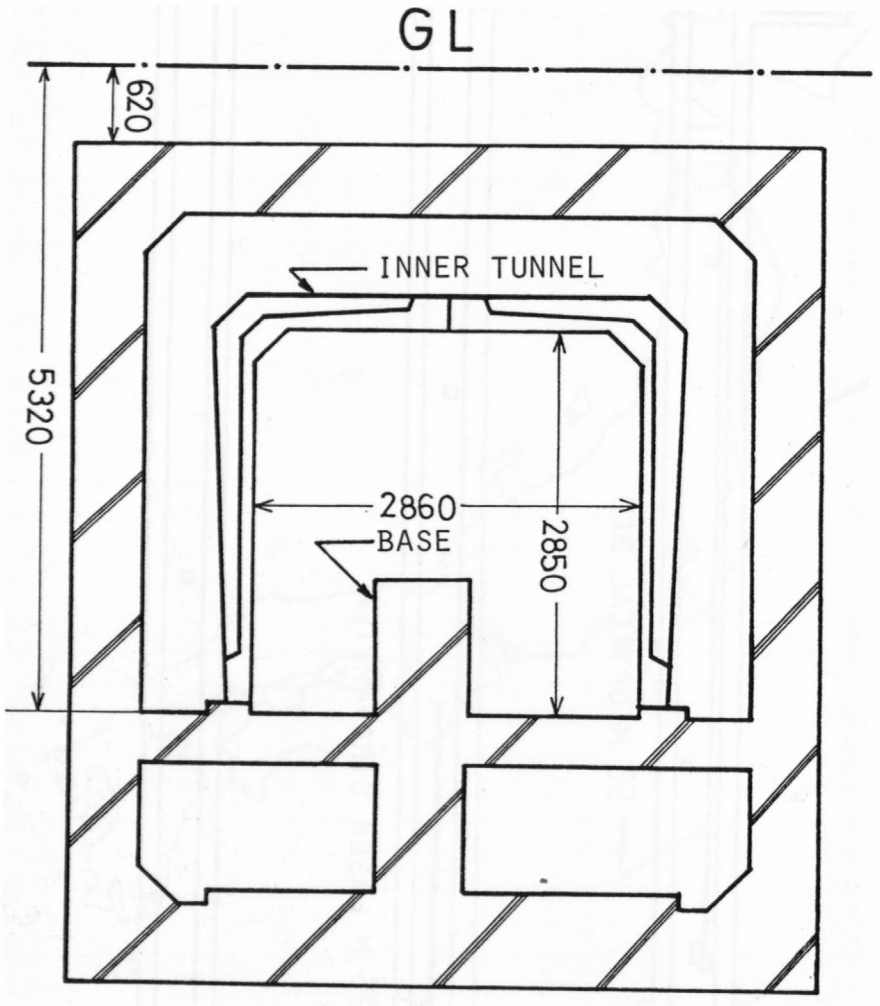

FIG.2(B) CROSS SECTION OF THE NRLM TUNNEL

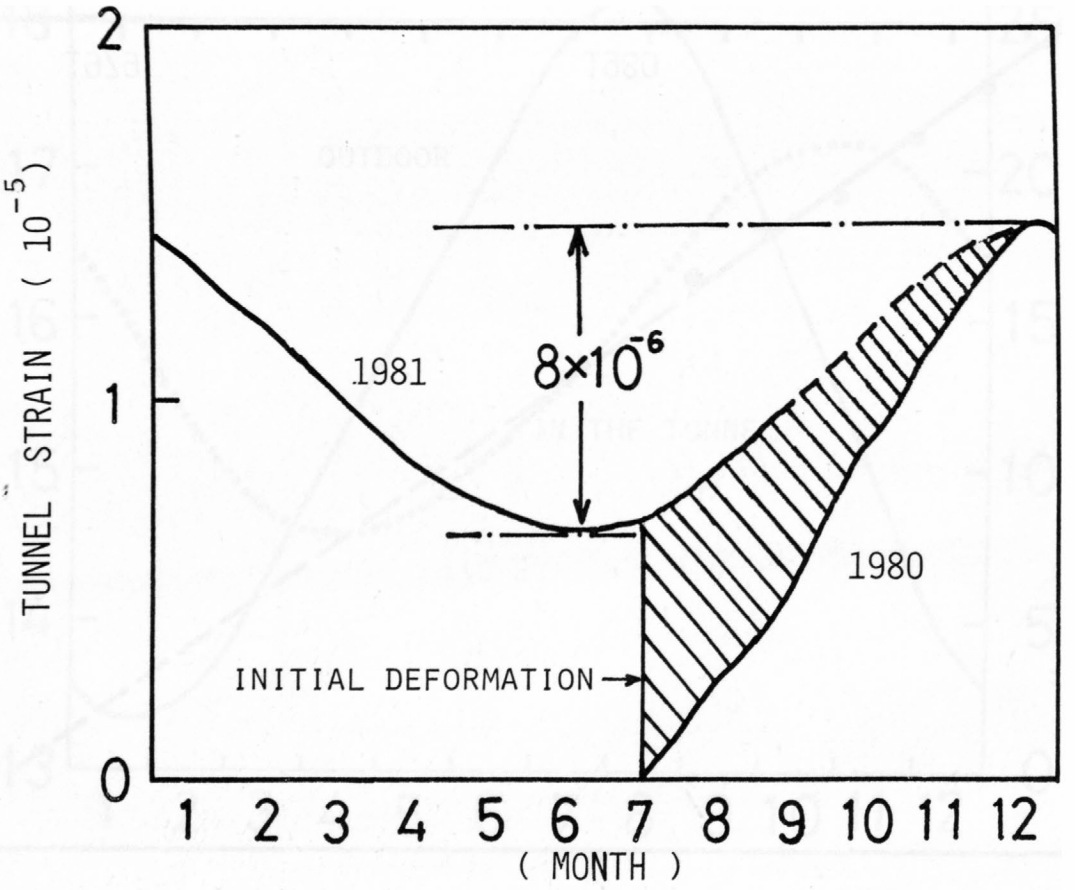

FIG.3 SECULAR CHANGE OF TUNNEL STRAINS.

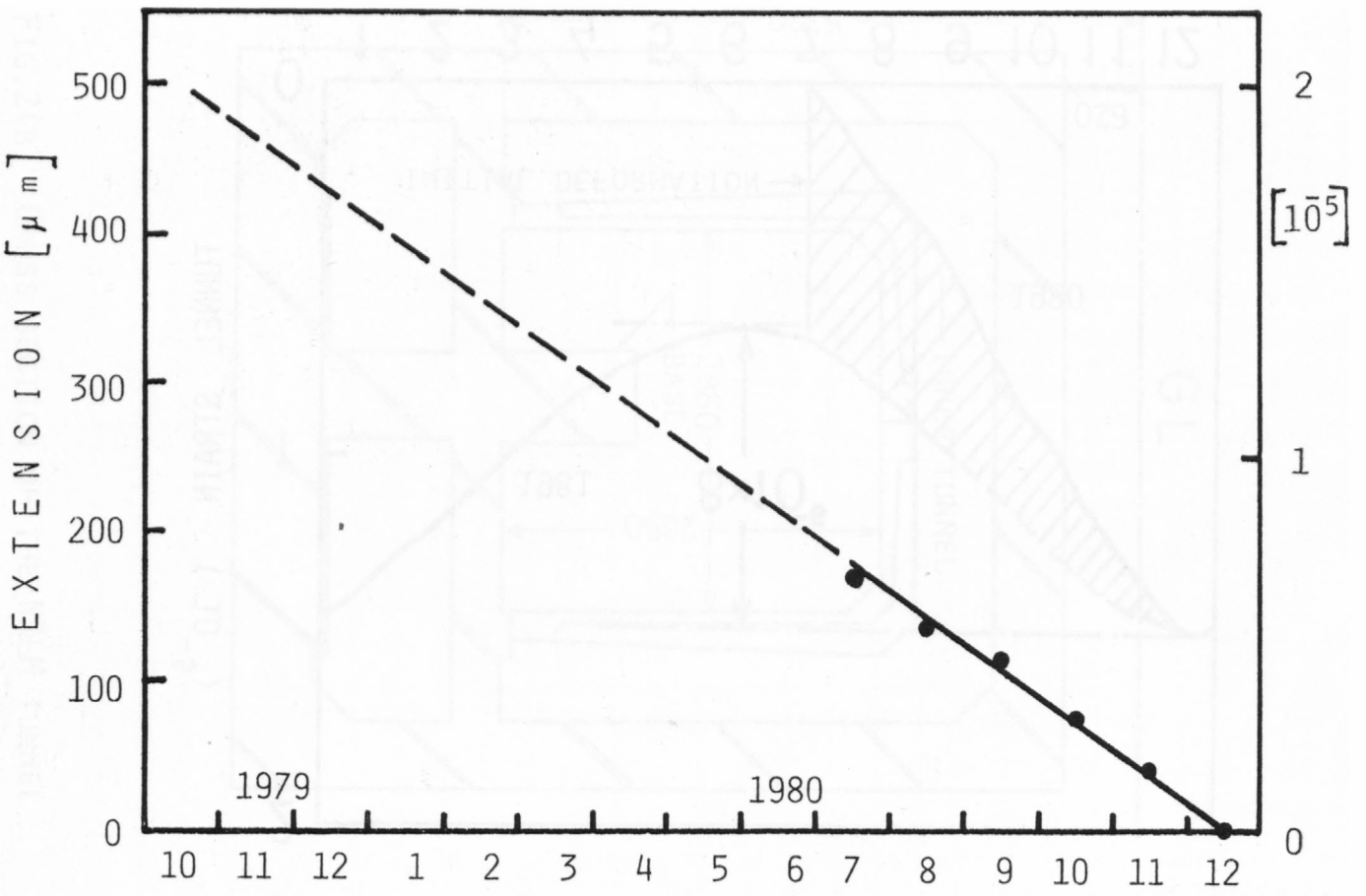

FIG.4 EXTRAPOLATION OF INITIAL DEFORMATION

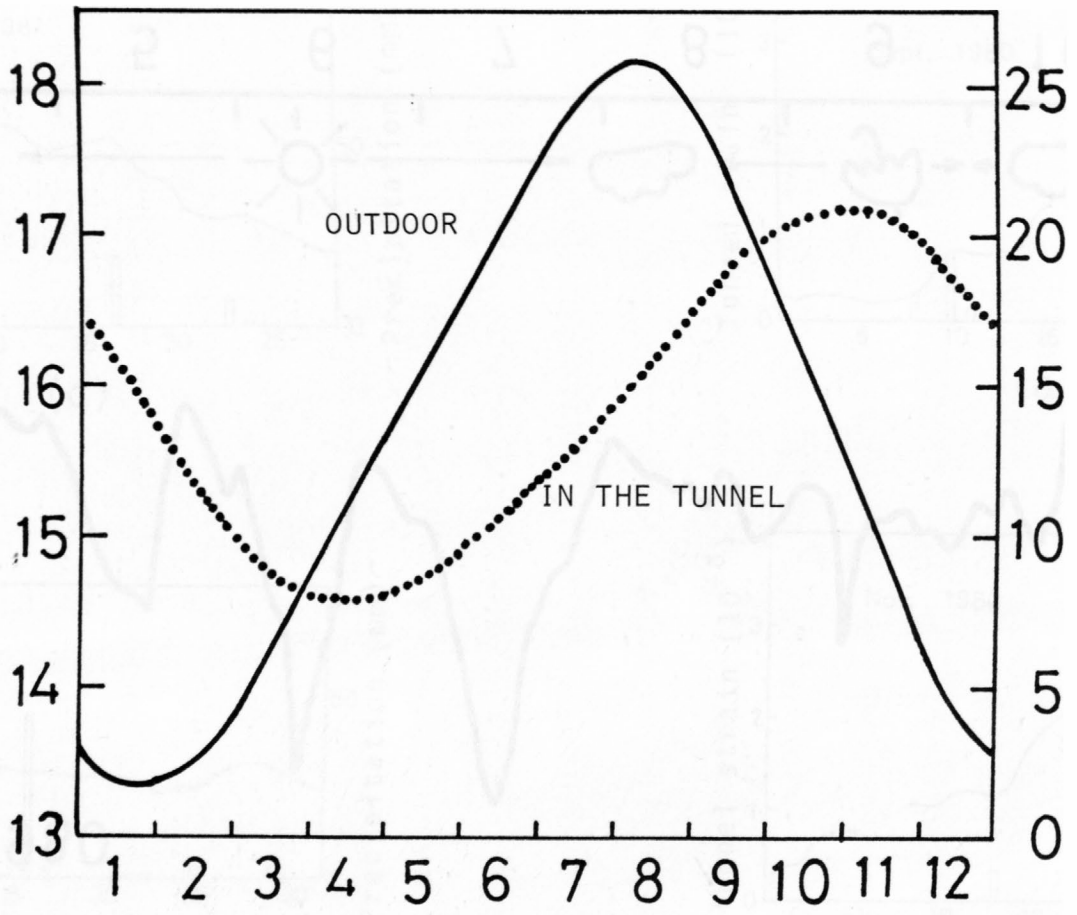

FIG.5 TEMPERATURE CHANGES OF OUTDOOR AND IN THE TUNNEL

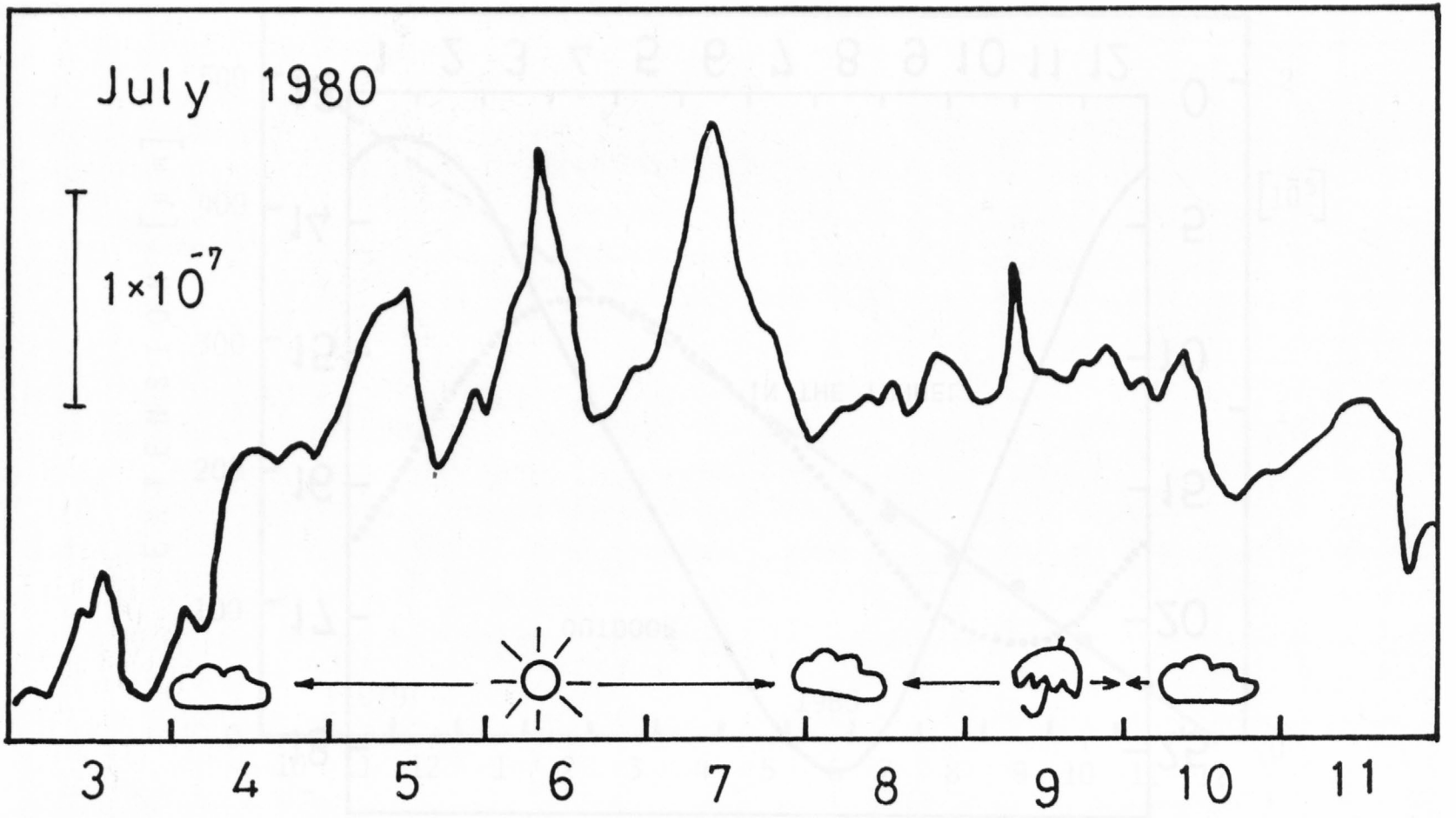

FIG.6 SHORT TERM CHANGE OF TUNNEL STRAIN

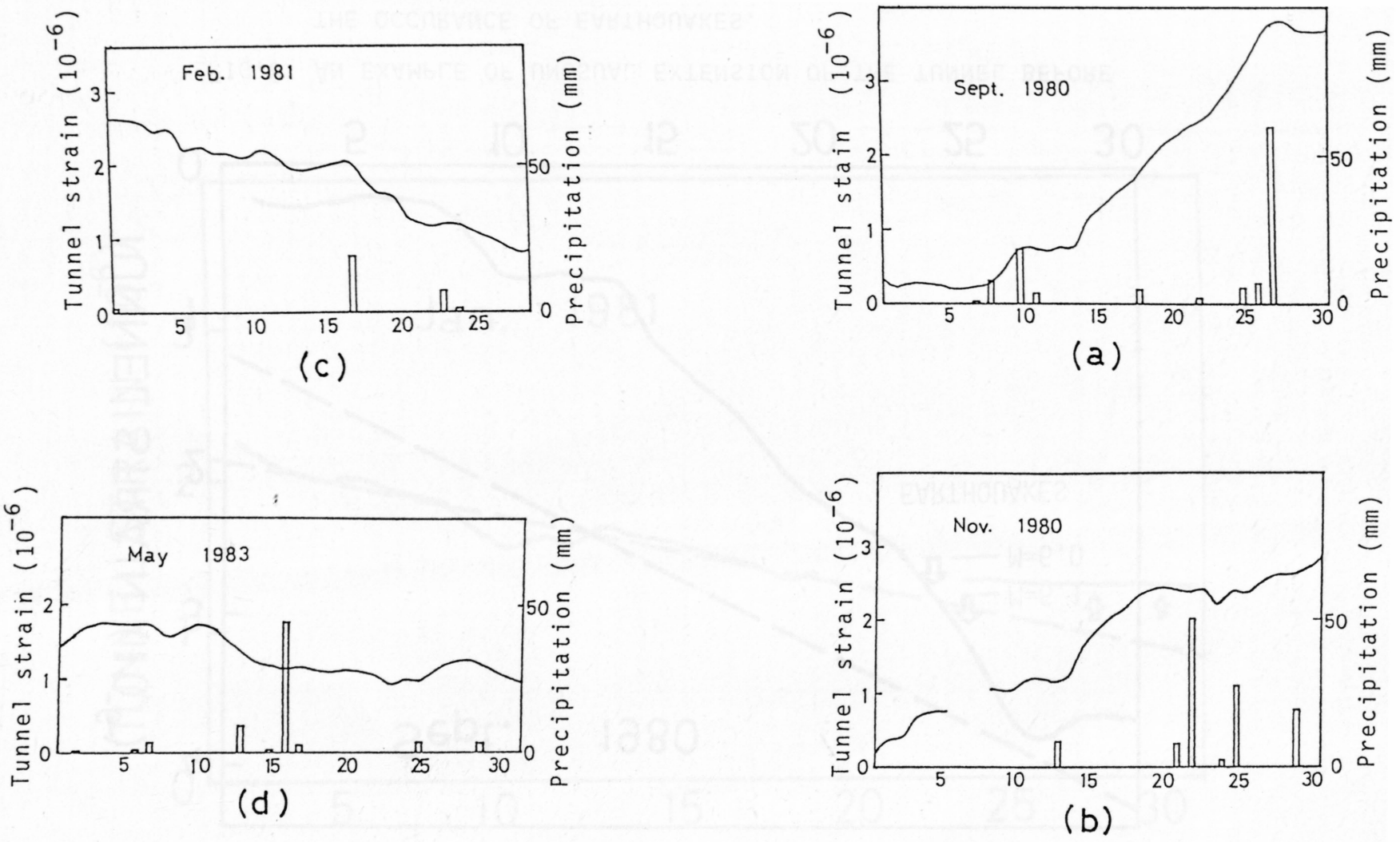

FIG. 7 TUNNEL STRAIN AND PRECIPITATION

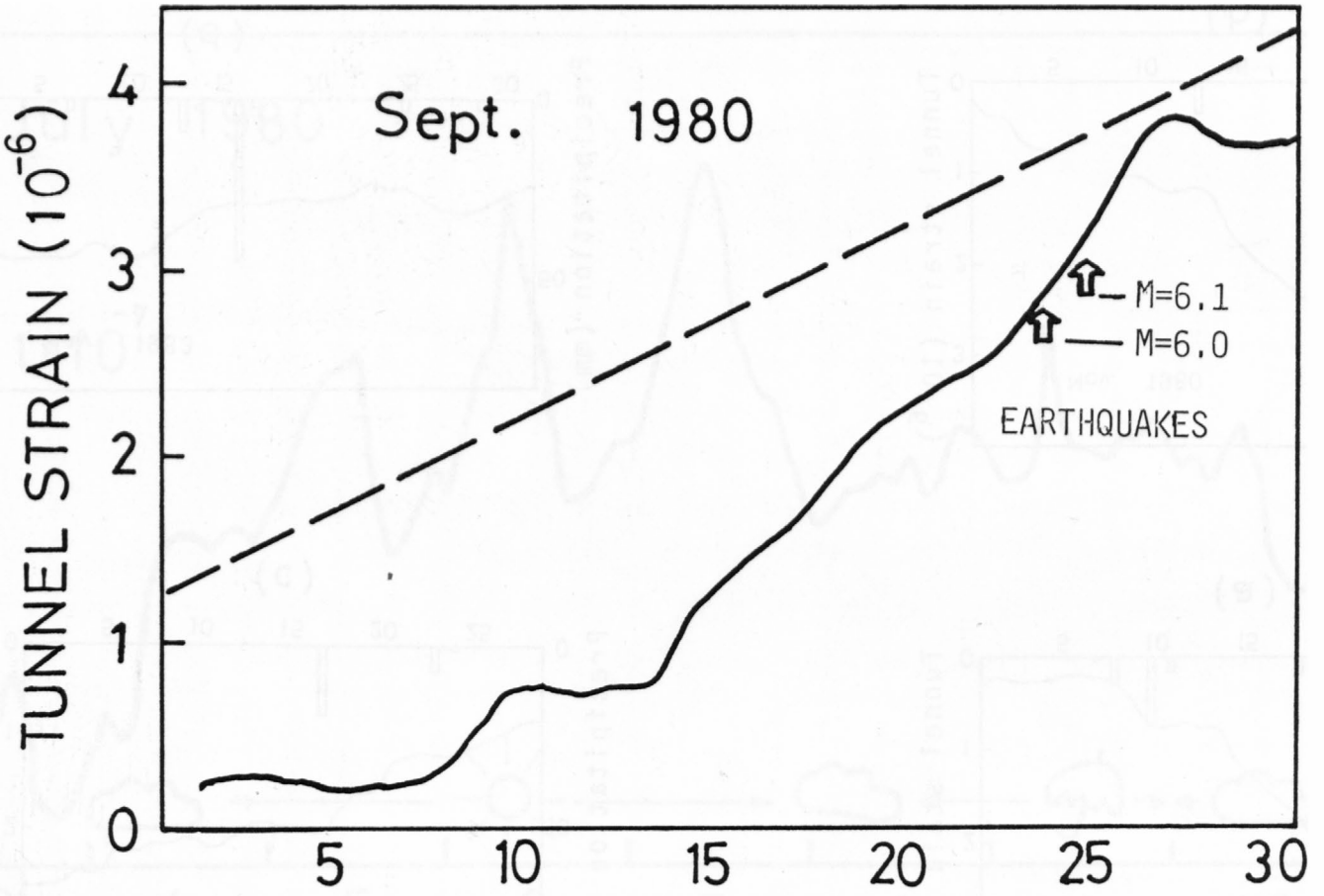

FIG.8 AN EXAMPLE OF UNUSUAL EXTENSION OF THE TUNNEL BEFORE THE OCCURANCE OF EARTHQUAKES.

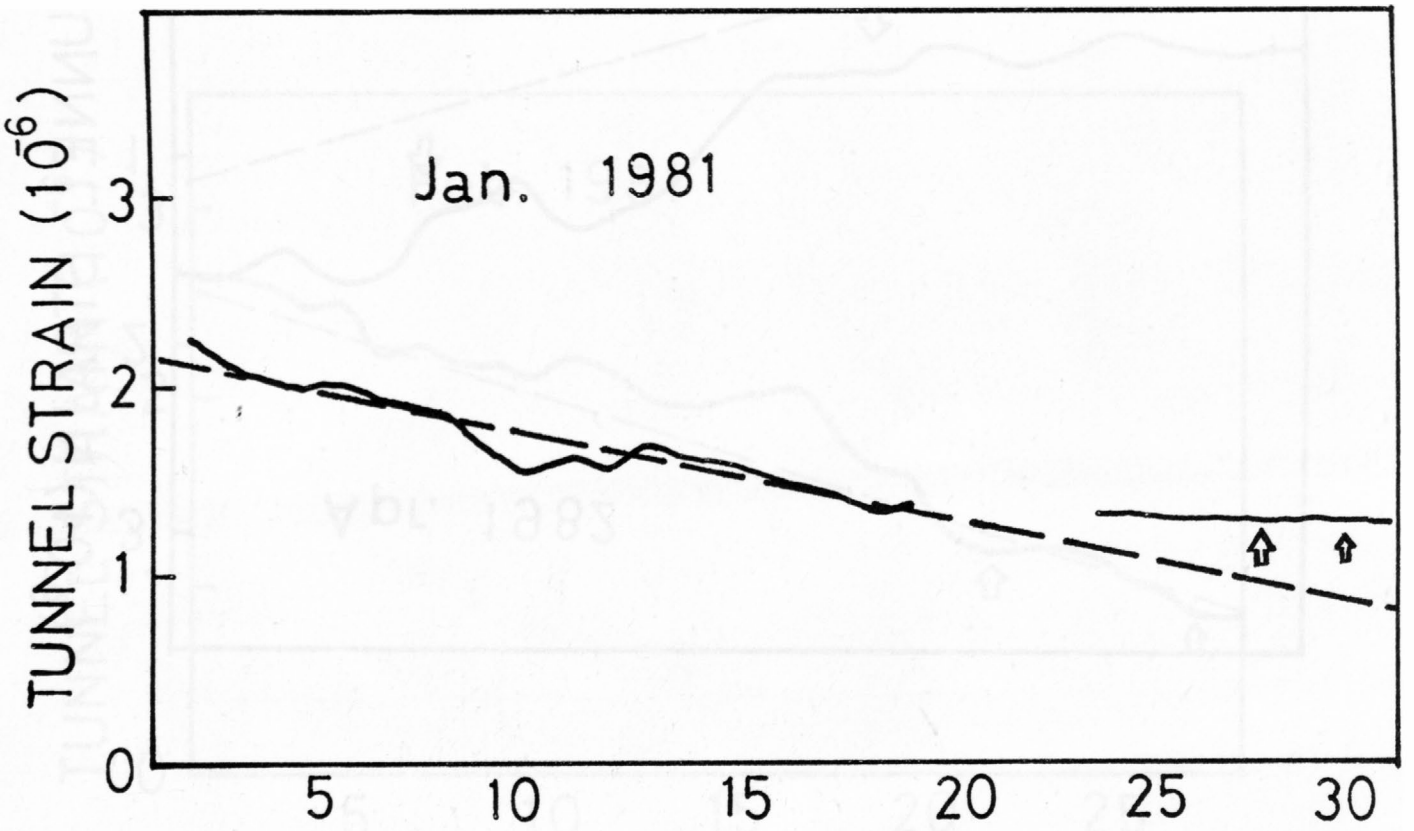

FIG.9 AN EXAMPLE OF APPARENTLY SMALL EXTENTION OF THE TUNNEL BEFORE THE OCCURANCE OF EARTHQUAKES.

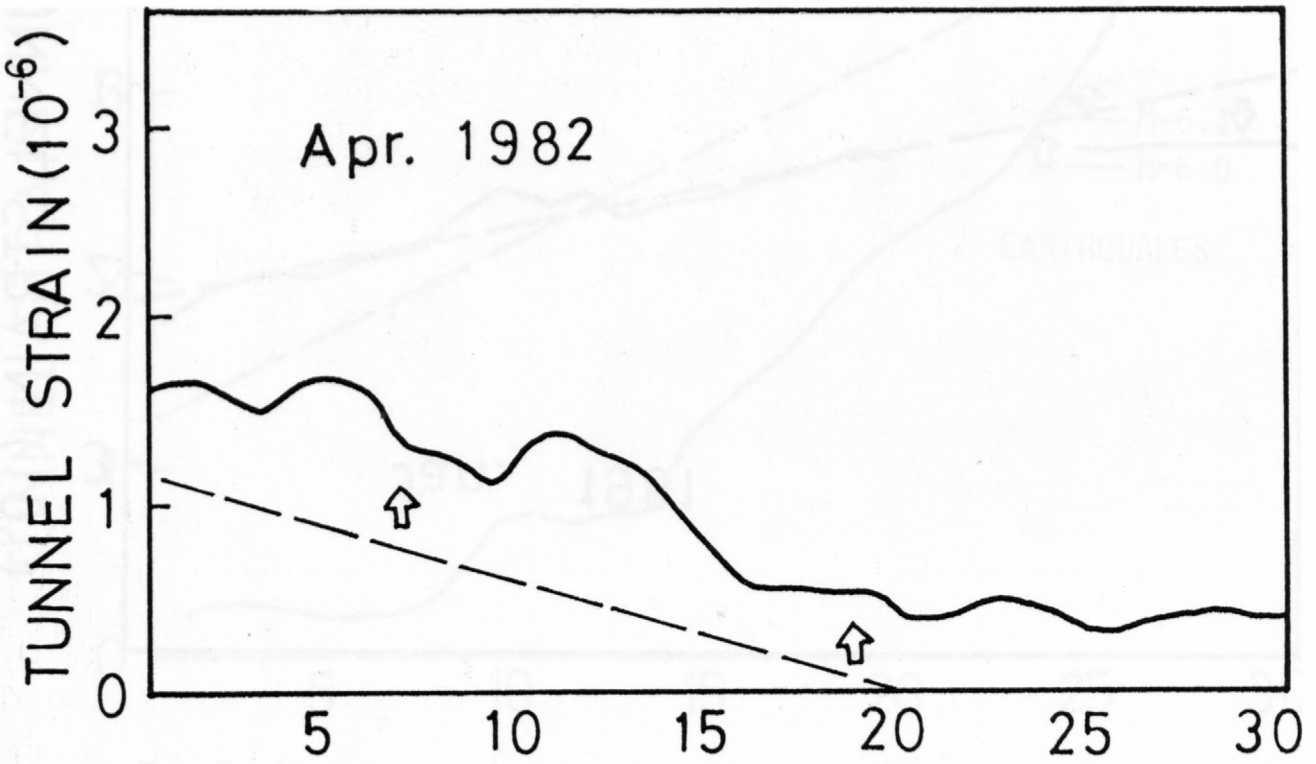

FIG.10 TUNNEL STRAIN BEFORE EARTHQUAKES: THE PRECEDING EARTHQUAKE OCCURED IN THE SEE OF KASHIMA; THE SUCCEEDING OCCURED AROUND TSUKUBA.

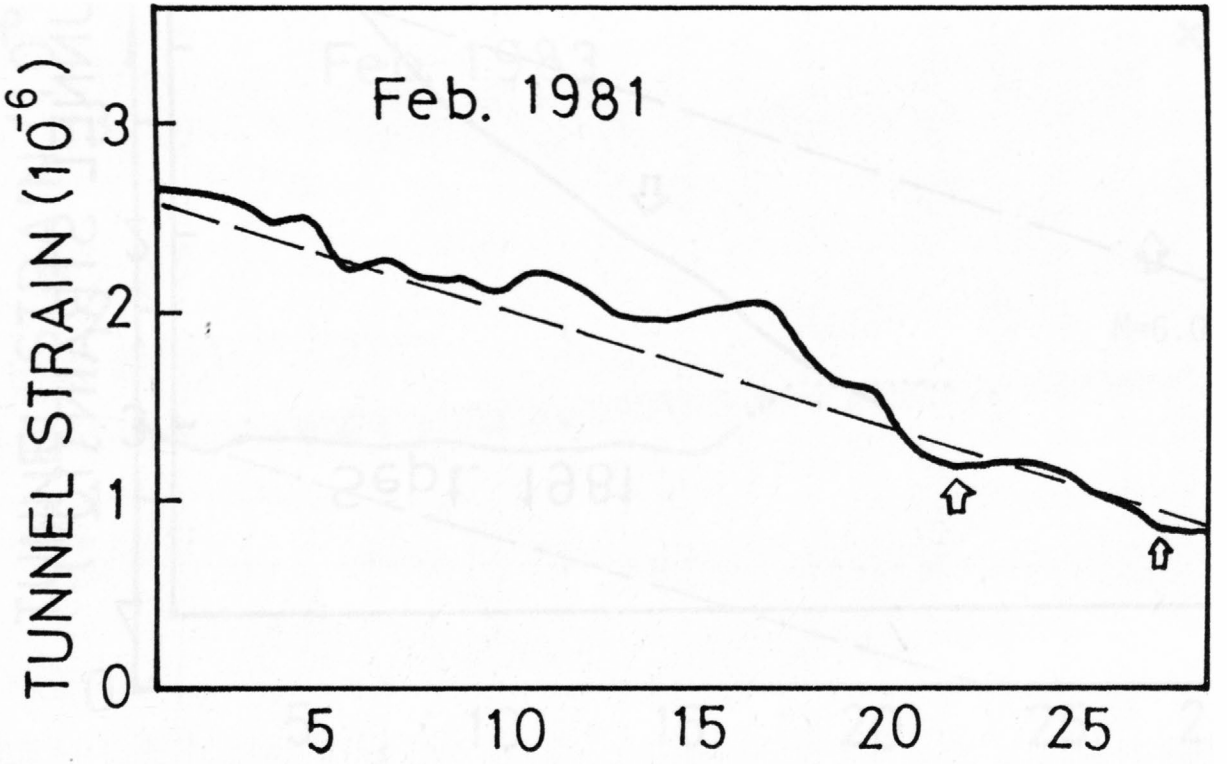

FIG.11 TUNNEL STRAIN BEFORE EARTHQUAKES: BOTH OCCURED OFF THE COAST OF IBARAKI.

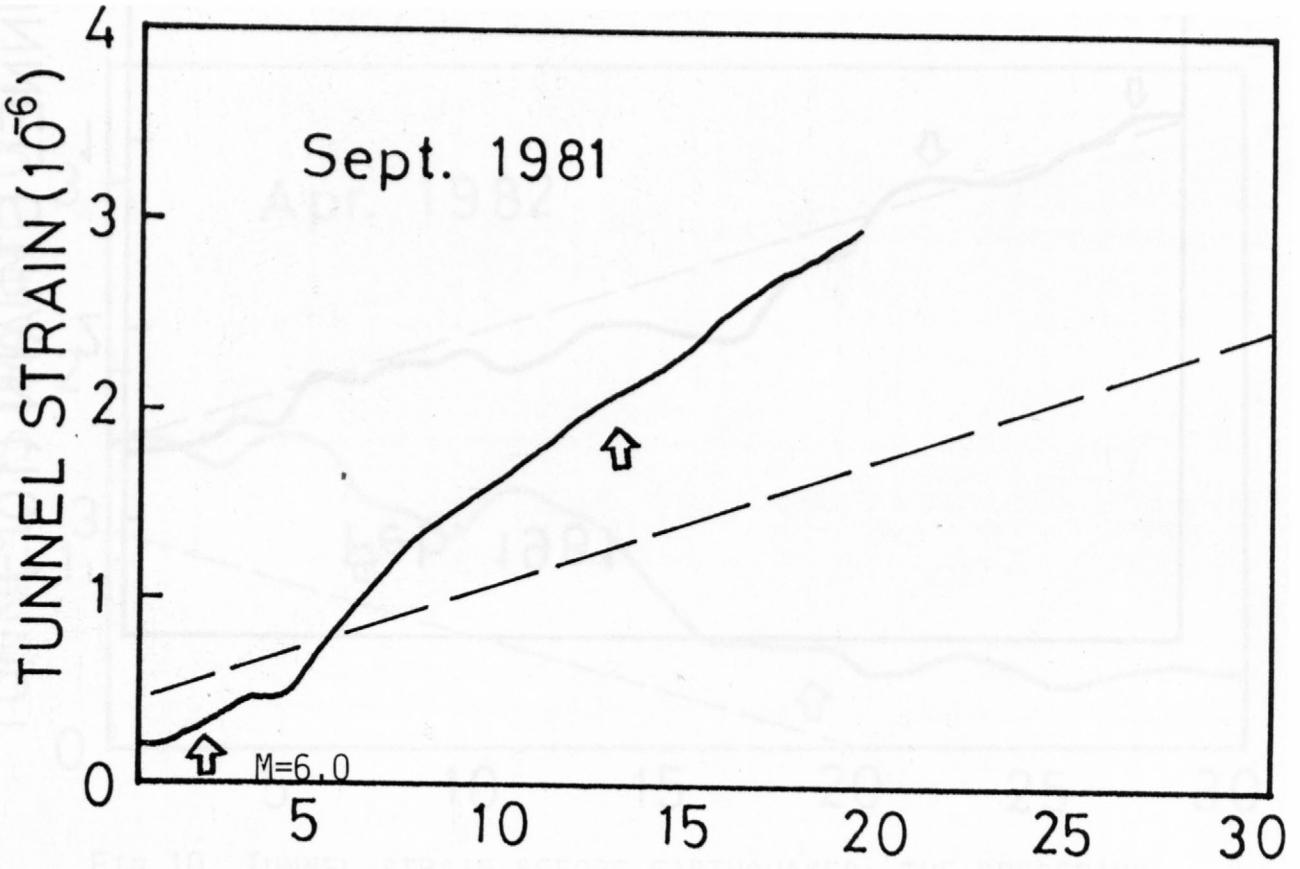

FIG.12 TUNNEL STRAIN BEFORE EARTHQUAKES: BOTH OCCURED OFF THE COAST OF IBARAKI.

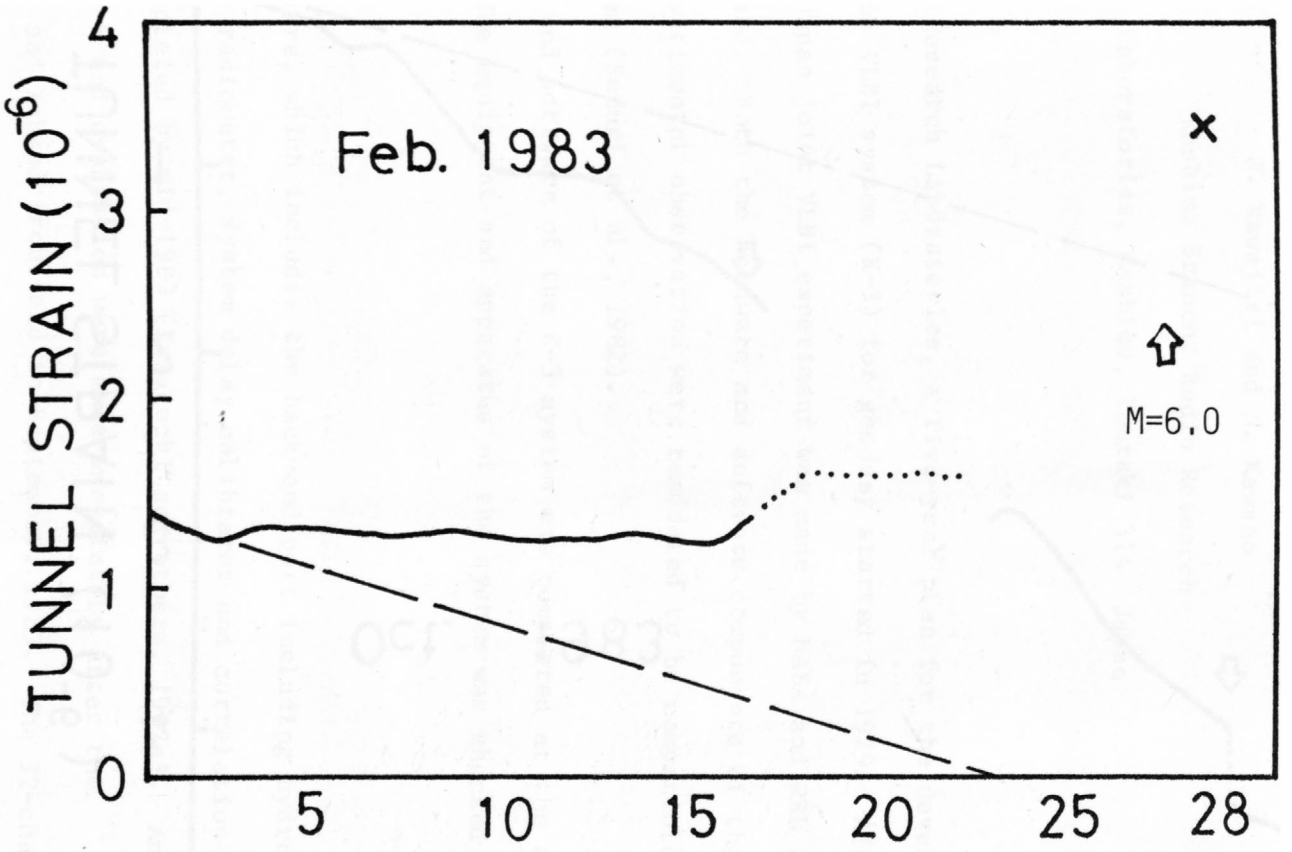

FIG.13 TUNNEL STRAIN BEFORE THE EARTHQUAKE OCCURED AROUND TSUKUBA.

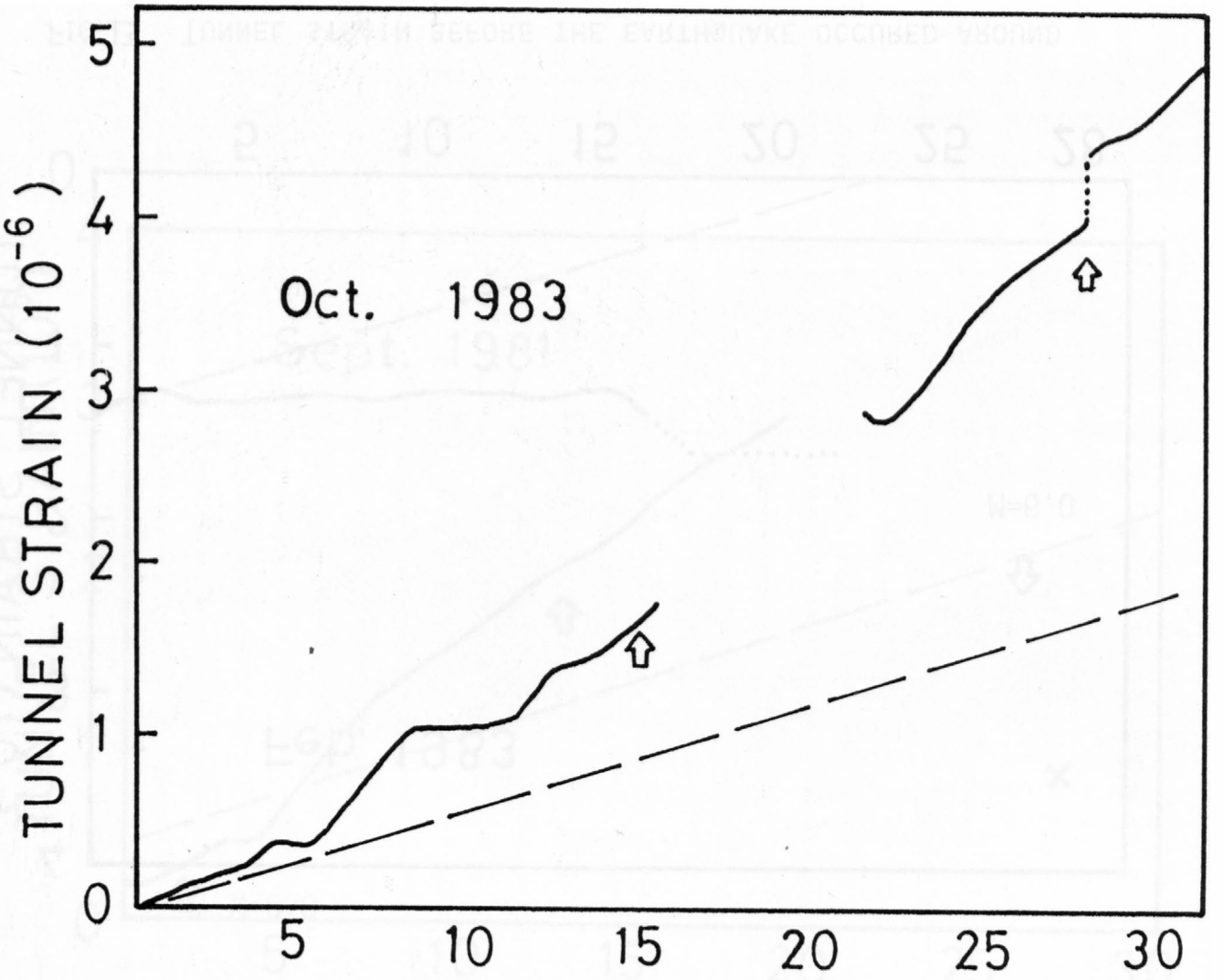

FIG.14 TUNNEL STRAIN BEFORE EARTHQUAKES: BOTH OCCURED AROUND TSUKUBA.

PRESENT STATUS OF K-3 VLBI SYSTEM DEVELOPED IN RADIO RESEARCH LABORATORIES

Y. Saburi and K. Yoshimura

Radio Research Laboratories

Koganei, Tokyo, 184 Japan

N. Kawajiri and N. Kawano

Kashima Branch, Radio Research

Laboratories, Kashima, Ibaraki 314 Japan

Introduction

In the Radio Research Laboratories, a five-year plan for the development of a high precision VLBI system (K-3) for geodesy started in 1979. After the agreement on the Japan joint VLBI experiment was made by NASA and RRL in 1980, the plan was revised. Both the hardware and software components of the K-3 system for intercontinental observation were remodeled to be compatible with the Mark III system (Saburi et al., 1982).

The hardware and software of the K-3 system was completed at the end of September 1983. The equipment and apparatus of the system was checked by successive tests.

K-3 Hardware

The K-3 hardware, which includes the back-end part including hydrogen maser, water vapor radiometer, system delay calibrator and correlation processor were completed by mid-1983 (Kawaguchi and others, 1982a). An overall system check and evaluation were made immediately after the installation of S- and X-band front-end in September, 1983. The 32-channel processor modules will perform data processing efficiently.

processor were completed by mid-1983 (Kawaguchi and others, 1982a). An overall system check and evaluation were made immediately after the installation of S- and X-band front-end in September, 1983. The 32-channel processor modules will perform data processing efficiently.

A hardware compatibility test was conducted at the Haystack Observatory in November 1982. The contents of the K-3 recorded tapes were successfully reproduced by using the Mark III recorder. In the summer of 1983, a more detailed compatibility test was made by using the Mark III data offered from NASA and NGS. The "correlation group" at Kashima succeeded in processing the Mark III data by use of K-3 correlator, obtaining the same result as that by the Mark III. That group used Polaris VLBI data of 3C 273B that was obtained from Westford-HRAS baseline of 3100 km.

Two hydrogen masers, made by Anritsu Electric Co., Ltd. were installed at Kashima at the beginning of September, 1983. The best stability of frequency attained is 2 to 3 x 10^{-15} for 500 to 5000 second averaging time.

The performances of 26 m antenna receiving systems were measured in the autumn of 1983, with a system noise temperature of 126.9 K and 94.6 K and antenna efficiency of 51.7% and 53.4% for S and X bands at their zenith, respectively.

The precision of the hardware system in determining the delay time is estimated to be 70 ps (2 cm in path length) between the Kashima 26 m and OVRO (Owens Valley Radio Observatory) 40 m antennas (Sugimoto and Kawaguchi, 1982).

K-3 Software

The K-3 software includes the programs for scheduling, automatic operation, correlator control, bandwidth synthesis, baseline analysis and data-base management. Unified management of VLBI data becomes possible with the aid of a data-base handler (Takahashi and others, 1982). The automatic operation software (KAOS) was developed previously. The KAOS and the corresponding Mark III software, Field System, are compatible as G.S.F.C. of NASA proved in March to April, 1983. The other software was completed early in 1983.

US-Japan Joint Experiment

Based on the various hardware/software tests mentioned in Section 2. and 3., Japan made the first fringe detection test for the transpacific baseline in November 1983 in cooperation with NASA/JPL. The test formed a part of that synthesized for the K-3 system, and the fringe peak was successfully detected.

The joint experiments between NASA and RRL, using the Mark III and K-3 system, respectively, started in January, 1984, under a five-year agreement between the two organizations. The so-called system-level experiments were made between Kashima and Mojave on January 23 to 24, 1984, and among Kashima, Mojave and Hat Creek on February 25 to 26, 1984. In July, 1984, we will take part in the global VLBI network which is formed of antennas of VLBI stations in North America, Alaska, Hawaii, Europe and Australia.

Domestic Experiment

In addition to the plan of the international observation, domestic VLBI experiments between Kashima (RRL) and Tsukuba (GSI) using the K-3 VLBI system is also expected to be made in 1984 (Kawaguchi and others, 1982b). Prior to the domestic VLBI experiment, an experimental correlation test was made at the beginning of October, 1983 over the 53 km-long Kashima-Tsukuba baseline. In order to connect the reference point (cross point of azimuth and elevation axes of 26 m antenna) at Kashima with the network of trigonometrical surveys in Japan, the staff of GSI made a measurement using a laser distance meter in December, 1983. A system-level VLBI experiment on the same baseline will start in 1984. Accuracy and repeatability of these VLBI results will be confirmed, by comparison with the data obtained separately by GSI by other means (e.g. laser ranging). The VLBI experiments for geodetic purposes between the Kashima 26 m and GSI 5 m antennas are planned to be made in 1985, along with the objectives of the Dynamics and Evolution of the Lithosphere Project.

Acknowledgement

We, the K-3 system developing group in RRL, would like to express our sincere thanks to many persons concerned in the organizations in U.S.A. and Japan during the stage of K-3 system development, especially to the members of geodynamics project in NASA Headquarters, GSFC, JPL and Haystack for their close cooperation and assistance.

References

Saburi, Y., Yoshimura, K., Kato, S., Tsukamoto, K., Yamashita, F., Kawajiri, N., and Kawano, N.: Development of VLBI system and future experimental plan in the Radio Research Laboratories, Proc. IAG Symp. No. 5 Tokyo, May 7-8, 1982, pp. 307-314.

Kawaguchi, N., Sugimoto, Y., Kuroiwa, H., Kondo, T., Hama, S., Amagai, J., Morikawa, T. and Imae, M.: The K-3 hardware system being developed in Japan and its capability, ibid 1982a pp. 163-176.

Sugimoto, Y. and Kawaguchi, N.: Performances and data processing of K-3 VLBI system for geodesy, the 3rd joint meeting of UJNR, Panel on Earthquake Prediction Technology, Tsukuba, Japan, September, 1982.

Takahashi, F., Yoshino, T., Murakami, H., Koike, K., Kunimori, H. and Kondo, T.: K-3 VLBI software development for international experiments, Proc. IAG Symp. No. 5, Tokyo, May 7-8, 1982, pp. 177-183.

Kawaguchi, N., Kawajiri, N., Kawano, N., Yoshimura, K., Ishii, H., Murakami, M., Nishimura, O., Yoshimura, Y. and Kaidzu, M.: A baseline determination between Kashima 26 m and Tsukuba 5 m antennas in joint VLBI experiment plan of RRL anbd GSI, ibid 1982b, pp. 325-334.

DEVELOPMENT OF THE GEOGRAPHICAL SURVEY INSTITUTE VLBI SYSTEM

The Geographical Survey Institute (GSI) has been developing a transportable VLBI system since 1981 for the purpose of adjustment of the geodetic network and monitoring of crustal movement.

The system has an antenna of 5 m in diameter and its acquisition system was designed to be compatible with the RRL's 26 m antenna station at Kashima.

Figure 1 shows the 5 m antenna installed on the grounds of GSI at Tsukuba. To achieve high efficiency, a shaped-beam cassegrain antenna is used. For transportability, the antenna can be divided into 3 parts, i.e. main dish, mount structure and pedestal. The main dish can be divided into 3 parts, so as to reduce the width of all the parts to less than 3 m. The side view of the antenna is illustrated in Figure 2. Three days, maximum, are required to disassemble the antenna and three vehicles, including a 10-ton trolley and a 10-ton crane, will be used for transportation. At the next station, ten days at maximum are required to re-assemble the antenna.

Most of the parts, including an acquisition terminal and a hydrogen maser oscillator, have already been constructed and a water vapor radiometer is to be constructed in fiscal year 1984. The principal specifications of the hardware are listed in Table 1. By the end of March, 1985, the system will be completed. After the system has been adjusted, joint experiments with RRL will be started on a baseline between Tsukuba and Kashima.

Table 1. The specification of hardware

	Items	specification
Antenna	Antenna diameter	5 meter
	Frequency range	X-band : 8180-8600 MHz S-band : 2220-2320 MHz
	Polarization	RHCP X and S-band
	Antenna efficiency (Gain)	X-band 61 %(50.7 dB at 8390 MHz) S-band 32 %(36.5 dB at 2260 MHz)
	Antenna noise temperature	X-band : 45 K(Elevation 45°) S-band : 120 K
	VSWR	1.3 X and S-band
	Axial ratio	3 dB X and S-band
	Slew rate	Azimuth 0 to 1 deg/sec Elevation 0 to 0.5 deg/sec
	Angle readout(resolution)	0.002 degree
Preamplifier	Bandwidth	X-band : 420 MHz S-band : 120 MHz
	Noise temperature	X-band : 75 K S-band : 55 K
	Gain stability	0.4 dB p-p/day X and S-band
	VSWR	1.25 X and S-band
Down converter	Input frequency range	X-band : 8170-8610 MHz S-band : 2200-2320 MHz
	Output frequency range	X-band : 90-530 MHz S-band : 180-300 MHz
	Off band attenuation	X-band : 30 dB(410 MHz off band) S-band : 60 dB(420 MHz off band)
	Local frequency	X-band : 8080 MHz S-band : 2020 MHz
	Phase stability	± 5° rms/10 min X and S-band
IF distributer	Number of channels Bandwidth/channel	14 channels LO and HI-band LO-band : 140 MHz HI-band : 320 MHz
Video converter	Number of channels	1 channel LSB and USB
	Output frequency range	800 Hz-8 MHz
	Local frequency range	99.99-519.99 MHz(10 KHz step)
Formatter	Input bandwidth	4 MHz
	Sampling frequency	8M, 4M, 2M, 1M, 0.5M,0.25MHz
Data recorder	Recording density	9 Mbps/ch at maximum
Hydrogen maser ocsillator	Stability	$< 5\times10^{-15}$ (τ= 1000 sec)
	Signal outputs	10MHz, 5MHz, 1pps
	Dimension	65cm wide, 67cm deep and 146cm high.

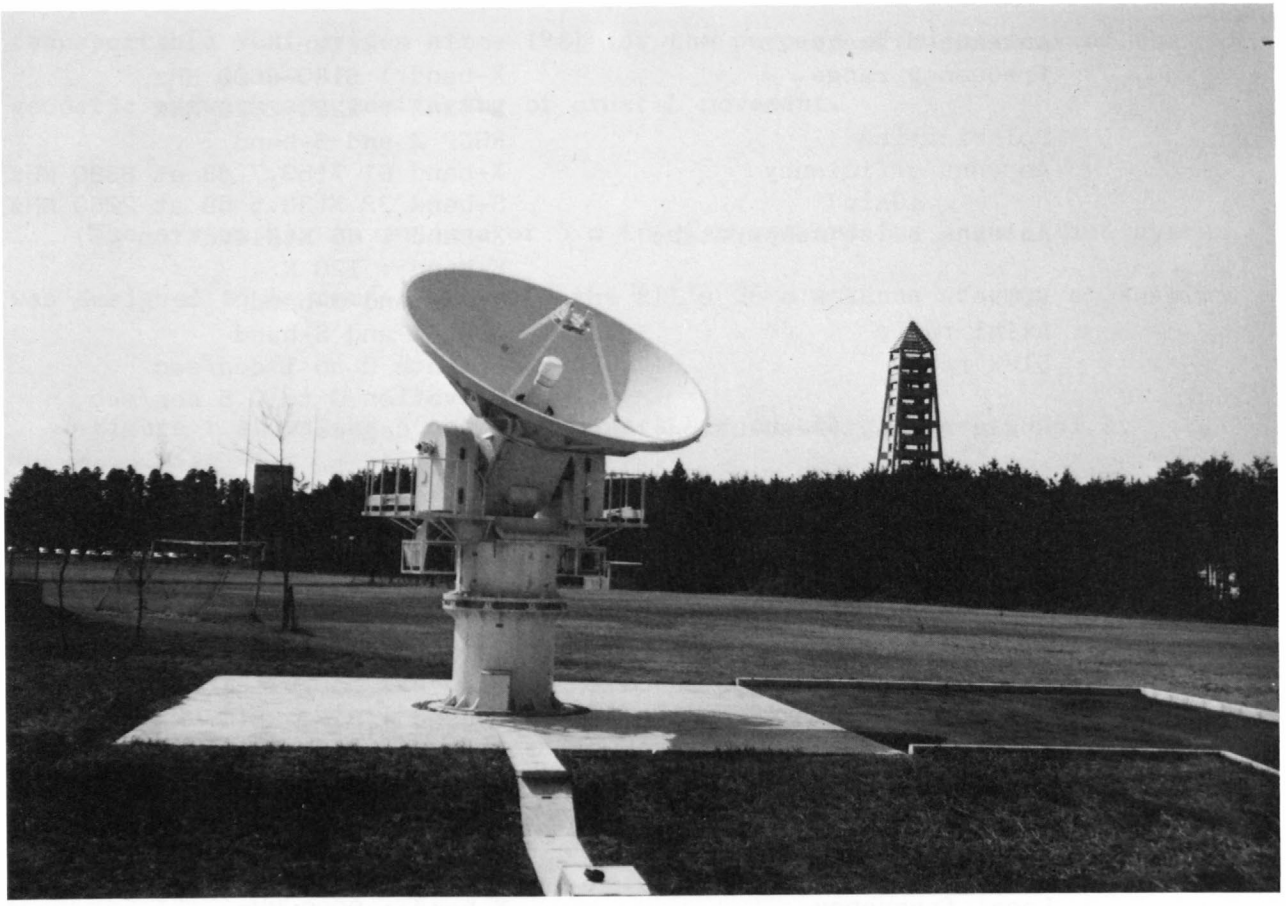

Fig. 1. The 5 m antenna in the grounds of GSI at Tsukuba

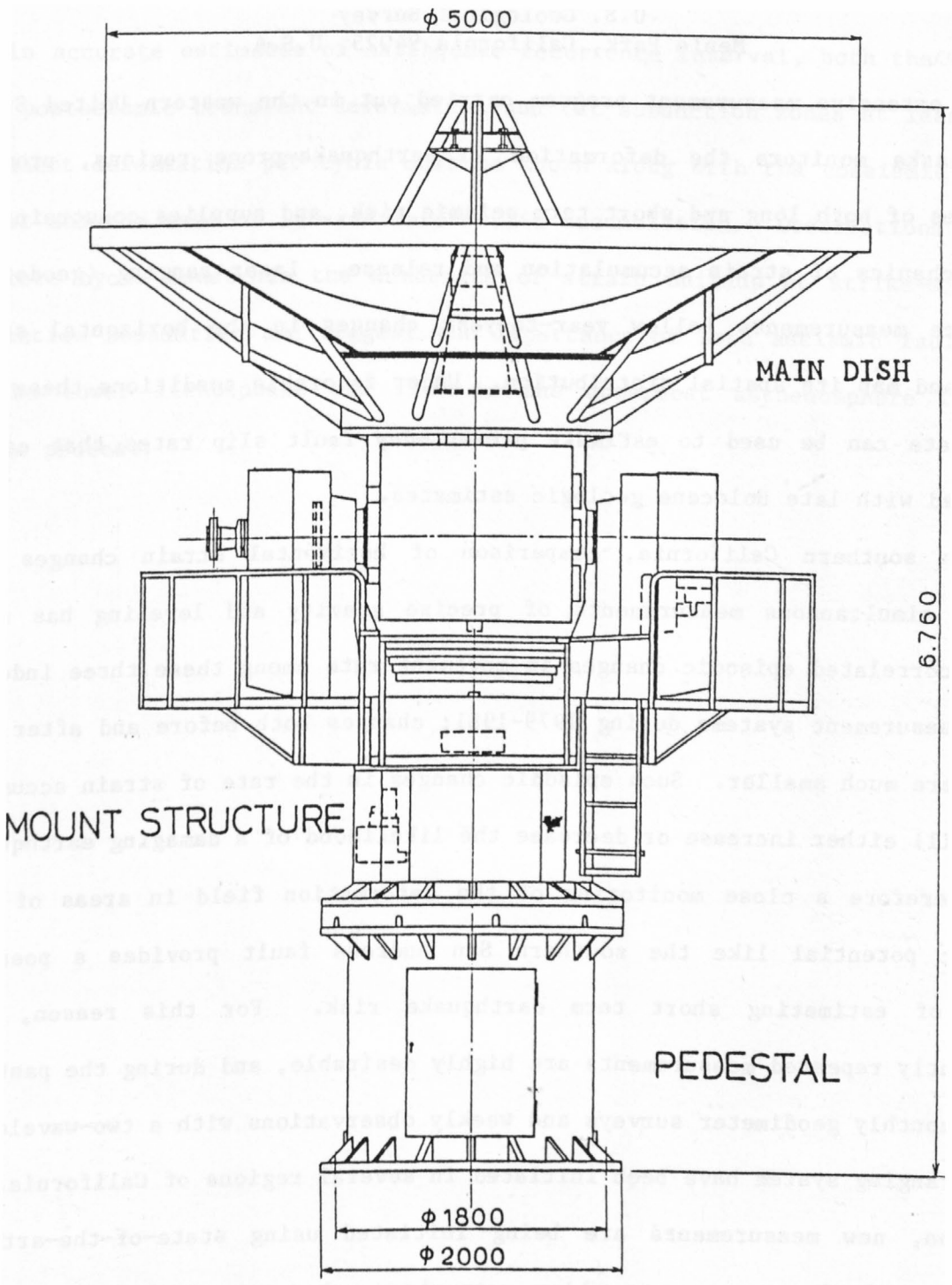

Fig.2 The schematic sketch of the 5 m antenna

Short and Long Term Geodetic Observations and Earthquake Prediction Research

Wayne Thatcher
U.S. Geological Survey
Menlo Park, California 94025, U.S.A.

An extensive measurement program carried out in the western United States and Alaska monitors the deformation in earthquake-prone regions, provides measures of both long and short term seismic risk, and supplies constraints on the mechanics of strain accumulation and release. Laser ranging (geodolite) distance measurements follow year-to-year changes in the horizontal strain field and map its spatial distribution. Under favorable conditions these network data can be used to estimate present-day fault slip rates that can be compared with late Holocene geologic estimates.

In southern California, comparison of horizontal strain changes with nearly simultaneous measurements of precise gravity and leveling has shown large correlated episodic changes in movement rate among these three independent measurement systems during 1979-1981; changes both before and after this time were much smaller. Such episodic changes in the rate of strain accumulation will either increase or decrease the likelihood of a damaging earthquake, and therefore a close monitoring of the deformation field in areas of high seismic potential like the southern San Andreas fault provides a possible means of estimating short term earthquake risk. For this reason, more frequently repeated measurements are highly desirable, and during the past two years monthly geodimeter surveys and weekly observations with a two-wavelength laser ranging system have been initiated in several regions of California. In addition, new measurements are being initiated using state-of-the-art GPS receivers, both to resurvey older networks, and to test their ultimately achievable precision on frequently-measured geodimeter monitoring nets in California and elsewhere.

Using both historic and modern geodetic measurements, long term features of the entire earthquake deformation cycle (coseismic strain release, postseismic transients, interseismic strain accumulation) can be constrained. To obtain accurate estimates of earthquake recurrence interval, both the cumulative postseismic transient deformation and (at subduction zones at least) the permanent deformation per cycle must be known along with the coseismic strain offset and the rate of interseismic strain accumulation. Observations of the complete cycle constrain the mechanics of strain buildup at strike-slip and subduction boundaries and suggest the importance of both aseismic fault slip in the lower lithosphere and flow in the uppermost asthenosphere in this cyclic process.

RELATION BETWEEN SEASONAL VARIATION OF THE OMAEZAKI PENINSULA AND SEA LEVEL CHANGE

Minoru Tazima and Masaru Kaidzu

Geographical Survey Institute

Norihisa Matsumoto

Public Works Research Institute

Abstract

As a part of an earthquake prediction project, GSI is conducting leveling surveys four times a year on the Omaezaki Peninsula. Through this frequent surveying, it was shown that the Omaezaki Peninsula uplifts and subsides once a year.

Among possible causes, elastic deformation through the effect of buoyancy was considered as the most important mechanism that causes the annual variation of the elevation of the Peninsula. The vertical motion, which was estimated through a two dimensional FEM model, is in the same order of that which was observed.

Introduction

As a part of the earthquake prediction project in the Tokai area, leveling surveys have been repeatedly performed in the Omaezaki Peninsula. In the Omaezaki area, it has been observed that the Peninsula has been subsiding secularly for the past 100 years. The subsidence is considered to be an indication of the subduction of the Philippine sea plate at the Suruga trough. In 1974, seismic activity in the adjacent Izu Peninsula increased suddenly. At the same time, the rate of subsidence at Omaezaki accelerated. This change in the mode of deformation drew wide attention. In order to watch

further developments, leveling has been performed four times a year since 1981. Through this frequent repetition of leveling the annual vertical movement of the Omaezaki Peninsula has been measured. Fig. 1-a shows the elevation change at Omaezaki relative to Kakegawa and the sea level change at Omaezaki. As the repetition of the leveling is not frequent enough, the phase difference between elevation changes and sea level changes is not clear. To improve the clarity, the results of weekly leveling surveys conducted by the local government of Shizuoka-ken was compared with sea level change (Fig. 1-b). Although the distance between the two bench marks is only 4 km or so, the elevation difference shows seasonal change. The phase difference between the elevation change and sea level change is less than one month in this case.

There are many natural phenomena which have annual periodicity and we have selected the most important factor among these.

It is well known that some clay minerals such as montmorillonite swell in water. Therefore, if rainfall varies seasonally, elevation may change annually. However, the average amount of rainfall does not have as large a horizontal gradient as that observed. In addition, the rainfall is not so seasonal, therefore this was not considered one of the most important factors.

Another annual phenomenon is the annual cycle of the Earth tide. The maximum range of actually observed tidal tilt is 0.017 arc seconds according to Vaníček (1981). As the distance between Kakegawa and Omaezaki is about 26 km, the maximum possible vertical motion of Omaezaki relative to Kakegawa is not greater than 2mm. Therefore, this also was not considered to be an important factor.

Another possible cause is atmospheric refraction. Atmospheric refraction effect on leveled height difference is given as

$$\Delta h = \sum Cs^2 (dT/dh) * (dh/ds).$$

Where s is the distance observed between the level and the rod, T is atmospheric temperature, h is elevation and C is a constant. The Omaezaki Peninsula is known for its flat top named Makinohara plane which is a dissected fan that formed about 100,000 BP. The refraction effect, therefore, is a serious problem. However the day to day variation in refraction effect will be much larger that the seasonal variation and the elevation change is too periodic to be the result of the refraction effect.

Rod calibration error is rejected because the height difference between Kakegawa and Omaezaki is negligibly small.

The remaining factor is ocean tide. The ocean tide may affect the elevation change through loading and a buoyancy effect. Fig. 2 shows the tidal spectrum at the Omaezaki tide gauge station. The annual cycle has an amplitude of about 12 cm. The problem to be answered is whether or not this 25 cm of annual variation of sea level can cause 2 cm of vertical motion.

Possible Mechanisms That Transfer the Sea Level Change to Vertical Motion of the Peninsula

There are several possible mechanisms that can transfer the sea level change to elevation change.

The first possible mechanism is an elastic response of a radially stratified model earth to surface loading. Obviously, this mechanism assumes that the effective thickness is large. The effective elastic constants are also large, therefore, the deformation will have a long wavelength. This mechanism has been well studied to assess the effect of ocean loading on gravity or earth tide observation. For example, for the most powerful partial tide M2, the amount of vertical displacement is estimated to be on the order of 1 cm (Sato and Sasao, 1980). However, the gradient of displacement is about 1 mm/10 km. This gradient is too small to explain the observed

phenomenon.

The next possible mechanism is an elastic response of young and soft rocks near the surface of the solid earth to surface loading. In the Omaezaki area, a detailed geological survey has been performed by Chubu Electric Power Co. Inc. for construction of a nuclear power plant. According to the report, the subsurface structure is as in Fig. 3. The Sagara group consists of alternating layers of sandstone and claystone. Young's modulus for these components is 1480 to 1940 kgf/cm^2 and 9800 to 10700 kgf/cm^2, respectively. In SI unit, 1 kgf/cm^2 corresponds to $9.8*10^{-4}$Pa. Poisson's ratio is 0.3 for both components. According to Kakimi (personal communication), the Sagara group overlies the Oigawa group, which is a bit harder, and the Oigawa group overlies Palaeogene or Mesozoic. Young's modulus of this ancient stratum is considered to be much larger that younger strata. Thus, we can treat the Peninsula as a bank-like structure on a rigid foundation. To assess the efect of sea level change on the deformation of the Peninsula, a two dimensional finite element model was used. This model is shown in Fig. 4. The number of nodes is 133, the number of elements is 106, Young's modulus of the Peninsula is assumed as 6000 kgf/cm^2 which is the average of both claystone and sandstone. The thickness of the Peninsula is taken to be 1200 m and the underlying foundation is assumed to be rigid. In this FEM model, because we are interested in near surface layers, the porosity of the rocks should be taken into account. If the rocks are permeable, the buoyancy effect becomes significant. The effect of buoyancy can also be assessed using the same FEM model.

The Result of Simulation

Using the FEM model, simulation was performed under the following assumptions:

1) The crust of the Peninsula is impermeable.

2) The crust of the Peninsula is perfectly permeable.

a. Impermeable Crust

Where the crust is impermeable, a rise in sea level causes an increase in pressure on the surface of the crust under the sea. Because Poisson's ratio is finite, the crust above the sea surface is uplifted. The calculated displacement of the nodes are shown in Fig 5. It is calculated that the uplift of the Peninsula is 1.2 cm for 30 cm of increase in sea level.

b. Perfectly Permeable Crust

When the crust is perfectly permeable, applied pressure is mostly born by infiltrated water. Therefore, the deformation of the crust due to surface pressure will be negligibly small and the most influential mechanism is buoyancy. The calculated displacement of nodes is shown in Figures 6 and 7. The uplift of the Peninsula is 0.6 cm for 30 cm of sea level rise.

In both cases, the rise of sea level caused the uplift of the Peninsula.

Conclusion and Discussion

Annual change of sea level with an approximate amplitude of 15 cm is observed at every tide gauge station in Japan. The cause of such annual sea level change is considered to be the annual variation of barometric pressure and water temperature. If this is the case, the pressure at the bottom of the sea, below a certain level, will be constant throughout the year and the uplift of the Peninsula caused by surface loading will be much smaller than the calculated value.

To verify the effect of buoyancy, we calculated the approximate uplift of the Peninsula using a one dimensional model. When L is the thickness of the elastic layer, F is the buoyancy, and E is Young's modulus, the amount of uplift is calculated as

$$\Delta L = FL/E = 30*1.2*10^5/(6*10^6*g) \approx 0.6 \quad (cm)$$

This is almost the same as the result of FEM simulation.

The actual amount of annual variaton in the elevation of the Omaezaki Peninsula relative to Kakegawa is 1.5 to 2.0 cm. This discrepancy will be explained in the following way.

The rocks located 0 to 100 m below the surface are weathered because of rainfall or cracks and the effective Young's modulus may be on the order of several hundred kgf/cm^2. Here, "effective" Young's modulus is different from the Young's modulus obtained from a small sample piece. "Effective" Young's modulus is the Young's modulus for the Peninsula as a single, macroscopic elastic body which is effective for geophysical phenomeona. As the effective Young's modulus is considered to be small, a few milimeters of uplift can occur in this top layer. The deeper the layer can be divided into two layers. The thickness of the Sagara group is about 880 m and the Young's modulus is several thousand kgf/cm^2 or less. The bottom layer is considered to be the Oigawa group, the thickness being 1440 m and the Young's modulus is estimated to be ten thousand kgf/cm^2. If we take this structure into account, it is quite possible to explain the observed 15 mm annual variation.

In the case where the crust near the sea surface is imperfectly permeable, assuming the water level under the Peninsula does not change rapidly, the pressure is transferred with the speed of sound in water. The resultant hydraulic gradient is converted into upward body force, the effect of which is similar to buoyancy. Therefore, the phase large of annual variation of elevation to annual change in sea level can be neglected.

Leveling surveys at Miura Peninsula play a role similar in the earthquake prediction project in Metropolitian area as the role of leveling at the Omaezaki Peninsula in the earthquake prediction project in the Tokai area. As

the topographic and geologic features of the Miura Peninsula are quite similar to the Omaezaki Peninsula, a similar annual variation of the elevation is expected in the Miura Peninsula. Re-investigation of the leveling data at other Peninsulas is important to the study of crustal dynamics through leveling data.

Acknowledgement

The authors wish to extend their thanks to Dr. Ryuichi Iida of the Public Works Research Institute and Dr. Toshihiro Kakimi of the Geological Survey of Japan for their fruitful discussions and advice to one of the authors (Tazima), and to the local government of Shizuoka-ken for permitting the authors to use the leveling data.

References

Vaníček, P. (1982): Geodesy the concepts, North Holland

Sato, T. and T. Sasao (1980): Influences of the Oceanic Tides upon the VLBI Observation. Proceedings of the Symposium on Geodetica and Geophysical application of VLBI. (in Japanese)

Figure captions

Fig. 1-a Elevation and sea level change at Omaezaki in recent five years. (?: expected but no real data)

Fig. 1-b Elevation difference between bench marks 2601 and SF2129 and sea level change at Omaezaki.

Fig. 2 Tidal spectrum at Omaezaki Tide gauge station. The leftmost component is the annual cycle.

Fig. 3 Subsurface structure at Omaezaki.

Fig. 4 Two dimensional model of the Omaezaki Peninsula.

Fig. 5 Deformation of impermeable crust when sea level rises 30 cm.

Fig. 6 Deformation of perfectly permeable crust when sea level rises 30 cm.

Fig. 7 Displacement of the nodes on the exterior boundary of the model Peninsula.

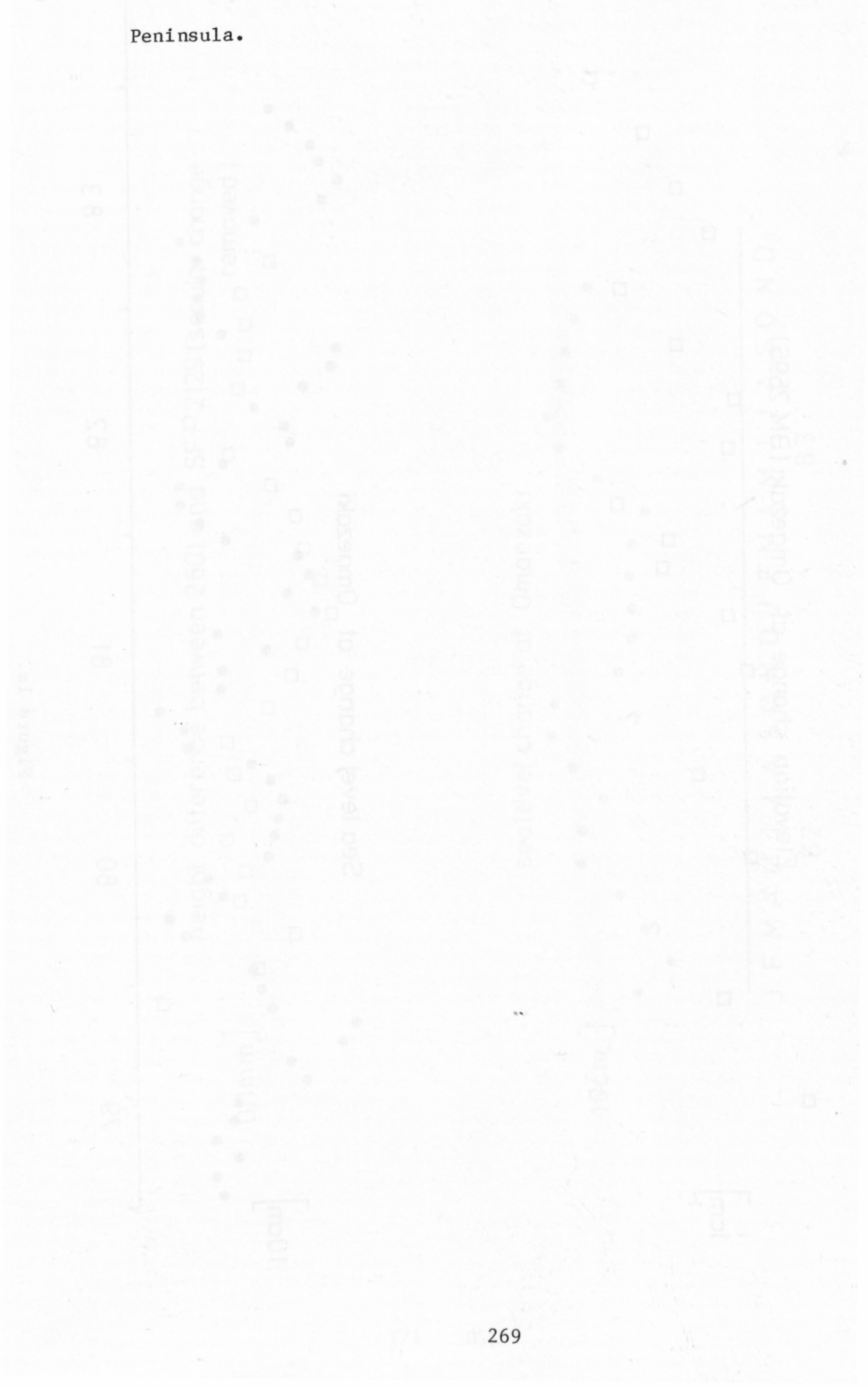

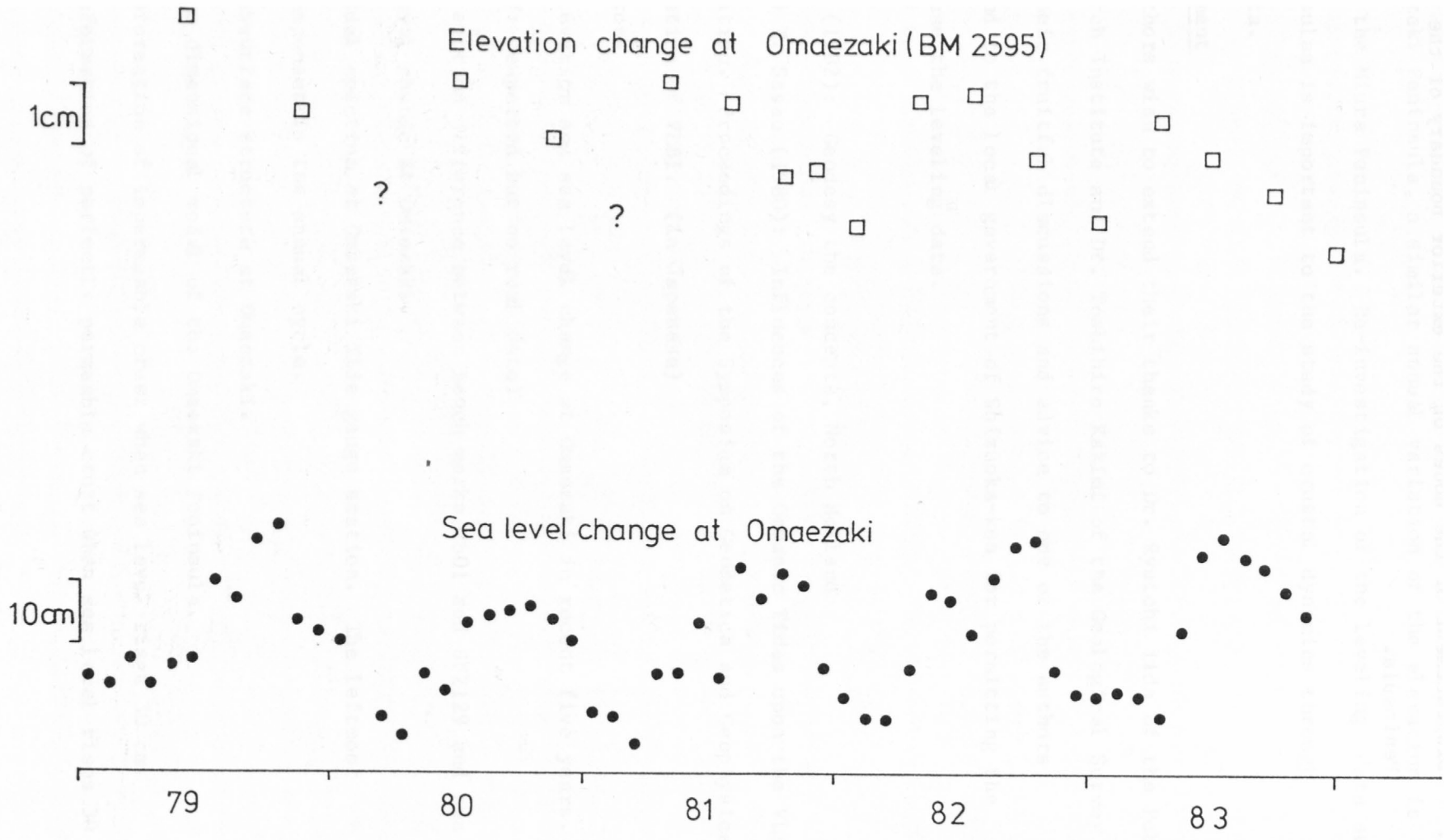
Elevation change at Omaezaki (BM 2595)
1cm
?
?
Sea level change at Omaezaki
10cm
79
80
81
82
83

Figure 1a.

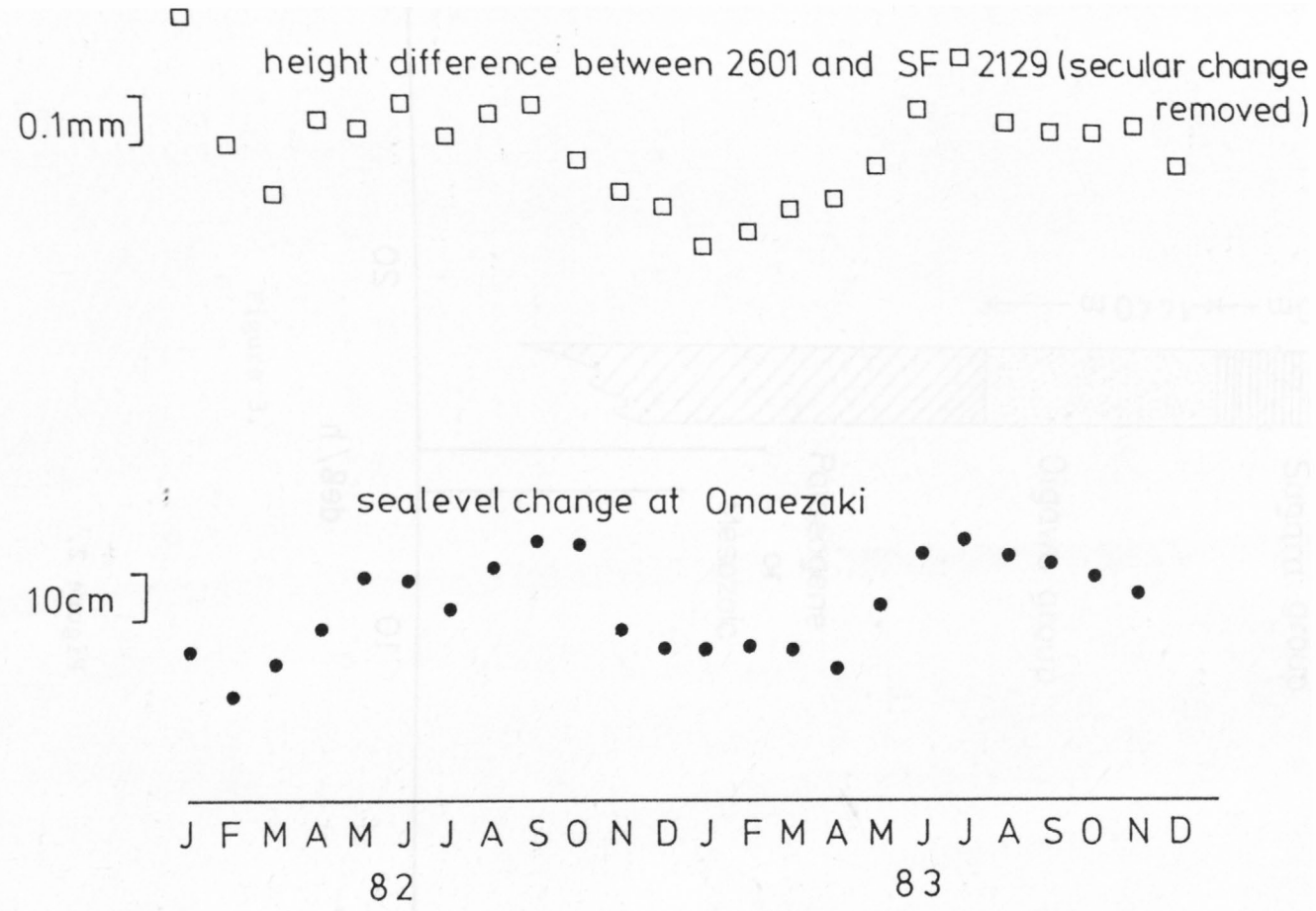
height difference between 2601 and SF 2129 (secular change removed)
0.1mm
sealevel change at Omaezaki
10cm
J F M A M J J A S O N D J F M A M J J A S O N D
82
83

Figure 1b.

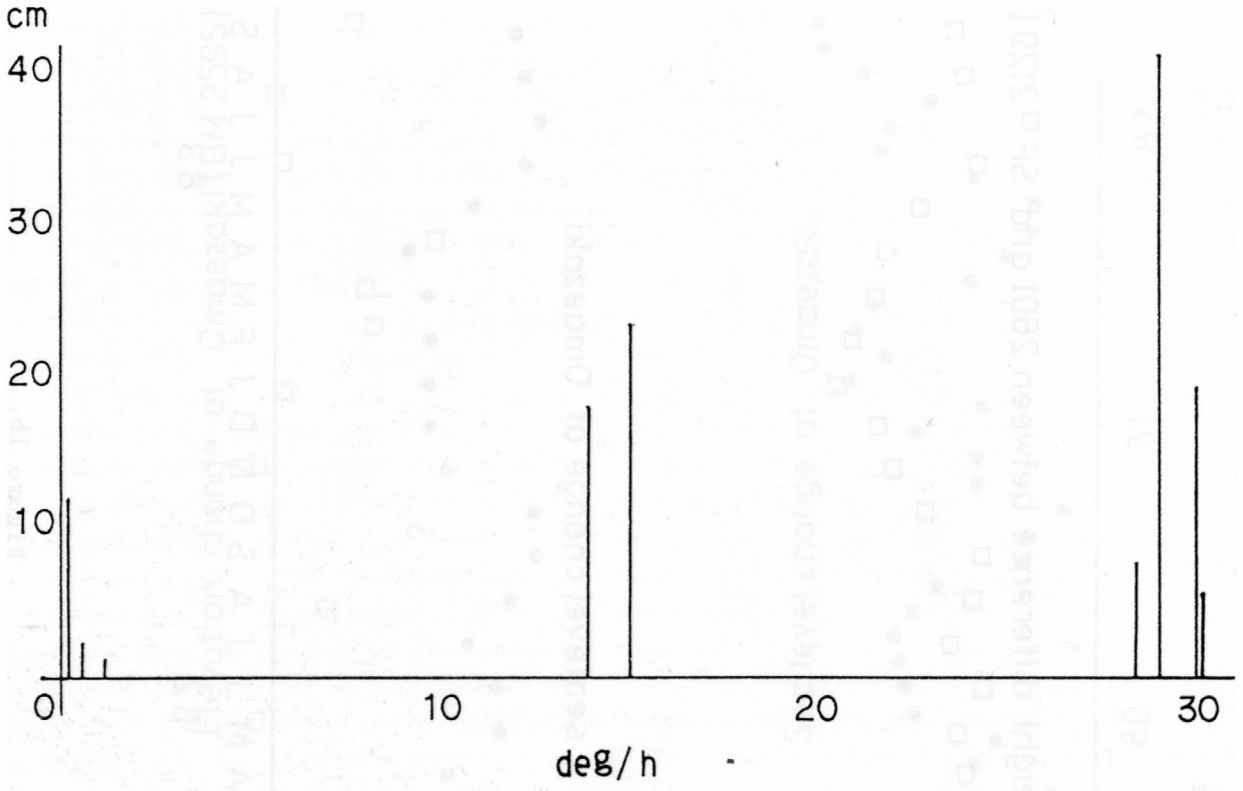

Figure 2.

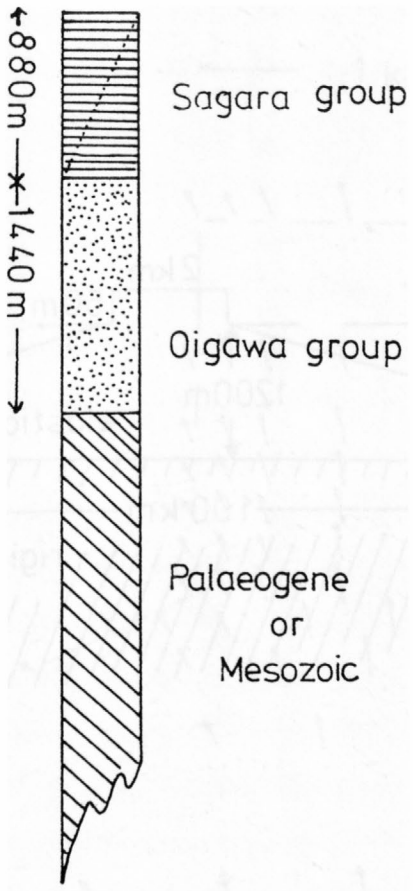
880m
1470 m
Sagara group
Oigawa group
Palaeogene
or
Mesozoic

Figure 3.

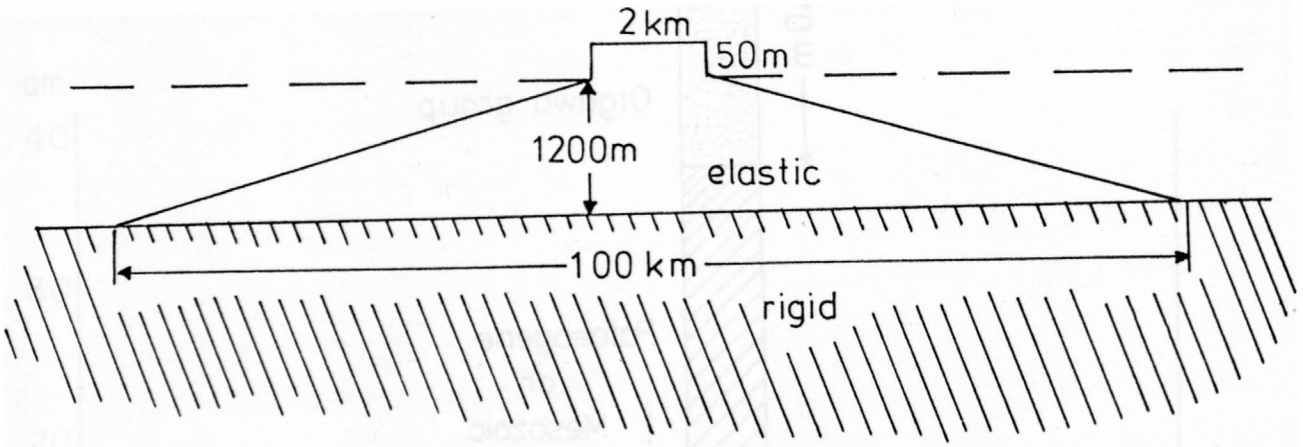

Figure 4.

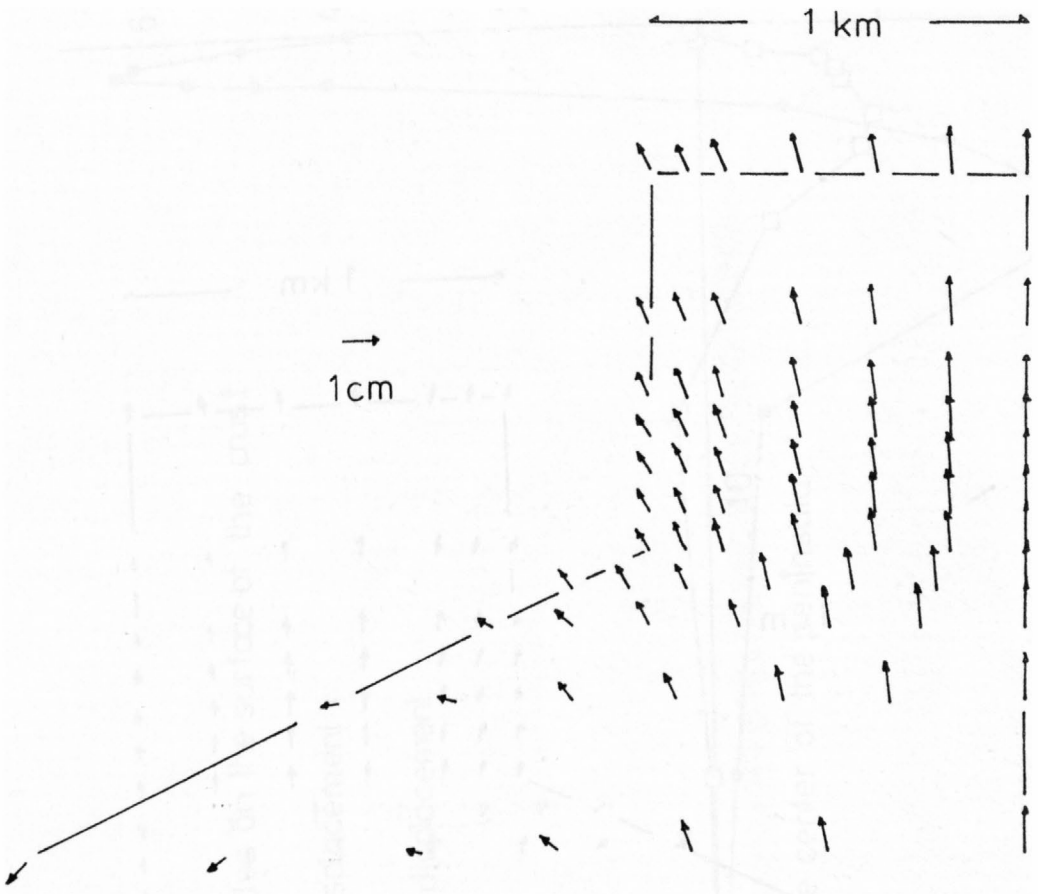

Deformation of Impermeable crust

Figure 5.

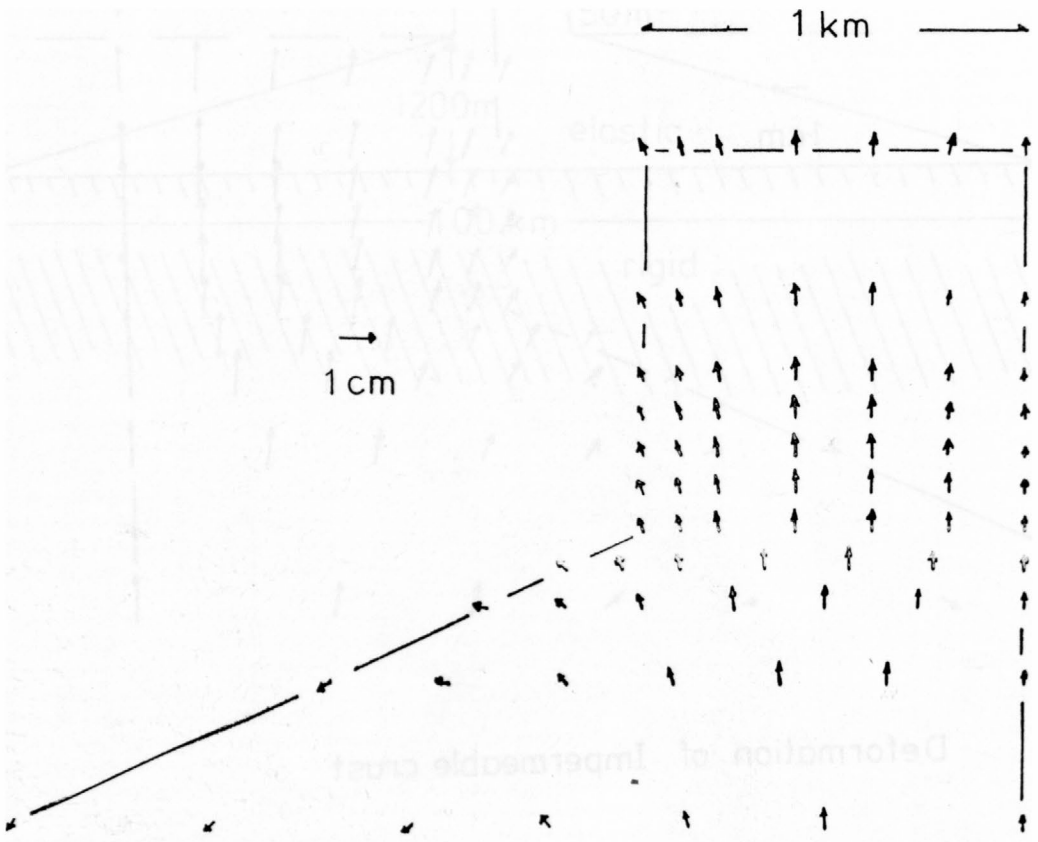

Figure 6.

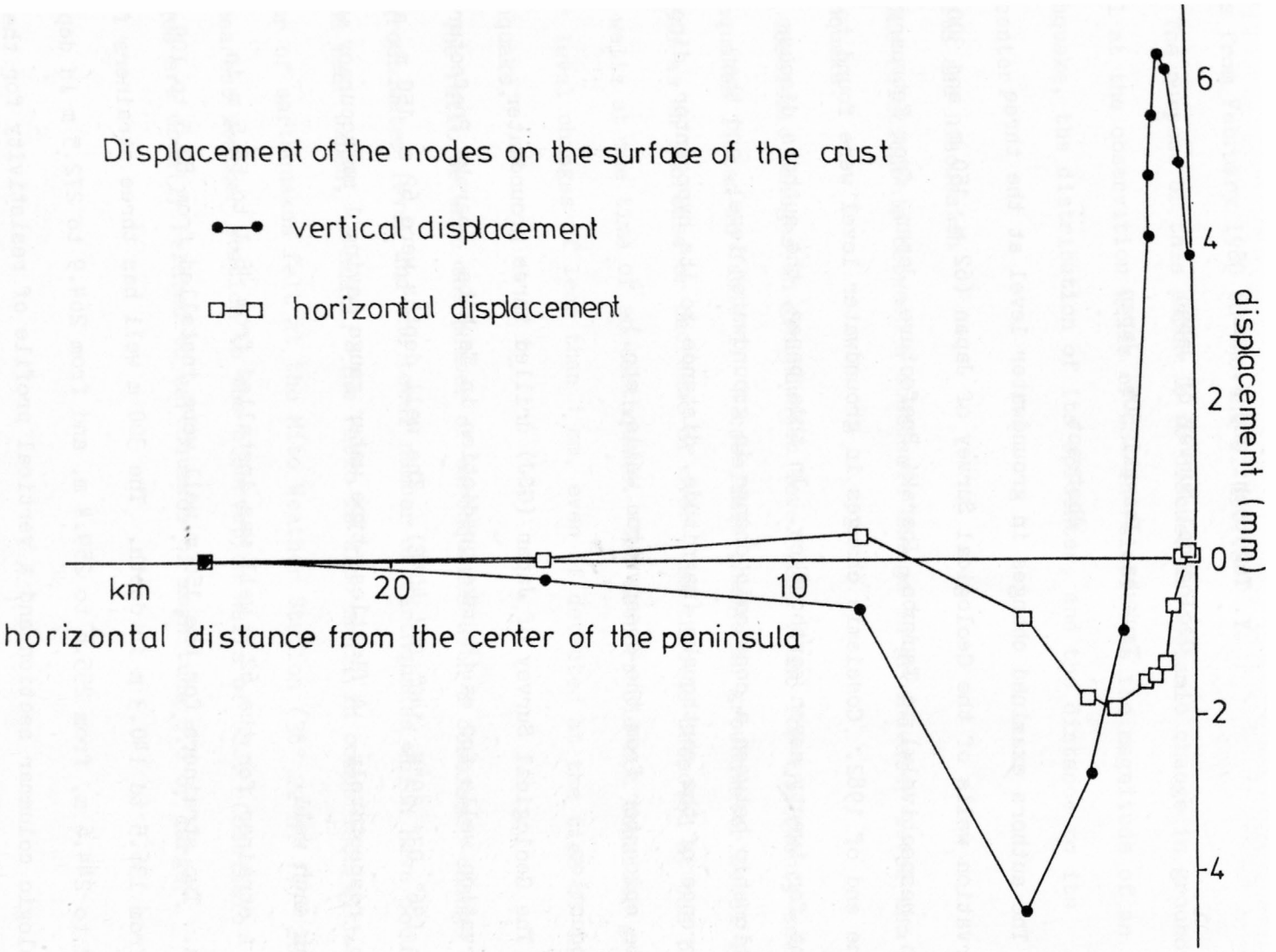
Displacement of the nodes on the surface of the crust
vertical displacement
horizontal displacement
km
20
10
horizontal distance from the center of the peninsula
6
4
2
0
-2
-4
displacement (mm)

Figure 7.

COSEISMIC CHANGES IN GROUNDWATER LEVEL AT THE OBSERVATION WELLS IN TSUKUBA, IBARAKI PREFECTURE AND THE DISTRIBUTION OF EPICENTERS

Y. Tagutschi and K. Ono

Geological Survey of Japan

Tsukuba, Ibaraki 305, Japan

Abstract

The authors examined changes in groundwater level at the three observation wells of the Geological Survey of Japan (62 m, 150 m, and 300 m in depth, respectively) in Tsukuba, Ibaraki Prefecture, Japan, from February 1980 to the end of 1982. Coseismic changes in groundwater level were found to some extent for twenty seven earthquakes. In this paper, the authors discuss the relationship between a coseismic change in groundwater level, and the occurrence of the earthquake (magnitude, distance to its hypocenter, direction to its epicenter from the observation wells, etc.).

Introduction

The Geological Survey of Japan (GSJ) drilled three groundwater observation wells for earthquake prediction in Tsukuba, Ibaraki Prefecture, Japan (36° 03' 39"N, 140° 07' 40"E). The well depths were 62 m, 150 m, and 300 m, respectively. A floatless-type water gauge having 1 mm accuracy was set at each well.

A strainer for the 62 m well was installed from 45.1 to 56.5 m in depth. Two strainers for the 150 m well were installed from 82.5 to 109.0 m and from 136.5 to 140.3 m in depth. The 300 m well has three strainers from 233.2 to 244.6 m, from 255.6 to 259.4 m, and from 264.9 to 272.5 m in depth. A geologic columnar section and a vertical profile of resistivity for the 300 m well are shown in Fig. 1.

The authors have been observing groundwater levels at these three wells since February 1980, and examined the change in groundwater level in these wells from February 1980 to the end of 1982.

The purpose of this paper is to discuss a coseismic change in groundwater level at the observation wells of GSJ in relation to the magnitude of an earthquake, the distribution of its epicenter, and the distance to its hypocenter.

Results and Discussion

1) The relationship between a coseismic change in groundwater level and an earthquake.

Coseismic changes in groundwater level were found for the twenty-seven earthquakes listed in Table 1. A coseismic change in groundwater level is defined as an increase or decrease of over 1 mm that is detected at one or more wells at the time of an earthquake. The authors did not consider ground water level changes of less than 1 mm, even if detected at the time of the earthquake.

The ratio between the number of earthquakes with a coseismic change in the groundwater level and the total number of earthquakes which have occurred in and near Japan, is small. The ratio is also small in comparison with the number of earthquakes felt at the Mito Weather Station (36° 22'N, 140° 28'E), the nearest weather station to the observation wells of GSJ. Coseismic changes are usually related to earthquakes of magnitude 5.0 or larger.

Table 1. List of earthquakes for which groundwater level of the observation wells of GSJ in Tsukuba was coseismically changed more than 1 mm (from February 1980 to December 1982)

No.	Origin Time, JST Date	Time	Name of District	Epicenter Long.	Lat.	H (km)	M	Well No. 1	2	3
1	'80 2/23	14:51	SE OFF Hokkaido	146,33'E	43,27'N	30	6.8	@	X	X
2	6/29	16:20	IZU PEN Region	139 14	34 55	10	6.7	@	@	@
3	9/24	04:10	Southern Kanto	139 48	35 58	80	5.4	@	@	X
4	9/25	02:54	SE Coast of Kanto	140 13	35 31	80	6.1	@	@	X
5	12/31	19:32	Kurile Is	152 22	46 14	70	7.1	@	?	@
6	'81 1/19	03:11	E Off N. Honshu	143 09	38 38	0	6.1	@	X	@
7	1/19	03:17	E Off Mid-Tohoku	142 58	38 36	0	7.0	@	@	@
8	1/23	04:34	E Off N Honshu	143 03	38 14	0	6.6	X	@	@
9	1/23	13:58	S Coast of Hokkaido	142 12	42 25	130	7.1	X	@	@
10	1/28	12:47	Northern Kanto	139 51	36 10	60	5.0	@	@	@
11	4/13	12:04	E Off S. Tohoku	142 21	37 16	30	5.7	@	@	-
12	9/02	18:24	E Off Kanto	141 08	35 48	40	5.8	@	@	?
13	9/03	14:35	SE Off Hokkaido	146 49	43 28	30	6.5	@	X	@
14	'82 2/21	04:18	SE Off Kanto	141 14	33 43	40	6.4	@	@	@
15	3/07	08:14	E Coast of Kanto	140 39	36 28	60	5.5	@	@	?
16	3/21	11:32	S Off Hokkaido	142 36	42 04	40	7.1	@	@	@
17	3/27	09:19	S Off Kanto	140 51	34 47	50	5.6	@	X	X
18	6/01	05:13	E Off Mid-Tohoku	142 20	38 41	40	6.2	@	X	X
19	7/23	23:23	E Off Kanto	141 57	36 11	30	7.0	@	@	-
20	7/24	02:53	E Off Kanto	142 03	36 07	30	6.2	@	@	-
21	7/25	17:01	E Off Kanto	141 56	36 20	10	5.9	@	@	-
22	8/03	01:26	E Off Kanto	141 22	36 13	30	4.5	@	X	-
23	8/12	13:33	S Off Kanto	139 34	34 53	30	5.7	@	-	X
24	9/30	01:10	Tokyo Bay Region	140 09	35 32	70	4.6	X	X	@
25	10/25	00:50	E Coast of Kanto	140 31	35 54	40	4.2	@	@	?
26	11/10	08:37	E Coast of Kanto	140 38	36 34	100	5.1	X	@	?
27	12/28	15:37	Near Miyakejima	139 27	33 52	20	6.4	@	@	@

Note: @; Changed, X; Not changed, ?; Under consideration, -; No record, Well No. 1; 62 m in depth, 2; 150 m in depth, 3; 300 m in depth (Data source of earthquakes: Japan Meteorological Agency)

Most coseismic changes in groundwater level are less than 10 mm. Coseismic changes greater than 10 mm were found only at the 62 m well (for earthquake numbers 15 and 19 - water level dropped) and at the 150 m well (for earthquake numbers 3, 12, and 15 = water level dropped, and number 19 - water level rose).

The groundwater change in different wells sometimes exhibited an opposite sense of movement for a single earthquake. For example, the groundwater level at well A increases but the level at well B decreases coseismically.

2) Distribution of epicenters

Figure 2 is a distribution map of 27 epicenters listed in Table 1. The area shown in Fig. 2 was divided into eight sectors and three concentric zones centering around the observation wells. Table 2 shows a frequency distribution of 27 epicenters in each sub-area.

Coseismic changes in the groundwater level appear only for the earthquakes which occurred in the upper or overlying plate (the Asian plate) along the Japan Trench in a N-SE direction. On the other hand, no coseismic change appears for those earthquakes which occurred in the upper plate, (the Asian Plate) along the Nankai Trough in SW direction.

Two possible explanations for this phenomenon are considered. One is that no big earthquakes have occurred in the upper or overlying crustal plate along the Nankai Trough during this observation period. The second reason may be related to the phenomenon called "region of anomalous seismic intensity:, whereby seismic intensity of an earthquake is not concentric around the hypocenter. Hypocenters of earthquakes which cause water level change are apparently distributed along the landward side of the Japan Trench. This distribution is probably due to smaller attenuation in the paths through the colder subducting Pacific Plate.

In Table 2 it seems that about 80% of epicenters are distributed within a radius of 500 km from the observation wells and about 60% of epicenters are in NE and E sectors.

A coseismic change in the groundwater level also appears for the big earthquakes which occurred at long distances in the N-NE sectors. Especially, hypocenters of earthquakes Nos. 1, 5, and 13 were located at distances of more than 1,000 km from the observation wells. In the E sector, a coseismic change is found only for the earthquakes which occurred within a radius of about 200 km from the observation wells.

3) The relationship between the magnitude of an earthquake, and distance and direction to its hypocenter.

The relationship between each magnitude of earthquake for which a coseismic change in the groundwater level was found, and distance and direction from the observation wells to each hypocenter is shown in Fig. 3. A straight line was drawn on a lower limit, which indicates a boundary of appearance of a coseismic change in groundwater level. It shows that some coseismic change appears in the area above the line. Fig. 3 indicates that a coseismic change in groundwater level, to some extent, may appear within a radius of 100 km even for an earthquake whose magnitude is less than four.

Table 2. Frequency of a coseismic change in groundwater level of the observation wells of GSJ in Tsukuba in each sector and the distance from the wells to the hypocenter

Direction / Radius	N	NE	E	SE	S	SW	W	NW	Total (%)
< 200 km		2	5	2	2	2	1	1	15(55.6%)
< 500 km		5			2				7(25.9%)
< 1,000 km	2								2(7.4%)
1,000 km <		3							3(11.1%)
Total	2	10	5	2	4	2	1	1	27(100.0%)

FIGURES AND TABLES

Fig. 1. A geologic columnar section and a vertical profile of resistivity of the 300 m well of GSJ in Tsukuba, Japan.

Fig. 2. Distributions of epicenters and the observation wells (G) of GSJ in Tsukuba.

Fig. 3. Relationship between the magnitude of the earthquake by which groundwater level of the observation wells of GSJ in Tsukuba was coseismically changed and the distance from the wells to its hypocenter in each sector.

Table 1. List of earthquakes for which groundwater level of the observation wells of GSJ in Tsukuba was coseismically changed more than 1 mm (from February 1980 to December 1982).

Table 2. Frequency of a coseismic change in groundwater level of the observation wells of GSJ in Tsukuba in each sector and the distance from the wells to the hypocenter.

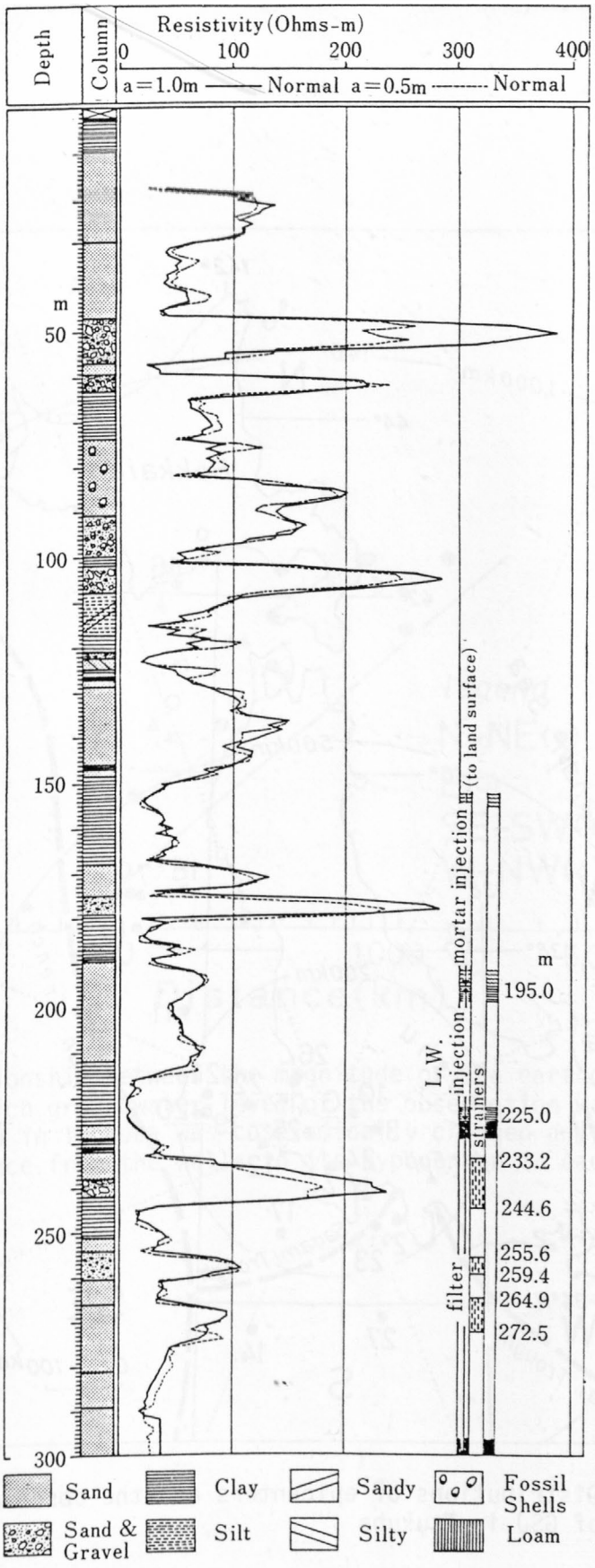

Fig.1 A geologic columnar section and a vertical profile of resistivity of the 300 m well of GSJ in Tsukuba, Japan

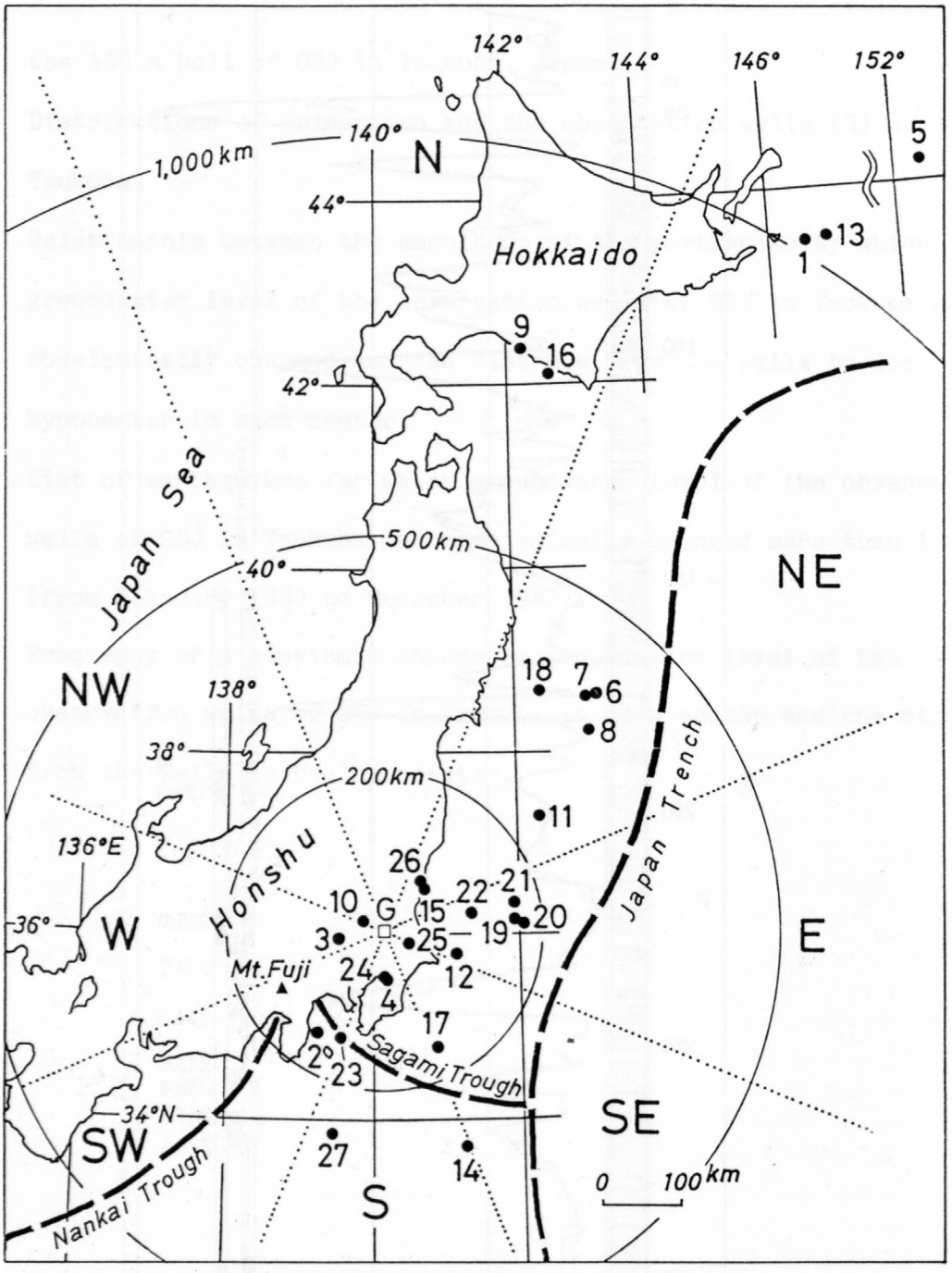

Fig.2 Distributions of epicenters and the observation wells(G) of GSJ in Tsukuba

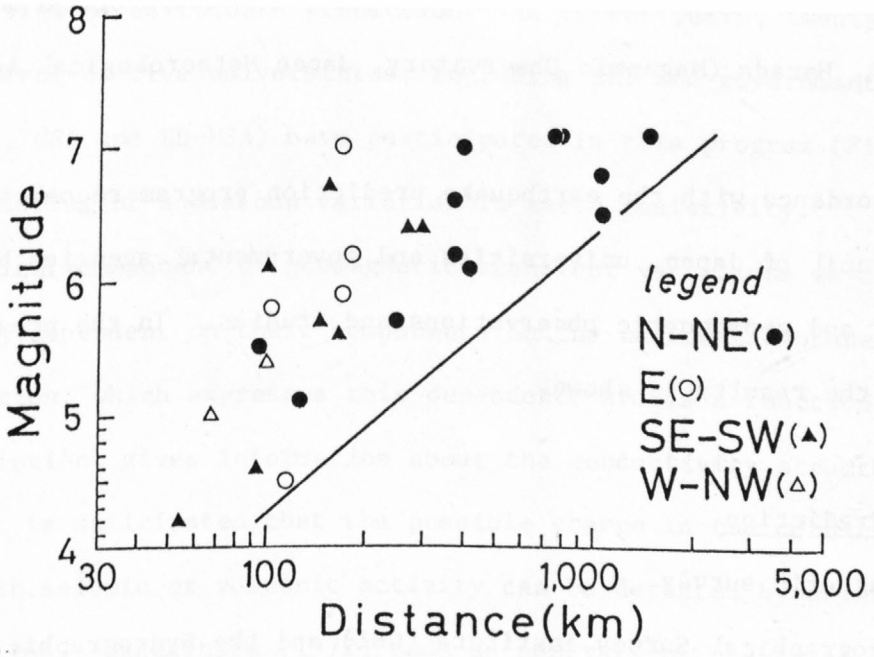

Fig.3 Relationship between the magnitude of the earthquake by which groundwater level of the observation wells of GSJ in Tsukuba was coseismically changed and the distance from the wells to its hypocenter in each sector

GEOMAGNETIC AND GEOELECTRIC WORK ON EARTHQUAKE PREDICTION IN JAPAN

T. Rikitake (Nihon University)

M. Tazima (Geographical Survey Institute)

M. Kawamura (Observations Department, Japan Meteorological Agency)

and A. Harada (Magnetic Observatory, Japan Meteorological Agency)

In accordance with the earthquake prediction program recommended by the Geodesy Council of Japan, universities and governmental agencies have made geoelectric and geomagnetic observations and studies. In the present paper, a summary of the results is shown.

Long-term Prediction

(1) Magnetic survey

The Geographical Survey Institute (GSI) and the Hydrographic Department of the Maritime Safety Agency (HD-MSA) have made magnetic measurements at approximately one hundred magnetic station which have been established over Japanese land at intervals of 1-5 years. The results have been analyzed to find out the regions of anomalous geomagnetic secular variations. Tazima and others (1976) determined the distribution of anomalous geomagnetic secular variations for the period 1967.5-1972.5, and showed their possible correlation with seismic or volcanic activities (Fig. 1).

(2) Continuous measurement of the geomagnetic secular variation

Since 1968, continuous total force measurements by proton magnetometers have been conducted at 12 stations. The data obtained are sent to the organization which operates the data analysis center. The center was

established in the Earthquake Research Institute, the University of Tokyo (ERI), and moved to GSI in 1973. Since 1980, the Magnetic Observatory of the Japan Meteorological Agency (MO-JMA) has been responsible for the data. Results have been periodically reported to the Coordinating Committee for Earthquake Prediction in order to examine anomalous phenomena, if any, from the point of view of earthquake prediction. In recent years, twenty stations under the control of five universities, including ERI and governmental agencies (JMA, GSI and HD-MSA) have participated in this program (Fig. 2).

(3) Monitoring of anomalous variation in earth resistivity.

The vertical component of geomagnetic transient variations is taken as being linearly dependent on their components on the horizontal plane. The transfer function, which expresses this dependence and is a function of the period of variation, gives information about the conductivity structure within the earth. It is anticipated that the possible change in the conductivity associated with seismic or volcanic activity can be detected by observing the transfer function. Yanagihara (1972) made an analysis of the ratio of the vertical to the horizontal component $\Delta Z/\Delta H$ and showed that it underwent a secular variation. He considered that the variation might be related to the Great Kanto Earthquake (M = 7.9) in 1923 (Fig. 3). Recently, Yanagihara and Nagano (1976) and Sano (1980) pointed out similar changes in the transfer of Kakioka and discussed a relation between the changes and earthquakes of magnitude 5 or greater which took place in the vicinity of Kakioka. MO-JMA is making continuous analysis of the transfer function of MMB, KAK, MTZ, OMZ and KNY. (The abbreviations of the name of the observatories and stations as well as their locations are given in Fig. 2). Miyakoshi (1975), Honkura (1980) and Sumitomo (1982) have also made extensive studies of the transfer function for the purpose of detecting anomalous changes of earth resistivity.

Short-Term Prediction in the Areas Under Intensified Measures Against Earthquake Disaster (Izu-Tokai area)

(1) Yamazaki (1974) of ERI developed a new instrument for measuring the apparent resistivity of rocks. Continuous measurements at Aburatsubo in Miura Peninsula south of Tokyo have been conducted with a hope of detecting a change of apparent resistivity. During the period from 1967 - 1974, he had observed pre-seismic anomalous changes twenty times, including a change corresponding in time to the 1974 Izu-Hanto-Oki earthquake (off Izu Peninsula, Fig. 4).

(2) ERI has conducted continuous measurements of the geomagnetic total intensity with proton magnetometers at SGH and KWZ in Izu Peninsula. Sasai and others (1980), detected a possible pre-seismic change of 6 nT preceding the aftershock (magnitude 5.0) of the 1978 Izu-Oshima-Kinkai earthquake (off Izu Oshima Island, Fig. 5).

(3) Yukutake and others of ERI conducted measurements of earth resistivity several times with the direct current method at Miharayama, a volcano in Izu Oshima Island. Remarkable variations of conductivity were observed preceding the 1978 Izu-Oshima-Kinkai earthquake and the 1980 Off Eastern Izu Peninsula earthquake (Fig. 6).

(4) MO-JMA established observation stations, MTZ and OMZ, which are located on the eastern and western sides of Suruga Bay. This area has been considered to be a possible place where a big earthquake will occur. Magnetic and earthcurrent observations have been conducted at the stations. The data obtained are sent to JMA by telemetering. Since 1982, earth resistivity measurements have also been carried out using the direct current method in the neighboring

areas of MTZ and OMZ.

(5) ERI, the Tokyo Institute of Technology (TIT) and other universities have cooperatively conducted geoelectric and geomagnetic observations in Izu Peninsula and the Tokai District. They established a dense network of magnetic stations over the region for earthquake prediction research and have made frequent repeated surveys.

Research Activities in Other Areas

(1) Investigation of fault activities based on geoelectric and geomagnetic measurements.

It is important for earthquake prediction and for prevention of disasters to investigate the activity of faults. The geoelectric and geomagnetic method are expected to be effective for this investigation. Universities (ERI, Akita University and others) and governmental agencies (MO-JMA, GSI and Geological Survey of Japan) applied these methods to the Yamasaki fault in 1975 - 1978 (located in western Honshu), the Tanna fault and the Ukihashi fault in 1979 (both in northern Izu Peninsula) and the Senya fault in 1980 (in northeastern Honshu). It was found that the faults had a low resistivity layer beneath them. Earth current vectors, electric potential, and magnetic field distributions often show anomalous character around the faults. These results suggest that the methods will contribute much to the investigation (Fig. 7-12).

(2) It is an important problem to develop a technique for prediction of earthquakes which have their foci directly under urban-areas, because they can cause serious damage and disaster. Extensive studies in this field have recently been started by universities and governmental agencies. The geoelectric and geomagnetic methods are also included in this project and the investigation is carried out in

the Kanto District.

References

Electromagnetic Research Group for the Active Fault, Study on fault activity using geoelectric and geomagnetic methods (by Ministry of Education, Science and Culture), 1981.

Electromagnetic Research Group for the Active fault, Low electrical resistivity along an active fault, the Yamasaki fault, J. Geomag. Geoelectr., 34, 103, 1982.

Electromagnetic Research Group for the Active Fault, Electrical resistivity structure of the Tanna and the Ukihashi Faults, Bull. Earthq. Res. Inst., 58, 265, 1983.

Handa, S., and N. Sumitomo, MT sounding around active faults by using natural electromagnetic noises in the ELF range, Tsukumo-Chigaku, 14, 21, 1979.

Honkura, Y., Geomagnetic changes associated with earthquakes in the Izu Peninsula, Proceedings of Earthquake Prediction Research, p. 65, 1980 (in Japanese).

Miyakoshi, J., Secular variation of Parkinson vectors in a seismically active region of Middkle Asia, J. Fac. General Education, Tottori Univ., 8, 209, 1975.

Sano, Y., Time changes of transfer functions at Kakioka related to earthquake occurrences (1), Geophys. Mag. 39, 98, 1980.

Sasai, Y. and Y. Ishikawa, Tectonomagnetic event preceding a M5.0 earthquake in the Izu Peninsula - Aseismic slip of a buried fault?, Bull. Earthq. Res. Inst., 55, 895, 1980.

Sumitomo, N., and M. Ohtsuda, CA observation in the Yanagase Fault, proceedings of CA symposium, p. 127, 1982 (in Japanese).

Tazima, M., H. Mizuno and M. Tanaka, Geomagnetic secular change anomaly in

Japan, J. Geomag. Geoelectr., 28, 68, 1976.

Yamazaki, Y., Electrical conductivity of strained rocks (6) - A resistivity change at Aburatsubo associated with the Izu-Hanto-Oki earthquake of 1974, Special Bull. Earthq. Res. Inst., 14, 121, 1974 (in Japanese).

Yanagihara, K., Secular variation of the electrical conductivity anomaly in the central part of Japan, Mem. Kak. Mag. Ovs., 15, 1, 1972.

Yanagihara, K., and T. Nagano, Time change of transfer function in the central Japan anomaly of conductivity with special reference to earthquake occurrence, J. Geomag. Geoelectr., 28, 157, 1976.

Yukutake, T., T. Yoshino, H. Utada, T. Shimomura and E. Kimoto, A change in the apparent electrical resistivity of Mt. Mihara of Oshima Volcano observed in association with the Izu-Hanto-Toho-Oki earthquake, 1980, Bull. Earthq. Res. Inst., 56, 623, 1981.

Figure Captions

Fig. 1: Results of magnetic surveying in Japan. The hatched areas show the anomalous secular variation of total magnetic field intensity (after Tazima and others, 1976).

Fig. 2: Distribution of stations for continuous measurements of geomagnetic secular variation. The stations are listed below.

MMB:	Memambetsu	(MO-JMA)	HAT:	Hatsushima	(ERI)
KMU:	Kamikineusu	(HU *)	HED:	Heda	(TIT)
OGA:	Oga	(TU *)	SGH:	Sugehiki	(ERI)
MIZ:	Mizusawa	(GSI)	KWZ:	Kawazu	(ERI)
KNK:	Kinkazan	(TU *)	NOM:	Nomashi	(ERI)
KAK:	Kakioka	(MO-JMA)	MTZ:	Matsuzaki	(MO-JMA)
KTR:	Kitaura	(MO-JMA)	OMZ:	Omaezaki	(MO-JMA)
YAT:	Yatsugatake	(ERI)	HJJ:	Hachijojima	(HD-MSA)
TOT:	Tottori	(KU *)	AHK:	Aso-sanroku	(MO-JMA)
KNZ:	Kanozan	(GSI)	KNY:	Kanoya	(MO-JMA)

* HU:Hokkaido University, TU:Tohoku University,
KU:Kyoto University

Fig. 3. Time change of the ratio $\Delta Z/\Delta H$ observed at Tokyo (1897-1912) and at Kakioka (1913-1973). (After Yanagihara and Nagano, 1976.)

Fig. 4. The change of apparent resistivity observed at Aburatsubo associated with the 1974 Izu-Hanto-Oki earthquake. (After Yamazaki, 1974.)

Fig. 5. Geomagnetic variation observed by proton magnetometers in Izu Peninsula. Left figure shows location of magnetic stations (large circle:continuous observation stations). A remarkable variation in the total force was observed at the Kawazu station before a major aftershock of the 1978 Izu-Oshima-Kinkai earthquake. (After Sasai

and Ishikawa, 1980.)

Fig. 6. Electrode arrangements are shown in the upper panel. I1, I2, and I3 denote the current electrodes and V1, V2, and V3 denote the potential ones. In the lower panel, time variations in apparent electrical resistivity of Miharayama volcano obtained by three pairs of electrodes as given in the upper panel (after Yukutake et al., 1981).

Fig. 7. A profile of apparent resistivity along a line crossing the Yamasaki fault. The curves of A, B and C are obtained by the VLF method, the horizontal prospecting method, and gradient method, respectively. (After Electromagnetic Research Group for the Active Fault, 1982.)

Fig. 8. A schematic illustration showing structures of the apparent resistivity near the Yamasaki fault. The Schumann resonance wave employed for this magnetotelluric analysis. (After Handa and Sumitomo, 1979.)

Fig. 9. An apparent resistivity profile across the faults. The central Ukihashi fault is located at the origin (0km) and the western Ukihashi fault at about 0.4km west. (After Electromagnetic Research Group for the Active fault, 1983.)

Fig. 10. In the left panel, apparent resistivity profiles are plotted against distance from the Senya fault. In the right, the phase differences are shown in the same way. (After Electromagnetic Research Group for the Active Fault, 1981.)

Fig. 11. The upper panel presents vectors of the electric potential gradient near the Senya fault and in the lower left is shown the comparison of the model with the observation. In the upper right, examples of anomalous behavior of electric potential profiles are shown. Dotted lines denote the location of the fault. The schematic illustration

of a model of the Senya fault is shown in the lower right. (After Electromagnetic Research Group for the Active Fault, 1981.)

Fig. 12. Examples of anomalous magnetic profiles (upper panel) and modeling (lower panel). (After Electromagnetic Research Group for the Active Fault, 1981.)

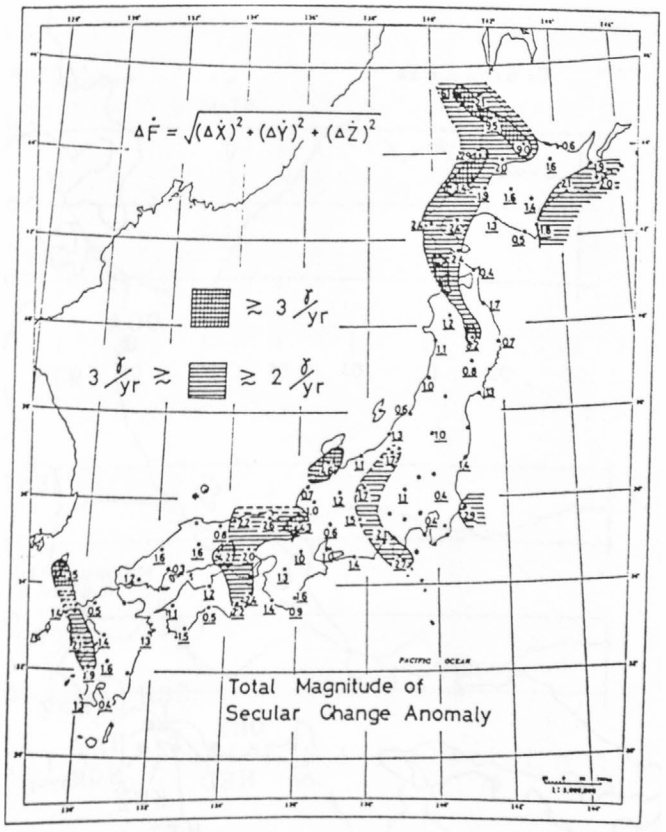
$\Delta\dot{F} = \sqrt{(\Delta\dot{X})^2 + (\Delta\dot{Y})^2 + (\Delta\dot{Z})^2}$
$\gtrsim 3\ \gamma/yr$
$3\ \gamma/yr \gtrsim \gtrsim 2\ \gamma/yr$
PACIFIC OCEAN
Total Magnitude of
Secular Change Anomaly

Figure 1.

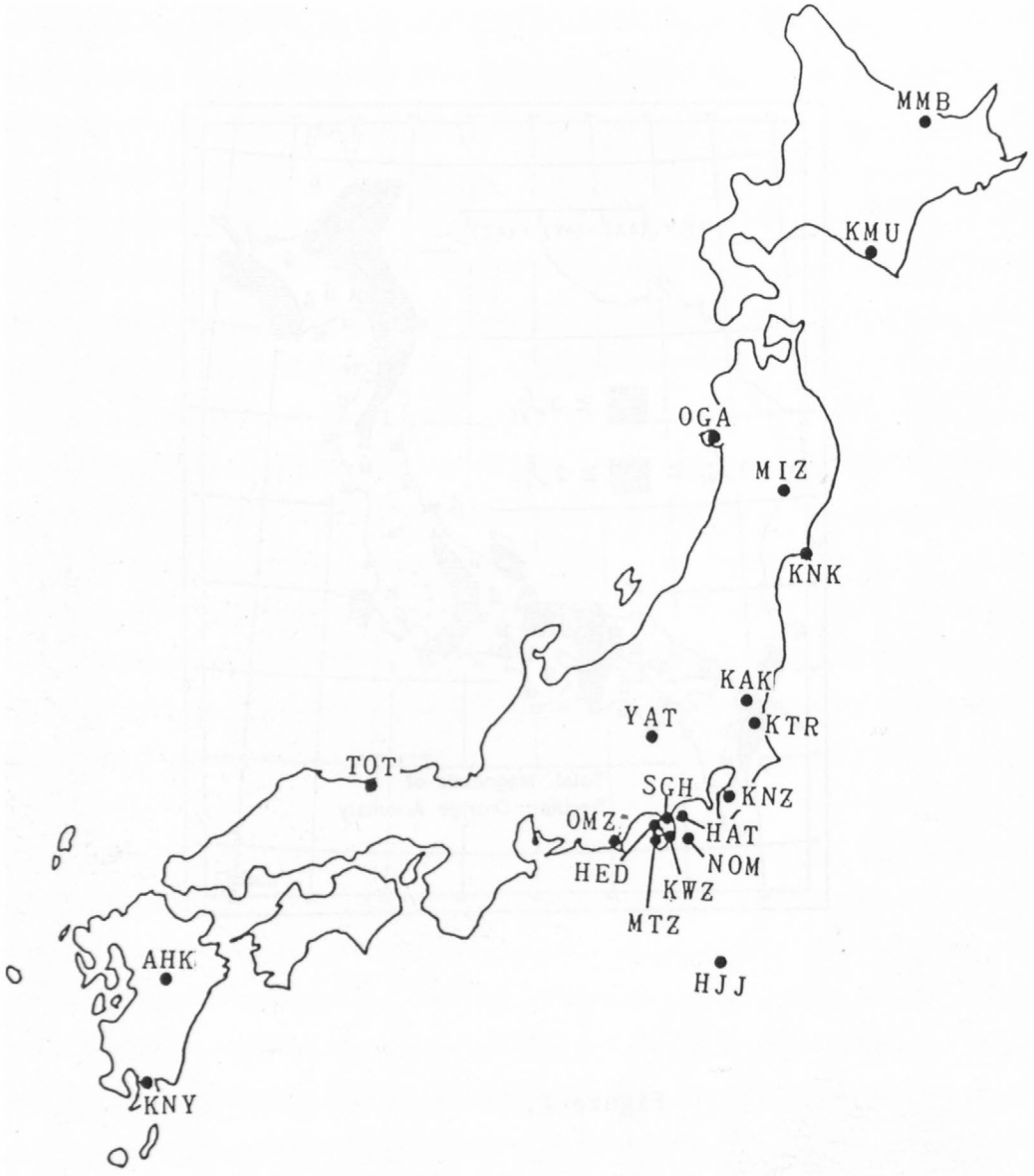
MMB
KMU
OGA
MIZ
KNK
KAK
YAT
KTR
TOT
SGH
KNZ
OMZ
HAT
NOM
HED
KWZ
MTZ
AHK
HJJ
KNY

Figure 2.

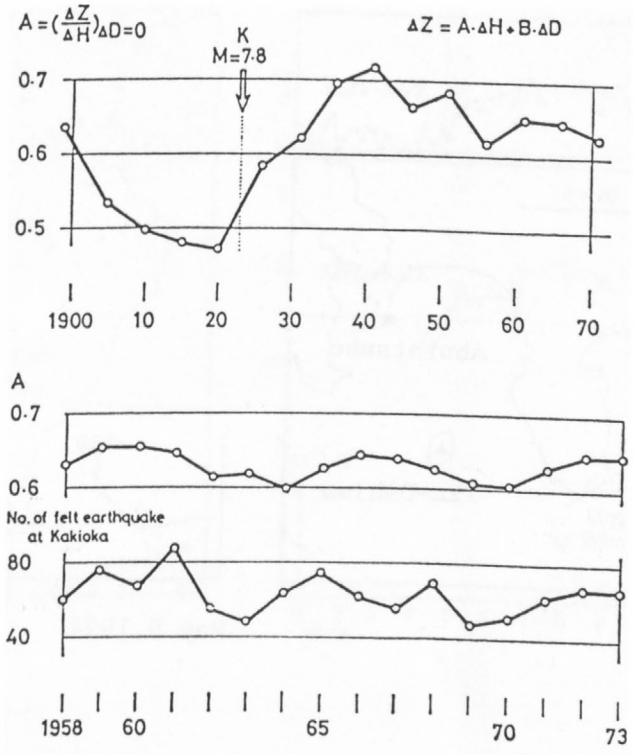
A = (ΔZ/ΔH)ΔD=0
K
M=7·8
ΔZ = A·ΔH + B·ΔD
0·7
0·6
0·5
1900
10
20
30
40
50
60
70
A
0·7
0·6
No. of felt earthquake at Kakioka
80
40
1958
60
65
70
73

Figure 3.

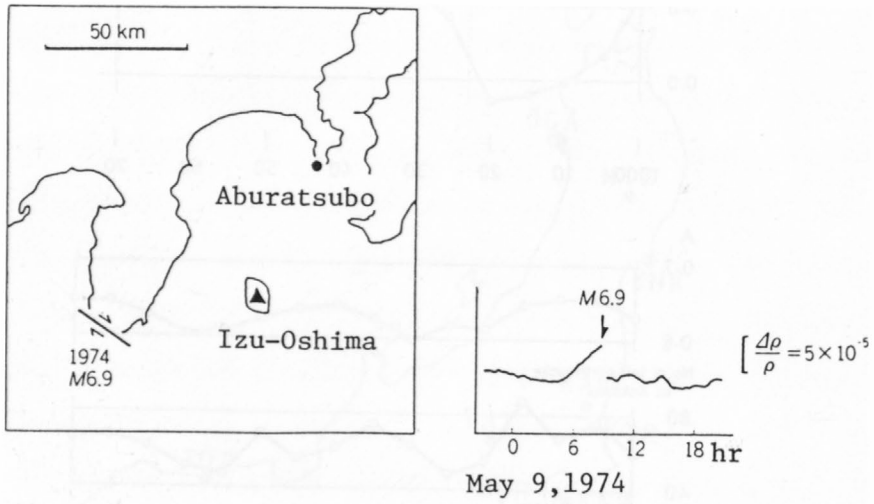
50 km
Aburatsubo
Izu-Oshima
1974
M6.9
M6.9
$\left[\frac{\Delta\rho}{\rho}=5\times10^{-5}\right.$
0
6
12
18 hr
May 9,1974

Figure 4.

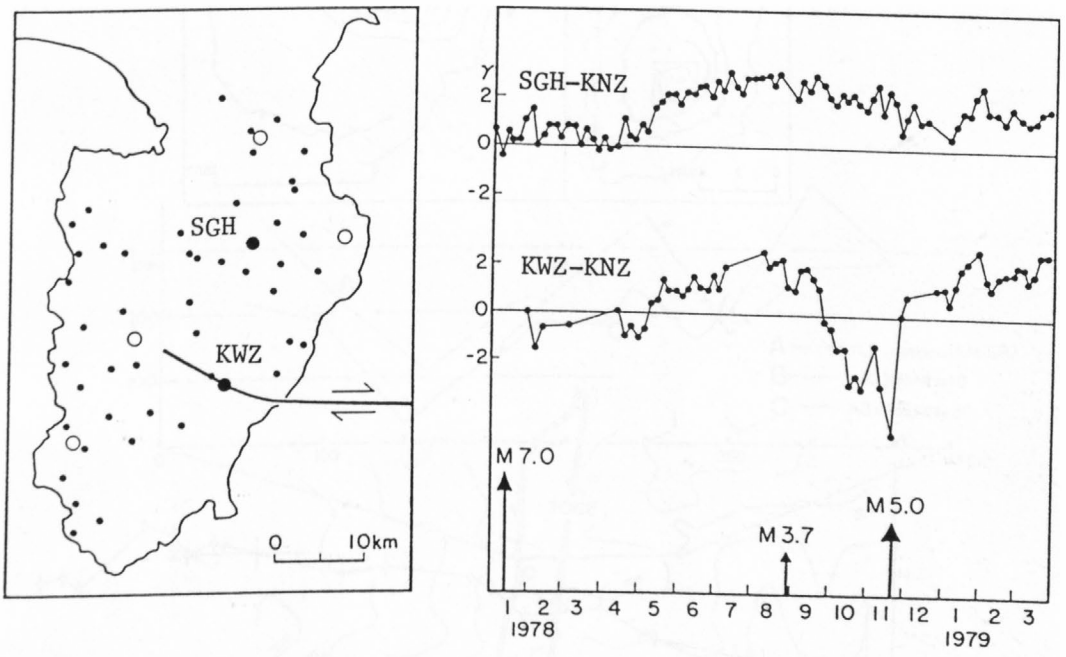
SGH
KWZ
0 10km
γ
SGH-KNZ
2
0
-2
KWZ-KNZ
2
0
-2
M 7.0
M 3.7
M 5.0
1 2 3 4 5 6 7 8 9 10 11 12 1 2 3
1978
1979

Figure 5.

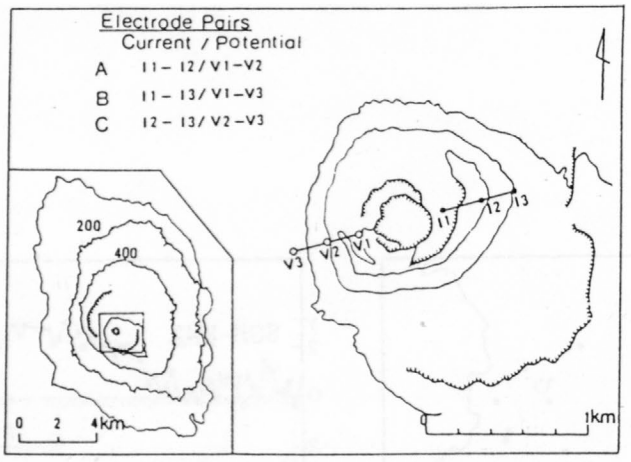
Electrode Pairs
Current / Potential
A I1 – I2 / V1 – V2
B I1 – I3 / V1 – V3
C I2 – I3 / V2 – V3
200
400
0 2 4km
I1
I2
I3
V1
V2
V3
1km

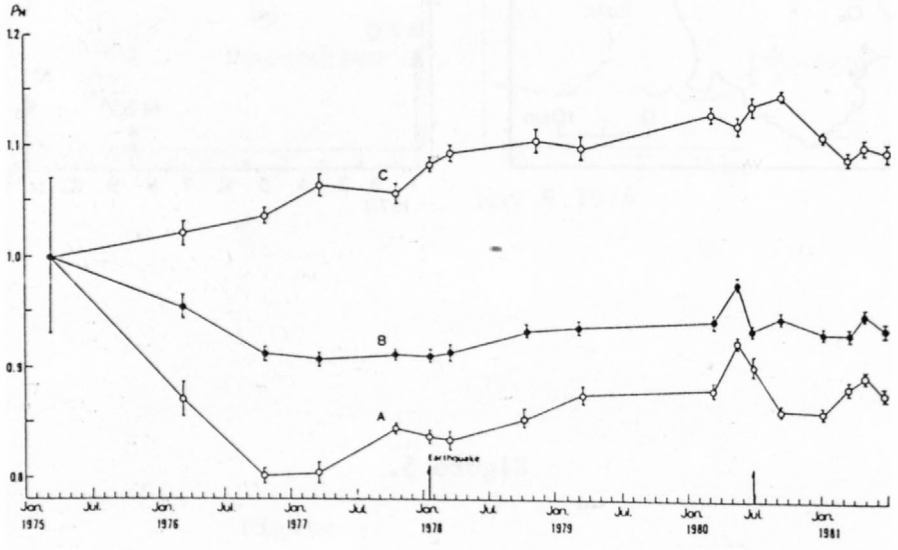
Pw
1.2
1.1
1.0
0.9
0.8
C
B
A
Earthquake
Jan. 1975
Jul.
Jan. 1976
Jul.
Jan. 1977
Jul.
Jan. 1978
Jul.
Jan. 1979
Jul.
Jan. 1980
Jul.
Jan. 1981

Figure 6.

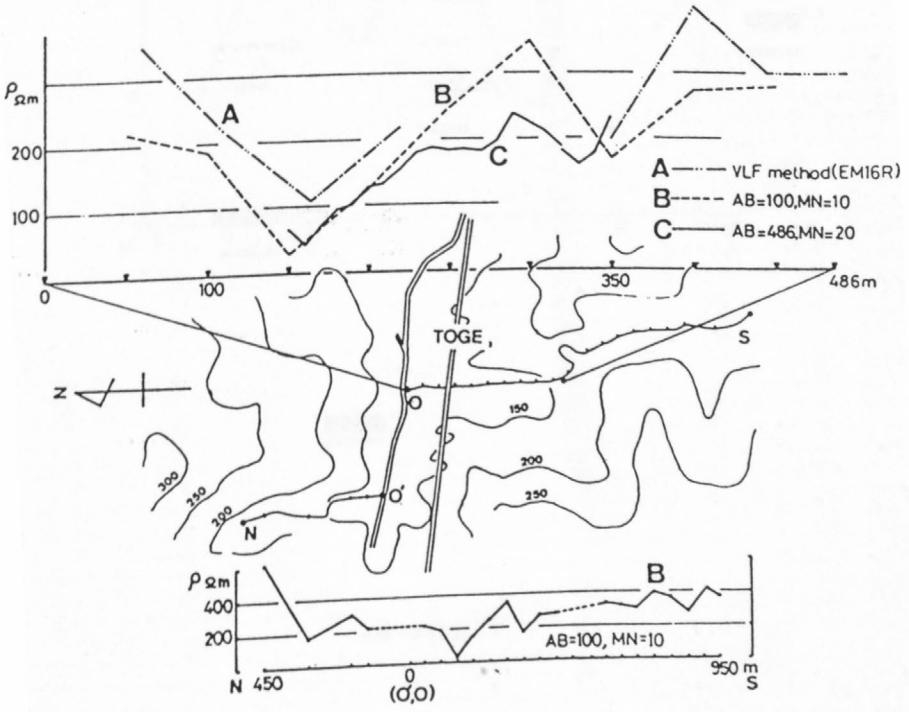
ρΩm
200
100
A
B
C
A—— VLF method(EM16R)
B---- AB=100,MN=10
C—— AB=486,MN=20
0
100
350
486m
TOGE
S
N
O
O'
150
200
250
300
ρΩm
400
200
B
AB=100, MN=10
N 450
0
(O,O)
950 m
S

Figure 7.

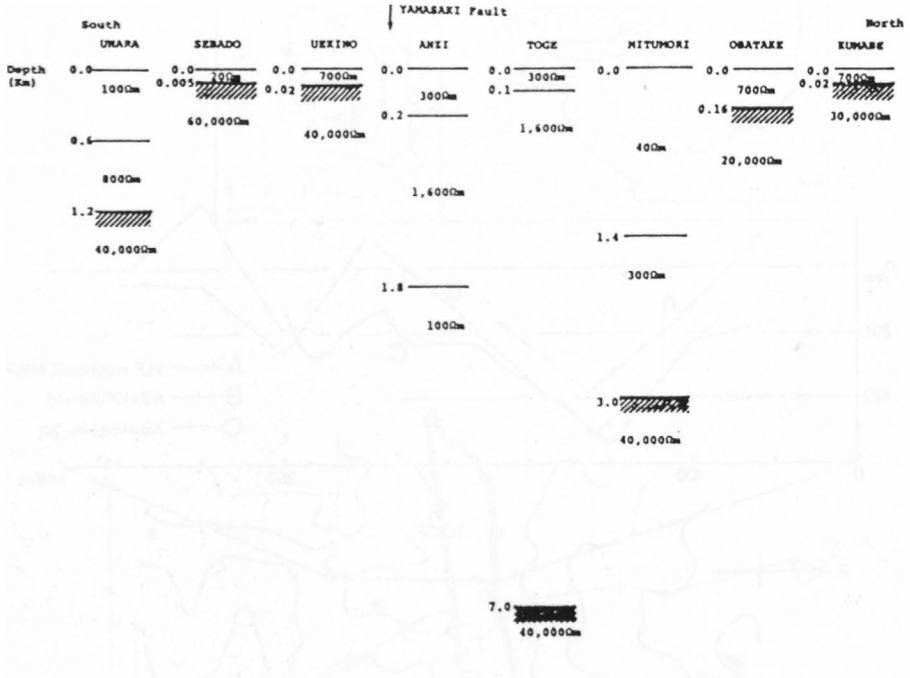
South
North
YAMASAKI Fault
UMARA
SEBADO
UEKINO
ANII
TOGE
MITUMORI
OBATAKE
KUMABE
Depth (Km)
0.0
100Ωm
0.5
800Ωm
1.2
40,000Ωm
0.005
200Ωm
60,000Ωm
0.02
700Ωm
40,000Ωm
0.2
300Ωm
1,600Ωm
1.8
100Ωm
0.1
300Ωm
1,600Ωm
7.0
40,000Ωm
40Ωm
1.4
300Ωm
3.0
40,000Ωm
0.16
700Ωm
20,000Ωm
30,000Ωm

Figure 8.

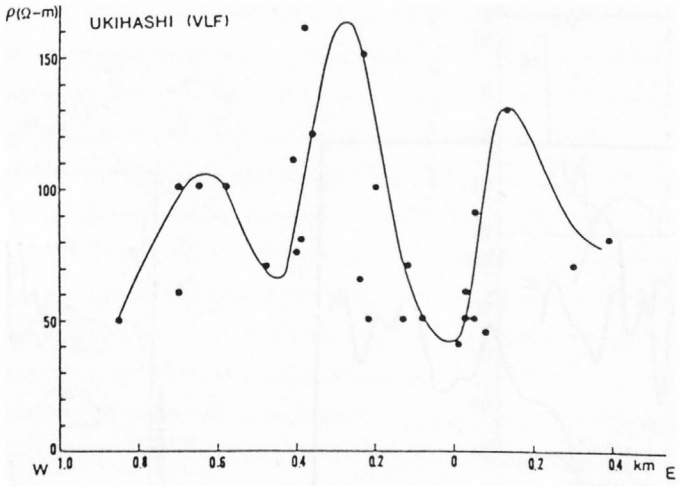

Figure 9.

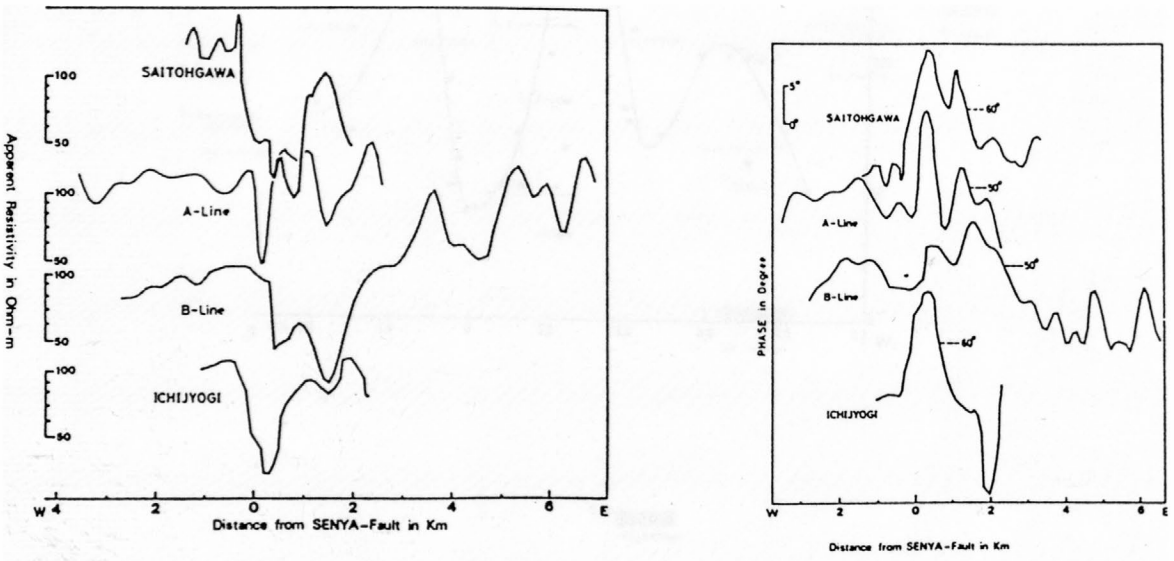
SAITOHGAWA
A-Line
B-Line
ICHIJYOGI
100
50
Apparent Resistivity in Ohm-m
W 4 2 0 2 4 6 E
Distance from SENYA-Fault in Km
5°
0°
60°
50°
50°
60°
PHASE in Degree
W 2 0 2 4 6 E
Distance from SENYA-Fault in Km

Figure 10.

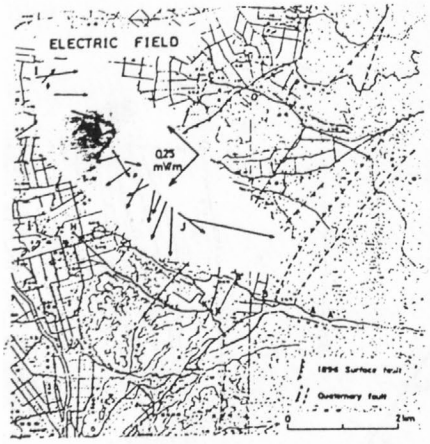
ELECTRIC FIELD
0.25 mV/m
1896 Surface fault
Quaternary fault
0
2km

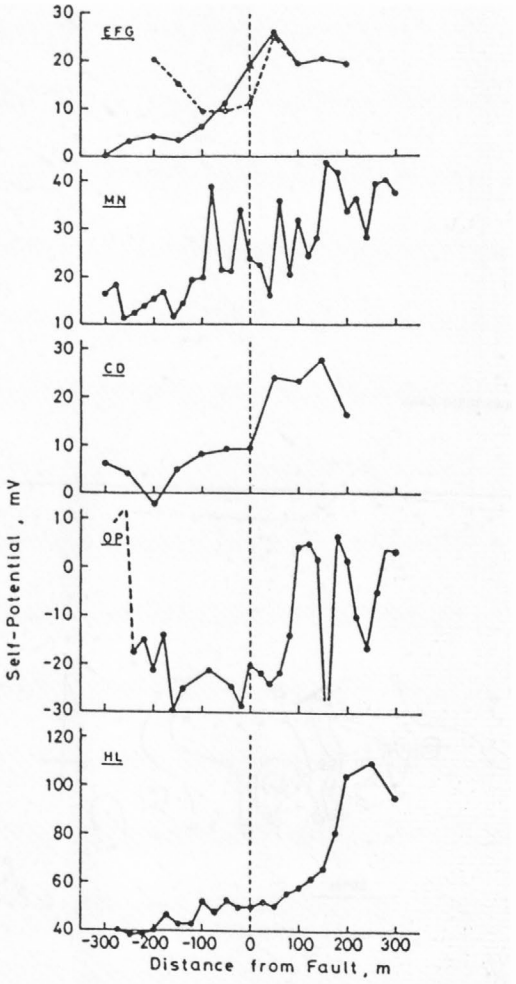
EFG
MN
CD
QP
HL
Self-Potential, mV
Distance from Fault, m

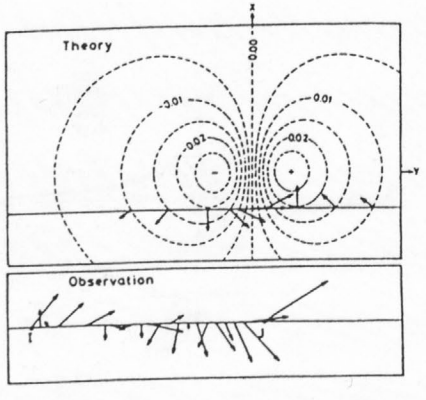
Theory
Observation
-0.01
0.01
-0.02
0.02

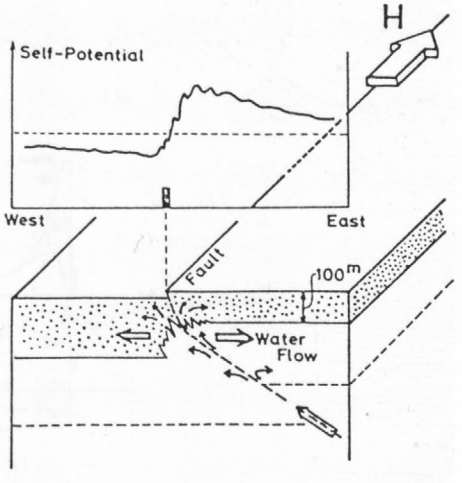
H
Self-Potential
West
East
Fault
100m
Water Flow

Figure 11.

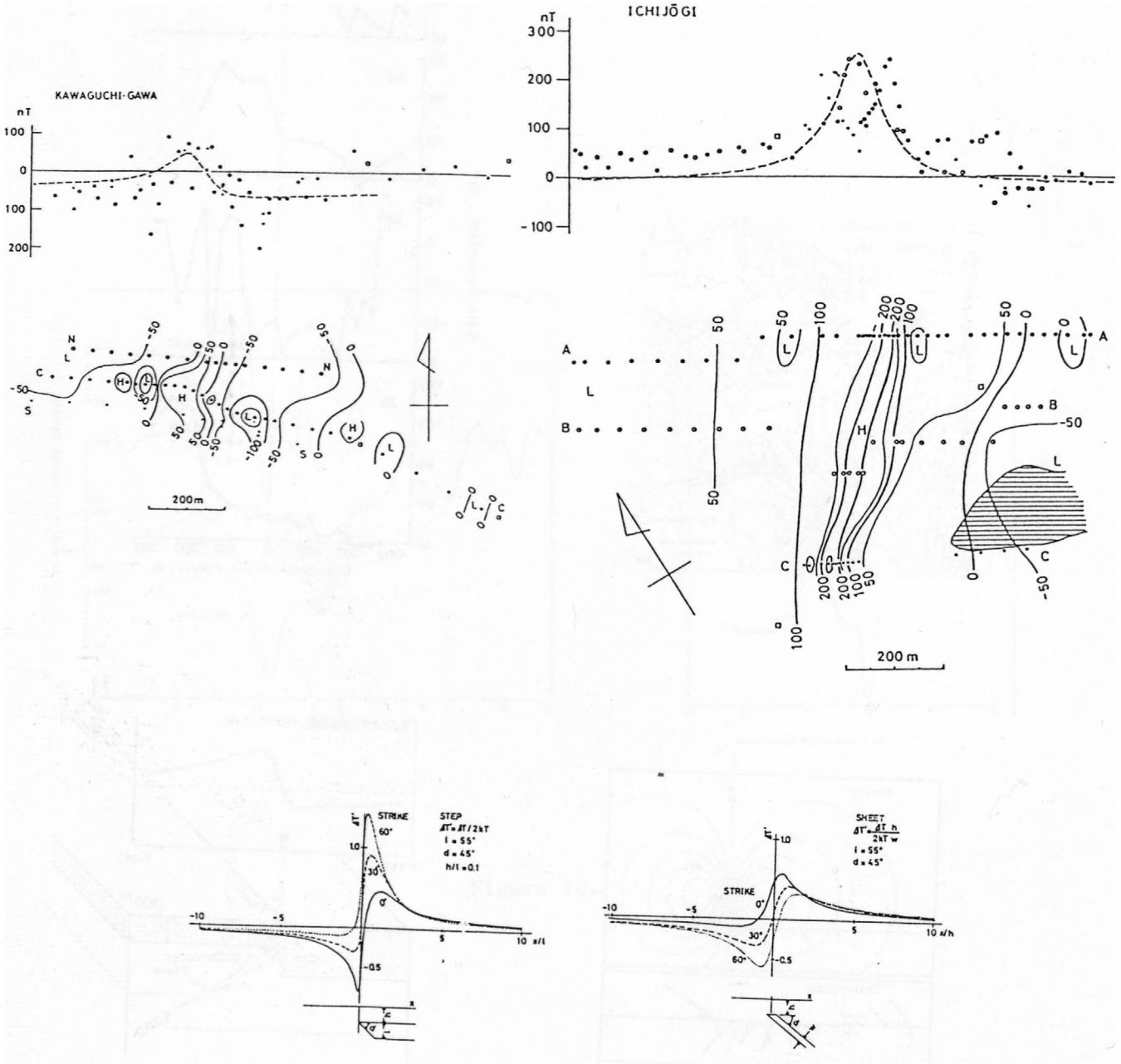
KAWAGUCHI-GAWA
nT
100
0
100
200
ICHIJŌGI
nT
300
200
100
0
-100
200m
A
B
L
C
H
200 m
STRIKE
STEP
ΔT = ΔT / 2kT
I = 55°
d = 45°
h/l = 0.1
60°
30°
0°
-0.5
-10
-5
5
10 x/l
SHEET
ΔT = ΔT h / 2kT w
I = 55°
d = 45°
1.0
30°
60°
-0.5
10 x/h

Figure 12.